TRANSPORTATION RESEARCH RECORD 725

Pavement Systems: Assessment of Load Effects, Design, and Bases

TRANSPORTATION RESEARCH BOARD

COMMISSION ON SOCIOTECHNICAL SYSTEMS
NATIONAL RESEARCH COUNCIL

NATIONAL ACADEMY OF SCIENCES
WASHINGTON, D.C. 1979

Transportation Research Record 725
Price $5.00
Edited for TRB by Mary McLaughlin

modes
1 highway transportation
4 air transportation

subject areas
11 administration
24 pavement design and performance
62 soil foundations

Transportation Research Board publications are available by ordering directly from TRB. They may also be obtained on a regular basis through organizational or individual affiliation with TRB; affiliates or library subscribers are eligible for substantial discounts. For further information, write to the Transportation Research Board, National Academy of Sciences, 2101 Constitution Avenue, N.W., Washington, DC 20418.

Library of Congress Cataloging in Publication Data
National Research Council. Transportation Research Board.
Pavement systems.

(Transportation research record; 725)
Reports prepared for the 58th annual meeting of the Transportation Research Board.

1. Pavements–Live loads–Addresses, essays, lectures. 2. Pavements–Design and construction–Addresses, essays, lectures. 3. Roads–Base courses–Addresses, essays, lectures. I. Title. II. Series.
TE7.H5 no. 725 [TE250] 380.5s [625.8] 79-607910
ISBN 0-309-02975-9 ISSN 0361-1981

Sponsorship of the Papers in This Transportation Research Record

GROUP 2–DESIGN AND CONSTRUCTION OF TRANSPORTATION FACILITIES
Eldon J. Yoder, Purdue University, chairman

Pavement Design Section
Carl L. Monismith, University of California, Berkeley, chairman

Committee on Flexible Pavement Design
Roger V. LeClerc, Washington State Department of Transportation, chairman
Leon M. Noel, Federal Highway Administration, secretary
Ernest J. Barenberg, Robert A. Crawford, R. N. Doty, W. B. Drake, Fred N. Finn, Wade L. Gramling, William Bryan Greene, R. G. Hicks, Michael P. Jones, David J. Lambiotte, J. W. Lyon, Jr., Richard A. McComb, Frank P. Nichols, Jr., Dale E. Peterson, William A. Phang, Carl L. Schulten, Donald R. Schwartz, James F. Shook, Eugene L. Skok, Jr., Richard L. Stewart, Loren M. Womack

Committee on Theory of Pavement Design
Ralph C. G. Haas, University of Waterloo, chairman
G. H. Argue, Yu T. Chou, Santiago Corro Caballero, M[illegible]
Darter, Paul J. Diethelm, David C. Esch, Fred N. Finn [illegible]
Fossberg, W. Ronald Hudson, Lynne H. Irwin, Ali S. K[illegible]
William J. Kenis, Ramesh Kher, Robert L. Lytton, Carl [illegible]
Leon M. Noel, Robert G. Packard, Dale E. Peterson, J[illegible]
William T. Stapler, Ronald L. Terrel, Kornelis Wester [illegible]

Committee on Shoulder Design
John F. Nixon, Texas State Department of Highways & Transportation, chairman
John S. Urban, Edwards and Kelcey, Inc., secretary
Donald K. Emery, Jr., Alvord C. Estep, Wade L. Gram[illegible]
L. Heimbach, R. G. Hicks, James W. Hill, John W. Hu[illegible]
Andrew D. Jones, Edwin C. Lokken, D. W. Loutzenhe[illegible]
A. McComb, Leon M. Noel, R. D. Pavlovich, Josette M[illegible]
James F. Roberts, Randolph W. Sanderson, James A. S[illegible]
F. W. Thorstenson, Graeme D. Weaver, W. A. Wilson, J[illegible]

Lawrence F. Spaine, Transportation Research Board st[illegible]

Sponsorship is indicated by a footnote at the end of ea[illegible]
The organizational units and officers and members are [illegible]
December 31, 1978.

Contents

Procedure for Evaluating the Effects of Legal Load Limits on Pavement Costs

R. Frank Carmichael III, Freddy L. Roberts, and Harvey J. Treybig, Austin
Research Engineers, Inc., Austin, Texas

A computer program that evaluates the effect of changes in legal load limits on the life-cycle costs of flexible, rigid, and composite pavements is described. The methodology of the NULOAD program for determining the effects of changes in truck size, weight, and configuration on pavement performance is examined, and these effects are related to maintenance and rehabilitation and their related costs. A sample problem from NULOAD is also discussed. Fifty representative sections can be grouped by type of system (such as Interstate sections) to reflect the effect of traffic loadings on the different classes of highways. The procedure permits inclusion of a maximum of 10 different truck types along with various axle and tire configurations, such as single axles with single tires and tridem-axle, single-axle, and tandem-axle configurations. Truck axle weight and configuration are the major variables considered, but the procedure can also handle new sizes of trucks, such as the triple-trailer units. The procedure also includes a computerized shifting procedure for gross vehicle weight and axle-load distribution.

This paper describes the development and use of a methodology for determining the effects of changes in truck size, weight, and configuration on pavement performance and relating these effects to pavement maintenance and rehabilitation and their related costs. The procedure was developed under a Federal Highway Administration (FHWA) project and is documented in the project final reports (1,2).

The objectives of this paper are

1. To provide a summary description of the evaluation procedure,
2. To describe the necessary input data for use of the procedure, and
3. To discuss an illustrative example run from the computerized procedure NULOAD.

SCOPE OF THE PROCEDURE

The NULOAD procedure evaluates the effect of changes in legal load limits on the life-cycle costs of flexible, rigid, and composite pavements. Fifty representative sections can be grouped by system (e.g., Interstate sections) to reflect the effect of traffic loadings on the different classes of highways. The procedure permits inclusion of a maximum of 10 truck types along with various axle and tire configurations, such as single axles with single tires or tridem axles, as well as conventional single- and tandem-axle configurations. Although truck axle weight and configuration are the major variables considered, new truck sizes, such as the triple-trailer units, can be handled in the procedure. The procedure includes a computerized shifting procedure for gross vehicle weight (GVW) and axle-load distribution that was first proposed by Whiteside and others (3). The user can select different representative sections. The cost predictions are prepared for any number of lane kilometers in each representative section so that evaluations at a variety of governmental levels can be performed. The procedure also uses a distribution by age and lane kilometers for each representative section.

EVALUATION CONCEPTS

The evaluation procedure permits estimates of costs associated with changes in routine maintenance and rehabilitation requirements that result from changes in the legal load limits. The four basic sets of computations included in the procedure are displayed graphically in the conceptual flowchart shown in Figure 1. They include

1. Determining the traffic loading in terms of 80-kN [18 000-lbf (18-kip)] equivalent single-axle loads (ESALs) for both present and proposed legal limits, including a load-distribution shifting procedure;
2. Predicting the expected life cycles for pavements of each age of the distributions by age and lane kilometers for all representative sections, including rate of deterioration, time of overlay, and overlay requirements;
3. Estimating the associated minor maintenance and rehabilitation (overlay) costs for all representative sections; and
4. Printing a summary of the cost and performance estimates by section, system, and/or entire network as specified by the user.

The life-cycle estimates are based on American Association of State Highway and Transportation Officials (AASHTO) performance equations (4). The overlay thickness is determined from the section condition [present serviceability index (PSI)] at the time of overlay and expected traffic for a 20-year overlay design life. In initial calculations, provision is made for considering the differences in AASHTO performance predictions and experience in the state through the use of average pavement ages at terminal serviceability and the application of "Iowa-type" survivor curves (5).

For each representative section, the user can consider routine maintenance costs in one of three ways: (a) not at all, if the user suspects that maintenance costs will not change with new loads; (b) by using cost-prediction models obtained from the EAROMAR program (6); or (c) based on historical cost information obtained from highway department records.

PROGRAM CAPABILITY

The NULOAD program has the capability to model various sizes of highway networks for which input data can be developed. The kilometers of a network should be distributed based on system classification (Interstate urban, Interstate rural, primary urban, and so on), section structure (asphalt concrete, portland cement concrete, or composite), and pavement age (time since construction or major reconstruction). A network can be divided into as many representative structural sections as necessary to adequately characterize the network. The lane kilometers of each representative section are distributed by pavement age.

The major capabilities of NULOAD include

1. The ability to handle as many as 10 representative sections for each system;
2. The ability to make predictions on the assumption either that the same total payload per year is car-

ried under present and proposed limits or that the same number of truck trips per year is made under both limits;

3. The choice of different maintenance cost models for each representative section;

4. Consideration of a traffic-stream mix of up to 10 trucks for both present and proposed regulations;

5. Variation in the percentage of each truck type as a percentage of all vehicles, by year in the analysis period;

6. The use of predictions of pavement performance that are based not only on pavement structure and traffic but also on existing pavement age;

7. A prediction of overlay cost, including the necessary costs to bring the shoulders up;

8. An estimate of remaining network functional life in terms of 80-kN ESALs to provide a measure of the structural condition of the system at the end of the analysis period;

9. Prediction and summarization by section, by system classification, and for the entire network of the expected economic effects of various proposed changes in legal load limits on maintenance and rehabilitation;

10. A number of options available to the user for handling those pavements in the category of pavements older than terminal serviceability (POTTS), i.e., pavements in such poor condition that the PSI at the beginning of the analysis period is below the terminal level;

11. Problem stacking for solution of many problems through the flexible input order of the NULOAD program;

12. The ability to consider asphalt concrete, p rtland cement concrete, and composite pavements in a single set of runs;

13. A provision to consider differences betwe n the AASHTO performance predictions and state experi nce through the use of various age parameters at terminal serviceability in conjunction with the use of Iowa survivor curves (5);

14. The ability to model the effect of different and multiple-trailer configurations by using vehicle designations and equivalency factors for single, steering tandem, and tridem axles; and

15. A slightly modified version of the load-distribution shifting procedure reported by Whiteside and others (3).

Figure 1. Flow of evaluation procedure to determine effect of new legal load limits.

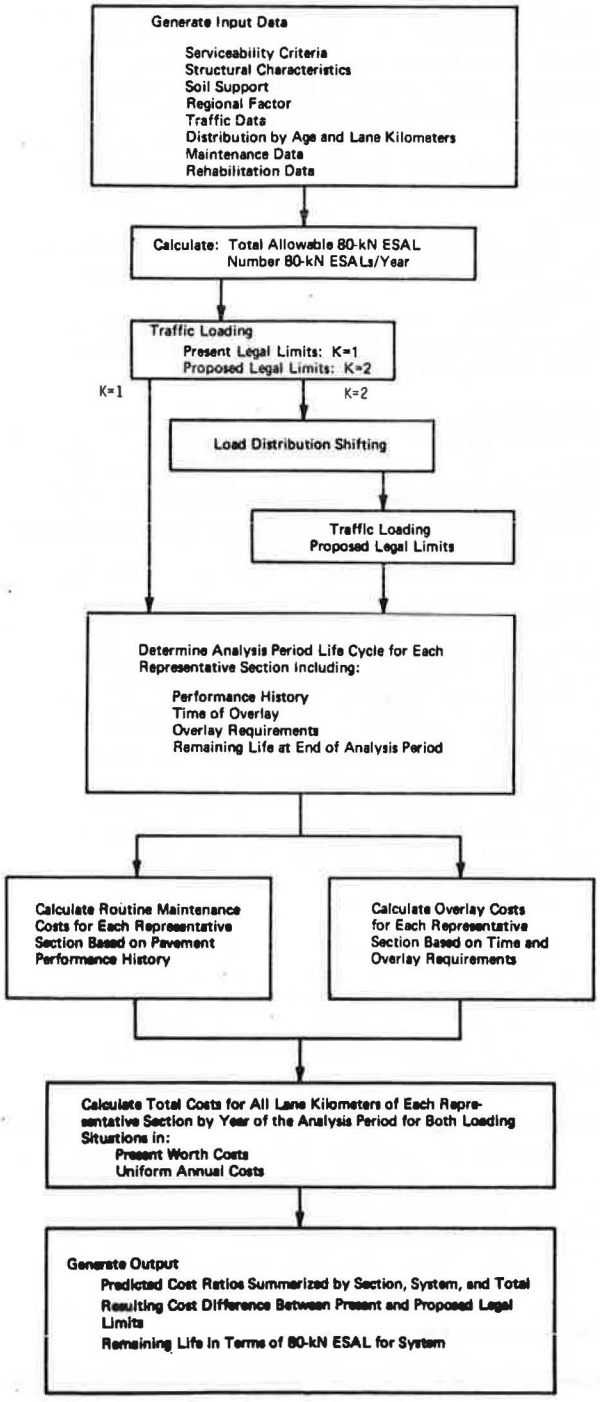

SUMMARY OF REQUIRED INPUT

Although no special field or laboratory studies are required, the use of NULOAD requires many data from highway agency records. The information required to determine input values for NULOAD is summarized as follows:

1. Traffic and load survey information includes the composition of the traffic stream; truck types; single-, tandem-, tridem-, and steering-axle-load distributions GVW distributions; empty vehicle weight; legal limits and expected growth in 80-kN ESALs.

2. Performance-prediction information includes highway network statistics, especially the kilometer breakdown by pavement type and age and system classification; representative design section structural information, including materials parameters and thicknesses and soil-support information; and performance parameters, such as regional factor, serviceability limits, an average pavement age at terminal PSI, and pavement ages when 25 and 75 percent of the length of each representative section should reach terminal PSI.

3. Economic prediction data include unit cost information, historical maintenance expenditures, geometric dimensions, interest rates, and pavement types.

The sample problem discussed in this paper uses realistic values for input, but specific data should be developed for each prediction desired.

DESCRIPTION OF THE PROCEDURE

The NULOAD computer program has been developed to use information currently available to state departments

of transportation. These data are used as input to the AASHTO performance model (4), the weight-distribution shifting procedures developed and included as a part of NCHRP Report 141 (3), and maintenance models from EAROMAR (6) to evaluate the difference in the life-cycle costs for the two different legal load limits selected by the user. The major calculation subsystems of the NULOAD procedure are discussed briefly in the following sections of this paper.

Remaining Life and Rehabilitation Calculations

NULOAD uses the performance equations from the AASHTO Interim Guide (4) as a basis for calculating the number of 80-kN ESALs that a typical representative section can withstand before reaching terminal PSI. At terminal PSI, the section under consideration can be overlaid in a timely manner or allowed to go below the prescribed PSI level—i.e., enter into the POTTS program. If the section enters POTTS, the layer coefficients are reduced in a manner prescribed by the Asphalt Institute (7, Table III-1). These reductions in the value of the layer coefficients were made to correspond to the different terminal PSI values in common use.

The kilometers of a particular age that require overlay rehabilitation during each of the years of the analysis period are determined by using a symmetrical type of Iowa survivor curve (5). One modification has been made to the application of these curves to enhance computer operations. This modification involves the assumption that the survivor curve for the pavement surface will not span a period of more than 13 years centered about the average life of the section. For example, if a representative section has an average life of 15 years, the life of various projects could be expected to range from 8.5 to 21.5 years, but most would require rehabilitation at around 15 years. The exact number of kilometers of pavement sections of a certain age that are reaching terminal PSI will be a function of the average age at terminal PSI and the standard deviation of the survivor curve. These concepts are discussed in more detail in the following sections.

AASHTO Performance Equation

The structural design equations for both flexible and rigid pavements developed at the AASHO Road Test are the basis of calculating the number of 80-kN ESALs that the typical pavement structure will sustain before reaching terminal PSI. This is accomplished by substituting the individual layer thicknesses and structural layer coefficients, a typical regional factor, and a typical soil-support value into the AASHTO equation. The total cumulative 80-kN ESAL is assumed to be applied over the years between initial construction and the average age before the pavement structure reaches terminal PSI (P_t). By using this average age at P_t, total cumulative ESAL, and the average growth rate of ESAL, NULOAD computes the rate of 80-kN ESAL applications per year and the number of ESALs remaining at the beginning of the analysis period on each pavement age of the distribution by age and lane kilometers. Traffic during the analysis period is applied at the calculated rate so that the pavement reaches P_t at the average age at P_t. The traffic level at the year of the analysis period when PSI reaches P_t is used along with the anticipated growth rate to calculate the number of 80-kN ESALs to which an overlay on the existing pavement will be subjected during its design life.

If the overlay is applied in a timely manner and if the P_t is 3.0, the structural coefficients assigned to the existing pavement are only slightly reduced when overlay thicknesses are calculated. However, for kilometers of pavement that are permitted to go below a selected value of P_t—i.e., pavement kilometers in POTTS—the structural coefficients are also reduced to reflect the decreased resistance of the structure to loads because of the effects of surface deterioration and the effects of moisture on the underlying layers and subgrade. Structural coefficients are increasingly reduced from their original values as the terminal PSI values decrease from 3.0 toward the commonly used values of 2.5 and 2.0. The overlay thickness required for the present load limits is calculated by using estimated future traffic, the appropriately reduced structural coefficients of the layers, and the typical soil-support value.

Use of Survivor Curves

The use of survivor curves is a standard method of making management decisions relative to future estimates of time to retirement of physical properties. Physical properties are said to be retired from service when, for one reason or another, they are removed from productive service or altered and used in a second service life (5). Winfrey (8) has developed 18 different survivor curves that fit into the three basic types: symmetrical, left modal, and right modal. The type selected for use in NULOAD is the symmetrical; the standard deviation of the survivor curve is defined by user input.

The application of these survivor curves in NULOAD can best be discussed by using an illustration. The upper part of Figure 2 shows the performance of a pavement that enters the analysis period at a PSI of 3.8 and reaches the terminal PSI (P_t) of 2.5 during the 10th year of the analysis period, the average age of the pavement at P_t. In the lower part of Figure 2, the histogram shows the kilometers of pavement that reach P_t at each of the 13 years centered about the average age of P_t by using the symmetric survivor-curve concept. These kilometers are calculated, by using the survivor curve, by first computing the probability that some number of kilometers will reach P_t, and then this probability is multiplied times the total pavement kilometers of that age. These probabilities are calculated by using the average age at terminal PSI and the standard deviation calculated from the following two input quantities: (a) the expected age by which 25 percent of the pavements have reached P_t and (b) the expected age by which 75 percent of the pavements have reached P_t. These kilometers of pavement are then either scheduled for overlay during the assigned years of the analysis period or placed into POTTS, depending on user-specified inputs.

The process discussed above is repeated once for each pavement age—i.e., years of service since construction or major reconstruction—and accumulated for each year of the analysis period. Kilometers that should have been rehabilitated—i.e., reached P_t before the beginning of the analysis period—represent the contents of POTTS.

Cost Calculations

Rehabilitation

The cost of rehabilitation is calculated by taking the kilometers that are overlaid and multiplying the unit cost of overlay for the additional thickness required to obtain the structural number sufficient to sustain the 80-kN ESALs expected during the design life of the overlay.

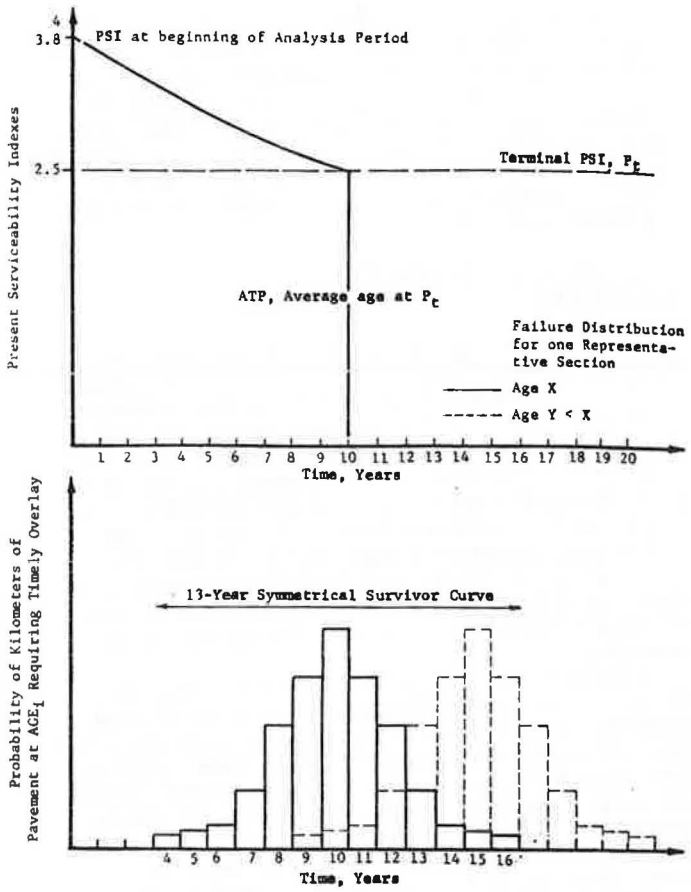

Figure 2. Application of survivor-curve concept in NULOAD to determine the time during the analysis period when kilometers of a certain age require a timely overlay.

In addition, the costs for raising the shoulders to the level of the new overlay are also included. These shoulders are categorized as either aggregate or asphalt concrete, and cost for the appropriate type and volume of material is included.

Maintenance

Maintenance costs can be input separately by the user or calculated by using internal models obtained from EAROMAR (6). These models predict routine maintenance items as a function of pavement age:

1. For flexible pavements, skin patching, base and surface repair, and crack sealing; and
2. For rigid pavements, joint sealing, mudjacking, blowups, and concrete surface patching.

These maintenance costs can be allocated in two different ways. First, the maintenance costs are calculated for current load-limit conditions only as a function of age by using regression models obtained from EAROMAR (6). This same set of models can be used to calculate maintenance as a function of age for the same pavements, but performance would be estimated by using loads applied under the new legal load limits. This option would represent a situation in which the level of maintenance funds is historically nearly constant or there are ceiling levels on employment that would prevent the maintenance level from being as responsive to distress in pavements as might otherwise be desired.

The second method for handling maintenance costs may best be called an accelerated maintenance method. This method is based on the assumption that a pavement will receive some prescribed amount of maintenance whether the life cycle is shortened by heavier loads or not. Layton and Hicks (9) used the assumption that cumulative maintenance costs expended on a roadway between initial construction and average time to terminal serviceability do not change with changes in load limits.

The procedure for accomplishing this acceleration of maintenance costs can best be illustrated by using Figure 3, which shows the technique for determining the cost of applied maintenance during each year of the analysis period under a proposed load-limit change. The cumulative maintenance cost shown in Figure 3 is calculated as a function of the age of the pavement by using regression models from EAROMAR. This cumulative cost curve is developed for pavements to present load limits but is also used to determine the amount of maintenance to be charged to each kilometer of pavement for the proposed load limits. The technique used to calculate accelerated maintenance is based on the assumption that the maintenance cost incurred between two different PSI levels is the same but the time during which the maintenance occurs changes. Therefore, as the rate of change of PSI per year increases, a larger increment of maintenance cost is charged to that year.

For example, in Figure 3, during the year between i and i + 1 and under the proposed load limits, the PSI changed from PSI_i to PSI_{i+1}. To calculate the accelerated maintenance cost applied to year i, extend the PSI lines from $year_i$ and $year_{i+1}$ from the proposed load-limit PSI curve to the present load-limit PSI curve. Extend vertically from the intersections of PSI_i and PSI_{i+1} with the present limit curve to the

cumulative maintenance cost curve. The difference between cumulative maintenance at PSI_{i+1} and PSI_i is the accelerated maintenance applied to $year_i$ under the proposed load limits. This level of maintenance under the proposed load limits is larger than the level applied to the same calendar year under present load limits.

SHIFTING OF LOAD DISTRIBUTION

The axle-load distributions for present load limits are shifted in order to evaluate the effect of changes in legal load limits on future truck-weight distributions. To do this, the user should supply the appropriate load information for each of the truck types to be used in the analysis: (a) GVW distribution, (b) single-axle-load distribution, (c) tandem-axle-load distribution, (d) tridem-axle-load distribution, and (e) steering-axle-load distribution. For example, a 3-S2 has a steering axle and two tandem axles; therefore, no single- or tridem-axle-load distributions are necessary and the steering-axle-load distribution is optional input. Once the appropriate axle-load distributions have been input for the present legal limit and the appropriate 80-kN ESALs have been computed, the distributions are shifted to simulate the anticipated effects of changes in legal load limits. If the legal load limits increase, the distributions are expected to shift toward higher loads. The result of such a shift will be that additional payload (GVW minus tare weight) can be carried by each truck and, if the same types of trucks are used with higher axle loads, the life cycle of the pavement will decrease because the damage per loaded truck increases exponentially as the payload increases linearly.

Figure 3. Procedure for determining cost of accelerated maintenance required because of increases in load limits.

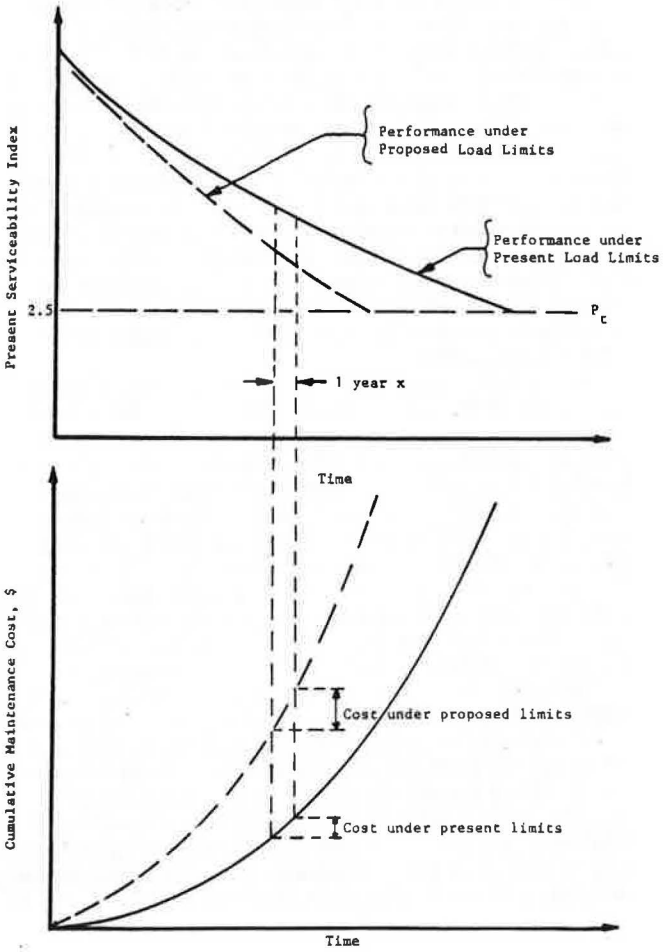

Data on load distributions obtained from W-4 loadometer tables are input into NULOAD and converted to cumulative distributions. An example of this type of information is shown in Figure 4, which represents the cumulative distribution of GVW for the 3-S2 truck. The solid line represents data taken from a W-4 table that have been smoothed. This cumulative distribution is shifted by using a procedure reported by Whiteside and others (3). The result of such a shift is also shown in Figure 4. The individual axle distributions are also shifted by using a procedure similar to that given by Whiteside and others.

Once the axle-load distributions are defined, the number of 80-kN ESALs can be calculated for both present and proposed load limits by multiplying equivalency factors for each weight interval from the AASHTO Interim Guide (4) by the percentage distribution of axle weights.

CHECK FOR CONSISTENCY

The procedure developed by Whiteside and others (3) includes calculation of the average payload for an average truck of each type that has been incorporated in NULOAD. At the point at which the average payload is calculated, the average number of 80-kN ESALs for an average truck of each type is also calculated. The total payload carried by all trucks of each type during each year under present legal load limits can also be calculated. At this point in the NULOAD procedure, the user has the choice of making either the number of trips or the total payload equal under both the present and the proposed legal load limits. If the user selects the equal-payload option, fewer trucks of each type will be required to carry the calculated total payload under the proposed than under the present load limits. If the user selects the equal-trips option, the number of 80-kN ESALs for the proposed legal load limits will be the number of trips of each truck type for present legal load limits times the number of ESALs for an average truck of that type under the proposed load limits. One

Figure 4. GVW distributions for present and proposed load limits.

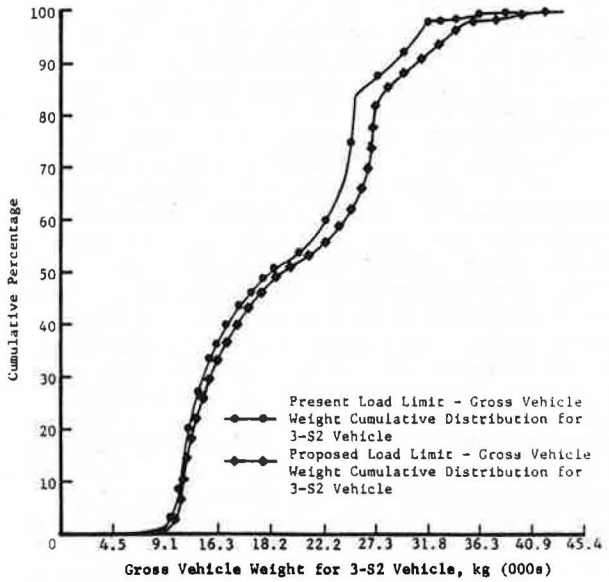

should understand that the implication associated with the equal-trips option is that either some freight will be diverted from other modes or that new freight will be generated to supply the extra payload difference between payload for a truck type under present and proposed legal load limits. The equal-total-payload option ensures a fair comparison for the effects of increased weights, whereas the second option, which may be more realistic for the actual situation, does not.

ECONOMIC EVALUATION

Engineering economy studies are conducted because of the need for making a choice between several alternative plans for accomplishing some objective of providing a given service. In order to make a selection between the several alternatives available, there should be a technique for normalizing the costs so that a clear decision between the alternatives can be made. The use of interest to accomplish this normalization and the fact that payments or costs that differ in total magnitude but are made at different dates may be equivalent to one another are both very important in engineering economy (11). To assist the user of NULOAD in making these comparisons, two types of economic analysis calculations are performed and are discussed in the following paragraphs.

Once the maintenance and overlay costs incurred during each year of the analysis period have been computed, they are converted by the use of interest factors to equivalent costs at the same time base. The present worth of all dollars to be spent in future years of the analysis period is calculated separately for both maintenance and overlay rehabilitation costs and for both present and proposed load limits. The ratio of the present worth of costs of maintenance and overlay under proposed load limits to that under present load limits is calculated and included in the output from NULOAD. In addition to the ratio of the present worth of costs, the difference in the present worth of total cost under proposed and present load limits is also included in the output. Because of the difficulty of assessing the worth of the system at the beginning of the analysis period, assessment of salvage value in monetary terms was beyond the scope of this project. However, salvage value is addressed from a structural standpoint by calculating the ratio of remaining 80-kN ESALs under proposed legal limits to remaining 80-kN ESALs under present legal limits.

There are those who contend that the use of interest factors in this type of analysis is not appropriate since no real assets that will be used to finance future payments are being placed in interest-bearing accounts. Such an argument ignores the fact that the real objective of such analyses is not to provide assets to pay for future expenses but to be able to rationally compare alternatives on a common basis. One should also recognize that there is a significant difference between cost estimates that are used for financial planning and those that are used in engineering comparisons between alternatives. If a financial plan is being prepared, inflation must be considered because of the effects of inflation on material and manpower costs; such is not necessarily the case, however, for engineering comparisons of alternatives. Unless the analyst is willing to predict different, individual inflation rates for each component considered in the cost proposal, the result of applying the same inflation rate for all components of an analysis is that the selection of the best alternative does not change but only the magnitude of the numbers involved in the calculations. The net result is that NULOAD, which is an engineering analysis tool, does not provide the option of considering inflation effects on unit costs of maintenance and overlay rehabilitation. NULOAD also outputs uniform annual cost differences and cost ratios to give the user a different type of reportable prediction.

SAMPLE PROBLEM

The illustrative problem represents the type of NULOAD solution that would be required to analyze an Interstate system that has two representative sections. All data used in the problem were gathered during the state visits conducted during this project. Although the solution is hypothetical in the sense that input data come from several states, it is real in the sense that actual data have been used.

The input for the problem has been prepared to demonstrate the following conditions and options of NULOAD:

1. One system—Interstate;
2. Two representative sections—flexible and rigid;
3. A 20-year analysis period;
4. Calculations based on (a) equal payload under present and proposed limits, (b) accelerated model maintenance, and (c) old sections (target value of 10 percent);
5. Four truck types—2D, 3A, 3-S2, and 2-S1-2; and
6. Legal load changes—(a) single axle, 80-89 kN (18 000-20 000 lbf); (b) tandem axle, 142-151 kN (32 000-34 000 lbf); and (c) gross weight, 356-534 kN (80 000-120 000 lbf).

Table 1 gives the most important summary output information. The total predicted additional cost of allowing new increased vehicle loads is $17 171 000 in present-worth terms for a 20-year analysis period. The rigid pavements contribute a majority of this difference because of their higher unit costs and twice as many lane kilometers. It should be noted, however, that at the end of the analysis period the concrete pavements are predicted to have 34 percent more remaining life under proposed than under present load limits and the flexible pavements to have 18 percent more remaining life. This means that the structural condition of the system has been improved as a result of overlay expenditures required to carry loads resulting from the load-limit changes.

As would be expected, the cost ratios are identical for the present-worth and uniform annual cost results. In the context of uniform annual cost, the increased cost of maintenance and rehabilitation on the 1776 lane-km (1101 lane miles) of flexible pavements is approximately $257/lane-km ($413/lane mile) more annually and, for the 3574 lane-km (2220 lane miles) of rigid pavement, the costs are increased by $292/lane-km ($470/lane mile) annually. On a system basis, this is a weighted value of approximately $280/lane-km ($451/lane mile) more annually. Although these numbers cannot be verified, the predictions are reasonable.

Tables 2 and 3 demonstrate some of the more detailed information concerning the calculation of the summary costs given in Table 1. In the procedure, five major tables for each of the representative sections are provided. They include (a) performance tables under present and proposed regulations (Tables 2 and 3), (b) POTTS tables under present and proposed regulations, and (c) undiscounted cost tables, including maintenance, overlay, and total costs estimated for both present and

Table 1. Differences between and ratios of costs for present and proposed legal load limits.

Section	Lane Kilometers	Present Worth				Uniform Annual Cost Delta Cost ($000s)	Ratio of Remaining Life (proposed limits/present limits)
		Delta Cost ($000s)	Cost Ratio	Delta Cost ($000s)	Cost Ratio		
1	1776	6 295.57	1.17	5 206.14	1.23	453.89	1.18
2	3580	20 713.24	1.39	11 965.35	1.47	1043.19	1.34
Total	5356	27 008.81		17 171.49		1497.08	

Note: 1 km = 0.62 mile.

Table 2. Performance table for present load regulations.

Lane Kilometers Overlaid	Year of Overlay	Overlay Design Structural Number	Overlay Thickness (cm)	PSI at End of Analysis Period	Remaining Life (million 80-kN ESALs)	Overlay Cost ($/lane-km)
45.7	1	5.19	4.6	2.81	9.142	8604
55.3	2	5.19	4.6	2.85	10.242	8604
67.1	3	5.19	4.6	2.90	11.320	8604
80	4	5.19	4.6	2.94	12.377	8604
93.2	5	5.19	4.6	2.99	13.414	8604
105.5	6	5.19	4.6	3.03	14.430	8604
117.3	7	5.19	4.6	3.08	15.426	8604
124	8	5.19	4.6	3.13	16.403	8604
126.3	9	5.19	4.6	3.18	17.361	8604
123.3	10	5.19	4.6	3.23	18.299	8604
114.9	11	5.19	4.6	3.28	19.22	8604
101.2	12	5.19	4.6	3.34	20.122	8604
84.6	13	5.19	4.6	3.39	21.007	8604
66.3	14	5.19	4.6	3.46	21.874	8604
48.3	15	5.19	4.6	3.52	22.724	8604
31.7	16	5.19	4.6	3.59	23.558	8604
18.8	17	5.19	4.6	3.68	24.375	8604
9.5	18	5.19	4.6	3.77	25.177	8604
3.8	19	5.19	4.6	3.90	25.962	8604
0.0						

Note: 1 km = 0.62 mile; 1 cm = 0.39 in; $1/lane-km = $1.61/lane mile.

Table 3. Performance table for proposed load regulations.

Lane Kilometers Overlaid	Year of Overlay	Overlay Design Structural Number	Overlay Thickness (cm)	PSI at End of Analysis Period	Remaining Life (millions of 80-kN ESALs)	Overlay Cost ($/lane-km)
46.5	0.72	5.43	5.96	2.79	12.182	11 167
56.5	1.45	5.43	5.93	2.82	13.221	11 123
68.4	2.18	5.42	5.91	2.85	14.241	11 080
81.3	2.91	5.42	5.88	2.88	15.240	11 038
95	3.65	5.41	5.86	2.92	16.220	10 996
107.3	4.40	5.41	5.86	2.95	17.182	10 955
119.4	5.14	5.41	5.84	2.98	18.124	10 914
126.3	5.89	5.40	5.81	3.02	19.048	10 875
128.6	6.65	5.40	5.78	3.05	19.954	10 836
125.5	7.40	5.40	5.76	3.09	20.842	10 797
117	8.16	5.39	5.73	3.12	21.713	10 759
103	8.93	5.39	5.73	3.16	22.567	10 722
86.2	9.70	5.39	5.71	3.20	23.403	10 685
67.4	10.47	5.38	5.68	3.24	24.224	10 648
49	11.24	5.38	5.66	3.28	25.028	10 613
32.3	12.02	5.38	5.66	3.32	25.816	10 578
19.1	12.80	5.37	5.63	3.37	26.589	10 543
9.6	13.59	5.37	5.61	3.42	27.347	10 509
4	14.38	5.37	5.58	3.47	28.090	10 475

Note: 1 km = 0.62 mile; 1 cm = 0.39 in; $1/lane-km = $1.61/lane mile.

proposed load limits. The following information is also provided:

1. The predicted increase in payloads and number of 80-kN ESALs by truck type and
2. The final shifted axle-load distributions, which can be compared with the input distributions to determine the effect of the shift.

SUMMARY

NULOAD is an implementable program that evaluates the effects of potential new legal load limits in terms of pavement maintenance and rehabilitation costs. Different axle configurations—such as tridems—or different truck sizes—such as triple-trailer units—can be evaluated. NULOAD cost predictions can be combined with benefit predictions to allow for a rational study of the effect of proposed legal limits on pavement costs. Complete documentation of the development of the procedure is available elsewhere (1). A user's manual has been prepared to provide the information necessary for using NULOAD, including (a) a summary description of the procedure, (b) a list and description of all inputs and outputs, (c) a complete illustrative problem, and (d) a detailed input guide (2).

NULOAD can be used to evaluate a city, a county, a district, or a state. It is conceivable that, if solutions were prepared for all 50 states, a prediction for the United States could be prepared. Other potential applications of the NULOAD program include an analysis of truck route networks, consideration of a modal shift in commodity hauling, and an evaluation of the effect of

different analysis periods on the failure of existing pavement and overlay life.

ACKNOWLEDGMENT

The work presented in this paper was accomplished in 1978 by a team that included R. Frank Carmichael III, Freddy L. Roberts, Peter R. Jordahl, Harvey J. Treybig, Harold Von Quintus, Larry L. Caldwell, Russell Catalano, Fred N. Finn, and W. R. Hudson. We wish to thank Peter R. Jordahl for his leadership in the development of analytical techniques and in the computer coding and other members of the team, including Harold Von Quintus, Larry L. Caldwell, and Russell Catalano, for providing development support. We especially thank F. N. Finn and W. R. Hudson for providing technical consultation.

Support for the project was provided by the Office of Research and Development of the Federal Highway Administration. We are grateful for the technical coordination, discussion, and participation of Richard McComb.

REFERENCES

1. R. F. Carmichael III, F. L. Roberts, P. R. Jordahl, H. J. Treybig, and F. N. Finn. Effects of Changes in Legal Load Limits on Pavement Costs: Volume 1—Development of Evaluation Procedure. Federal Highway Administration, U.S. Department of Transportation, Rept. FHWA-RD-78-98, Sept. 1978.
2. R. F. Carmichael III, F. L. Roberts, P. R. Jordahl, H. J. Treybig, and F. N. Finn. Effects of Changes in Legal Load Limits on Pavement Costs: Volume 2—User's Manual for Program NULOAD. Federal Highway Administration, U.S. Department of Transportation, Rept. FHWA-RD-78-98, Sept. 1978.
3. R. E. Whiteside, T. Y. Chu, J. C. Cosby, R. L. Whitaker, and R. Winfrey. Changes in Legal Vehicle Weights and Dimensions. NCHRP, Rept. 141, 1973.
4. AASHTO Interim Guide for Design of Pavement Structures. AASHTO, Washington, DC, 1972.
5. R. Winfrey. Economic Analysis for Highways. International Textbook Co., New York, 1969.
6. B. C. Butler, Jr. Economic Analysis of Roadway Occupancy for Freeway Pavement Maintenance and Rehabilitation. Federal Highway Administration, U.S. Department of Transportation, Rept. FHWA-RD-76-14, Vols. 1, 2, and 3, 1974.
7. Asphalt Overlays and Pavement Rehabilitation. Asphalt Institute, College Park, MD, Manual Series 17, 1st Ed., Nov. 1969.
8. R. Winfrey. Statistical Analyses of Industrial Property Retirements. Iowa Engineering Experiment Station, Iowa State Univ., Ames, Bull. 1935, republished 1967.
9. R. D. Layton, and others; Oregon State Univ. The Energy, Economic and Environmental Consequences of Increased Vehicle Size and Weight. U.S. Department of Transportation, Final Rept. Vols. 1 and 2, Nov. 1977.
10. The AASHO Road Test: Report 5—Pavement Research. HRB, Special Rept. 61E, 1962.
11. E. L. Grant and W. G. Ireson. Principles of Engineering Economy, 5th Ed. Ronald Press, New York, 1970.

Publication of this paper sponsored by Committee on Flexible Pavement Design.

Heavy Trucks on Texas Highways: An Economic Evaluation

C. Michael Walton, Department of Civil Engineering, University of Texas at Austin
James L. Brown, Asphalt Institute, Austin, Texas
Dock Burke, Texas Transportation Institute, Texas A&M University, College Station

A study undertaken to assess the effects of projected truck traffic on the highway system of Texas is described. The study included the evaluation of costs and benefits for a 20-year planning horizon. Alternative scenarios of future truck traffic were assessed. The study considered only an increase in gross vehicle weights and axle loads and not the effects of changes in the size of trucks or the effects of heavy trucks on county roads and city streets. The major approach to the study involved estimating the comparative pavement maintenance and rehabilitation costs of perpetuating the state highway system under current weight limitations and of future use under different weight conditions. It is concluded that, if changes in weight laws are undertaken, further analysis will be needed to select those routes that would carry relatively large freight tonnages and cost relatively less to upgrade.

The objective of this study was to assess the effects of projected truck traffic on the Texas highway system for a 20-year analysis period. Selected costs and benefits were calculated to show some of the measurable effects of increasing the legal weight limits for trucks that operate on the state network.

The study included the evaluation of costs and benefits for a 20-year planning horizon. Alternative scenarios of future truck traffic were assessed. The study did not consider the effects of changes in the size of trucks, only an increase in gross weights and axle loads. The study did not evaluate the effects that heavy trucks would have on county roads or city streets.

SELECTION OF SCENARIOS

The identification of alternative scenarios was accomplished through analysis, discussion, and evaluation of

Figure 1. Selected truck configurations for scenarios A and B.

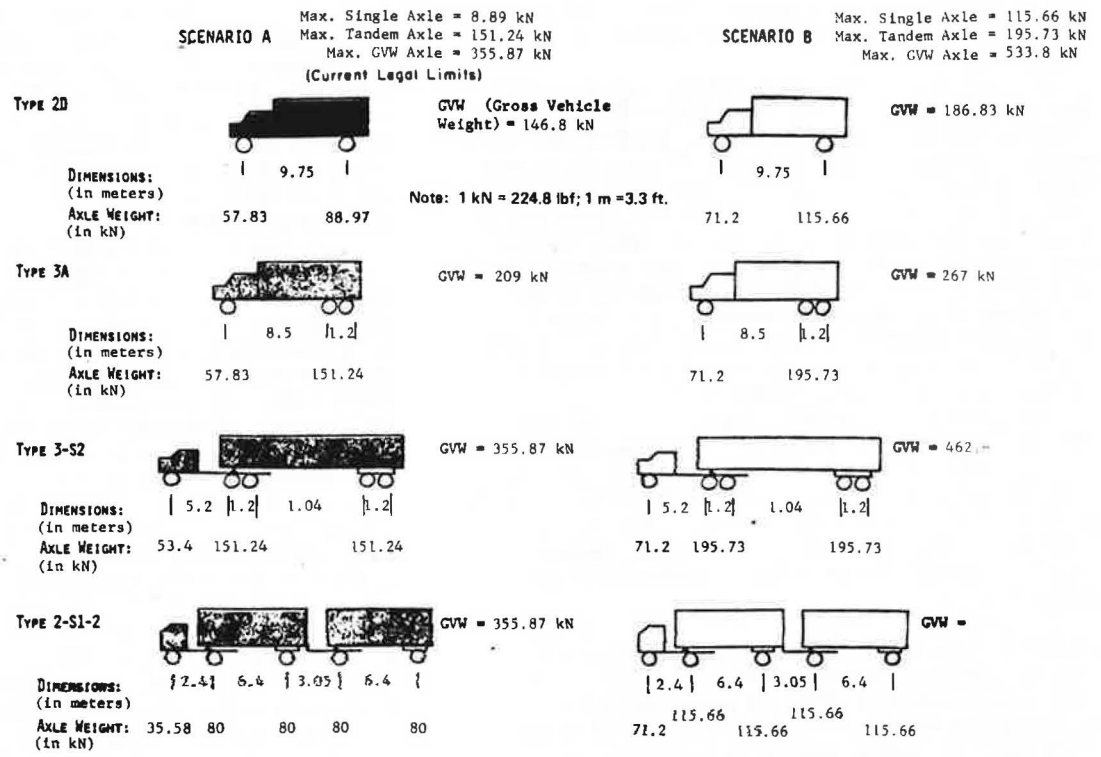

Figure 2. Truck populations and changes resulting from an increase in maximum legal GVW.

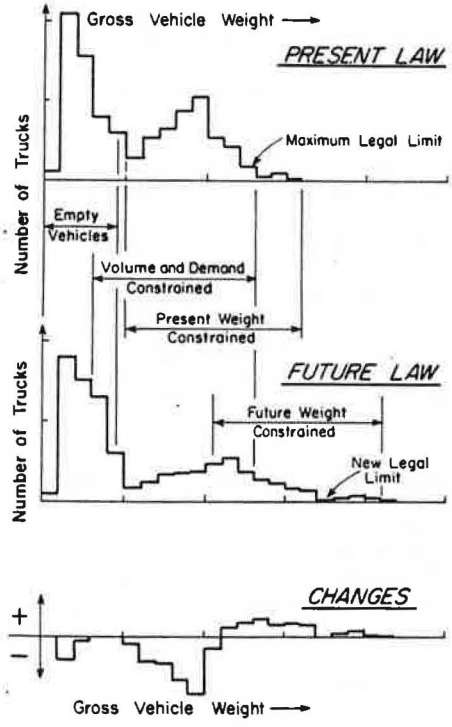

both existing weight limits and those that might be likely candidates for the near future. It was decided that two scenarios would be considered. Scenario A would include the continued application of existing law on truck weights and sizes. Scenario B would include increasing the maximum allowable truck weights to those studied by the federal government (1) but would retain current restrictions on the size of vehicles.

Four different types of trucks were selected as representative of the fleets of trucks that now operate and will be operating in the future on Texas highways. Diagrams of these vehicles, and the maximum legal gross vehicle weight (GVW) and axle loads considered for each of the two scenarios, are shown in Figure 1.

The following restrictions on vehicle dimensions were considered applicable for both scenarios and are based on existing law: (a) maximum length of 13.72 m (45 ft) for single-unit trucks and 19.81 m (65 ft) for trailer and semitrailer combinations and (b) maximum width of 244 cm (96 in).

A bridge formula that limits truck axle loads and configurations to protect bridges from excessive [illegible] was considered in both scenarios (2).

PROJECTED TON KILOMETERS OF TRUCK TRAVEL

To facilitate the forecast of truck types and their assignment to highway classes, a projection of future ton kilometers of truck travel in the state of Texas from 1977 to 1997 was required. The total projection was divided into two major categories: intercity and urban. Intercity ton kilometers were allocated to three functional highway classes: Interstate highways, farm-to-market roads, and all other state highways. The urban figures were also allocated to three functional highway classes: Interstate highways, other state freeways and arterials, and collectors.

The total projected Texas ton kilometers ranged from 65.7 billion t-km (45 billion ton miles) in 1977 to 131.4 billion t-km (90 billion ton miles) in 1997. Of the total 131.4 billion t-km projected, only 17.52 billion t-km (12 billion ton miles) was forecast for urban travel, whereas 113.88 billion t-km (78 billion ton miles) was forecast for intercity traffic. This intercity figure was then allocated as follows: 47 percent to Interstate highways, 8 percent to farm-to-market roads, and 45 per-

cent to all other state highways. The forecast ton kilometers was assumed to remain constant in both scenarios.

To illustrate the basic procedure, Figure 2 shows how the truck population is likely to be affected by a change in the maximum legal GVW. First of all, more trucks will operate above the current legal limit, and these will replace some that had been operating near and below the old limit. This means that there will be an overall reduction in the number of loaded vehicle trips and, correspondingly, a decrease in the number of empty trips. At the same time, a portion of the truck population will be unaffected by the change in maximum legal GVW. The loads on these trucks are either low-density commodities (volume constrained) or partial loads (demand constrained).

The procedure used data collected by the Texas State Department of Highways and Public Transportation (TSDHPT) over the past 20 years (3). The data represent vehicle (empty and loaded) weight intervals sampled at designated highway locations around the state. The distribution of gross weights for specific classes of trucks under existing legal limits was established from these data.

The process required the development of a technique for computing average empty-vehicle weights, average payload carried, and 80-kN [18 000-lbf (18-kip)] single-axle load (SAL) for each vehicle type and each highway system. The number of 80-kN SALs, truck operating costs, and fuel consumption for each highway class for each year over the forecast period (20 years) are calculated by using the truck-freight ton-kilometer allocation for each class, the average payload per kilometer of a system for each year, and the total number of vehicles required to carry the freight allocated to that vehicle type. The actual procedure used in the computations was obtained from a National Cooperative Highway Research Program (NCHRP) study of truck sizes and weights (4). The NCHRP model was modified and adapted for use in this study.

MODIFICATIONS OF NCHRP METHODOLOGY

Initial efforts in this study used the methodology contained in NCHRP Report 141 with only minor modifications. However, an examination of the preliminary estimates of costs and benefits led to a more extensive critique and modification.

The NCHRP researchers examined historical GVW distributions before and after changes in size and weight laws. There is a pattern in these data that shows a shift to heavier trucks and a small shift on the empty weight portion of the distribution. A shift that is approximately proportional to the ratio of the practical maximum gross weight under the new law to the practical maximum gross weight under the old law exists on the loaded weight portion of the distribution.

The results of applying this type of shift to scenario A for one hundred 3-S2 trucks on a representative 1.6 km (1 mile) of Interstate highway are shown in Figure 3. Figure 3(a) shows a large decrease in 80-kN SALs for trucks that are operating near the current legal limit. This decrease is negated by the increase caused by the new heavy trucks. Figure 3(b) is similar except that a large savings in truck operating costs is indicated for empty and lightly loaded vehicles. Such data caused us to reexamine the shifting procedure.

If weight laws (only) were changed, certain consequences might be expected. Those trucks that operate near the legal axle or GVW limit would increase their loads, and this would result in fewer loaded and empty trips. Vehicles that carry low-density cargo and are constrained by vehicle volume (size) would be unaffected. A significant number of partially loaded vehicle trips are made. Some of these are delivery trips in which vehicle weight decreases or increases along the route. Segments of these trips could be affected by the change in the weight laws, whereas the less-loaded trips, which are made because the demand is only for a partial load, would be unaffected.

It was concluded that a shifting procedure would be used that would have the following characteristics: (a) heavily loaded vehicle trips would shift to a larger GVW in proportion to the previously mentioned ratio of practical maximum gross weights, (b) lightly loaded vehicles would be unaffected by the change in the law, and (c) empty-vehicle trips would be reduced in proportion to the reduction of loaded-vehicle trips.

It is postulated that the historical changes in GVW distributions that were used as a basis for the NCHRP shift were the result of factors other than changes in weight laws. To explore this phenomenon, a sensitivity study was conducted to examine the effects of several possible shifts on the computed savings in truck operating costs and increased 80-kN SALs. In general, truck operating cost savings are more sensitive than 80-kN SAL to shifts that increase the weight of lightly loaded trucks. Furthermore, for shifts that primarily affect heavily loaded vehicles, neither output is extremely sensitive to the shifting procedure.

The results obtained by using the shifts are shown in Figures 4-7. Results for the NCHRP procedure are based on one hundred 3-S2 trucks in scenario A and 61.7 trucks with the same payload in scenario B on a representative 1.6 km (1 mile) of Interstate highway. Results for the Texas procedure are based on one hundred 3-S2 trucks in scenario A and 85.7 trucks with the same payload in scenario B.

Note that for the adopted (TSDHPT) shift the following results were obtained:

1. Fewer empty trips resulted in savings.
2. Some partially loaded or lightly loaded trucks were unaffected.
3. The number of trucks possibly constrained by axle or GVW laws was reduced.
4. The number of trucks that exceed the present law (but are constrained by the future law) was increased. This resulted in increased savings.
5. Net savings in truck operating costs were affected much more than was the net increase in 80-kN SALs by the adopted shift versus the NCHRP shift.

Figure 8 shows the NCHRP and TSDHPT shifting factors. The TSDHPT shift is considered a "most likely" outcome; it must be pointed out, however, that the basis for its selection lacks precision. For much cargo, the point of diminishing returns as far as gross- or axle-weight limitations are concerned may already have been reached.

IMPLEMENTATION OF SCENARIOS

Currently, many farm-to-market roads and bridges are load-zoned for less than the vehicle weights considered for scenario A. But it was considered more reasonable to implement scenario A as if no restrictions existed since enforcement is difficult.

It was found that a significant number of existing bridges would require restrictive load zoning until replacement if the load limits were eased as in scenario B. In this study, it was assumed that the scenario B increase in the legal limit would be effective in 1980.

Figure 3. Results of use of NCHRP shift: (a) decrease in 80-kN SAL and (b) savings in truck operating costs.

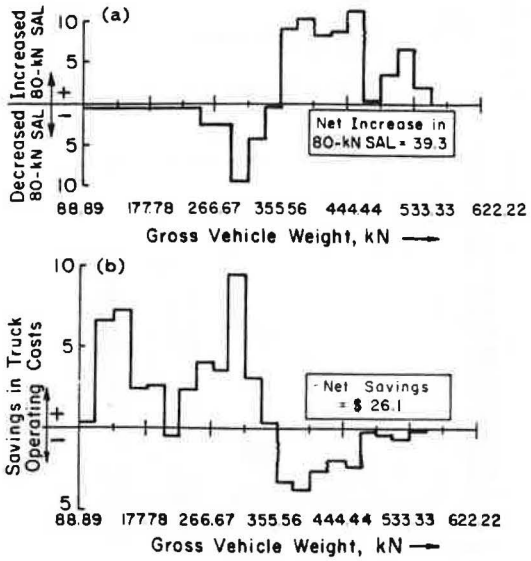

Figure 4. Change in 80-kN SAL versus GVW: NCHRP shift.

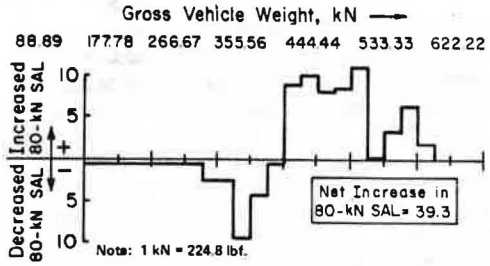

Figure 5. Change in 80-kN SAL versus GVW: TSDHPT shift.

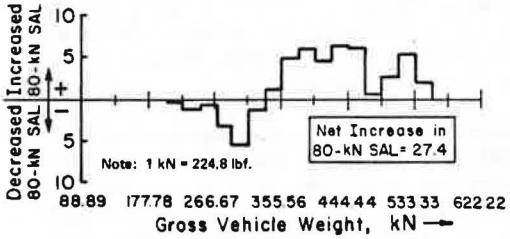

Figure 6. Change in truck operating costs versus GVW: NCHRP shift.

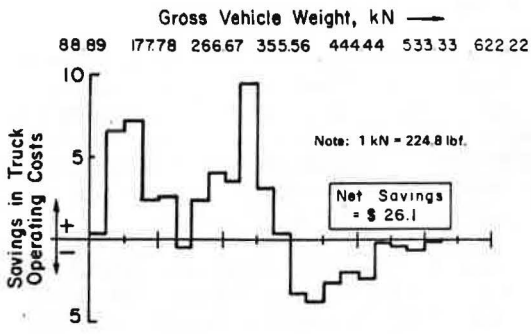

As a result of the load restriction on bridges, it was estimated that a 14-year program of bridge replacements would be necessary to fully implement scenario B.

HIGHWAY COSTS

Costs to maintain the existing network of pavements in good condition for the next 20 years were first estimated for scenario A. A second estimate was made for scenario B that considered only those items of highway maintenance and construction that would be affected by an increase in gross weight and axle loads. Included in the pavement costs were the costs of routine pavement maintenance, seal coats, and pavement rehabilitation. Also included were the estimated costs of upgrading structurally deficient bridges to carry the loadings of the two scenarios. Because pavement deterioration is caused by both truck loading and environmental stresses, the routine maintenance and seal-coat costs were assumed to remain constant in both scenarios. This assumption implies that routine maintenance and seal coats are sufficient to handle the environmental deterioration. Pavement rehabilitation costs were estimated to increase with the heavier trucks.

The resulting annual and cumulative cost estimates are shown in Figures 9 and 10. No data were available to estimate the costs of roads and streets off the state system. Table 1 gives the costs accumulated for the analysis period.

Other smaller but still significant increases in highway construction costs will be incurred. These costs have not been estimated because of either time limitations or lack of data.

BASIS FOR ESTIMATES OF PAVEMENT COST

A computer program entitled REHAB, originally developed in the McKinsey study (5), was improved and used to estimate the costs of pavement rehabilitation. Inputs to this program include the number of lane kilometers of pavement, their age, unit costs for rehabilitation, and survivor curves that portray the expected life of the pavements.

Data on lane kilometers and age (the time elapsed since construction, reconstruction, or rehabilitation) were obtained from files maintained by TSDHPT. The greatest number of recently constructed pavements has been on the Interstate system. Many non-Interstate lane kilometers have not been rehabilitated or reconstructed in the past 20 years. A proportionate mix of minor and major rehabilitations was used as input to REHAB to represent the rehabilitations that are most likely to occur.

Survivor curves that show the percentage of each pavement type that is expected to survive to a certain age were estimated by a panel of experienced pavement

Figure 7. Change in truck operating cost versus GVW: TSDHPT shift.

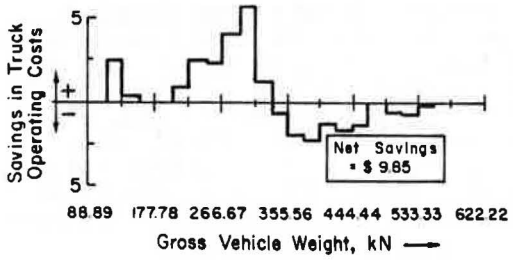

Figure 8. Multipliers adopted for shifting GVW distributions from scenario A to scenario B.

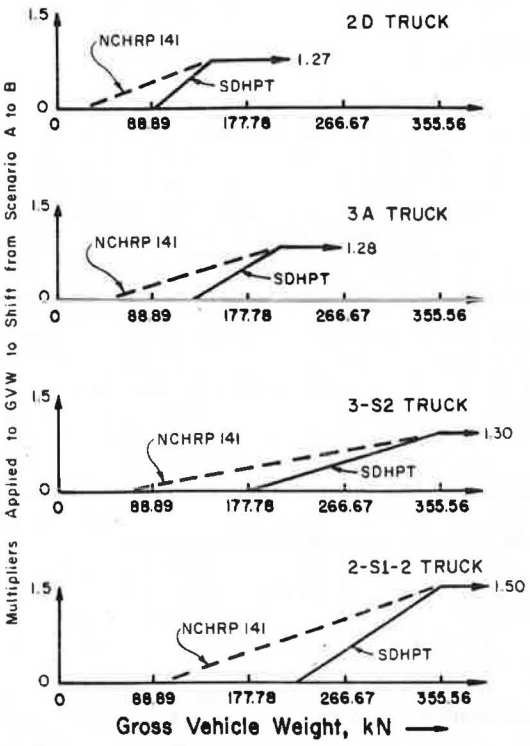

Figure 9. Cost to maintain existing pavement system, including maintenance, replacement, and rehabilitation.

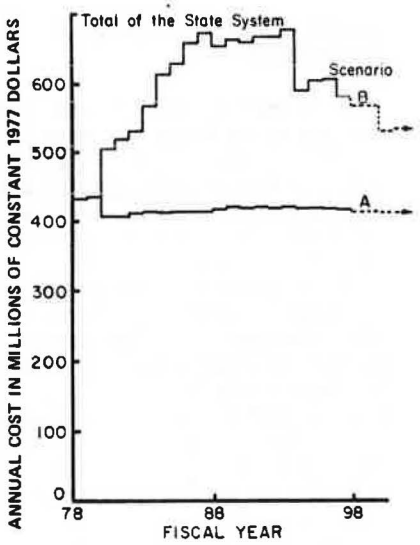

engineers for use by McKinsey and Company when the original REHAB model was developed. These curves were updated for this study by using unpublished information made available to the panel after the original estimate.

It was necessary to devise a method for adjusting pavement life when truck volume increases or heavier trucks are operated over a road segment. This adjustment procedure was based on the results of the AASHO Road Test (6). The expected pavement lives, i.e., the survivor curves, were shortened in proportion to the increase in equivalent axle loads supplied from the projected traffic discussed previously. It was also necessary to institute this additional aging of the pavements at the expected time of occurrence of the heavier trucks.

Figure 10. Cost to maintain existing pavement systems over 1977-1997 analysis period.

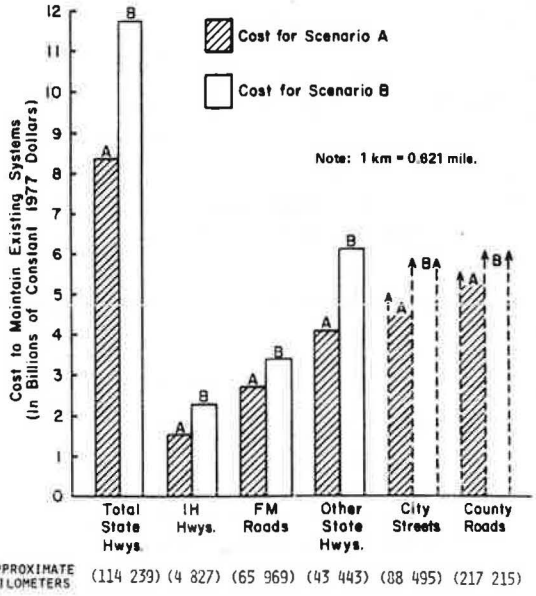

Another revision to REHAB was necessary. After the accelerated wearing out of the existing pavements, it would be desirable to redesign pavement structures to handle the heavy trucks properly. The program was revised to accomplish this for that portion of the pavements that receive major rehabilitation. The original survivor curves (those developed under more recent weight standards with longer lives) were then applied to these pavements. The increased cost to accommodate heavier trucks was estimated to be proportional to the ratio of the logarithm of the heavy traffic equivalencies to the logarithm of the original traffic equivalencies. This methodology is also based on the findings of the AASHO Road Test (7).

In summary, the necessary revisions changed the REHAB program so that when heavier trucks are applied the life curves are shortened, which causes the pavements to wear out faster. The "worn-out" pavements are then rehabilitated. Those that receive minor rehabilitation (thin overlays) continue to wear out at the accelerated rate. However, those that receive major rehabilitation are redesigned at an increased cost to handle the heavier trucks. These redesigned pavement structures now begin to wear out at a slower rate. The slower rate is the same rate as the original life curves for these pavements.

BASIS FOR ESTIMATES OF BRIDGE COST

The Federal Highway Administration (FHWA) and the American Association of State Highway and Transportation Officials (AASHTO) have developed a formula for calculating a sufficiency rating for bridges. This formula takes into consideration structural adequacy and safety features, serviceability and functional obsolescence, and essentiality for public use.

By using the above formula and current bridge-inspection data, a sufficiency rating was calculated for all bridges on the state highway system. The bridge-replacement costs for scenario A were developed by applying the same criteria used by FHWA in the National

Table 1. Comparative 20-year costs for scenarios A and B.

Scenario	Cost Category	Cost (millions of constant 1977 dollars) Interstate Highways	Farm-to-Market Roads	Other State Highways	Total State System
A	Pavement maintenance and seal coats	240	1 100	960	2 300
	Pavement rehabilitation	1 334	1 512	3 084	5 930
	Bridge replacements	4	76	50	130
Total		1 578	2 688	4 094	8 360
B	Pavement maintenance and seal coats	240	1 100	960	2 300
	Pavement rehabilitation	1 888	1 953	4 618	8 459
	Bridge replacements	172	376	554	1 102
Total		2 300	3 429	6 132	11 861

Figure 11. Savings in truck operating costs from 1977 to 1997: scenario B over scenario A.

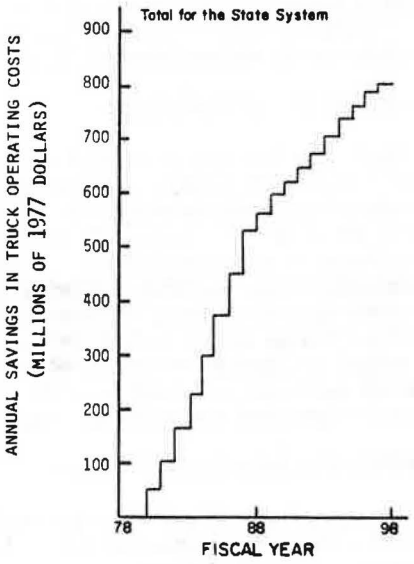

Figure 12. Truck fuel savings from 1977 to 1997: scenario B over scenario A.

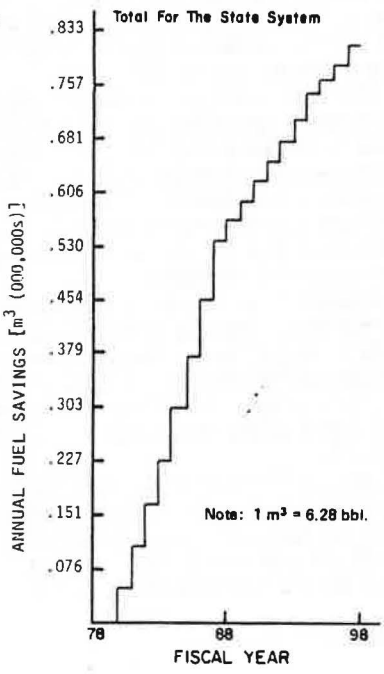

Special Bridge-Replacement Program and adding additional load-restricted bridges.

Scenario B required evaluation of the effect of increased truck loading on bridges. This was performed generally in accordance with the methodology of the NCHRP procedure.

From computer listings that represented all of the bridges on the Texas highway system, 12 bridge types were selected as representative of the entire system of bridges. The usual ratio of dead-load moment to live-load moment was established for each type by calculations and estimates. These vary slightly from those reported in the NCHRP procedure to correspond more nearly to Texas conditions. Spans of each structure type were considered for four design loadings—H10, H15, H20, and HS20—and on each of three types of highway systems—Interstate, farm-to-market, and all others. Live-load moments attributable to one design truck or lane were taken from Appendix A of the AASHTO Bridge Specification for each span. Moments caused by one truck from the proposed legal loading, scenario B, were calculated for each span by using a computer program called BMCOL 43 (8). Trucks represented by scenario B were considered, and the absolute maximum moment for the span was used. The ratio of the scenario B moment to the design-load moment represents the increase in live-load moment for each span of each structure type. To convert this to stresses, the ratio of dead to live load was used. The formula selected for calculating overstress is that used in NCHRP Report 141.

In order to evaluate the effects of the overstress, allowable values for the various types of bridges were established. Whenever the calculated overstress exceeded the allowable overstress, all bridges represented by the type-span loading were considered inadequate for scenario B loads and therefore required replacement. Where the overstress was less than that allowable, the bridges were considered adequate.

The deck area of bridges that are currently load restricted was tabulated and subtracted from the total to provide the bridge deck area that would be affected by the proposed changes for scenario B. The bridge replacement costs calculated are given in Table 1.

DECREASED TRUCK OPERATING COSTS

The primary benefit obtained by the hypothesized change in the weight limit accrues in the form of reduced operating costs in the trucking industry. The projected savings are shown in graphical form in Figure 11. The projected $9.12 billion savings that occurs within the 20-year analysis period was calculated by using a procedure similar to that used in NCHRP Report 141. The data base for operating costs was obtained by updating the cents-per-ton-mile numbers described in the NCHRP report. The components of the total operating costs per ton kilometer are (a) repair and servicing,

Table 2. Twenty-year incremental costs and savings associated with shift to heavier trucks.

Type of Road	Additional Highway Costs (billions of 1977 dollars)	Savings in Truck Operating Costs (billions of 1977 dollars)	Fuel Savings (millions of cubic meters)
Interstate	0.72	4.57	4.58
Farm-to-market	0.74	0.71	0.68
Other state highways	2.04	3.84	3.90
Total for highway systems	3.50	9.12	9.16

Note: 1 m^3 = 6.28 bbl.

(b) tires and tubes, (c) fuel, (d) driver wages and subsistence, (e) overhead and indirect costs, and (f) depreciation and interest.

After several different cost indices were considered, the general consumer price index (CPI) was finally selected as the mechanism for updating 1970 truck operating costs to current 1977 levels. A recent study conducted by the Hertz Corporation suggests that increases in truck operating costs since 1975 were larger than those reflected in the CPI. The Hertz data, however, were not incorporated in this analysis primarily because of time constraints. The savings shown in Figure 11 are probably on the low side because of the relatively more rapid increase in fuel costs, which is not reflected in the estimates.

The projected ton-kilometer data were allocated to the three highway systems and to the selected vehicle types within each system. The hypothesized change in truck weight limits allowed the heavier vehicles to haul more ton kilometers, which resulted in fewer trips and therefore lower aggregated costs for truck operations in scenario B.

Cost savings by types of systems were calculated on a disaggregated basis. The major finding is that 50 percent of the calculated savings occur on the Interstate system, 43 percent on all other highways, and only 8 percent on the farm-to-market network.

FUEL SAVINGS

A separate analysis was conducted to examine what, if any, fuel savings might result from an increase in truck weights. The following model was selected from a review of the literature (9-13) to relate liters of fuel per kilometer and GVW:

$$L/km = 0.327 + 0.003\,41\ GVW \quad (1)$$

Intercity ton-kilometer fuel consumption rates were calculated by using the above equation. Projected fuel savings are shown in Figure 12. The fuel saved would be about 1.8 percent of the amount needed without the increase in truck weights. The total 20-year savings—9.16 million m^3 (2.42 billion gal)—represents an amount approximately equal to 28 percent of all the motor fuel used in Texas in 1975.

EFFECTS OF AIR AND NOISE POLLUTION

Some analyses were completed in an attempt to relate pollution from vehicles and changes in vehicle weights. The results are derived from previously developed models (14-16). In the three major Texas metropolitan areas (Dallas-Fort Worth, Houston-Galveston, and San Antonio), a 3-6 percent reduction in air pollution caused by heavy trucks was calculated. This calculated decrease represents a less than 1 percent reduction in transportation-generated pollution.

The available data and research on noise pollution indicated that the hypothesized increase in axle-weight limits should generate only small increases in noise along highways. Estimates of these reductions were not calculated because of the incompleteness of techniques in the state of the art (17-24).

OTHER CONSIDERATIONS

Many significant considerations that are involved in size and weight changes in truck use were not considered explicitly in this study. These include, but are not limited to, geometric redesign of streets and highways to accommodate larger trucks, highway safety considerations, costs of replacing bridges and pavements other than those on major highways, implications of new design trucks and performance, changes in technology, and externalities associated with heavier truck loads and the freight shares of rail pipelines and waterways attributable to the modal shifts.

FINDINGS AND CONCLUSIONS

The major approach used in this study involved estimating the comparative maintenance and rehabilitation costs of perpetuating the state highway system under current limitations on vehicle weights and on future use under different weight conditions. These costs were based on alternative weight limitations on trucks and did not consider alternative vehicle sizes.

The incremental costs for scenarios A and B associated with heavier truck loads and the corresponding savings in truck operating costs for the 20-year analysis period were computed for the three highway classes. Also included was an estimate of fuel savings. These are given in Table 2.

It was determined in the study that, if changes in legal weight limitations were undertaken, further analysis would be justified to select those routes that would carry relatively large freight tonnages and would cost relatively less to upgrade.

It can also be inferred that, once the highways have been upgraded to handle heavier trucks, the additional cost to maintain the system for the heavier trucks will decrease. In other words, annual additional costs beyond 1997 would be less than the annual costs that would occur during upgrading.

ACKNOWLEDGMENT

The research from which this paper was developed was sponsored by the Texas State Department of Highways and Public Transportation. We, the authors, and not the sponsoring agency, are responsible for the material presented here.

REFERENCES

1. R. Winfrey and others. Economics of the Maxi-

mum Limits of Motor Vehicle Dimensions and Weights. Federal Highway Administration, U.S. Department of Transportation, Vols. 1 and 2, 1968.
2. Texas Regulations Governing the Size and Weight of Commercial Vehicles. Texas Department of Public Safety, Austin, 1975.
3. Truck Weight and Vehicle Classification Study. Planning Survey Division, Texas Highway Department, Austin, 1960-1971; Federal Highway Administration, U.S. Department of Transportation, 1973-1975.
4. Robert E. Whiteside and others. Changes in Vehicle Weights and Dimensions. NCHRP, Rept. 141, 1973.
5. Guide to the Highway Rehabilitation Forecasting Model. McKinsey and Co., San Francisco, 1966.
6. The AASHO Road Test: Report 1—History and Description of Project. HRB, Special Rept. 61A, 1962.
7. The AASHO Road Test: Report 5—Pavement Research. HRB, Special Rept. 61E, 1962.
8. H. Matlock and T. Taylor. A Computer Program to Analyze Beam-Columns Under Movable Loads. Center for Highway Research, Univ. of Texas at Austin, Rept. 56-4, 1968.
9. W. L. Hall. Financing Modern Highways for Montana. Montana Fact-Finding Committee on Highways, Streets, and Bridges, Helena, 1956.
10. M. F. Kent. Fuel and Time Consumption Rates for Trucks in Freight Service. HRB, Bull. 276, 1960.
11. Line-Haul Trucking Cost in Relation to Vehicle Gross Weights. HRB, Bull. 301, 1961.
12. Supplementary Report of the Highway Cost Allocation Study. 89th Congress, 1st Session, House Doc. 124, Washington, DC, 1961.
13. E. K. Bender and M. C. Kaye; Bolt, Beranek, and Newman, Inc. Truck Noise III-g: Field Test of Freightliner Guided Truck. U.S. Department of Transportation, Sept. 1975.
14. M. W. Ingalls and K. J. Springer; Southwest Research Institute. Mass Emissions from Ten Pre-Controlled Gasoline Trucks and Comparisons Between Different Trucks on a Road Course. U.S. Environmental Protection Agency, April 1975.
15. M. W. Ingalls and K. J. Springer; Southwest Research Institute. Mass Emissions from Diesel Trucks Operated Over a Road Course. U.S. Environmental Protection Agency, Aug. 1974.
16. 1972 National Emissions Report. U.S. Environmental Protection Agency, June 1974.
17. A Review of Road Traffic Noise. British Road Research Laboratory, Crowthorne, Berkshire, England, Rept. LR 357, 1970.
18. R. L. Staadt. Truck Noise Control. In Reduction of Machinery Noise, Rev. Ed. (J. C. Malcomb, ed.), 1975.
19. W. H. Close and J. E. Wesler. Vehicle Noise Sources and Noise-Suppression Potential. In Motor Vehicle Noise Control, TRB, Special Rept. 152, 1975, pp. 14-33.
20. T. Priede. Noise and Vibration Problems in Commercial Vehicles. Journal of Sound and Vibration, Vol. 5, No. 1, 1967, pp. 129-154.
21. Transportation Noise and Its Control. U.S. Department of Transportation, June 1972.
22. Alan M. Voorhees and Associates, Inc. An Analysis of the Economics of Truck Sizes and Weights in Relation to State and Federal Regulations. Motor Vehicle Manufacturers Assn., Detroit, Sept. 1973.
23. K. R. Agent and R. L. Rizenbergs. Vehicle Noise Survey in Kentucky. HRB, Highway Research Record 580, 1976, pp. 70-75.
24. Noise: New Federal/EPA Regulation Governing Interstate Motor Carriers. U.S. Environmental Protection Agency, April 1975.

Publication of this paper sponsored by Committee on Flexible Pavement Design.

Fatigue Damage to Flexible Pavements Under Heavy Loads

James H. Havens, Herbert F. Southgate, and Robert C. Deen,
Bureau of Highways, Kentucky Department of Transportation,
Lexington

A modified Chevron N-Layer computer program has the capability of calculating the "work" done on pavements by the total load of various types of trucks. Seven truck groups are examined: two-tire and four-tire single axles, tandems, triaxles, and four-, five-, and six-axle groups. The two-tire (front steering) axle has the most severe damage relationship. Damage factors based on the AASHO Road Test and factors based on the concept of strain energy density are compared in the analyses. Various vehicle configurations and ranges of loads are discussed and evaluated in terms of damage per trip.

In the past, pavement design engineers have generally sought merely to sustain current statutory limits on axle loads—that is, to avoid destructive or catastrophic damage to pavements and premature depletion or ruination of physical assets (premature in this context implies that the damage occurs before the responsible agency is fiscally capable of restoring and maintaining the system under the changed circumstances). If it were feasible and practical to manufacture highway truck-trains that had perfect cornering and guidance capabilities in their trailing axles, bulk raw materials such as ores, coal, logs, and freight could be transported on highways more efficiently than they can by some of the simpler types of trucks, which are currently being overloaded by some owners and operators. These ideas issue from the "centipede concept", which fostered railroads and freight trains. These factors should be, and perhaps are being, considered by automotive designers and

truck manufacturers. Inputs may take the form of comparative analyses of damage factors and optimization of tire and axle sizes and configurations.

Flexible pavement designs for heavy loads are primarily a function of traffic volume, material characteristics, and the relative damage caused by various load configurations. Material characteristics and traffic volume are assumed to have been determined, and variations in thicknesses would be a function of relative damage factors. The effects revealed are specific for flexible pavements, and further analyses of effects on bridges need to be performed. The analyses are predicated on the concept of the "strain energy density" exerted by the pavement to resist the loadings. Strain energy is the work done internally by the body and is equal to and opposite in direction to the work done on the body by the external force. Strain energy is the integral of strain energy density.

STRAIN ENERGY DENSITY

Sokolnikoff's Equation 26.8 (1) defined strain energy as

$$U = \int_{\tau} W d\tau \tag{1}$$

where

- U = strain energy of the body,
- τ = a stress component, and
- W = volume density of strain energy at a specific point in the pavement structure, strain energy density, or elastic potential.

This relation can be expanded to yield Sokolnikoff's Equation 26.16, as follows:

$$W = (1/2)\lambda\vartheta e_{ii} + G e_{ij} e_{ij}$$
$$= (1/2)\lambda\vartheta^2 + G(e_{11}^2 + e_{22}^2 + e_{33}^2 + 2e_{12}^2 + 2e_{23}^2 + 2e_{13}^2) \tag{2}$$

where

- e_{11} = strain component in the ii direction,
- ϑ = $e_{11} + e_{22} + e_{33}$,
- λ = $E\mu/(1 + \mu)(1 - 2\mu)$,
- E = Young's modulus of elasticity for the material in which W is to be calculated,
- G = $E/2(1 + \mu)$ and is called the modulus of rigidity or the shear modulus, and
- μ = Poisson's ratio.

Young's modulus E and Poisson's ratio μ are input values to the Chevron N-Layer computer program (2); the strain components (e_{11}, etc.) are outputs of the program.

Noting that Young's modulus E and the fraction (1/2) are present in each term of Equation 2, Equations 3 and 4 can be obtained as follows:

$$\epsilon_w^2 = 2W/E \tag{3}$$

$$\epsilon_w^2 = (2W/E)^{1/2} \tag{4}$$

where ϵ_w = "work strain" and has the same order of magnitude as the strain components e_{11}. Since the strain components and the sum of the principal strains are squared, taking the square root, as in Equation 4, eliminates any direction and identification as tension or compression. Thus, ϵ_w can be used only as an indicator of the total effect of all strain components.

Stress components can be used to calculate W by using Sokolnikoff's Equation 26.17 (1):

$$W = \mu\psi^2/2E + (1 + \mu)(\tau_{11}^2 + \tau_{22}^2 + \tau_{33}^2)/2E + (1 + \mu)$$
$$(2\tau_{12}^2 + 2\tau_{23}^2 + 2\tau_{31}^2)/2E \tag{5}$$

where $\psi = \tau_{11}^2 + \tau_{22}^2 + \tau_{33}^2$ and τ_{11} = stress component in the ii direction. Noting that $W = (1/2)\,\epsilon_w^2 E$ and $W = \tau_w^2/2E$, then

$$\epsilon_w^2 E/2 = \tau_w^2/2E \tag{6}$$

where τ_w = "work stress". Multiplying both sides by 2E gives

$$\epsilon_w^2 E^2 = \tau_w^2 \tag{7}$$

Work stress is given by

$$\tau_w = \epsilon_w E \tag{8}$$

Squaring the stresses and taking the square root of a summation eliminate, as before, any direction and identification as tension or compression.

Research that has not yet been published indicates that there is a direct correlation between the tensile strain component at the bottom of the asphaltic concrete layer and work strain. Thus, fatigue calculations based on the tensile strain component can be directly converted to a relation between work strain and fatigue.

INPUT PARAMETERS AND COMPUTATIONAL PROCESSES

The Chevron N-Layer (2) program was modified to perform calculations of strain energy density for specified depths and radial distances from the center of the load. Computations were requested for the bottom fiber of the asphaltic concrete and the top fiber of of the subgrade.

Superposition principles (1) apply when deflections, stresses, and strains are sufficiently small that they do not substantially affect the action of external forces. The nine basic superposition equations are summarized in Figure 1. The input format to the Chevron N-Layer program was modified for this analysis so that the loads and desired locations for computations are read in terms of an X-Y coordinate system and all stresses and strains are resolved and are compatible with the coordinate system.

Layer thicknesses of the asphaltic concrete pavement sections used in this analysis were those used at the AASHO Road Test (3), and the matrix resulted in 100 combinations. Only 67 of the possible combinations were constructed at the Road Test. The modulus of the asphaltic concrete was assumed to be 4140 MPa (600 000 lbf/in^2), determined from a typical temperature distribution for the AASHO Road Test site, and the Poisson's ratio was 0.4. The subgrade modulus was 41.1 MPa (6000 lbf/in^2), and the Poisson's ratio was 0.45.

Previous work (4) had shown that changes in tire pressures have an effect so minor as to be negligible in comparison with the effects of other variables. For this analysis, a tire pressure of 551 kPa (80 lbf/in^2) was used. The numbers of tires and axles on a vehicle were varied to simulate a front steering axle with 2 tires, a 4-tire single-axle tractor and/or trailer, an 8-tire tractor and/or trailer tandem-axle group, and a 12-tire trailer triaxle group. Analyses were also made to simulate a 16-tire, four-axle group; a 20-tire, five-axle group; and a 24-tire, six-axle group. Dimensions between tires and axles were the average of test vehicles used on loops 3-6 of the AASHO Road Test (5).

Tire loads were the same for every tire in a given

Figure 1. Basic equations by superposition principles.

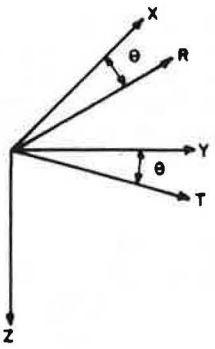

$$\sigma_x = \sigma_R \cos^2\theta + 2\tau_{RT} \cos\theta \sin\theta + \sigma_T \sin^2\theta$$

$$\tau_{xy} = \sigma_R \cos\theta \sin\theta + \sigma_{RT}(\cos^2\theta - \sin^2\theta) - \sigma_T \sin\theta \cos\theta$$

$$\tau_{xz} = \tau_{RZ} \cos\theta - \tau_{TZ} \sin\theta$$

$$\sigma_y = \sigma_R \sin^2\theta + 2\tau_{RT} \sin\theta \cos\theta + \sigma_T \cos^2\theta$$

$$\tau_{yz} = \tau_{RZ} \sin\theta + \tau_{TZ} \cos\theta$$

$$\sigma_z = \sigma_z$$

$$\tau_{yx} = \tau_{xy}$$
$$\tau_{zx} = \tau_{xz}$$
$$\tau_{zy} = \tau_{yz}$$

group. The load ranged from 8.9 to 35.6 kN (2000-8000 lbf) on 2.2-kN (500-lbf) increments.

COMPARATIVE RESULTS

Deacon (6) also used superposition principles, but he assumed one circular loaded area to represent a dual tire arrangement. His fatigue criteria were based on the maximum principal tensile strain at the bottom of the asphaltic concrete layer.

Previous analyses (4) have indicated that the location of the most severe strain is under the center of a single tire or the center of the inside tire of a dual arrangement and at the top of the subgrade. Calculations of strain energy density indicate that the most severe strain is located at the bottom of the asphaltic concrete layer beneath the outer edge of the inside tire. Thus, the location shifted from the center of the inner tire to the outside edge. This significant change was the result of two conditions: (a) Previously, only one component of strain at each depth had been used as the criterion, and (b) the shear component is zero under the center of the load but becomes significant at the outer edge of the loaded area. In the case of two tires per axle, the critical point is the inside edge of the tire print. Thus, when all components of stress or strain are included, the location of the highest magnitude of total strains has shifted both vertically and horizontally within the pavement structure from the location that was previously thought to be the most severe.

The average work strain of the 100 structures and the load matrix described above for the four-tire, single-axle group was computed, and the value of work strain for the 80-kN (18 000-lbf) axle load for each respective pavement section was used as the basic value for all other groups for the same pavement section. Thus, Figure 2 shows the ratio of work strain at any given load to work strain for the 80-kN axle load. Therefore, the same amount of damage is caused by the total load on the group described in the table below (1 kN = 225 lbf):

Axle Group		Load (kN)	
Number of Axles	Number of Tires	Total	Per Axle
1	2	63.6	63.6
1	4	80.0	80.0
2	8	166.4	83.2
3	12	250.0	83.3
4	16	333.6	83.4
5	20	415.0	83.0
6	24	496.4	82.7

Since the damage factors for the steering axle on 5-cm (2-in) asphaltic concrete sections were five to eight times those on thicker sections, the values given in the table above and in Tables 1 and 2 are averages for the thicker pavements only.

Table 1 compares damage factors by the American Association of State Highway and Transportation Officials (AASHTO) and those developed based on "equal work" for the test vehicles used at the AASHO Road Test. Because the curves in Figure 2 represent the mean of the pavement thicknesses and vehicle dimensions, they are not necessarily those related to optimum conditions. Lanes 1 and 2 were the inner and outer lanes, respectively, and the test vehicles were classified as 2-S1 and 3-S2, respectively (2-S1 is a two-axle tractor and one-axle semitrailer; 3-S2 is a three-axle tractor and two-axle semitrailer). A total of 556 880 vehicle trips (1 113 760 applications) were made in each traffic lane. Thus, the loaded axles were the axles on the rear of the tractor and on the trailer. All analyses of relative damage have been based on the magnitude of the loaded axles. Therefore, the fatigue damage caused by steering axles was included as a part of the damage of the loaded axles. The advent of wide tires and heavily loaded steering axles has further emphasized the need for damage-factor relations for two-tire axles. Transit-mix and coal- and stone-haul single-unit trucks typically have steering axle loads of 70-80 kN (16 000-18 000 lbf). Figure 2 shows that these loads are approximately 10 times more damaging than the steering axle loads used on the AASHO Road Test.

Figures 3 and 4 show the relation between AASHO Road Test damage factors and damage factors based on analyses of strain energy density. The circled points are the sum of the damage factors for all axle groups for the particular test vehicle by the strain energy density method versus the sum of the AASHTO damage factors for the two loaded axles. Inserts to Figures 3 and 4 show that the steering axle loads were not truly proportional to the loaded axles. For example, the steering axle loads for vehicles of loops 4 and 5 were the same for the respective vehicle classifications, yet the loaded axles were greater on loop 5 than on loop 4. For purposes of illustration, a line drawn through the loop 3 and loop 6 points provides one way of proportioning the steering axle load to the loaded axles.

Analyses by the strain energy density method indicate that damage factors for the steering axle on 2-S1 vehicles used on lane 1 of loops 3-6 were approximately 4 percent of the damage factor for a single, four-tire, loaded axle of those vehicles. However, damage factors for the steering axles of the 3-S2 vehicles used on lane 2 of loops 3-6 were approximately equal to 10-100 percent of the damage factors of a tandem axle load of those vehicles. Thus, the steering axles of the 3-S2 vehicles caused a far greater proportion of the damage per trip than the steering axles of the 2-S1 vehicles.

For 2-S1 vehicles, the relative accumulated damage per trip was 2.1 times the damage done by the four-tire, single-axle load. For 3-S2 vehicles, the relative ac-

cumulated damage per trip was 2.1-3.0 times the damage done by the tandem axle load. If the steering axle loads for 3-S2 vehicles had been reduced so as to cause a damage of only 10 percent of the tandem axle load damage, an increase in the magnitude of the tandem axle load would have been required to cause the same damage as that caused by the four-tire, single-axle loads of the 2-S1 vehicles. Because AASHTO (7) equated a 146.8-kN (33 000-lbf) tandem axle load to an 80-kN (18 000-lbf) four-tire, single-axle load, the above logic indicates that the tandem axle load would be greater than 146.8 kN. Thus, by strain energy density methods, a

Figure 2. Damage factors versus total load for various axle groupings.

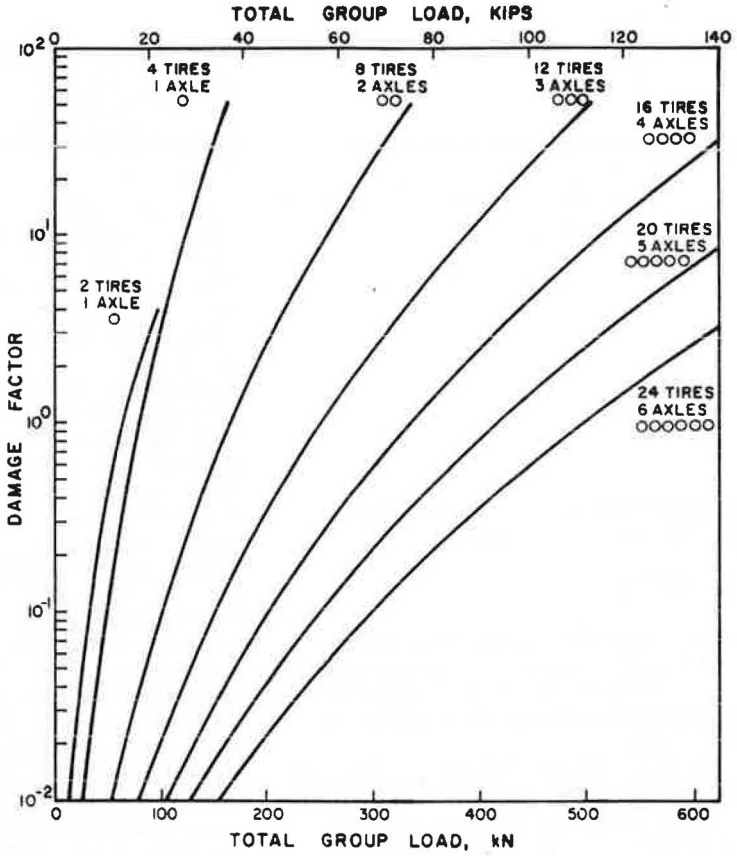

Table 1. Damage factors for AASHO Road Test vehicles based on concept of "equal work".

		Front Axle		Tractor Axle		Trailer Axle		Total Vehicle		Total AASHTO
Loop	Lane	Load (kN)	Damage Factor	Load (kN)	Damage Factor	Load (kN)	Damage Factor	Load (kN)	Damage Factor	Damage Factor
2	1	8.9	0.005	8.9	0.003			17.8	0.010	0.0004
3	1	18.7	0.025	54.3	0.016	54.3	0.016	126.8	0.345	0.440
4	1	24.9	0.045	80.5	1.01	81.4	1.05	186.8	2.105	2.09
5	1	24.9	0.045	101.4	3.45	100.5	3.30	226.9	6.795	4.75
6	1	39.6	0.205	134.8	17.50	133.0	16.0	306.9	33.705	13.90
2	2	8.9	0.005	26.7	0.055			35.6	0.060	0.010
3	2	24.5	0.043	108.1	0.132	109.9	0.144	242.4	0.319	0.63
4	2	39.1	0.20	143.2	0.480	144.6	0.500	326.9	1.18	1.85
5	2	39.1	0.20	177.5	1.39	179.3	1.47	395.9	3.06	4.11
6	2	48.5	0.40	217.1	4.12	214.8	3.90	480.4	8.42	8.35

Note: 1 kN = 225 lbf.

Table 2. Damage factors and payloads for various vehicle configurations.

	Total Vehicle Load (kN)			Front Axle (2 tires)		Single Axle (4 tires)			Tandem Axle (8 tires)			Triaxle (12 tires)			Total Vehicle		
Configuration Number	Gross Weight	Tare Weight	Payload	Axle Load (kN)	Unit Damage Factor	Axle Load (kN)	Number of Units	Unit Damage Factor	Axle Load (kN)	Number of Units	Unit Damage Factor	Axle Load (kN)	Number of Units	Unit Damage Factor	Total Vehicle Damage Factor	Total Number of Axles	Payload per Unit of Damage kN
1	326.0	115.7	210.3	41.3	0.24				142.3	2	0.465				1.17	5	179.7
2	355.9	133.4	222.5	41.3	0.24				157.3	2	0.750				1.74	5	127.9
3	355.9	133.4	222.5	53.4	0.56				151.2	2	0.620				1.80	5	123.6
4	355.9	133.4	222.5	40.0	0.24				157.9	2	0.770				1.755	5	125.0
5	533.8	186.8	347.0	53.4	0.56				240.2	2	7.10				14.76	5	23.5
6	533.8	186.8	347.0	40.0	0.24				246.9	2	8.40				17.015	5	20.4
7	533.8	186.8	347.0	53.4	0.56							240.2	2	0.810	2.18	7	159.2
8	533.8	186.8	347.0	40.0	0.24							246.9	2	0.940	2.095	7	165.6
9	533.8	186.8	347.0	40.0	0.24				123.4	4	0.240				1.175	9	295.3
10	533.8	169.0	364.8	40.0	0.24	89.0	2	1.70	202.4	2	2.80				5.815	7	62.7
11	533.8	169.0	364.8	40.0	0.24	80.1	2	1.00	166.8	2	1.00				4.215	7	86.5
12	355.9	133.4	222.5	71.2	1.42				284.7	1	19.3				20.72	3	10.7

Note: 1 kN = 225 lf.

166.4-kN (37 400-lbf) tandem axle load is equivalent to an 80-kN four-tire, single-axle load. Figure 2 shows that damage factors appropriate to a four-tire single axle should not be used for two-tire single axles.

Figure 2 also shows that the relation between load and damage factor for a two-tire axle group is roughly parallel to the relation for the single-axle, four-tire group, particularly in the range of normal loads. If one uses the concept of "influence lines" from structures, the single tires on either end of an axle are far enough apart that one tire has little influence on the other and a severe "punching" action results. However,

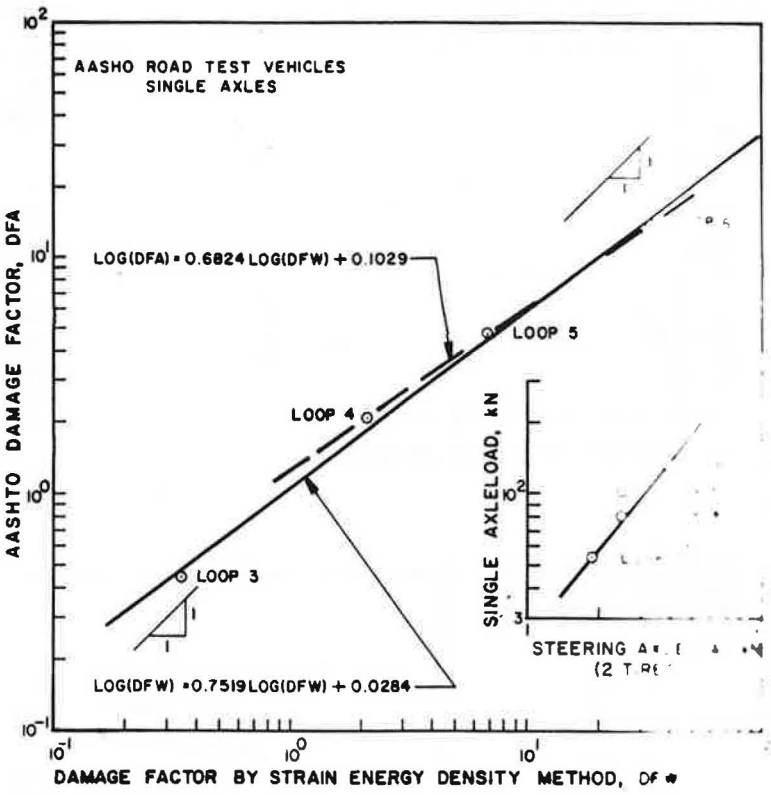

Figure 3. Comparison of damage factors by AASHTO method and strain energy density method for single-axle vehicles used at the AASHO Road Test.

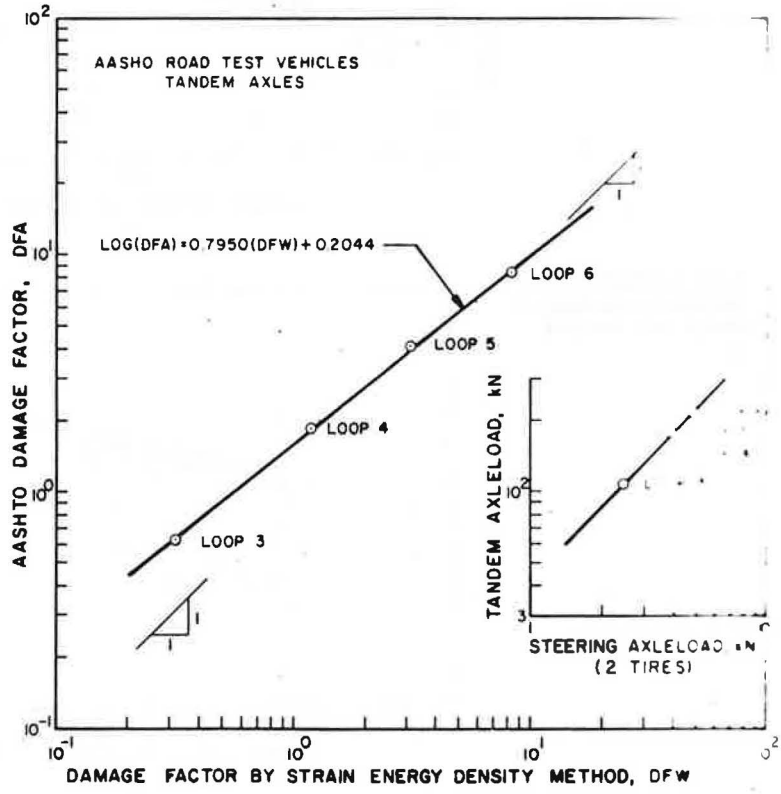

Figure 4. Comparison of damage factors by AASHTO method and strain energy density method for tandem-axle vehicles used at the AASHO Road Test.

when another tire is placed quite close to the single tire (to constitute a dual tire), the sharp bending caused by one tire is considerably reduced, or flattened, by the adjacent tire, and the deflection bowl is extended horizontally. For most highway vehicles, the deflections caused by a set of dual tires will be influenced by the dual tires on the opposite end of the axle. Similarly, the addition of another axle has a modifying influence on the deflection bowl of the single axle. In a three-axle group, maximum deflection will occur beneath the inner tire on the center axle. However, fourth and/or succeeding axles are located far enough from the "center" axle of the triaxle group as to have almost no effect on the magnitude of the deflection, but such additional axles do affect the horizontal dimension of the deflection bowl. Thus, the total load on a given group divided by the number of axles (see Figure 5) indicates that, for four or more axles, the total load can be increased by approximately 83.5 kN (18 800 lbf) for each additional axle.

Figure 5. Load per axle versus number of axles in group.

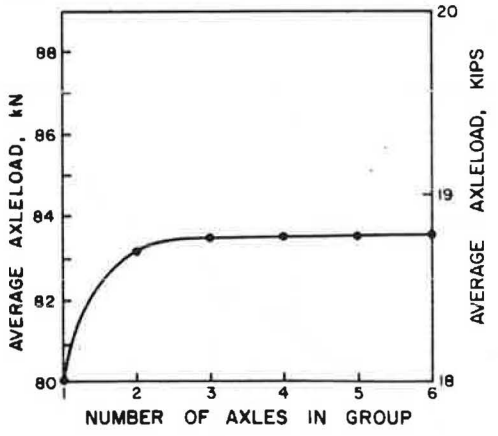

Table 2 gives the effects of (a) different magnitudes of loads, (b) different configurations, and (c) differences in the total damage factor attributable to load distribution for the same total load and configuration. Winfrey and others (8) give a gross vehicle weight (GVW) of 535 kN (120 000 lbf) as proposed in research by the Federal Highway Administration for the 1985 proposed weight limits. Careful study of Table 2 illustrates that specifying total load only does not account for accumulated fatigue. Proposals of GVW limits without some restrictions on configuration could prove disastrous in terms of fatigue.

Table 2 gives another interesting comparison. Empty weights were obtained from manufacturers'

Figure 6. Total load versus damage factor for various vehicle configurations.

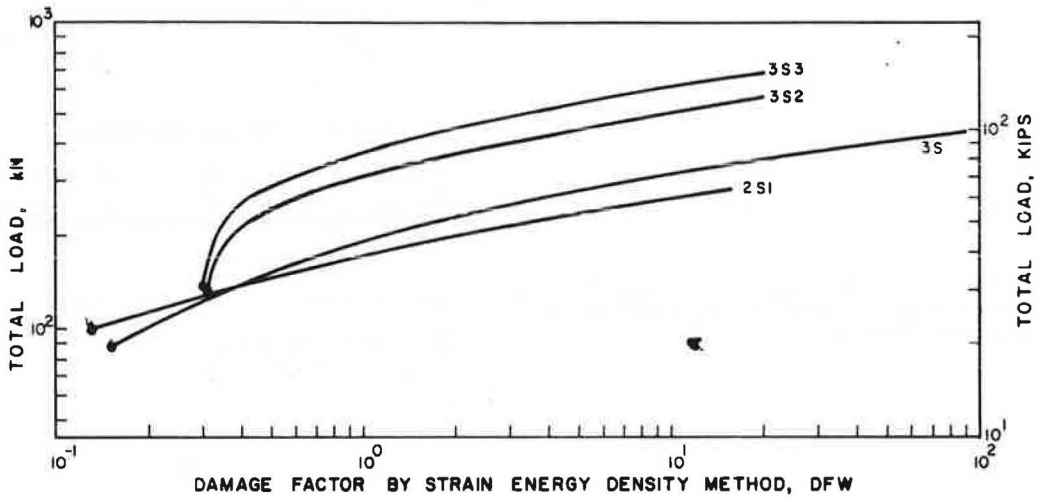

Figure 7. Effects of front axle load damage factor on damage factor for total load.

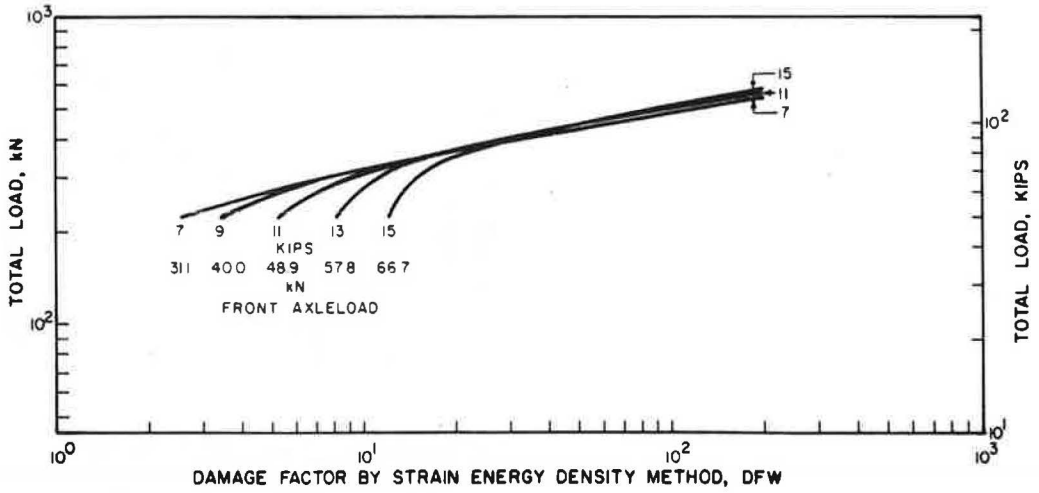

Figure 8. Front axle load versus position of kingpin assembly relative to center of tractor tandem.

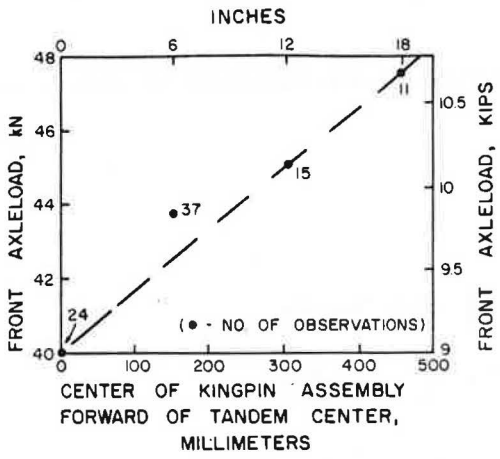

published data, and corresponding payloads were selected to be within a realistic range. Thus, the payload per unit of total damage certainly shows some optimum load distributions as well as configurations to minimize damage. The empty weights and axle loads given in Table 2, which are representative of vehicles currently in use in Kentucky and the eastern part of the United States, differ considerably from those used in analyses by Layton and others (9).

Figure 6 shows the relation between total load and damage factor for several configurations. The circled points at the lower end of each curve represent empty weight for that vehicle. Two curves are shown in Figure 6 for the single-unit, three-axle truck to illustrate the variability among manufacturers in the intended use of the vehicle. The two curves are so close together, however, that one curve can be used for both vehicles.

Figure 7 shows the effects of front axle loads on total load and total damage factor for a five-axle semitrailer (3-S2) vehicle. The obvious conclusion is that the front axle load should be minimized and the remainder of the load should be evenly divided over the other two sets of tandems. The front axle load should range between 31.1 and 62.3 kN (7000 and 14 000 lbf) to provide adequate and safe steering. Figure 2 indicates that the remainder of the load is far less damaging when it is distributed over tandem or triaxle groups.

In August 1978, 129 vehicles of the 3-S2 classification were inspected and weighed at a scale on I-64 in Kentucky. The axles were weighed individually, and the location of the kingpin assembly relative to the center of the tandem on the tractor was measured. More than 80 percent of the kingpins were located ahead of the center of the tandem by as much as 46 cm (18 in). Figure 8 shows that the front axle load generally increased as the kingpin assembly was located farther from the center of the tandem. The increase from 40.0 to 47.6 kN (9000-10 700 lbf) on the front axle causes the damage factor to increase from 0.2 to 0.4. However, a 7.6-kN (1700-lbf) increase of the tandem axle load to 151.2 kN (34 000 lbf) causes an increase in the damage factor of only 0.18. Analysis indicates that simply moving the kingpin assembly back to the center of the tandem on the tractor will not increase pavement life significantly. However, the addition of a third axle to form a triaxle trailer group will substantially increase pavement life if the load is uniformly distributed among the three axles.

SUMMARY

Based on the concept of "equal work", damage factors have been developed and presented for seven axle groups—2-tire and 4-tire single axles, 8-tire tandem axles, 12-tire triaxles, 16 tires on four axles, 20 tires on five axles, and 24 tires on six axles. The damage factors and equivalent loads for all groupings are based on the amount of work caused by an 80-kN four-tire, single-axle load (see Figure 2 and text table given earlier, respectively). These damage-factor relations were used to compute the total damage for the test vehicles used at the AASHO Road Test and to compare it with values computed from the 1972 AASHTO Interim Guide (7) (Table 2).

Not only are magnitudes of loads important, but so is the way the load is distributed on a given type of vehicle. Additional load is placed on the front axle when the kingpin assembly is shifted forward of the center of the tandem of the tractor (see Figure 8). Weight shifted to the front axle can be two times more damaging than if it were placed on the tandem axles. Approximately 80 percent of the three-axle tractors have the kingpin assemblies located forward of the center of the tandem. Pavement life could be extended considerably if a triaxle group were used on the trailer instead of a tandem group.

If the proposed GVW is raised to 535 kN (120 000 lbf), the configuration of the vehicle should be specified to minimize the fatigue damage.

ACKNOWLEDGMENT

The concepts, data, and analyses reported in this paper are partly a result of a research study conducted as part of a work program funded by the Federal Highway Administration and the Kentucky Department of Transportation. The contents of the report reflect our views, and we are responsible for the facts and accuracy of the data presented. The contents do not necessarily reflect the official views or policies of the Kentucky Department of Transportation or the Federal Highway Administration. This report does not constitute a standard, specification, or regulation.

REFERENCES

1. I. S. Sokolnikoff. Mathematical Theory of Elasticity. McGraw-Hill, New York, 1956.
2. H. F. Southgate and J. G. Mayes. Chevron N-Layer Program Modified for Strain Energy Density Calculations. Kentucky Department of Transportation, Lexington (in preparation).
3. The AASHO Road Test: Report 5—Pavement Research. HRB, Special Rept. 61E, 1962.
4. H. F. Southgate, R. C. Deen, J. H. Havens, and W. B. Drake. Kentucky Research: A Flexible Pavement Design and Management System. Proc., 4th International Conference on the Structural Design of Asphalt Pavements, Univ. of Michigan, Ann Arbor, 1977, pp. 269-297.
5. The AASHO Road Test: Report 3—Traffic Operations and Pavement Maintenance. HRB, Special Rept. 61C, 1962.
6. J. A. Deacon. Load Equivalency in Flexible Pavements. Proc., AAPT, Vol. 38, 1969.
7. AASHTO Interim Guide for Design of Pavement Structures, 2nd Ed. AASHTO, Washington, DC, 1974.
8. R. Winfrey and others. Economics of Maximum

Limits of Motor Vehicle Dimensions and Weights. Federal Highway Administration, U.S. Department of Transportation, Rept. FHWA-RD-73-70, Vol. 2, 1968.
9. R.D. Layton and others. The Energy, Economic, and Environmental Consequences of Increased Vehicle Size and Weight. Research and Special Programs Administration, U.S. Department of Transportation, Rept. DOT/RSPA/DPB-50/78/27, Vol. 2, 1978.

Publication of this paper sponsored by Committee on Flexible Pavement Design.

Factorial Study of Relations Between Pavement Cost and Legal Axle Loads

J. Brent Rauhut, Austin Research Engineers, Inc., Austin, Texas
William J. Kenis, Federal Highway Administration, U.S. Department of Transportation

Results are presented of a study conducted to estimate lifetime costs for flexible pavements as a function of legal axle-load limits by using an improved version of the VESYS IIM computer program. VESYS IIM was modified to include capabilities for (a) seasonal characterizations of pavement materials, (b) a discretized representation of axle-load distribution, and (c) predictions of low-temperature cracking. A literature survey and a laboratory testing program were combined to produce definitions of the variations in permanent deformation parameters as important material characteristics vary seasonally with the environment. These data and other information and experience were applied to produce input data that would yield realistic performance predictions. A factorial of 64 solutions was obtained by using the input data and the improved version of VESYS IIM to study the effects of truck traffic for four levels of legal axle-load limits, two levels of traffic, two levels of pavement-section thickness, and four environmental zones. When failures were predicted, an overlay was applied and a new solution obtained until a pavement life of at least 20 years was attained. Initial and overlay costs were estimated, and these costs, for 20 years of pavement service, were related to legal axle-load limits. Estimated costs for 20 years of pavement service were considerably increased by increasing legal axle loads, and estimated cost increases were more severe for the northern than for the southern environmental zones of the United States.

Significant efforts are under way to evaluate the effects on pavement performance and maintenance costs of the increasing levels of traffic being imposed on U.S. highway systems. The results of one study in this overall effort are reported here.

This study was conducted by using an improved version of the Federal Highway Administration computer program VESYS IIM for predicting pavement distress and performance (1, 2). Briefly, VESYS IIM consists of a set of mechanistic models that are uniquely integrated for use in analyzing the structural integrity and performance of flexible highway pavements. The working hypothesis for the VESYS model assumes that all responses of the pavement can be stated in terms of the geometry of the pavement structure, the physical properties of the material layers, and the effect of climate and load on these properties. The material properties can be characterized for primary response behavior as linear elastic and/or linear viscoelastic, and temperature and stress in the appropriate layers are accounted for.

Laws of cumulative damage exist for several distress mechanisms that cause pavement damage. These laws are formulated from observations of the distress behavior of the materials. The serviceability of a pavement is hypothesized to be represented by the linear accumulation of the distress parameters (cracking, rutting, and roughness), which can be expressed similarly as the American Association of State Highway and Transportation Officials definition of present serviceability index (PSI).

More precise verification of the model was necessary in this study than had previously been attained (3-6). However, such precise verification requires more realistic measurement of traffic and environmental effects. To account for these effects, the program was modified to include all the capabilities of VESYS IIM plus capabilities for (a) seasonal characterizations of stiffness and permanent deformation properties of materials, (b) a discretized representation of axle-load distribution for more accurate axle-load characterization, and (c) predictions of low-temperature cracking (1). This new version of VESYS (currently called VESYS A) is believed to provide greatly improved predictions of rutting, slope variance, PSI, and expected life.

Verification of the modified program and its associated sets of input data was accomplished by comparing predicted distress and performance with measured values from four sections of the AASHO Road Test, four sections from the Brampton Test Road, and data available for sections of I-80N in Utah and I-10 in Florida. This verification effort involved an iterative procedure that required exercising the model to arrive at predictions, comparing the predictions with measured performance, analyzing differences to assess their cause, and making rational modifications to problem input where they were indicated to sharpen up the predictions. The only revisions made to input values were those that could be justified through analysis.

Once the modified VESYS IIM subsystem had been verified and rational material, traffic, and environmental characterizations established, a factorial of 64 solutions was developed in order to arrive at a basis for establishing relations between cost and legal axle load. This factorial included four levels of legal axle load [80, 89, 98, and 107 kN [18 000, 20 000, 22 000, 24 000 lbf (18, 20, 22, and 24 kip)]], two levels of pavement section called thin and thick, two levels of truck traffic called low and high, and four different environmental zones, including wet-freeze, dry-freeze, wet/no freeze, and dry/no freeze. The solutions were run as a full factorial of 64. The environmental zones were repre-

sented by conditions at a section of I-80 in Illinois for wet-freeze, a section of I-80N in Utah for dry-freeze, a section of I-10 in Florida for wet/no freeze, and a section of I-20 in Texas for dry/no freeze.

DEVELOPMENT OF REALISTIC INPUT DATA

Modifications to the computer program were accompanied by a rather detailed study to determine (a) how the permanent deformation characteristics of the surface asphalt concrete, base material, and subgrade materials vary seasonally with variations in density, moisture content, stress, and temperature; (b) what the axle-load distributions might be expected to be in the event of higher legal axle-load limits; (c) how the layer stiffnesses could be expected to vary seasonally in view of freeze-thaw conditions, temperature, moisture content, density, and stress; (d) what low-temperature model should be incorporated into the VESYS system and how to obtain the necessary input values; (e) what pavement temperatures should be assigned for the various environmental zones to be considered; and (f) how moisture content varies in base and subgrade layers.

To develop a general range of input data on the permanent deformation characteristics of materials subjected to seasonal changes of temperature and moisture, a factorial test series was run in the laboratory. A total of 18 tests were run for a typical asphalt concrete, and duplicate tests were run for three levels of stress and three levels of temperature. Each test was continued for 100 000 cycles of loading. A typical silty clay was similarly tested at three levels of moisture content and three levels of density. The test procedures and results are described in detail by Rauhut and Hordahl (7).

One of the most important decisions in a study of the effects of increased legal axle loads is what the resulting axle-load distribution may be. Accordingly, the axle-load distributions selected were arrived at after careful study of the work of Winfrey and others (8) and Whiteside and others (9), correspondence with agencies that represent the trucking industry, and study of W-4 tables from a number of states, including those that have relatively high limits on legal axle loads. The resulting axle-load distributions expected for the four legal axle-load limits considered are given in Table 1. It can be reasonably argued that more overloaded trucks than the 0.5 percent shown operate on U.S. highways and evade weighing, but only data from weight measurements are available. A higher incidence of heavily loaded trucks would, of course, result in a higher rate of damage.

The same distributions of truck traffic in time were used for all legal axle loads, which implies an increase in megagrams with increasing legal limits on axle loads. An alternative approach could have been decreases in traffic with increases in axle-load distributions to maintain constant megagrams, but this was the less severe condition and the relative realism of either extreme is moot.

PAVEMENT DISTRESS AND PERFORMANCE PREDICTIONS

Since the reporting of the performance predictions for all 64 solutions would require a great deal of space, typical plots for 80- and 107-kN legal axle loads are shown in Figures 1-4. One figure for each environmental zone has been included; both low- and high-traffic cases and some variation in pavement section are also shown.

Study of distress and performance predictions for the entire factorial indicated the following:

1. Expected increases in cracking and rutting with increased traffic and increased axle loads were predicted. The magnitudes of predicted cracking damage and rut depths were less for thick than for thin pavements.
2. Predicted "failures" were caused by cracking in all environmental zones, except for the quite warm wet/no freeze environment represented by Florida. Overlays for the wet/no freeze environment were necessitated by excessive rutting and consequent loss of serviceability.
3. Cracking failures occurred much more rapidly in the colder wet-freeze and dry-freeze environments than in the dry/no freeze environment represented by Texas. Low-temperature cracking also added to the higher levels of fatigue cracking in the colder [illegible] and affected the shapes of the cracking curves [illegible] time. (The nature of the fatigue equation is such that the curve tends to become horizontal as it approaches 1000 m^2 cracked/1000 m^2, but the linear addition of low-temperature cracking causes it to reach failure before the curve approaches the horizontal.)
4. PSI remained relatively high where cracking necessitated use of an overlay since serious rutting did not have time to develop (see Figure 1 for example).
5. Although the expected increase in incidence of higher axle loads for higher axle limits is numerically minor, it can be seen that failures are predicted considerably earlier for the higher legal axle-load limits than for the usual 80-kN limit. In fact, twice as many cases (8:4) of legal axle-load limits of 98 and 107 kN required two overlays than the corresponding 80-kN case. This results, of course, from the increased rate of damage caused by the higher axle loads.

COST EVALUATIONS AND RELATION BETWEEN COSTS AND LEGAL AXLE LOADS

It was originally intended that cost estimates would be performed in terms of present worth, but the unpredictable variability in time of interest rates and differential inflation, plus the fact that interest rates and inflation rates have been similar and off-setting in recent years, resulted in a decision to base cost estimates on 1977 costs for both initial construction and subsequent overlays. This means, in effect, that present worth is based on assumption of a zero discount rate. The probability of inaccuracy, however, is no higher than it would be were we to attempt to predict these rates in time.

One of the very difficult decisions made during the research effort was how to meaningfully express the relations between costs and legal axle loads. One type of cost that must be considered is the total cost of obtaining 20 years of acceptable pavement service. Although it is meaningful, this cost does not discriminate with much sensitivity between the real costs of operating real pavements that are certainly not to be abandoned after 20 years. As can be seen later, the same number of overlays may suffice for several axle-load distributions, although the relative distresses and performances may differ. Consequently, it was decided that "value of remaining pavement life" or "salvage value" beyond 20 years should also be included as a part of the analysis

and presentation. It was also apparent that the costs of maintaining an existing pavement in service under increased axle-load distributions were at least as important as the costs of building and maintaining new pavements under various axle-load distributions.

From the many types of costs that might have been used in this comparative study, four were selected:

1. Total cost, which consists of the initial construction costs and costs of necessary overlays to maintain satisfactory service for 20 years;
2. Average annual cost, which is calculated by dividing the total cost by the total life of the pavement;
3. Total cost of overlays, or the cost for the overlays necessary to attain 20 years of satisfactory service (the same as total cost less initial construction cost); and
4. Average annual cost for overlays, or the total cost of overlays divided by the life of the pavement after the first overlay.

Table 1. Axle-load distribution (percentage of total representing the four legal axle-load limits studied).

Axle-Load Range (kN)	Axle-Load Distribution (%)			
	80 kN	89 kN	98 kN	107 kN
9-18	7.5	5.8	2.5	2.0
18-27	11.2	9.7	9.2	8.1
27-35	15.4	14.9	15.5	13.6
35-44	30.8	27.7	23.8	23.2
44-53	11.1	13.9	16.9	17.8
53-62	8.1	9.1	10.5	11.3
62-71	11.5	11.6	12.5	13.1
71-80	3.9	5.3	6.1	7.1
80-89	0.4	1.4	1.9	2.2
89-98	0.1	0.4	0.6	1.0
98-107	-	0.1	0.2	0.2
107-115	-	0.1	0.2	0.2
115-124	-	-	0.1	0.2

Notes: 1 kN = 224.8 lbf.
Fifty-two percent of the total number of axles were found to be tandem axles, and one set of two axles in tandem was considered as 2.25 single axles instead of 2.0 to approximate equivalency between tandem and single axles.

Total cost and average annual cost include initial construction costs and therefore relate to relative costs for new pavements subjected to truck traffic that represents different legal axle loads, whereas the other two types of costs relate in an approximate fashion to major maintenance costs for existing pavements that are subjected to different legal axle loads. Total cost, average annual cost, and total cost of overlays appear to be rather straightforward and their relation to real situations direct. The cost type termed average annual cost of overlays is not as direct but does give a measure of sorts for relating axle loading to the cost of maintaining pavement serviceability. Other cost terms can be defined and considered for existing pavements, but none have any more general applicability. Both average annual cost and average annual cost of overlays bring the value of the remaining pavement life after 20 years of service into consideration.

Figure 1. Predicted pavement performance under high and low traffic volumes for wet-freeze environment and thin pavement.

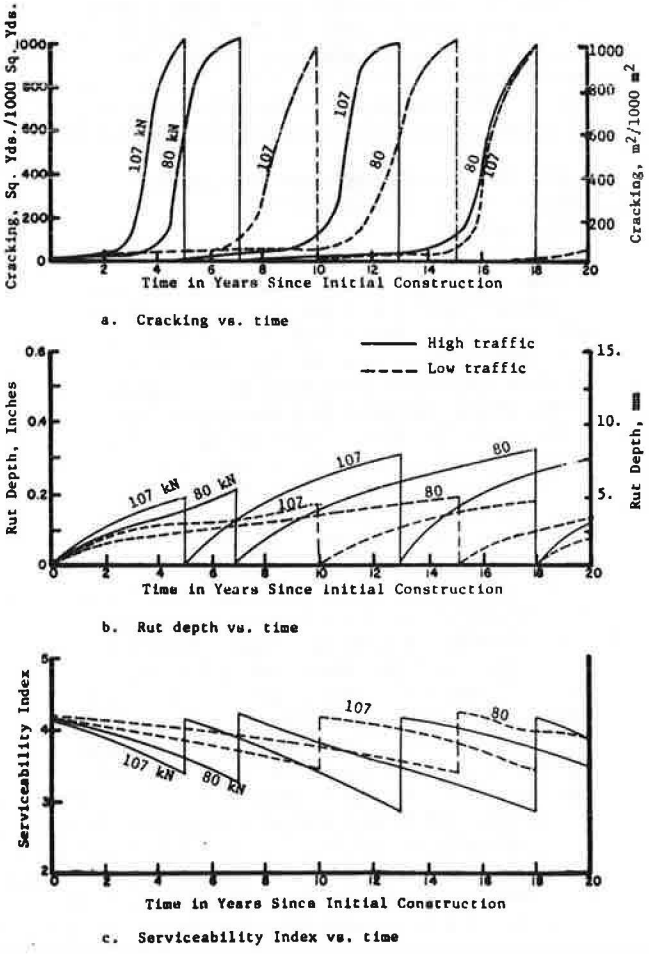

Figure 2. Predicted pavement performance under high and low traffic volumes for dry-freeze environment and thick pavement.

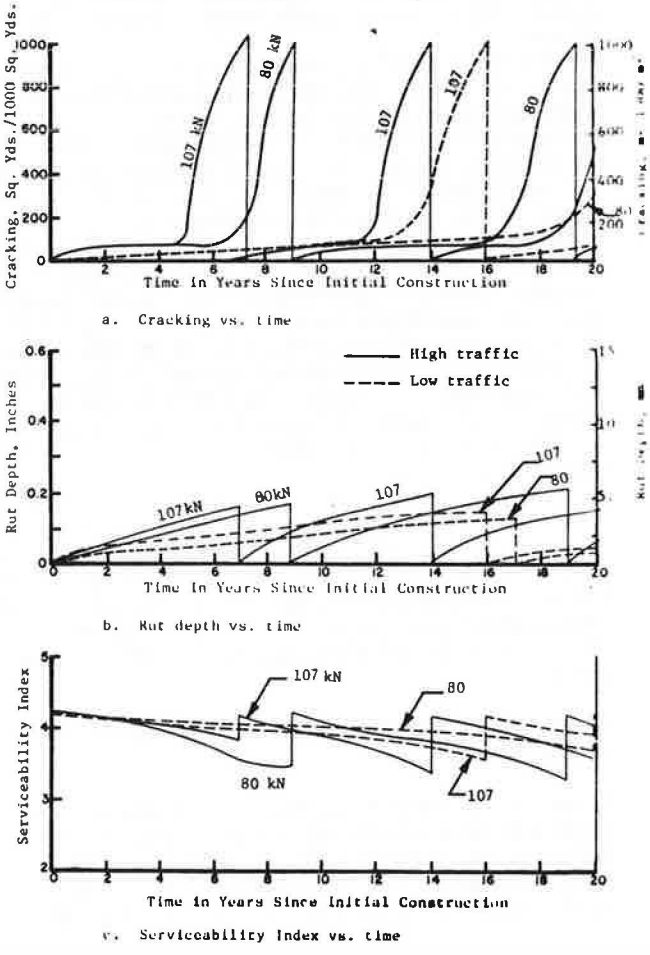

Figure 3. Predicted pavement performance under high and low traffic volumes for wet/no freeze environment and thick pavement.

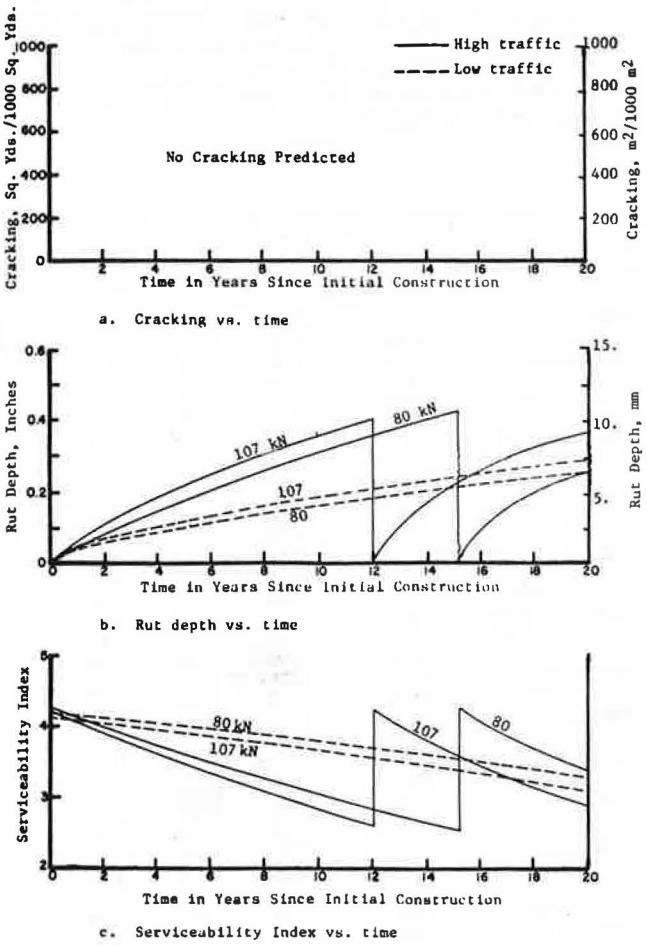

Figure 4. Predicted pavement performance under high and low traffic volumes for dry/no freeze environment and thin pavement.

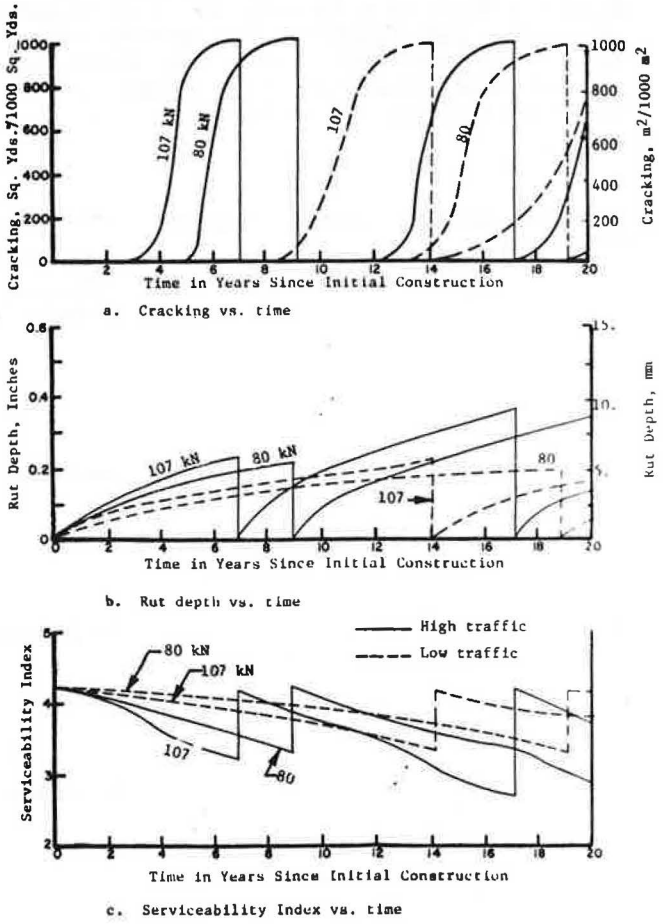

Table 2. Predicted pavement life and pavement age when overlaid, by legal axle load: low traffic volume.

Environmental Zone	Age Category	Age (years) Thin Section 80 kN	89 kN	98 kN	107 kN	Thick Section 80 kN	89 kN	98 kN	107 kN
Wet-freeze	At first overlay	15	13	11	10				19
	At second overlay				18				
	Life of system[a]	25	22	20	28E	26	23	21	33
Dry-freeze	At first overlay	12	10	9	8			17	16
	At second overlay		18	16	15				
	Life of system[a]	21	28E	24E	22E	23	20	30E	27E
Wet/no freeze[b]	Life of system[a]	29	28	26	25	37	35	34	33
Dry/no freeze[c]	At overlay	19	17	15	14				
	Life of system[a]	32	28	25	24	31	27	25	23

Note: E = estimated.
[a]As repaired to serve at least 20 years. [b]No overlays. [c]Single overlay.

Table 3. Predicted pavement life and pavement age when overlaid, by legal axle load: high traffic volume.

Environmental Zone	Age Category	Age (years) Thin Section 80 kN	89 kN	98 kN	107 kN	Thick Section 80 kN	89 kN	98 kN	107 kN
Wet-freeze	At first overlay	7	6	5	5	11	10	9	8
	At second overlay	18	16	14	13			18	17
	Life of system[a]	29E	27E	24E	21E	24	21	29E	27E
Dry-freeze	At first overlay	6	5	5	4	9	8	8	7
	At second overlay	15	13	12	11	19	17	15	14
	Life of system[a]	25E	23E	21E	20E	30E	28E	25E	22E
Wet/no freeze	At first overlay	11	11	10	10	15	13	11	11
	At second overlay			18	18				
	Life of system[a]	21	20	25E	24E	28	26	25	24
Dry/no freeze	At first overlay	9	8	7	7	15	13	11	11
	At second overlay			18	17				
	Life of system[a]	23	20	30E	28E	30	26	22	21

Note: E = estimated.
[a]As repaired to serve at least 20 years.

The total costs for the 64 combinations of conditions studied can be developed by taking the appropriate initial cost ($8.05 for a thin or $10.37 for a thick pavement section) and adding to that the cost of the overlays. Tables 2 and 3 indicate the number of overlays and the point in time at which they were used. Their thicknesses and costs were as follows (2):

1. Pavements for all environmental zones except wet/no freeze received 7.6-cm (3-in) overlays at $4.25/m² ($3.55/yd²) for low traffic and 10.2-cm (4-in) overlays at $5.65/m² ($4.71/yd²) for high traffic.
2. Five-centimeter (2-in) overlays at $2.85/m² ($2.39/yd²) were placed on pavements in the wet/no freeze environmental zone.

Table 4. Pavement cost by legal axle load: low traffic volume.

Environmental Zone	Type of Cost	Type of Section	Cost ($/m²) 80 kN	89 kN	98 kN	107 kN
Wet-freeze	Total	Thin	13.87	13.87	13.87	18.12
		Thick	12.40	12.40	12.40	16.65
	Average annual cost	Thin	0.55	0.63	0.69	0.64
		Thick	0.48	0.54	0.58	0.50
	Total for overlays	Thin	4.24	4.24	4.24	8.49
		Thick	0	0	0	4.24
	Average annual cost for overlays	Thin	0.43	0.46	0.46	0.46
		Thick	0	0	0	0.30
Dry-freeze	Total	Thin	13.87	18.12	18.12	18.12
		Thick	12.40	12.40	16.65	16.65
	Average annual cost	Thin	0.66	0.64	0.75	0.72
		Thick	0.54	0.62	0.55	0.72
	Total for overlays	Thin	4.24	8.49	8.49	8.49
		Thick	0	0	4.24	4.24
	Average annual cost for overlays	Thin	0.46	0.46	0.56	0.56
		Thick	0	0	0.32	0.32
Wet/no freeze	Total	Thin	9.63	9.63	9.63	9.63
		Thick	12.40	12.40	12.40	12.40
	Average annual cost	Thin	0.33	0.34	0.37	0.37
		Thick	0.33	0.36	0.37	0.37
	Total for overlays	Thin	0	0	0	0
		Thick	0	0	0	0
	Average annual cost for overlays	Thin	0	0	0	0
		Thick	0	0	0	0
Dry/no freeze	Total	Thin	13.87	13.87	13.87	13.87
		Thick	12.40	12.40	12.40	12.40
	Average annual cost	Thin	0.43	0.49	0.55	0.55
		Thick	0.39	0.45	0.49	0.54
	Total for overlays	Thin	4.24	4.24	4.24	4.24
		Thick	0	0	0	0
	Average annual cost for overlays	Thin	0.32	0.38	0.43	0.43
		Thick	0	0	0	0

Note: 1 m² = 1.196 yd²

Table 5. Pavement cost by legal axle load: high traffic volume.

Environmental Zone	Type of Cost	Type of Section	Cost ($/m²) 80 kN	89 kN	98 kN	107 kN
Wet-freeze	Total	Thin	20.89	20.89	20.89	20.89
		Thick	18.03	18.03	23.67	23.67
	Average annual cost	Thin	0.72	0.77	0.87	0.87
		Thick	0.75	0.86	0.81	0.81
	Total for overlays	Thin	11.26	11.26	11.26	11.26
		Thick	5.63	5.63	11.26	11.26
	Average annual cost for overlays	Thin	0.51	0.54	0.59	0.59
		Thick	0.43	0.51	0.56	0.56
Dry-freeze	Total	Thin	20.89	20.89	20.89	20.89
		Thick	23.67	23.67	23.67	23.67
	Average annual cost	Thin	0.84	0.91	0.99	1.04
		Thick	0.79	0.85	0.94	1.07
	Total for overlays	Thin	11.26	11.26	11.26	11.26
		Thick	11.26	11.26	11.26	11.26
	Average annual cost for overlays	Thin	0.60	0.64	0.70	0.70
		Thick	0.54	0.56	0.66	0.75
Wet/no freeze	Total	Thin	12.48	12.48	15.34	15.34
		Thick	15.26	15.26	15.26	15.26
	Average annual cost	Thin	0.60	0.62	0.61	0.63
		Thick	0.55	0.58	0.61	0.63
	Total for overlays	Thin	2.86	2.86	5.72	5.72
		Thick	2.86	2.86	2.86	2.86
	Average annual cost for overlays	Thin	0.29	0.32	0.38	0.40
		Thick	0.21	0.24	0.24	0.24
Dry/no freeze	Total	Thin	15.26	15.26	20.89	20.89
		Thick	18.03	18.03	18.03	18.03
	Average annual cost	Thin	0.67	0.76	0.69	0.74
		Thick	0.60	0.69	0.82	0.86
	Total for overlays	Thin	5.63	5.63	11.26	11.26
		Thick	5.63	5.63	5.63	5.63
	Average annual cost for overlays	Thin	0.40	0.46	0.49	0.54
		Thick	0.37	0.43	0.51	0.56

Note: 1 m² = 1.196 yd².

The cost estimates developed in this manner are given as total cost in Table 4 for low truck traffic and in Table 5 for high truck traffic. The other three types of costs are also given in Tables 4 and 5.

All the basic data are now tabulated. Costs are now considered in relation to legal axle loads in terms of new pavements (initial construction costs are considered) and existing pavements (only overlay costs are considered).

COST RELATIONS FOR NEW PAVEMENTS

A review of Tables 4 and 5 shows that, for a given climatic region, total cost is independent of the legal

Table 6. Normalized pavement cost by legal axle load: low traffic volume.

Environmental Zone	Type of Cost	Type of Section	Normalized Cost[a] 80 kN	89 kN	98 kN	107 kN
Wet-freeze	Total	Thin	1.00	1.00	1.00	1.31
		Thick	1.00	1.00	1.00	1.34
	Average annual cost	Thin	1.00	1.14	1.25	1.17
		Thick	1.00	1.13	1.23	1.05
	Total for overlays	Thin	1.00	1.00	1.00	2.00
		Thick	1.00	1.00	1.00	-[b]
	Average annual cost for overlays	Thin	1.00	1.08	1.08	1.08
		Thick	1.00	1.00	1.00	-[b]
Dry-freeze	Total	Thin	1.00	1.31	1.31	1.31
		Thick	1.00	1.00	1.34	1.34
	Average annual cost	Thin	1.00	0.98	1.14	1.25
		Thick	1.00	1.15	1.03	1.14
	Total for overlays	Thin	1.00	2.00	2.00	2.00
		Thick	1.00	1.00	-[b]	-
	Average annual cost for overlays	Thin	1.00	1.00	1.21	1.31
		Thick	1.00	1.00	-[b]	-
Wet/no freeze	Total	Thin	1.00	1.00	1.00	1.00
		Thick	1.00	1.00	1.00	1.00
	Average annual cost	Thin	1.00	1.02	1.10	1.15
		Thick	1.00	1.06	1.09	1.12
	Total for overlays	Thin	1.00	1.00	1.00	1.00
		Thick	1.00	1.00	1.00	1.00
	Average annual cost for overlays	Thin	1.00	1.00	1.00	1.00
		Thick	1.00	1.00	1.00	1.00
Dry/no freeze	Total	Thin	1.00	1.00	1.00	1.00
		Thick	1.00	1.00	1.00	1.00
	Average annual cost	Thin	1.00	1.14	1.28	1.33
		Thick	1.00	1.15	1.24	1.35
	Total for overlays	Thin	1.00	1.00	1.00	1.00
		Thick	1.00	1.00	1.00	1.00
	Average annual cost for overlays	Thin	1.00	1.19	1.33	1.33
		Thick	1.00	1.00	1.00	1.00

[a] Normalized by dividing all values by the corresponding 80-kN legal axle-load costs.
[b] Intermediate since the divisor is zero.

Table 7. Normalized pavement cost by legal axle load: high traffic volume.

Environmental Zone	Type of Cost	Type of Section	Normalized Cost[a] 80 kN	89 kN	98 kN	107 kN
Wet-freeze	Total	Thin	1.00	1.00	1.00	1.00
		Thick	1.00	1.00	1.00	1.31
	Average annual cost	Thin	1.00	1.07	1.21	1.45
		Thick	1.00	1.14	0.87	1.02
	Total for overlays	Thin	1.00	1.00	1.00	1.00
		Thick	1.00	1.00	2.00	2.00
	Average annual cost for overlays	Thin	1.00	1.05	1.16	1.37
		Thick	1.00	1.19	1.31	1.39
Dry-freeze	Total	Thin	1.00	1.00	1.00	1.00
		Thick	1.00	1.00	1.00	1.00
	Average annual cost	Thin	1.00	1.09	1.19	1.25
		Thick	1.00	1.07	1.27	1.36
	Total for overlays	Thin	1.00	1.00	1.00	1.00
		Thick	1.00	1.00	1.00	1.00
	Average annual cost for overlays	Thin	1.00	1.08	1.18	1.18
		Thick	1.00	1.04	1.22	1.40
Wet/no freeze	Total	Thin	1.00	1.00	1.23	1.23
		Thick	1.00	1.00	1.00	1.00
	Average annual cost	Thin	1.00	1.05	1.03	1.08
		Thick	1.00	1.08	1.12	1.17
	Total for overlays	Thin	1.00	1.00	2.00	2.00
		Thick	1.00	1.00	1.00	1.00
	Average annual cost for overlays	Thin	1.00	1.12	1.33	1.42
		Thick	1.00	1.11	1.11	1.11
Dry/no freeze	Total	Thin	1.00	1.00	1.37	1.37
		Thick	1.00	1.00	1.00	1.00
	Average annual cost	Thin	1.00	1.15	1.05	1.12
		Thick	1.00	1.15	1.36	1.43
	Total for overlays	Thin	1.00	1.00	2.00	2.00
		Thick	1.00	1.00	1.00	1.00
	Average annual cost for overlays	Thin	1.00	1.15	1.21	1.32
		Thick	1.00	1.16	1.39	1.52

[a] Normalized by dividing all values by the corresponding 80-kN legal axle-load costs.

Table 8. Mean values of pavement costs, by legal axle load, normalized by dividing by 80-kN axle-load costs.

Cost Item	Normalized Cost			
	80 kN	89 kN	98 kN	107 kN
Total				
All thin pavements	1.00	1.04	1.12	1.16
All thick pavements	1.00	1.00	1.05	1.12
All low traffic volumes	1.00	1.02	1.09	1.14
All high traffic volumes	1.00	1.04	1.09	1.16
Wet-freeze environment	1.00	1.00	1.08	1.12
Dry-freeze environment	1.00	1.00	1.00	1.23
Wet/no freeze environment	1.00	1.08	1.16	1.16
Dry/no freeze environment	1.00	1.00	1.06	1.06
All pavements	1.00	1.02	1.08	1.14
Average annual costs				
All thin pavements	1.00	1.08	1.16	1.22
All thick pavements	1.00	1.12	1.15	1.20
All low traffic volumes	1.00	1.10	1.17	1.20
All high traffic volumes	1.00	1.10	1.14	1.23
Wet-freeze environment	1.00	1.12	1.14	1.18
Dry-freeze environment	1.00	1.07	1.16	1.23
Wet/no freeze environment	1.00	1.01	1.03	1.04
Dry/no freeze environment	1.00	1.05	1.09	1.13
All pavements	1.00	1.10	1.15	1.21

Figure 5. Average annual pavement cost by environment and legal axle load: low traffic volume.

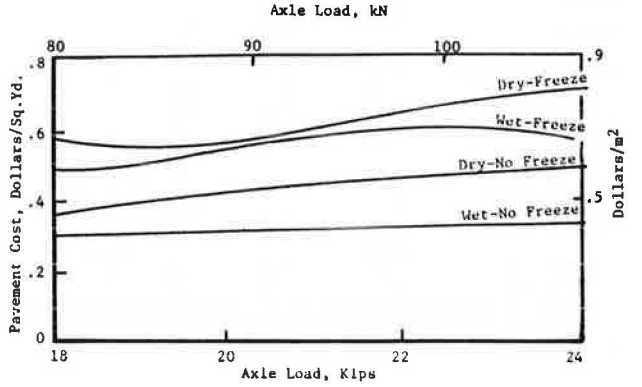

a. Thin pavement section

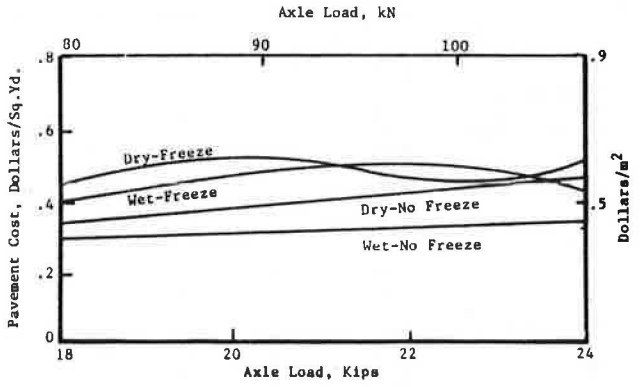

b. Thick pavement section

axle load for 9 of the 16 cases considered. This occurred because either the pavement did not require an overlay to reach a 20-year design life or an equal number of overlays were required for each of the legal axle loads considered.

Because of the higher frequency of cracking in colder climates and the lower frequency of overlays required when the failure mode was rutting rather than cracking, costs for thin pavements for the northern environmental zones were higher than those for the south environmental zones. For thick pavements, the differences in costs among environmental zones were

Figure 6. Average annual pavement cost by environment and legal axle load: high traffic volume.

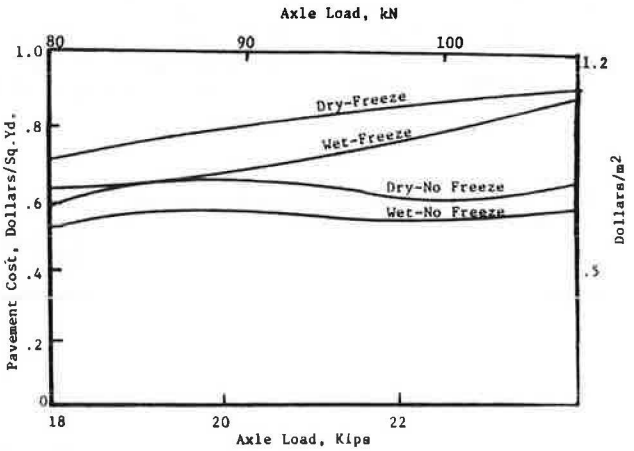

a. Thin pavement section

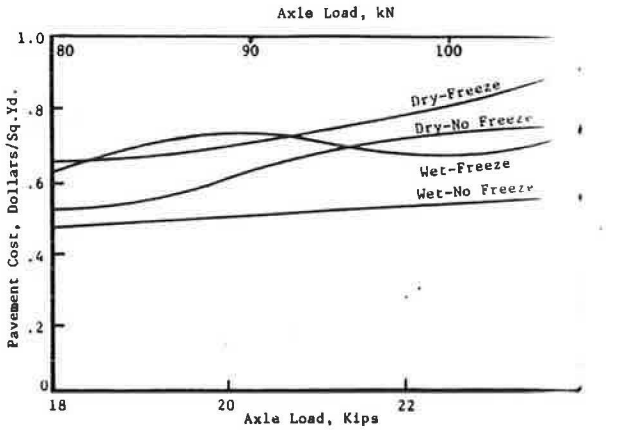

b. Thick pavement section

Another useful way to consider the data developed by normalizing all results given in Tables 4 and 5 by dividing each value by its corresponding value for the 80-kN legal axle load. These normalized values, given in Tables 6 and 7, indicate rather directly the increases in costs that are produced by increases in legal axle loads. This information has been summarized statistically in Table 8 for new pavements by obtaining mean values for the various groupings of cases and environmental zones as well as for all cases combined.

To make it easier to observe trends and identify some unexpected results, average annual cost (which is probably more meaningful than total cost because it considers pavement life after 20 years) from Tables 4 and 5 is plotted in Figures 5 and 6. These figures indicate that average annual costs generally increase as expected with increasing legal axle loads. However, an apparent anomaly occurs in some cases; see the dry-freeze plot in Figure 5b, where cost is shown decreasing with increasing legal axle load. This is not generally consistent with expectations from field experience, partly because accelerating deterioration as moisture percolates through surface cracks into underlying layers and reflection cracking are not modeled by mechanistic models such as VESYS.

Cost decreases with increasing legal axle load because damage predictions necessitate an overlay

Table 9. Mean values of pavement costs for overlays, by legal axle load.

Cost Item	Cost ($/m²)			
	80 kN	89 kN	98 kN	107 kN
Total for overlays				
All thin pavements	5.46	6.00	7.05	7.59
All thick pavements	3.17	3.17	4.41	4.94
All low traffic volumes	1.59	2.13	2.65	3.72
All high traffic volumes	7.05	7.05	8.45	8.45
Wet-freeze environment	5.28	5.28	6.70	8.81
Dry-freeze environment	6.70	7.76	8.81	8.81
Wet/no freeze environment	1.43	1.43	2.14	2.14
Dry/no freeze environment	3.87	3.87	5.28	5.28
All pavements	4.32	4.59	5.74	6.27
Average annual costs for overlays				
All thin pavements	0.378	0.411	0.454	0.483
All thick pavements	0.195	0.219	0.287	0.354
All low traffic volumes	0.152	0.165	0.222	0.274
All high traffic volumes	0.419	0.465	0.519	0.563
Wet-freeze environment	0.344	0.380	0.406	0.518
Dry-freeze environment	0.400	0.418	0.562	0.613
Wet/no freeze environment	0.125	0.141	0.155	0.161
Dry/no freeze environment	0.275	0.320	0.359	0.383
All pavements	0.286	0.314	0.371	0.418

Table 10. Mean values of pavement costs for overlays, by legal axle load, normalized by dividing by 80-kN axle-load costs.

Cost Item	Normalized Cost			
	80 kN	89 kN	98 kN	107 kN
Total for overlays				
All thin pavements	1.00	1.10	1.29	1.40
All thick pavements	1.00	1.00	1.39	1.56
All low traffic volumes	1.00	1.34	1.67	2.34
All high traffic volumes	1.00	1.00	1.20	1.20
Wet-freeze environment	1.00	1.00	1.27	1.67
Dry-freeze environment	1.00	1.16	1.32	1.32
Wet/no freeze environment	1.00	1.00	1.49	1.49
Dry/no freeze environment	1.00	1.00	1.36	1.36
All pavements	1.00	1.06	1.33	1.45
Average annual costs for overlays				
All thin pavements	1.00	1.09	1.20	1.28
All thick pavements	1.00	1.12	1.47	1.82
All low traffic volumes	1.00	1.09	1.46	1.80
All high traffic volumes	1.00	1.11	1.24	1.34
Wet-freeze environment	1.00	1.10	1.18	1.50
Dry-freeze environment	1.00	1.05	1.40	1.53
Wet/no freeze environment	1.00	1.12	1.24	1.29
Dry/no freeze environment	1.00	1.17	1.30	1.39
All pavements	1.00	1.10	1.30	1.46

which in turn sufficiently increases predicted pavement life so that its effect in decreasing average annual costs is greater than the increase caused by the added overlay cost. This may well be realistic in a dry climate if reflection cracking can also be controlled, but it may be the exception rather than the rule.

It should be remembered, however, that the modeling limitations mentioned above apply not only to overlays but also to initial construction predictions; that is, pavement life should always be overpredicted if the modeling limitation is serious. Since the predictions do not appear unrealistic for either original pavements or overlays, it can be concluded that the model limitations may not be the primary cause of this apparent anomaly. It may simply mean that an overlay may not only meet an immediate need to maintain service but may also be cost effective. The Florida Department of Transportation has in fact found it cost effective to extend the life of a pavement through a relatively thin overlay when cracking begins at the bottom of the surface layer rather than to apply a thicker overlay after the cracks have propagated to the surface.

A fact that tends to lend credence to the predicted costs is that the axle-load distributions (Table 1) that result from a change in legal axle limit are not very severe. There is no real similarity at all, for instance, in a road test such as the AASHO Road Test, in which an increase in test axle load means that essentially all subsequent traffic has that axle load.

Although it may not be appropriate to claim quantitative accuracy for the predicted costs, it does appear reasonable to expect that all the results will be biased in the same way; the trends would thus be reliable and the cost err, if at all, toward the low side.

To continue with analysis of the cost predictions developed, the following general conclusions can be drawn from the summary values given in Table 8:

1. The total cost for a 20-year service life can be expected to (a) increase as much as 8 percent for an increase in legal axle-load limit from 80 to 89 kN and, on the average, increase 2 percent for all pavements; (b) increase as much as 16 percent for an increase in legal axle-load limit from 80 to 98 kN (depending primarily on pavement thickness and environment) and, on the average, increase 8 percent for all pavements; and (c) increase from 6 to 23 percent for an increase in legal axle-load limit from 80 to 107 kN and, on the average, increase 14 percent for all pavements.
2. The average annual cost (considering the value of remaining pavement life after 20 years) can be expected to (a) increase from 1 to 12 percent for an increase in legal axle-load limit from 80 to 89 kN and, on the average, increase by 10 percent; (b) increase from 3 to 17 percent for an increase in legal axle-load limit from 80 to 98 kN and, on the average, increase by 15 percent; and (c) increase from 4 to 23 percent for an increase in legal axle-load limit from 80 to 107 kN and, on the average, increase by 21 percent.
3. The overall effect of increased axle loads is more severe for thin than for thick pavements and for wetter than for warmer climates.
4. Although the effect on damage caused by different levels of truck traffic volume on a pavement section is obvious, the relative costs (or rates of increase in costs) for accommodating traffic at different legal axle-load limits are not very sensitive to levels of truck traffic.

COST RELATIONS FOR EXISTING PAVEMENTS

The cost types previously described as total costs for overlays and average annual costs of overlays permit an analysis of the effects of increased legal axle-load limits on existing highways because the initial construction costs are not included in the analysis. The overlay costs for overlays given in Table 9 were arrived at as previously described for new highways except that initial construction costs were omitted. These values were normalized by dividing by the corresponding 80-kN axle-load costs; the normalized values are given in Table 10.

As would be expected, the percentage increases in overlay costs for increases in legal axle-load limits are much greater when a relatively large fixed initial construction cost is not included. Analysis of the results in Tables 9 and 10 indicates that

1. The predicted overlay costs for the higher legal axle-load limits in the wet/no freeze environmental zone (or warm temperature) represented by Florida I-10 are nominal.
2. As would be expected, the total cost for maintaining the highway is much less for low than for high

traffic volumes, but the percentage increase in total overlay costs with increase in axle loads is much higher for the low-traffic case. For instance, a mean predicted total overlay cost for a 107-kN legal axle load on all low traffic volumes is 2.34 times as much as that for an 80-kN legal axle load as opposed to only 20 percent more for all high traffic volumes.

3. The predicted overlay costs themselves are much higher for northern than for southern environments, but the percentage increases in overlay costs with increasing legal axle load are similar to those for southern highways.

4. The cost of overlaying pavements was logically predicted to be greater for thin than for thick pavements, but the percentage increase in overlay cost with increasing legal axle load was greater for thick pavements.

5. In general, total overlay costs can be expected to increase by about 6 percent for an increase in legal axle-load limit from 80 to 89 kN, 33 percent for an increase from 80 to 98 kN, and 45 percent for an increase from 80 to 107 kN.

6. An increase in legal axle-load limit from 80 to 89 kN increases the average annual cost of overlays about 10 percent, an increase from 80 to 98 kN increases it about 30 percent, and an increase from 80 to 107 kN increases it about 46 percent.

SUMMARY

Relations have been reported between costs for 20 years of acceptable pavement service and established legal single-axle-load limits. These relations are based on distress and performance predicted by a modified version of the VESYS IIM computer program by using the best traffic, environment, and materials characterizations possible in a factorial study of 16 cases with legal single-axle loads of 80, 89, 98, and 107 kN for each.

It is clear that the accuracy of the cost relations depends on the ability of the flexible-pavement structural model to simulate real pavements and on the accuracy of the characterizations of traffic, axle-load distribution, environment, and material input to the model. The modified version of VESYS IIM is certainly one of the most complete mechanistic models of a flexible pavement, but it shares the limitation of most, if not all, other such models in that it does not model reflection cracking or the accelerating deterioration of its structural components as surface cracking progresses and moisture enters the base and subgrade layers nor does it consider loss of stiffness in the asphalt concrete surface caused by cracking or changes in stiffness and viscoelastic properties as the asphalt hardens over time. In addition, distress and performance predictions are very sensitive to materials characteristics. These characteristics are, however, limited to relatively typical materials from several specific locations. Thus, exceptional quantitative accuracy cannot be claimed, but all solutions are subject to the same biases so that the trends established can be expected to be reasonably reliable and the quantitative relations sufficiently accurate to offer valuable insight until the results of other, much more comprehensive, studies are completed.

ACKNOWLEDGMENT

The research reported here was conducted by Austin Research Engineers, Inc. We wish to thank the sponsor—the Federal Highway Administration, U.S. Department of Transportation—and the many others that furnished information useful to the project. The opinions, findings, and conclusions expressed in this paper are ours and not necessarily those of the Federal Highway Administration.

REFERENCES

1. W. J. Kenis. Predictive Design Procedures. Proc., 4th International Conference on the Structural Design of Asphalt Pavements, Univ. of Michigan, Ann Arbor, Vol. 1, 1977.
2. W. J. Kenis. Predictive Design Procedures: VESYS Users Manual. Federal Highway Administration, U.S. Department of Transportation, Rept. FHWA-RD-77-154, 1978.
3. B. Rauhut and others. Comparison of VESYS IIM Predictions to Brampton/AASHO Performance Measurements. Proc., 4th International Conference on the Structural Design of Asphalt Pavements, Univ. of Michigan, Ann Arbor, Vol. 1, 1977.
4. D. I. Anderson and others. Field Verification of the VESYS IIM Structural Subsystem in Utah. Proc., 4th International Conference on the Structural Design of Asphalt Pavements, Univ. of Michigan, Ann Arbor, Vol. 1, 1977.
5. G. Sharma and others. Implementation and Verification of Flexible Pavement Design Methodology. Proc., 4th International Conference on the Structural Design of Asphalt Pavements, Univ. of Michigan, Ann Arbor, Vol. 1, 1977.
6. G. Sharma and others. Evaluation of Flexible Pavement Design Methodology Based upon Field Observations at PSU Test Track. Proc., 4th International Conference on the Structural Design of Asphalt Pavements, Univ. of Michigan, Ann Arbor, Vol. 1, 1977.
7. J. B. Rauhut and P. R. Hordahl. Effects on Highways of Increased Legal Vehicle Weights Using VESYS IIM. Federal Highway Administration, U.S. Department of Transportation, Rept. FHWA-RD-77-134, Jan. 1978.
8. R. Winfrey and others. Economics of the Maximum Limits of Motor Vehicle Dimensions and Weights. Federal Highway Administration, U.S. Department of Transportation, Rept. FHWA-RD-73-69, Vol. 1, Sept. 1968.
9. R. E. Whiteside, T. Y. Chu, J. C. Cosby, R. L. Whitaker, and R. Winfrey. Changes in Legal Vehicle Weights and Dimensions: Some Economic Effects on Highways. NCHRP, Rept. 141, 1973.

Publication of this paper sponsored by Committee on Theory of Pavement Design.

Allowable Load on Multiple-Axle Trucks

Jacob Uzan and Gdalyah Wiseman, Department of Civil Engineering, Technion—Israel Institute of Technology, Haifa

A methodology is proposed by which, for flexible pavements, the equivalency of various loading configurations with respect to cumulative pavement damage can be computed by using the criterion of maximum shear stress at the top of the subgrade. Computations can be performed with sufficient accuracy by replacing the real pavement with a two-layer elastic model. The results of this approach are found to be in good agreement with equivalencies established by the AASHO Road Test for dual and dual-tandem truck loadings. Good agreement is also found with the results of tests performed by the U.S. Army Corps of Engineers on airfield flexible pavements. Finally, an industry-oriented approach to the analysis of equivalent loads, based on a tonnage criterion and the serviceability index of the road, is presented. It is concluded that the methodology can be used with confidence by highway agencies to determine allowable loads for multiple-axle trucks.

The cost of truck transportation has always been and remains of prime importance in every national economy. Available truck and highway-pavement technologies and their aircraft and runway-pavement counterparts allow for a wide range of alternative policies. In recent years, increases in freight rates and in the cost of road construction and maintenance have led to a search for a means of reducing costs, the criteria being increased load capacity on the one hand and reduced (or at least stabilized) wear and damage to roads on the other. Among the factors involved is the fact that truck manufacturers have been marketing trailers that have multiple axles instead of the dual-axle vehicles used in the past. The profitability of multiple-axle trucks depends on the allowable axle load.

It should be noted that pavement technology is still largely based on full-scale experimentation, and theoretical extrapolation is likewise subject to experimental verification. Fortunately, since wheel-assembly configurations on airfields are more numerous and diverse than those on roads, they can be put to use in tackling the problem.

This paper deals with the concept of equivalent single-wheel load (ESWL) for different wheel-assembly configurations on flexible pavements. The model used is calibrated on the basis of data from the AASHO Road Test (1) and from the U.S. Army Corps of Engineers multiple-wheel heavy-gear-load pavement tests (2, p. 198; 3, p. 43). The paper concludes with an industry-oriented approach based on a tonnage criterion. The proposed model can therefore be used in determining allowable loadings for multiple-axle trucks.

EQUIVALENT WHEEL LOAD

Each pavement is designed for a certain volume of traffic and/or cargo tonnage. This volume is reflected in design formulas in the form of two major factors: (a) the design load per wheel or per axle and (b) the number of repetitions or coverages of this load. In design methods based on single-wheel load, any other configuration is translated to its equivalent single-wheel load, which is defined as causing an equal magnitude of a preselected parameter stress, strain, or deflection as the configuration in question. In design methods based on single-axle load, any other situation in terms of configuration and/or load repetitions is translated to design single-axle-load repetitions by means of traffic equivalency factors, which are generally derived from observations of pavement performance.

Although this measurement is uniformly adopted in many states, there is no unified approach among the design methods in the selection of a procedure for computing equivalent single-wheel load [see Yoder and Witczak (4) for a survey of design methods for flexible pavements]. Gerrard and Harrison (5) have shown that the equivalent wheel load depends largely on the stressing criterion and on the structural stiffness of the pavement.

DESCRIPTION OF PROPOSED MODEL

The model discussed here is based on the original thickness design formula of the Corps of Engineers (since the formulas are calibrated in U.S. customary units of measurement, no SI equivalents are given):

$$z = (0.144 + 0.231 \log N)\sqrt{(1/8.1\,CBR) - (1/\pi p)}\cdot\sqrt{Q} \qquad (1)$$

where

z = thickness of pavement (in),
N = number of load coverages,
CBR = design California bearing ratio (here, <12),
p = contact pressure of wheel (lbf/in²), and
Q = single-wheel load (lb), or ESWL.

Table 1. Ratio of ESWL to load on a single truck-assembly wheel for 4.5-in radius of contact area and $E_1/E_2 = 5$.

Configuration	Assembly	13.5-in Depth	22.5-in Depth	31.5-in Depth	45.0-in Depth
2A	Dual	1.384	1.700	1.831	1.912
4A	Dual-tandem	1.360	1.673	1.954	2.321
6A	Dual-triple	1.354	1.703	2.085	2.610
2B	Dual	1.482	1.755	1.863	1.929
4B	Dual-tandem	1.424	1.772	2.083	2.488
6B	Dual-triple	1.422	1.843	2.274	2.868
2C	Dual	1.583	1.807	1.893	1.945
4C	Dual-tandem	1.504	1.908	2.257	2.700
6C	Dual-triple	1.497	1.969	2.403	3.025

Table 2. Ratio of ESWL to load on a single truck-assembly wheel for 22.5-in pavement thickness and 4.5-in radius of contact area.

Configuration	Assembly	$E_1/E_2 = 1.0$	$E_1/E_2 = 2.5$	$E_1/E_2 = 5.0$	$E_1/E_2 = 10.0$
2A	Dual	1.639	1.672	1.700	1.728
4A	Dual-tandem	1.563	1.584	1.673	1.821
6A	Dual-triple	1.548	1.601	1.703	1.871
2B	Dual	1.705	1.732	1.755	1.777
4B	Dual-tandem	1.623	1.688	1.772	1.929
6B	Dual-triple	1.645	1.732	1.843	2.027
2C	Dual	1.768	1.789	1.807	1.825
4C	Dual-tandem	1.741	1.819	1.908	2.070
6C	Dual-triple	1.759	1.852	1.969	2.138

Wiseman and Zeitlen (6), Ahlvin and others (2), and other authors have shown that this formula, although based on full-scale testing, can be derived from considerations of shear failure of the subgrade or, in other words, that the design criterion is the maximum shear stress in the subgrade (this criterion and its analogs, such as maximum shear strain or the vertical strain in the subgrade, are compatible with strength theories). In this context it should be noted that determination of maximum shear stress according to a multilayer structure is feasible in specific cases in which the thicknesses and moduli of the layers are known; an approximate solution is obtainable by replacing the multilayer structure with a two-layer one in which the upper layer represents the pavement (7).

The procedure presented here for calculating ESWL is based on equal shear stress and consists of the following steps: (a) determination of the stress tensor for each point of a grid covering the space between the wheels, (b) determination of the principal stresses at each such point, (c) comparison of the maximal shear stresses for the assembly and for a single wheel with the same contact radius, and (d) correction of the ESWL for number of repetitions. The results are formulated as the ratio of the ESWL to one wheel load of the gear.

Tables 1 and 2 give the results of calculations for the road wheel assemblies shown in Figure 1 [partly reproduced from the work of Gerrard and Harrison (5)], and Tables 3 and 4 give results for aircraft gears. It can be seen that the ESWL increases with decreasing wheel spacing, increasing number of wheels, increasing depth, and increasing stiffness of the top layer. For roads, a variation of the pavement/subgrade modular ratio (E_1/E_2) from 3 to 5 or from 5 to 7 [the 3-7 interval is commonly accepted for conventional

Figure 1. Wheel-assembly configurations.

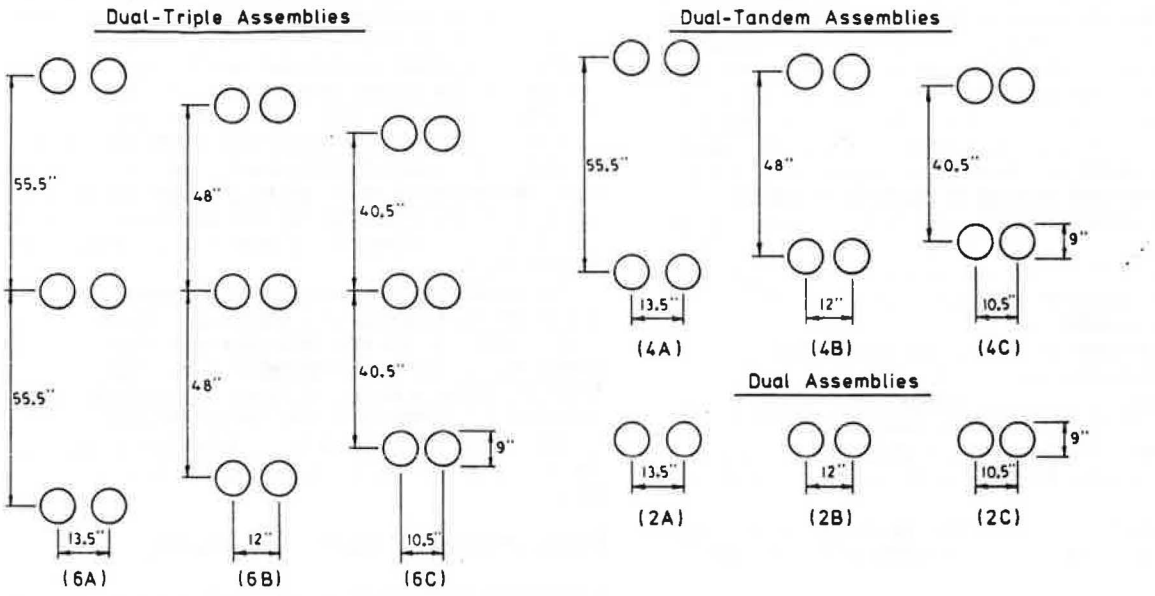

Table 3. Ratio of ESWL to load on a single aircraft-assembly wheel for $E_1/E_2 = 5$.

No. of Wheels	Aircraft	Radius of Contact Area (in)	Contact Pressure (lbf/in²)	Ratio by Depth in Contact Radii			
				3	5	7	10
2	B-727-100	8.587	166.0	1.210	1.521	1.719	1.851
	B-737-220	7.442	148.0	1.286	1.614	1.778	1.884
	DC-9-32	7.265	152.0	1.290	1.619	1.781	1.885
4	B-707-120B	7.514	170.0	1.317	1.719	2.154	2.729
	DC-8-63F	8.359	196.0	1.362	1.865	2.376	2.965
	DC-10-10	9.395	175.0	1.248	1.619	2.062	2.669
	Cv-880	6.800	150.0	1.473	1.989	2.461	3.045
	Concorde	8.928	184.0	1.456	1.924	2.364	2.934
6	L-1011-8	8.768	196.0	1.327	1.853	2.561	3.542
8	B-747F	8.843	185.0	1.300	1.781	2.353	3.244

Table 4. Ratio of ESWL to load on a single aircraft-assembly wheel for 22.5-in pavement thickness and 4.5-in radius of contact area.

No. of Wheels	Aircraft	Depth (in)	$E_1/E_2 = 1$	$E_1/E_2 = 2.5$	$E_1/E_2 = 5$	$E_1/E_2 = 10$
2	B-727-100	60.11	1.663	1.693	1.719	1.745
	B-737-200	52.10	1.733	1.758	1.778	1.799
	DC-9-32	50.86	1.737	1.761	1.781	1.801
4	B-707-1208	52.60	1.728	1.907	2.154	2.490
	DC-8-63F	58.51	2.015	2.168	2.376	2.647
	DC-10-10	65.77	1.542	1.792	2.062	2.401
	Cv-880	47.60	2.157	2.300	2.461	2.780
	Concorde	62.50	2.080	2.214	2.364	2.664
6	L-1011-8	61.38	2.064	2.320	2.561	2.950
8	B-747F	61.90	1.719	1.987	2.353	2.938

pavements, the vertical strain in the subgrade being used as the criterion (7)] changes the wheel-load ratio by about 5 percent and the ratio for airfield runways by about 10 percent. Accordingly, the ESWL determined for a modular ratio of 5 covers a wide range of conventional pavements with sufficient accuracy.

CALIBRATION OF THE MODEL

AASHO Road Test

The configurations used on the AASHO Road Test sections fall in the "wide" and "average" categories. The ESWL was determined from the performance data, as follows:

$$\log(4.2 - p)/2.7 = \beta(\log W - \log \rho) \quad (2)$$

where

$$\rho = 10^{5.93}(D + 1)^{9.36} L_2^{4.33}/(L_1 + L_2)^{4.70} \quad (2a)$$

$$\beta = 0.4 + 0.081(L_1 + L_2)^{3.23}/(D + 1)^{5.19} L_2^{3.23} \quad (2b)$$

$$D = a_1 D_1 + a_2 D_2 + a_3 D_3 \quad (2c)$$

and

- p = final serviceability index of pavement,
- W = number of repetitions,
- D = thickness index or structural number,
- L_1 = assembly load, and
- L_2 = coefficient = 1 for a single assembly and 2 for a tandem assembly.

The results of load on a tandem, equivalent to that on a single assembly (at the same W), for p = 1.5-2.5 and D = 2-6 are given below:

Load on Single Axle (lb)	Load on Tandem Assembly (lb)
24 000	44 000-44 800
22 000	40 400-41 000
20 000	36 600-37 300
18 000	33 000-33 600
16 000	29 300-29 800

As the table indicates, the load ratio ranges from 1.83 to 1.87.

At the same time, Table 1 gives, for the same pair of assemblies, a ratio range of 1.55-2.08 (for loads that have the same ESWL) that decreases with increasing depth (2.04-2.08 for 13.5 in, 1.90-2.01 for 22.5 in, 1.79-1.87 for 31.5 in, and 1.55-1.65 for 45.0 in). (The maximum pavement thickness in the AASHO test was 31 in.) This range stems from the lengthwise distribution pattern of τ_{max}; Figures 2-4 show that for the smaller depth (13.5 in) one pass of the tandem assembly is equivalent to two repetitions, since the maximum occurs twice in a conspicuous manner; by contrast, for the larger depths (>31.5 in), the distribution is flat and each pass is in practice one repetition. According to Equation 1, for small depths and in the $N = 10^4$-10^6 interval, the load ratio corrected for the difference in number of repetitions drops to 1.83-1.90. In summary, for depths corresponding to D = 2-6 (up to 31.5 in in thickness), the ratio equals 1.80-1.90 and decreases with increasing thickness (or D) beyond the results of the AASHO Road Test.

It can therefore be concluded that there is good agreement between ratios of tandem to single load calculated by using the proposed model, taking into account the influence of depth on the number of stress repetitions and load ratios determined from the AASHO Road Test. It should, however, be noted that extrapolation of the AASHO results for pavements with D > 5 may lead to overestimation of the equivalent loads and to underdesign of the pavement. Hence, the model is acceptable or, at worst, slightly on the conservative side.

For the triple-dual assemblies of the A and B classes, the ratio (after correction for shear stress repetitions) is 2.5 for thicknesses less than 31.5 in, and, for 45 in, 2.2 and 2.0 in A and B, respectively. Accordingly, in the first case, under a single-axle load of 12 tons, the equivalent load on a tandem assembly is 21.5 tons and, on a triple assembly, 30 tons; for larger thicknesses, the equivalent load is smaller, as explained above.

Corps of Engineers Test

The U.S. Army Corps of Engineers design method consists of determining the equivalent wheel load according to the criterion of maximum settlement of the subgrade by using Boussinesq's theory and disregarding the stiffness of the pavement—an unrealistic approach, both in terms of the failure mechanism of the subgrade and the properties of the pavement materials. With the advent of B-747, C5A, DC-10, and L-1011 aircraft, the Corps of Engineers undertook one-to-one scale experiments and found that the actual performance of flexible-pavement test sections under the twin-tandem and 12-wheel gear was substantially better than had been predicted under the flexible-pavement design methodology that existed prior to the multiple-wheel heavy-gear-load tests (3). This resulted in modification of Equation 1 by means of the so-called load repetition factor α [see Figure 5(8)], which replaced the expression (0.144 + 0.231 log N) and is a function of the number of wheels in the assembly or gear and of the number of cycles. It should be noted that, even for a single wheel, the factor is no longer linear with log N as its predecessor was. The proposed model is therefore based on the modified design thickness formula, as follows:

$$z_w = \alpha_w \sqrt{(1/8.1\,CBR) - (1/\pi p_{ew})} \cdot \sqrt{Q_w} \quad (3)$$

Here, the subscript w refers to the criterion (subgrade deflection and Boussinesq theory) by which the equivalent wheel load Q was determined, and p_e is the pressure of the equivalent single wheel on a contact area equal to that of one of the wheels.

In the case of ESWL computed according to maximum shear stress, the corresponding equation is

$$z_\tau = \alpha_\tau \sqrt{(1/8.1\,CBR) - (1/\pi p_{e\tau})} \cdot \sqrt{Q_\tau} \quad (3a)$$

where α_τ is the fatigue factor for one wheel. Equating the two expressions, we find

$$\alpha_w/\alpha_\tau = \sqrt{Q_\tau/Q_w} \quad (3b)$$

Figure 6 shows values of Q_τ/Q_w for different aircraft (based on Q, data from Table 3). In the thickness range of 20-40 in, the following values are obtained for α_w/α_τ: Two wheels = 0.91-0.95, four wheels = 0.85, and six and eight wheels = 0.76.

Figure 5 yields the thickness reduction factor (depending on the number of wheels) obtained under the modified approach. The results given below for N = 1000, 10 000, and 100 000 are seen to be close to those obtained

Figure 2. Pattern of distribution of maximal shear stress for single-axle dual assembly.

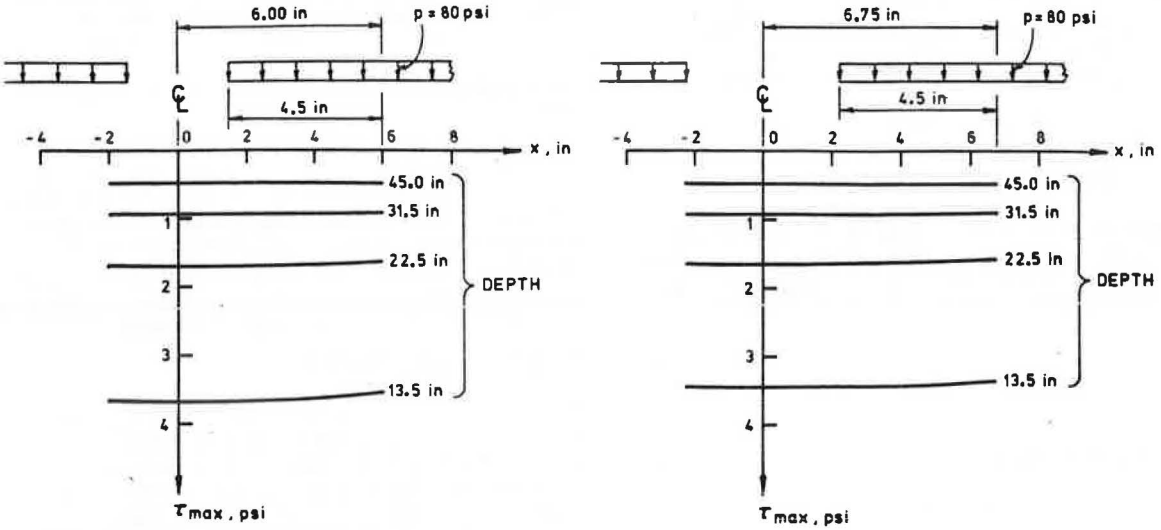

Figure 3. Pattern of distribution of maximal shear stress for dual-tandem assembly.

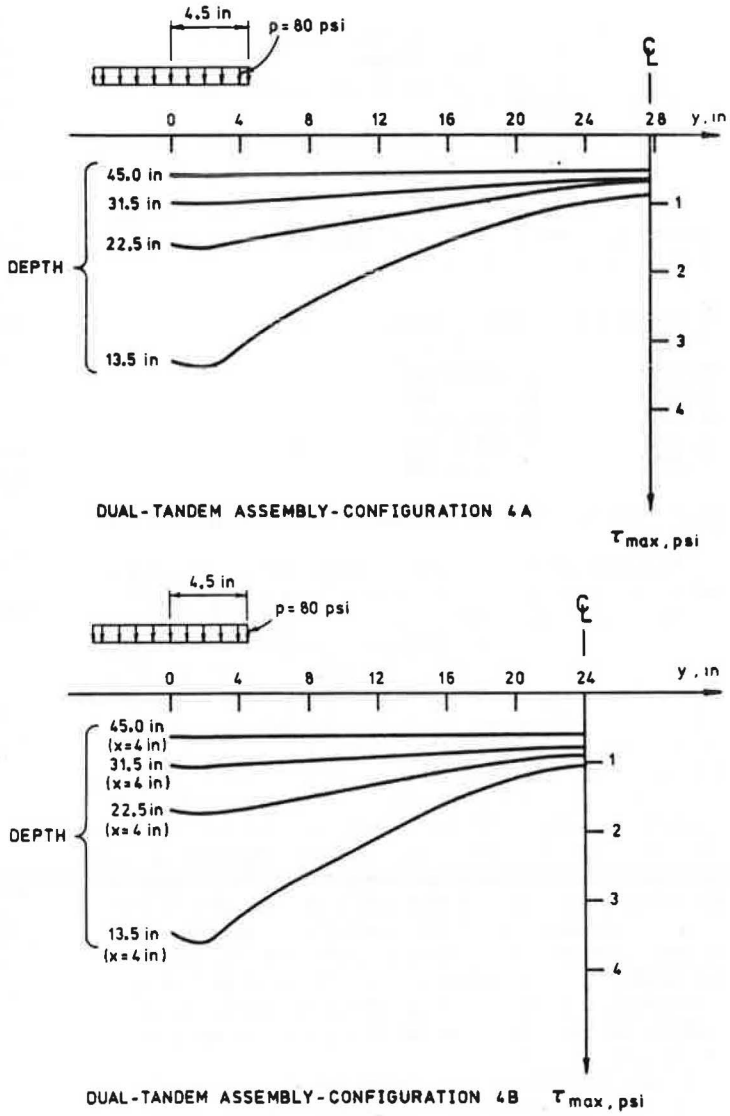

Figure 4. Pattern of distribution of maximal shear stress for dual-triple assembly.

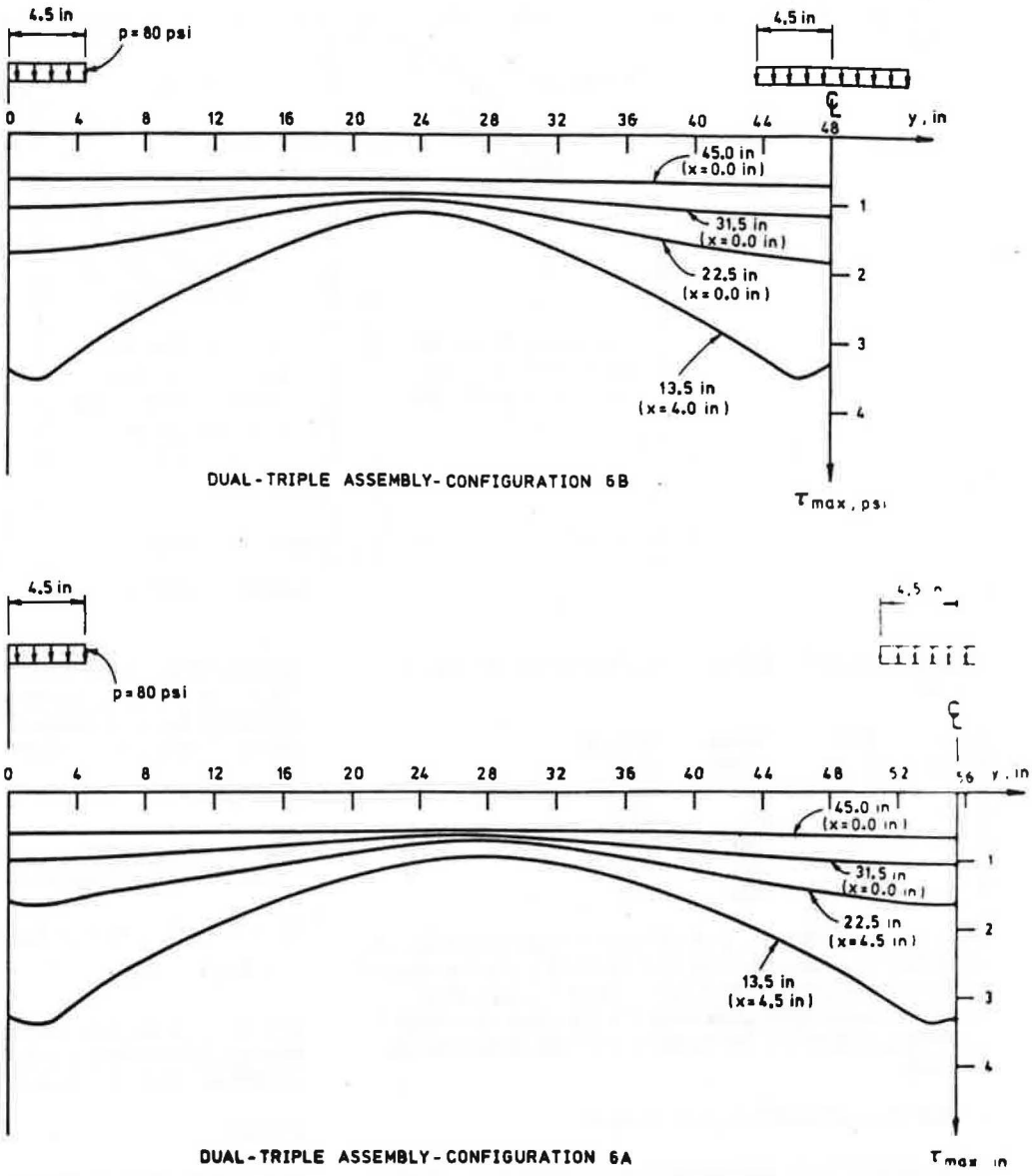

Figure 5. Load repetition factor α versus aircraft traffic volume factors.

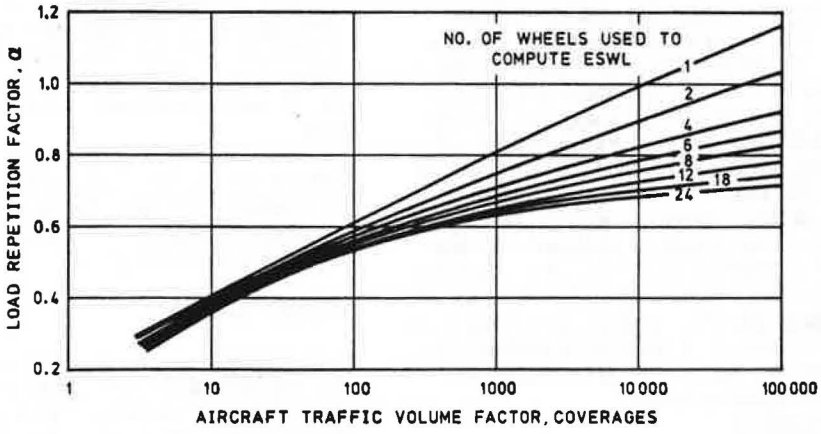

Figure 6. Q_T/Q_W for different aircraft.

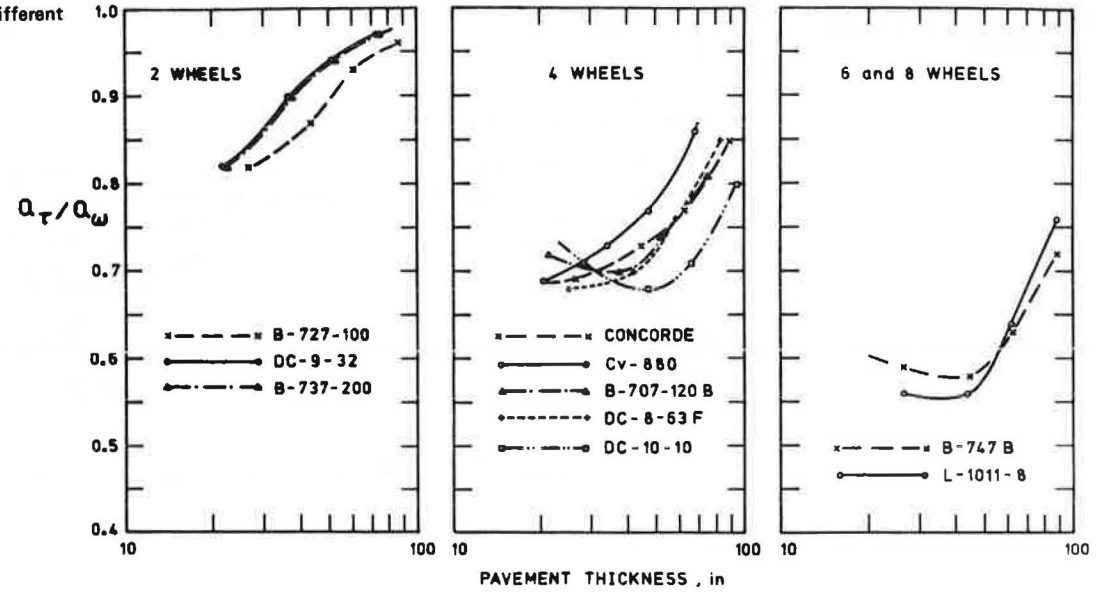

in determining the ESWL according to the proposed model:

No. of Wheels	1000 Cycles	10 000 Cycles	100 000 Cycles
1	1.00	1.00	1.00
2	0.92	0.90	0.89
4	0.87	0.83	0.79
6	0.84	0.79	0.75
8	0.82	0.76	0.71

Thus, $\alpha_r \cong 1$; that is, if the Corps of Engineers design formula for a single wheel (corrected for the number of cycles) is adopted in conjunction with the proposed model, the resulting pavement thicknesses are close to those obtained under the modified Corps of Engineers method.

INDUSTRY-ORIENTED APPROACH

In the conventional approach used in the preceding sections, the ESWL was determined for a given wheel-assembly configuration at a constant number of load cycles (the equivalent load obtained with the model calibrated according to the AASHO Road Test was reduced to preserve this constancy). However, economic considerations make it preferable to use an approach based on the tonnage carried by the road, i.e., on the equivalent load that corresponds to transportation of a given tonnage, subject to the same reduction in the serviceability index of the road. (Although it is the net tonnage that counts in the economic analysis, the present calculation is based on the gross; it is known that the net increases with the number of axles.) For example, if we compare simple dual axles and tandems, then, since for equal damage and one pass the allowable load on the tandem axle is larger, a smaller N suffices for the given tonnage and the load on the tandem can be further increased for equal damage.

Tonnage T is defined as

$$T = \sum_i W_i P_i \qquad (4)$$

where W_i is the number of repetitions of configuration i under load P_i.

In comparing the equivalent loads for a single-axle assembly and a tandem according to the AASHO Road Test, we refer to tables given in the AASHO Interim Guide (9) for the necessary values of the traffic equivalence factor, defined as

$$F_j = W_{18}/W_j \qquad (4a)$$

where j represents a given traffic class with a uniform configuration. Combining the above two equations yields

$$T = W_j P_j = (W_{18}/F_j)P_j = W_{18}P_{18}(P_j/P_{18}) \cdot (1/F_j)$$
$$= (T/P_{18}) \cdot (P_j/F_j) \qquad (4b)$$

where P_j is the load (in thousands of pounds) for the configuration alternative to a single axle under P_{18} = 18 000 lb (18 kip). Hence,

$$P_j = 18F_j \qquad (4c)$$

The tables given in the AASHO Interim Guide (9) show that the equivalent load on a tandem is 39 000 lb for a structural number of 1-6. In other words, a given tonnage can be carried on a single-axle assembly under 18 000 lb, or a tandem under 39 000 lb, and the numbers of repetitions corresponding to these would result in the same reduction in the serviceability index of the road.

For other configurations (triple assemblies and still larger ones), the same model used before can be used in similar analyses. Equation 4c applies for economic analyses that include truckage, construction, and maintenance strategies.

CONCLUSIONS

The theoretical model proposed here for determining the equivalent loads for different wheel-assembly configurations is based on a simple and realistic representation of the pavement (a two-layer structure) and on a criterion that is compatible with the failure mechanism of flexible pavements (the maximal shear stress at the top of the subgrade). By this means, minimal deviation is assumed from the expected behavior of the pavement. The model was first calibrated on the basis of AASHO Road Test results by comparing the equivalent loads for a single-axle and a tandem-axle assembly, and the re-

sults were in good agreement. Calibration was then carried out on the basis of U.S. Army Corps of Engineers testing, which covers a wider variety of configurations, and, again, the results provided justification for the model.

Finally, an industry-oriented approach is presented for the analysis of equivalent loads, the criterion being transportation of a given tonnage and similar reduction of the serviceability index of the road. According to this approach, the equivalent allowable load on tandem- and triple-axle assemblies in relation to design single-axle load can be determined.

The model is a useful tool for determining allowable loads for different wheel-assembly configurations and for slightly unconventional conditions, such as excessive pavement thickness. Further improvement, as well as adaptation to specific local conditions, can be achieved through field performance studies.

REFERENCES

1. The AASHO Road Test: Report 5—Pavement Research. HRB, Special Rept. 61E, 1962.
2. R. G. Ahlvin and others. Multiple-Wheel Heavy Gear Load Pavement Tests. U.S. Air Force Weapons Laboratory, NM, Tech. Rept. AFWL-TR-70-113, Vol. 1, 1971.
3. D. N. Brown and J. L. Rice. Airfield Pavement Requirements for Multiple-Wheel Heavy Gear Loads. Federal Aviation Administration, U.S. Department of Transportation, Rept. FAA-RD-70-77, 1971.
4. E. J. Yoder and M. W. Witczak. Principles of Pavement Design. Wiley, New York, 2nd Ed., 1973.
5. C. M. Gerrard and W. J. Harrison. A Theoretical Comparison of the Effects of Dual-Tandem and Dual-Wheel Assemblies on Pavements. Proc., 5th Conference of the Australian Road Research Board, Vol. 5, Part 4, Paper 645, 1970, pp. 112-137.
6. G. Wiseman and J. G. Zeitlen. A Comparison Between CBR and the Shear Strength Methods in the Design of Flexible Pavements. Proc., 5th International Conference on Soil Mechanics and Foundation Engineering, Paris, 1961, pp. 359-366.
7. J. Uzan, M. Livneh, and I. Ishai. Thickness Design of Flexible Pavements with Different Layer Structures. Technion, Haifa, Israel, 1978.
8. U.S. Army Corps of Engineers. Criteria for Airport Pavements: Chapter 7—New Criteria for Pavement Design and Construction. Federal Aviation Administration, U.S. Department of Transportation, Final Summary Rept. FAA-RD-74-35, 1974, pp. 1-14.
9. AASHO Interim Guide for Design of Pavement Structures. AASHO, Washington, DC, 1972.

Publication of this paper sponsored by Committee on Flexible Pavement Design.

Evaluation of Full-Depth Asphalt Pavements

Erland O. Lukanen, Research and Development Section, Minnesota Department of Transportation, St. Paul

A research investigation begun in 1971 by the Minnesota Department of Transportation to learn more about the behavior of full-depth asphalt pavements is reported. The project has 26 test sections, each 365.8 m (1200 ft) long, of a variety of thicknesses, and on a variety of soils. The major portion of the research consisted of Benkelman beam measurements at 15.2-m (50-ft) intervals, taken weekly during the spring, biweekly in the summer, and monthly in the fall. The temperature of the upper 3.8 cm (1.5 in) of the mat was measured each time the Benkelman beam deflections were measured. These data were then used to determine the effect of temperature and season on deflections and to create a set of correction factors to apply to the measured deflections so as to adjust them to a 26.7°C (80°F) peak season deflection. This peak season deflection was then taken to be the standard deflection for each test section. These standard deflections were compared with the deflections of aggregate-base pavements, and a relation was developed between the full-depth thickness and the granular equivalency of an aggregate-base pavement with an equal deflection. That relation was used to develop a design chart for full-depth bituminous pavement, which is the deflection equivalent of the flexible-pavement design chart currently used by the Minnesota Department of Transportation.

The purpose of pavement design is to provide a structure of adequate thickness and strength to carry expected traffic loads. Various designs that are considered to be adequate are then examined for construction and maintenance costs so that the engineer can choose the most economical pavement design.

Before 1969, the Minnesota Department of Highways had to choose between rigid pavement or flexible pavement with an aggregate base. In June 1969, "full-depth" asphalt was approved and included as a design alternative, adding a third choice for pavement selection. The alternate allowed 2.5 cm (1 in) of bituminous base to replace 5.1 cm (2 in) of aggregate base. But, although full-depth pavement was approved, very little was known about its structural response to axle loads or its performance under traffic.

The Physical Research Unit of the Minnesota Department of Highways began evaluation of full-depth pavements in 1971 with the prime objective of determining a unit granular equivalent (GE) value for hot-plant-mix bituminous base. The Minnesota project consists of 26 test sections that cover a range of soil types and full-depth thicknesses (see Table 1). To include new test sections on new construction projects, four test sections were designed and constructed: one flexible pavement section with an aggregate base that represents the typical section from the project plans, one full-depth section with an equal GE, and two additional full-depth test sections, one of which had a 5.1-cm (2-in) reduction in full-depth thickness and the other a 10.2-cm (4-in) reduction in full-depth thickness. The reduced sections were included to reduce the time required to make performance

Table 1. Test sections.

Test Section	Highway	Year Built	Surface Thickness (cm)	Base Thickness (cm)	Subgrade	R-Value	Approximate Location
201	MN-23	1970	9	30.5	A-6	8.5	Marshall
202	MN-23	1970	7.5	25.5	A-6	10	Marshall
203	MN-23	1970	7.5	10	A-3	72	Marshall
204	US-212	1971	7.5	12.5 30.5[a]	A-4	23	Madison
205	US-212	1971	7.5	25.5	A-4	21	Madison
206	US-212	1971	7.5	23	A-4	17	Madison
207	US-212	1971	7.5	15	A-6	20	Madison
208	MN-13	1972	5	15	A-6	19.7	Prior Lake
209	MN-13	1972	5	10	A-6	18.7	Prior Lake
210	MN-13	1972	5	20	A-6	21.5	Prior Lake
211	US-169	1974	4	8.5	A-4	58	Princeton
212	US-169	1974	4	16	A-4	59	Princeton
213	US-169	1974	4	23	A-4	52	Princeton
CS 212	US-169	1974	4	8.5 15[a]	A-4	59	Princeton
CS 213	US-169	1974	4	3 46[a]	A-4	60	Princeton
214	US-10	1976	11.5	16.5	A-2-4	12	New York Mills
215	US-10	1976	11.5	16.5	A-6	21	New York Mills
216	US-10	1976	7.5	16.5	A-2-4	65	New York Mills
217	US-10	1976	7.5	14	A-2-4	70	New York Mills
218	US-10	1976	7.5	21.5	A-2-4	57	New York Mills
219	US-10	1976	11.5	16.5	A-6	10	New York Mills
220	US-10	1976	6.5	35.5	A-2-4	18	New York Mills
1	Kandiyohi County Road 1	1970	13.5		A-6	26	Willmar
2	Kandiyohi County Road 1	1970	18		A-4	26	Sunberg
3	Kandiyohi County Road 20	1970	10.5		A-7-6	21	Willmar
4	Kandiyohi County Road 4	1970	14.5		A-6	18	Lake Lillian
102	MN-109	1963	5	21.5 5[a]	A-4	17	Wells

Note: 1 cm = 0.39 in.
[a]Aggregate.

evaluations and to provide more thickness variables for purposes of analysis.

Materials sampled for the investigation consisted of core samples and subgrade samples. Tests conducted on the test sections consisted of periodic Benkelman beam deflection measurements and corresponding measurements of pavement temperature, annual measurements of rut depth, roughometer index measurements, Mays road meter measurements, and surface condition ratings.

Laboratory work consisted of measurements of bituminous layer thickness from the cores, densities, extractions, gradation, penetration, and air voids. The subgrade samples were examined for Hveem stabilometer R-value, AASHO T-99 moisture density relations, gradations, and Atterberg limits.

The analytic work on this project had two objectives: (a) to determine the temperature and seasonal effects on deflections and (b) to determine how many centimeters of aggregate base it takes to reduce the Benkelman beam deflection to the same amount as that of bituminous base. The objectives were ranked in this order because the second was not possible without the first.

The loss in serviceability is too small at this time to determine the performance of full-depth pavements on all but two sections. Evidence is available, however, from the Brampton Test Road and the San Diego County Experimental Base Project, that the performance of full-depth pavement is at least as good as that of aggregate-base flexible pavement if the two have equal deflection values. This investigation will be continued until the test sections yield sufficient data to determine the performance capabilities of full-depth pavement.

CURRENT DESIGN OF FLEXIBLE PAVEMENT

A brief description of the basis for the current design of flexible pavement is included here to provide a better understanding of the basis of the research on full-depth pavement. Current flexible-pavement design is a product of Minnesota Investigation 183 (1). It combines the relation between deflection and 80-kN (18 000-lbf) standard axle loads (see Figure 1) derived from the AASHO Road Test (2, p. 110) with the relation between deflections, pavement GE, and embankment R-value (see Figure 2) derived from Minnesota test sections in Investigation 183 (1, p. 50). These two relations were algebraically combined, and the deflection terms were canceled. The resulting equation was then solved for GE. The following equation results:

$$GE = -69.6 + 35.8 \log(\Sigma N18) - 60.5 \log R \quad (1)$$

where

GE = granular equivalent (cm),
ΣN18 = sum of the 80-kN axle loads carried to a present serviceability index (PSI) of 2.5, and
R = Hveem stabilometer value at 1.65 MPa (240 lbf/in^2).

This equation is the basis of the Minnesota flexible-pavement design chart. Since the Minnesota relations used to develop the design equation were based on conventional aggregate-base flexible pavements, there was a concern for extending the design chart to include full-depth pavements.

Figure 1. AASHO Road Test relation between peak average spring deflections and standard equivalent 80-kN axle loads at PSI of 2.5.

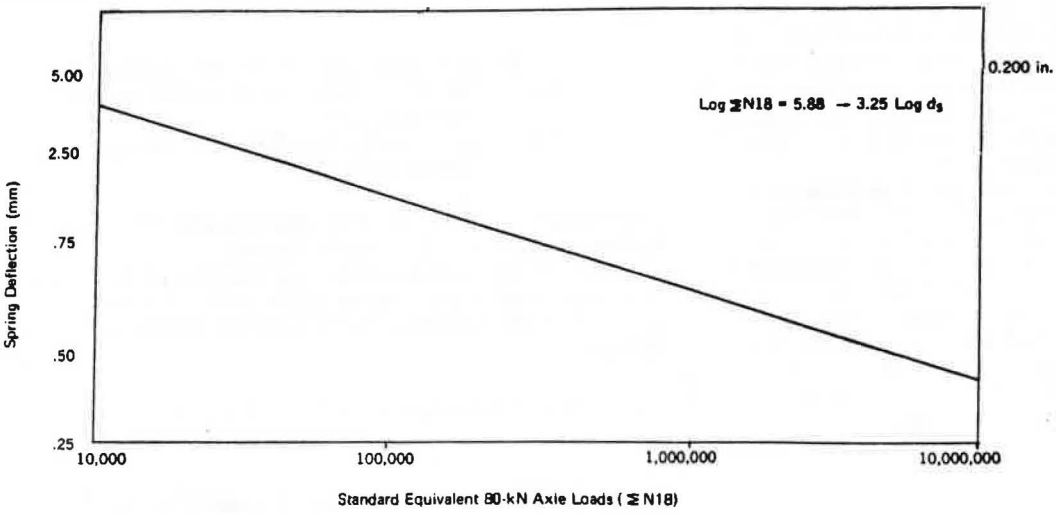

Figure 2. Relation between pavement deflection, GE, and R-value.

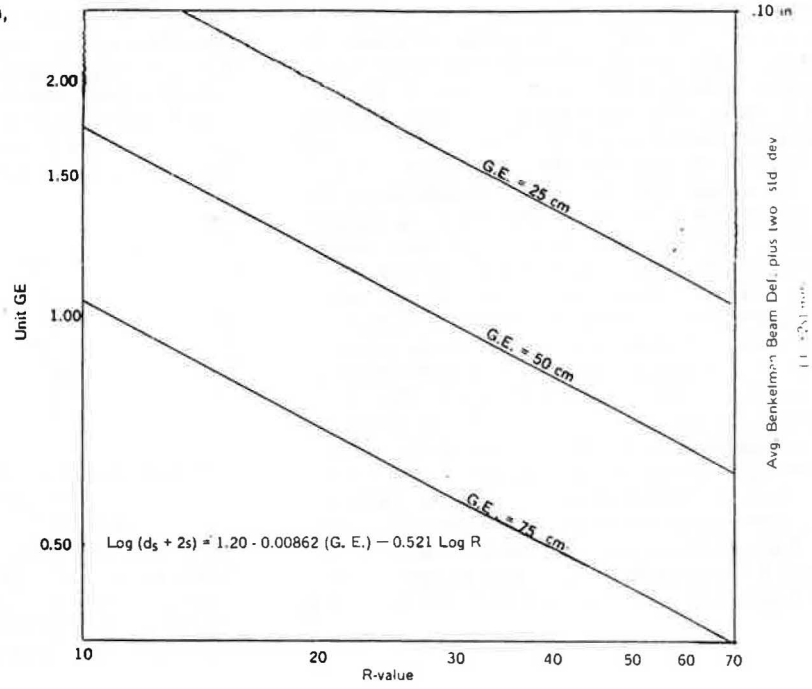

DATA ACQUISITION

Materials samples of all of the pavement materials and subgrade were obtained from the test sections. The bituminous samples were obtained by taking 15.2-cm (6-in) diameter cores from the test sections. A minimum of three bituminous samples (consisting of three cores) were generally taken from each section. The individual thickness of each layer was measured from the cores. Other tests, such as aggregate gradation, asphalt content, and density, were run to verify that the mix was within specifications.

Subgrade samples were also obtained from the test sections and sent to the central office laboratory, where they were analyzed for gradation, Atterberg limits, American Association of State Highway and Transportation Officials (AASHTO) soil classification, and Hveem stabilometer R-values (3) at a 1.65-MPa (240-lbf/in^2) exudation pressure. (The subgrade R-value has been found to have a good correlation with the maximum spring deflections for aggregate-base flexible pavements and is used in this investigation to characterize soil strength.)

Deflection measurements were made at 15.24-m (50-ft) intervals throughout the test section; this produced 25 deflection measurements in 365.76 m (1200 ft). The average of the 25 deflections is then the representative deflection for that test section, uncorrected for temperature and season.

To determine the seasonal deflection response of the test sections, deflections were taken as follows: weekly from mid-March to the end of May, biweekly from June through August, and monthly in September and October.

To find the effect of temperature on the test section deflections, pavement temperature was measured each time the deflections were measured. Pavement temper-

ature was measured by driving a hole in the pavement 3.8 cm (1.5 in) deep, filling it with light machine oil, and placing a thermometer in the hole. The temperature was allowed to come to equilibrium while the deflections were taken and then read. It should be noted that this is not a surface temperature but an average temperature of the upper 3.8 cm of the mat. This method of measurement was found to be adequate for correlating pavement deflection with pavement temperature.

Ride, rut depth, cracking, and patching were also measured on each test section each year. Ride was measured by using two devices: the PCA road meter and the BPR roughometer. Rut depths were measured in the outer wheel path at 15.24-m (50-ft) intervals by use of an A-frame. These measurements were then averaged to produce one representative rut depth per test section. The survey of surface condition conducted in this investigation was very limited. Basically, it included only multiple cracking and patching.

ANALYSIS

Adjusting Deflections for Temperature

When the data analysis began, the first task was to characterize each test section by a Benkelman beam deflection value. This initially caused concern because of the variance in deflection values on the test sections throughout the year. Figure 3 shows the typical deflection response exhibited by a section from March through October. Since it was felt that the deflections of full-depth pavements were quite temperature dependent, the first task was to find a way to correct for temperature.

Since most of the data spanned a period from early March to mid-October and a 50° C (90° F) temperature range, there were no direct methods available to determine a temperature-deflection relation that was independent of date. Statistical regression techniques were then used to determine the effect of temperature and date. The first attempt was a three-variable regression of the average deflection of the test sections versus mat temperature and date. The results were surprising in that, for most of the sections, the date was not a significant factor in the regression and the mat temperature explained nearly all of the deflection variance. The sections were then rerun in a two-variable regression of deflection versus temperature. From each regression, a set of factors were developed, as follows:

$$MTCF = \text{def } 26.7°C/\text{def } (T) \quad (2)$$

where

MTCF = mat-temperature correction factor,
def 26.7°C = 26.7°C (80°F) deflection predicted by regression, and
def (T) = deflection predicted by regression at temperature T.

The factors for the individual sections and years used in the analysis are shown in Figure 4.

A two-variable regression was then run to relate the mat-temperature correction factor to the mat temperature. The best correlation resulted in the following relation:

$$\overline{MTCF} = 111.791\,81\,[(9/5)C + 32]^{-1.075\,31} \quad R = 0.95$$
$$SE = 0.05(\log) = 1.75 \text{ percent} \quad (3)$$

where $\overline{MTCF}$ = the average mat-temperature correction factor and C = mat temperature of the upper 3.8 cm (1.5 in) (°C).

The correlation is good, and the standard error is small enough to suggest that there is little difference in the correction factors from one test section to another. The above expression can thus be used to generate a set of MTCFs for mean deflections at mat temperatures other than 26.7°C (80°F). MTCFs are plotted in Figure 5 and given in the table below [$t°C = (t°F - 32)/1.8$]:

Mat Temperature (°C)	$\overline{MTCF}$	Mat Temperature (°C)	$\overline{MTCF}$
5	2.06	30	0.93
10	1.67	35	0.84
15	1.39	40	0.76
20	1.20	45	0.69
25	1.05	50	0.64
26.7	1.00		

It is interesting to note that the factors increase quite rapidly at mat temperatures below 26.7°C, which indicates significant increases in pavement strength at those lower temperatures. Above 26.7°C, the pavement continues to become weaker as indicated by the fractional correction factors above that temperature. This is in contrast to the conventional aggregate-base flexible pavements that have thinner bituminous layers; in these

Figure 3. Deflections for test section 207 in 1972.

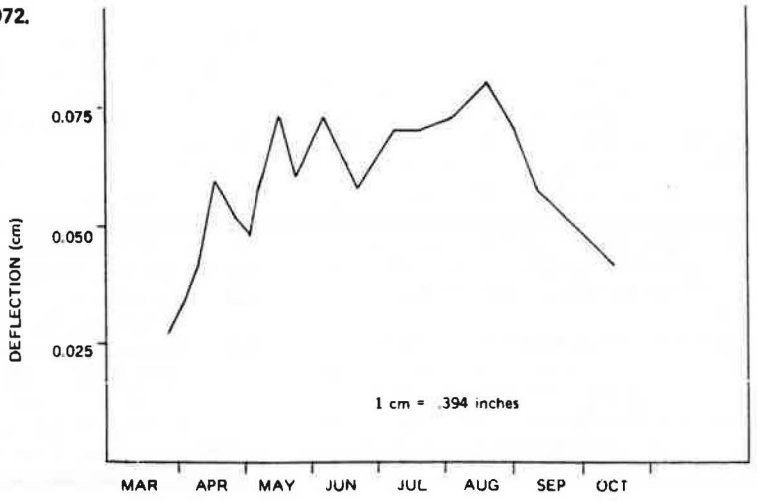

Figure 4. Correction factors for correcting full-depth 26.7°C deflections to deflections at any temperature.

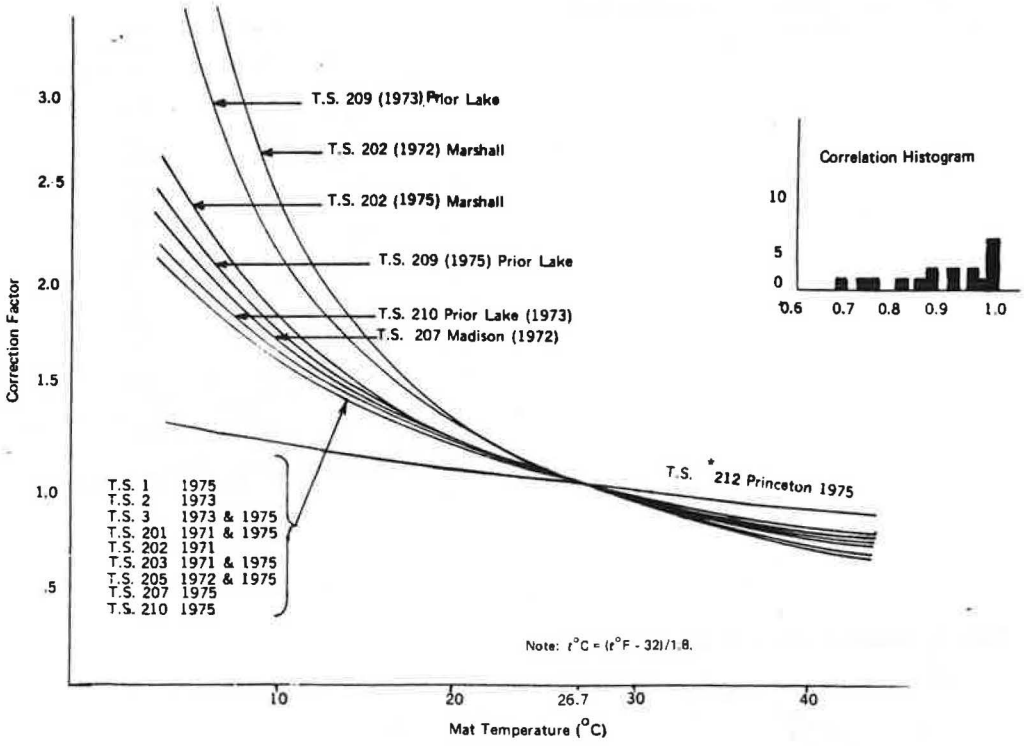

Figure 5. Temperature adjustment factors for Benkelman beam deflections on full-depth pavement.

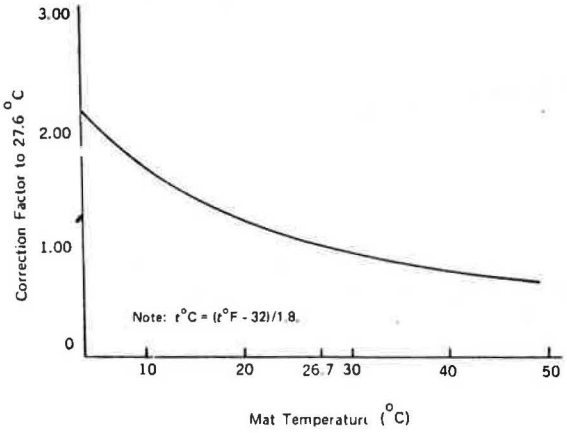

pavements, the mat temperature does not appreciably affect pavement strength above 26.7°C. The shape of the curve in Figure 5 for factor versus temperature is similar to a curve recommended by the Asphalt Institute.

Once the approximate mat-temperature effect on the mean spring recovery deflections had been determined, the spring recovery deflections for each test section were corrected to a mat temperature of 26.7°C by using the temperature correction factors. An analysis of the temperature-corrected deflections showed a definite relation between deflection and date. A suitable relationship between the corrected deflections and the date at which they were recorded was then determined. The relation took the following form:

$$\ln \overline{BB}_{26.7} = \ln a_0 + a_1 \ln D + a_2 D \quad (4)$$

where

$\overline{BB}_{26.7}$ = average mat-temperature-corrected spring recovery deflection,
D = day of the year, and
a_0, a_1, and a_2 = regression coefficients.

In all instances, time significantly affected the the average mat-temperature-corrected defle

To aid in comparing the effect of time on the recovery deflection of each test section, the m $\overline{BB}_{26.7}$ predicted by the relation and the averag which it occurred were calculated. The result given in Table 2. The data show that the maxi spring 26.7°C deflection occurs between about t of May and the middle of June.

To determine the average time effect, spring covery correction factors were generated for e section in Table 2 by determining the ratio betw deflections calculated for other times in the yea the calculated maximum 26.7°C deflection. Th were then compared with the corresponding dat a correlation. The result of the analysis was a

$$\overline{SRCF} = 24.281\,82\,(D)^{-0.808\,75}\, e^{0.005\,788\,(D)}$$

R = 0.86 SE = 0.05 on ln $\overline{SRCF}$

where $\overline{SRCF}$ = average spring recovery correction f and D = number of days into the year (April 26 is 11

The correlation is good, and the standard error is small enough to suggest that there is little differenc in the correction factors from one test section to anot r The above expression can thus be used to generate a average set of spring recovery factors for the mean m at temperature-corrected deflection. The spring recover correction factors are given below:

Date	Factor	Date	Factor
March 1	1.25	June 29	1.03
March 16	1.14	July 24	1.06
March 31	1.07	July 29	1.08
April 15	1.03	August 13	1.12
April 30	1.01	August 28	1.16
May 15	1.00	September 12	1.20
May 30	1.01	September 18	1.25
June 14	1.02	October 12	1.31

Table 2. Date of peak-temperature-corrected deflection by test section and year.

Test Section	Year	Predicted Peak $\overline{BB}_{26.7}$* (mm)	Day into Year of Maximum Deflections	Pavement Thickness (cm)	Embankment	
					Subgrade	R-Value
102	1973	0.85	117	25.4	A-4	17
102	1974	0.86	131	25.4	A-4	17
102	1975	0.76	142	25.4	A-4	17
201	1971	0.38	137	39.4	A-6	8.5
201	1975	0.39	128	39.4	A-6	8.5
202	1971	0.46	138	33.0	A-6	10
202	1975	0.47	145	33.0	A-6	10
203	1971	0.36	136	17.8	A-3	72
203	1972	0.32	132	17.8	A-3	72
203	1975	0.25	162	17.8	A-3	72
207	1972	0.57	148	22.9	A-6	20
208	1975	1.63	150	20.3	A-6	20[b]
209	1975	1.88	141	15.2	A-6	19°[c]
210	1975	0.81	167	25.4	A-6	22[b]
212	1975	0.85	128	19.7	A-4	59

Note: 1 mm = 0.039 in; 1 cm = 0.39 in; $t°C = (t°F - 32)/1.8$.

* The maximum deflection value as determined from $\overline{BB}_{26.7} = a_1 (D)^{a_2} 1e^{a_2 D}$, not the maximum observed deflection corrected to 26.7°C.

[b] R-value given is that obtained prior to paving.

[c] Subgrade samples taken from the subgrade in the northbound lane, during later maintenance repair, resulted in R values between 8 and 10.

Figure 6. Benkelman beam deflection response to season.

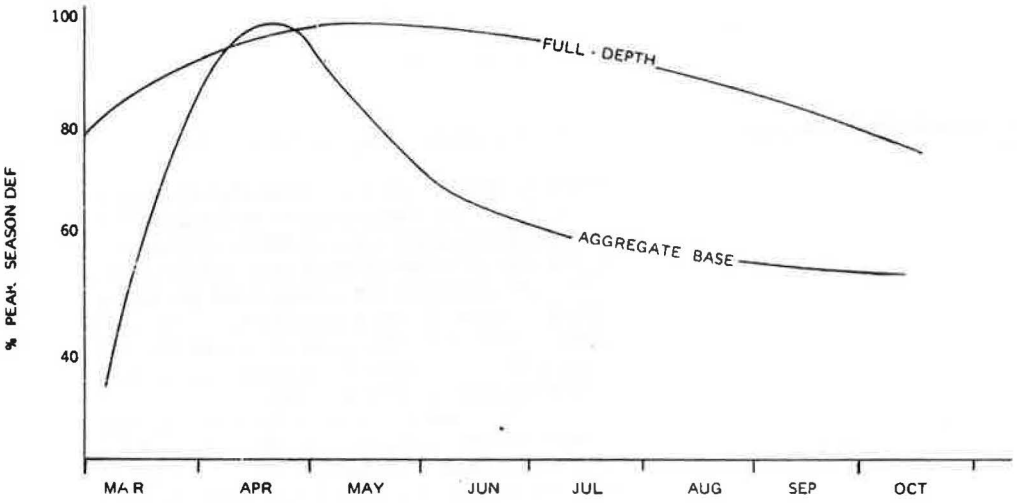

Figure 7. Full-depth correction factors to correct deflections for season and temperature.

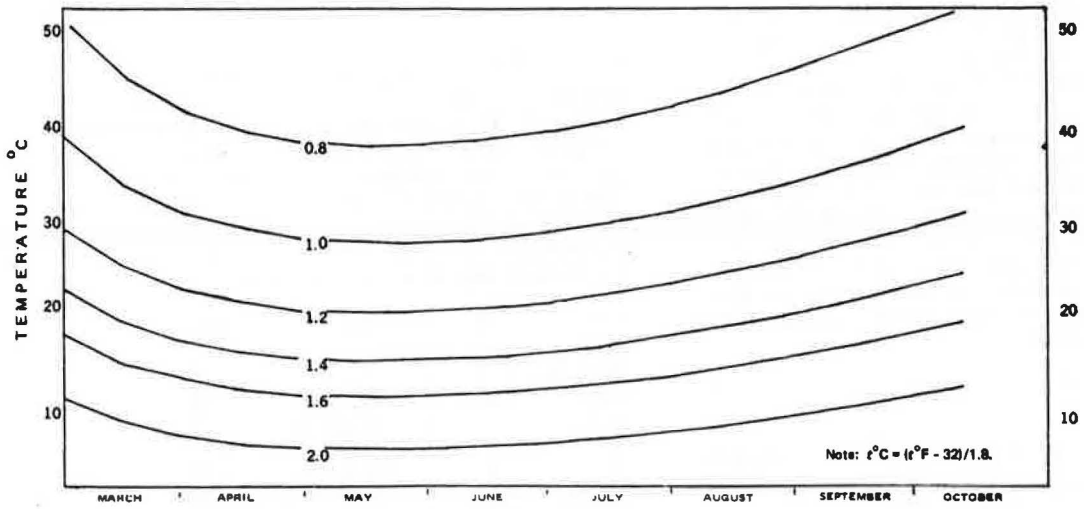

It can be seen that the peak seasonal deflection can be expected from the middle of April through the end of June. In addition, the correction factors are small in comparison with the seasonal correction factors developed for flexible pavements that have aggregate bases (4), as shown in Figure 6.

The factors obtained in this investigation represent mostly plastic soil subgrades, which are found exclusively in the southern half of the state. Early- and late-season factors given above may be low when they are used to adjust the deflection of a full-depth pavement in the northern part of the state because of the later spring thaw and earlier freeze.

Correction Factor for Date and Temperature

To quicken the process of correcting deflections for temperature and date, the above two relations were combined and put into graph form, as shown in Figure 7. To use this graph, the Benkelman beam operator enters the graph on the right or left side at the measured mat temperature and goes horizontally into the graph to the date on which the deflection was taken. The factor is then interpolated by its position between the factor contour lines. For example, a 15.6°C (60°F) mat temperature on April 15 has a correction factor of 1.42; or a 43.3°C (110°F) mat temperature on August 15 has a correction factor of 0.80. It should be noted that the mat temperature for which Figure 7 was developed is the average temperature of the upper 3.8 cm (1.5 in) of the pavement surface. For the greatest possible accuracy, low mat temperatures or early- or late-season deflection measurements should be avoided if possible.

Deflection Behavior in Full-Depth Pavements

The following observations can be made concerning deflection behavior in full-depth pavements:

1. Full-depth pavement deflections, when corrected for temperature, generally peak in mid-May, whereas conventional pavements generally peak in mid-April. The actual uncorrected deflection peak for full-depth pavement occurs from mid-June to mid-July because of the high pavement temperatures.
2. Mat temperature has a marked moderating effect on the spring recovery in full-depth pavement. Deflections will peak in late spring and will not drop off significantly until late summer or early fall.
3. The thinner the pavement becomes, the larger the spring recovery correction factors tend to be. Deflection for full-depth pavements that are less than 14 cm (5.5 in) thick should not be corrected by use of the spring recovery factors given in this paper.
4. The spring recovery factors given in the table above are typical of full-depth thicknesses of ≥14 cm on weak soils such as plastic A-4 and A-6 soils in the Stabilometer R-value range of 5-25. Although there have been indications that the factors apply to other soils (test section 203 on an A-3 soil), there are not enough data at this time for valid conclusions.
5. Because of the small spring recovery factors, a weak period for full-depth pavement cannot be sharply defined. For that reason, it would be very risky to build a thin full-depth pavement with the intention of restricting axle loads in the spring. To protect a full-depth pavement by means of axle-load restrictions during its peak deflection period, the restrictions would have to remain in effect until fall.

Full-Depth Granular Equivalency

Now, with the ability to assign a standardized deflection value to a full-depth pavement, structural analysis can be done. Several methods were used and are briefly described here.

The first method described involved computing a GE for each full-depth test section from the temperatures, seasonally corrected deflections, and subgrade R-values of the sections. The equation used for this computation relates the average peak spring deflection of a flexible pavement with an aggregate base to its GE and subgrade R-value. The computed GE was then correlated with the thickness of the full-depth test sections to produce a GE-thickness relation (see Figure 8). This relation is used to develop the full-depth design chart shown in Figure 9. Minimum thickness designs, based on the R-values included in the full-depth design chart, are based on the full-depth thickness, which is equivalent to the GE required to limit the average deflection plus two standard deviations to 1.9 mm (0.075 in). It should be noted that this method does not result in a single fixed GE for a full-depth pavement.

Another GE analysis compared the deflections of full-depth test sections with the adjacent control sections.

A determination of the GE of bituminous base of the aggregate-base control sections yields a unit GE of 2.57 for test sections 205 and 206 in comparison with test section 204. A unit GE of 2.32 is obtained for test sections 208, 209, and 210 in comparison with the deflection behavior of the aggregate-base test sections on the adjoining project. Comparison of test sections 211 and 213 with control sections 212 and 213 yields a unit GE of 1.81 and 2.51, respectively.

Test sections 214-216 and 218 and 219 provide a unique opportunity to evaluate bituminous base. These test sections are all in the outside lanes of a four-lane roadway and can be compared with aggregate-base test sections adjacent to them in the inside lanes. These test-section pairs are used to directly compare the deflection resistance capabilities (GE) of bituminous base and aggregate base. Because these sections occur on the same embankment side by side, all other factors should be about as close to equal as can be expected in the field. A deflection analysis of these sections yields an average unit GE of 2.78. This result is based on only one set of deflection measurements that were obtained late in the fall of a drought year. Additional deflection measurements are needed to substantiate these results.

Edge Effect on Deflections

A special deflection study was run to determine the deflection behavior of a full-depth pavement near its edge. There were two objectives in this study: (a) to determine the design thickness of full-depth widenings next to a portland cement concrete pavement and (b) to determine the distance the bituminous base should extend beyond the outer wheel track of a full-depth pavement.

The deflections that have been discussed so far are slab deflections that were taken about 1.5 m (5 ft) from the edge of the bituminous base. These deflections are fairly representative of the interior portion of a uniformly supported slab. Full-depth widenings, however, are narrow and thus approach the behavior of a strip foundation rather than that of a slab.

A special deflection study was conducted on test sections 201 and 203 to quantify this difference in deflection. To ensure equal field conditions, deflections were first measured at 0.3-m (1-ft) intervals from 2.74 to 3.66 m (9-12 ft) from the centerline, at 0.15-m (0.5-ft) intervals to the edge of the bituminous base 4.56 m (15 ft)

from the centerline, and then at 0.3-m intervals to the edge of the shoulder at three locations per test section. No increase in deflections (attributable to the edge effect) was noted until beyond the 3.66-m (12-ft) edge stripe, which indicates that the standard 9.14-m (30-ft) width of bituminous base could be reduced to 8.53 m (28 ft) without excessive deflections in the outer wheel path. On four-lane roadways, the center of the base should be shifted 0.3 m to the right to provide the protection required for right-shoulder traffic encroachment.

After the first set of deflections was measured, the slab was sawed longitudinally 3.66 m (12 ft) from the centerline for 12.2 m (40 ft). Deflections were then taken at 2.44, 2.74, 3.05, 3.35, and 3.96 m (8, 9, 10, 11, and 13 ft) from the centerline. The deflection at 3.96 m is of particular interest here because it is the deflection of a strip footing rather than a slab. The deflection was found to increase by about 30 percent for the

Figure 8. Full-depth thickness versus GE.

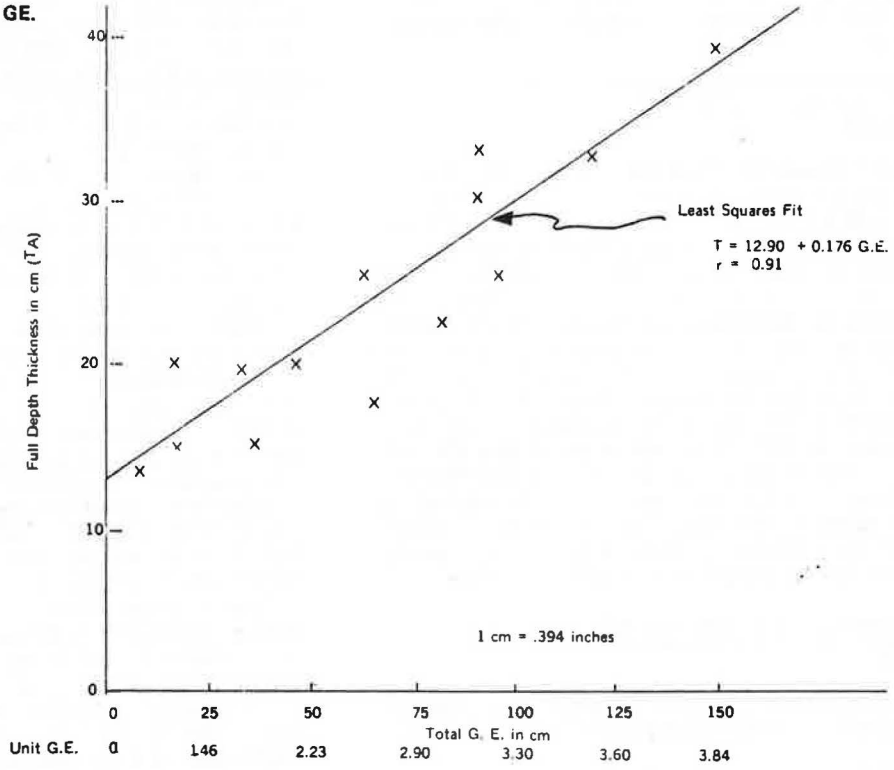

Figure 9. Design chart for full-depth bituminous pavement.

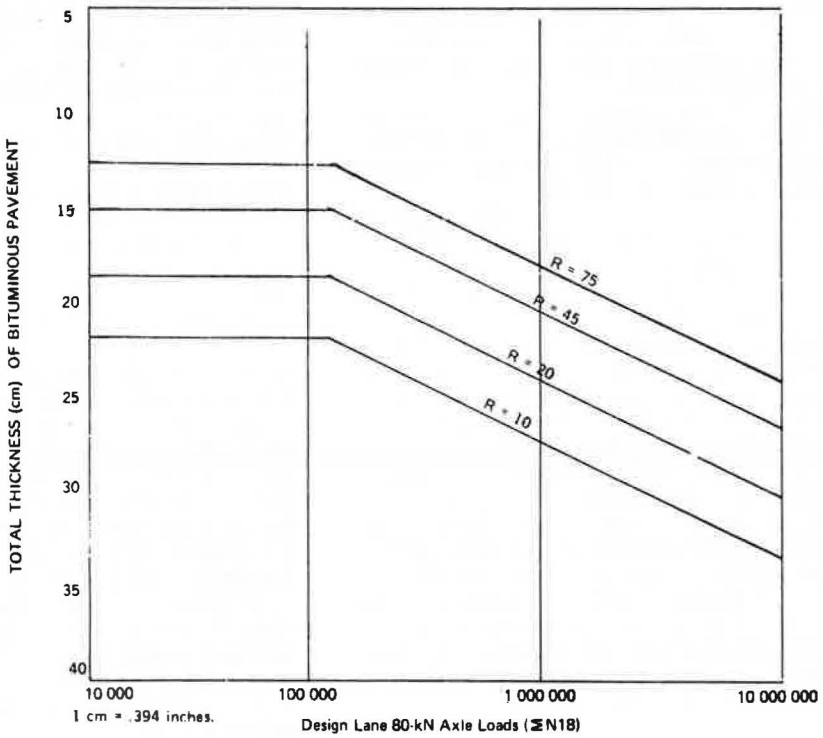

A-6 embankment (test section 201). No noticeable increase was found on the A-3 embankment (test section 203) after the longitudinal saw cut. Finally, transverse saw cuts across the shoulder were made at the ends of the longitudinal saw cut, and the deflection measurements were repeated; no increase in deflections was noted, however.

Based on the deflections obtained after the saw cut, if widening of an existing narrow, rigid pavement is based on the full-depth design, the thickness of the full-depth pavement should be increased by 20 percent. This additional thickness will result in approximately the same deflection intended in the design.

FINDINGS AND CONCLUSIONS

Full-depth pavements do not exhibit the same Benkelman beam deflection behavior as aggregate-base flexible pavements. The deflections are much more sensitive to the temperature of the bituminous. The deflections are, in fact, so dependent on temperature that this effect nearly masks the seasonal effect. The seasonal effect can only reduce the deflections by about 30 percent (at most) from the peak seasonal deflection and then only at the seasonal extremes, such as early March or October. Temperature, on the other hand, can vary the deflection by as much as 300 percent at any time of the year. For instance, a deflection of 0.25 mm (0.010 in) at a 4.4°C (40°F) mat temperature can increase to 0.76 mm (0.030 in) if the mat temperature increases to 43.3°C (110°F).

Analysis of the deflections, adjusted to peak season deflections at a 26.7°C (80°F) mat temperature, shows that the deflections are very sensitive to pavement thickness in the 12.7- to 22.9-cm (5- to 9-in) range. But, as pavement thickness increases beyond 30.5-33.0 cm (12-13 in), there is little decrease in measured deflections. This implies that assigning a single unit GE value to full-depth pavement is not appropriate. Our comparisons of the full-depth and aggregate-base flexible test sections on this project show that a 17.8-cm (7-in) full-depth pavement has the same deflection as a flexible pavement with 27.9 cm (11 in) of GE and that a 27.9-cm full-depth pavement has the same deflection as a flexible pavement with 85.1 cm (33.5 in) of GE. The unit GE of full-depth pavement varies with the pavement thickness; for example, it is 1.5 at a thickness of 17.5 cm (6.9 in) and 3.0 at a thickness of 27.4 cm (10.8 in).

In the special study of the edge effect, it was found that full-depth pavement on plastic soils deflects about 30 percent more at the edge of the pavement than it does 0.6 m (2 ft) from the edge. This same increase in deflections also occurs in full-depth widenings that are less than 1.22 m (4 ft) in width. To reduce the deflection of a widening to the deflection of a normal pavement, the full-depth thickness should be increased by 20 percent.

Early indications show that the performance of full-depth pavement is comparable to that of aggregate-base flexible pavement if both types have the same peak season 26.7°C (80°F) Benkelman beam deflection.

REFERENCES

1. M. S. Kersten and E. L. Skok. Minnesota Department of Highways Flexible Pavement Design—1969. Minnesota Department of Highways, St. Paul, Investigation 183, Annual Rept., June 1969.
2. The AASHO Road Test: Report 5—Pavement Research. HRB, Special Rept. 61E, 1962.
3. W. A. Fingalson and J. C. Hale. Test Method for Resistance R-Value and Expansion Pressure of Compacted Soils and Base Aggregates. Minnesota Department of Highways, St. Paul, Investigation 176, 2nd Revision, Dec. 1973.
4. C. G. Kruse and E. L. Skok. Flexible Pavement Evaluation with the Benkelman Beam. Minnesota Department of Highways, St. Paul, Investigation 603, Revision to Table 2 of 1968 Summary Rept., Feb. 26, 1975.

Publication of this paper sponsored by Committee on Flexible Pavement Design.

Analysis of a Cracked Pavement Base Layer

E. Otte, Van Wyk and Louw, Inc., Pretoria, South Africa

A study is reported whose objectives were to investigate the effect of the presence of a crack in a treated pavement layer on the stresses and strains induced in the layer by traffic loading and to formulate a procedure for including the effect of the crack during structural pavement design. Prismatic-solid finite-element analysis was used to calculate the stress next to a wide crack, and the ratio of this stress to the stress calculated in an uncracked pavement was taken to quantify the effect of the crack on the stress developed. An increase in stress usually resulted. The study shows that the maximum tensile stress in the treated layer occurs adjacent to the crack at the bottom of the layer and that it acts parallel to the crack. The magnitude of the increase in stress depends on the thickness of the treated layer and the width of the crack, and the maximum increase appears to be 1.4 times. The increase in vertical compressive strain in the subgrade in the vicinity of the crack may be considerable—as much as 14 times—although it is likely to be much less some distance away from the crack.

Treating road-building materials with cement or lime has always been a popular practice because it increases the strength of the material. Both cement- and lime-treated materials do, however, have a tendency to exhibit initial cracking—also called shrinkage cracking—soon after construction. For structural design purposes, materials treated with cement or lime should therefore be considered in the same way; a general term for both—treated material—is used in this paper.

Examples of the extent and width of the initial cracks in pavements that have cement-treated crushed-stone bases are shown in Figure 1. The width generally depends on the quality of the treated material and the position of the layer in the pavement structure. In an ex-

Figure 1. Extent and width of initial cracking in cement-treated crushed stone.

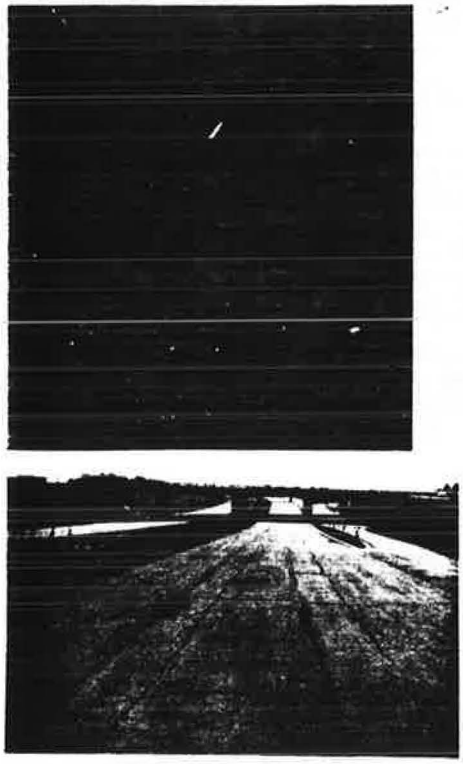

Figure 2. Finite-element mesh.

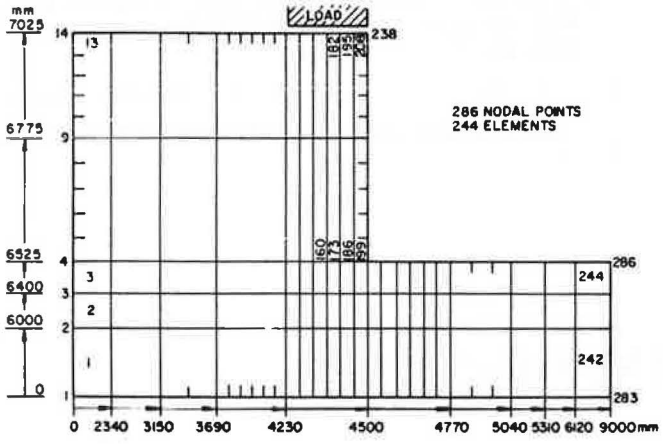

treme case, I have observed cracks as wide as 10 mm in cement-treated crushed-stone bases (the specifications for this material have since been altered to prevent such wide cracking).

Until recently, the effect and influence of initial cracks on the performance of pavements could only be studied and evaluated by visual observation and speculation (1-3). It is difficult to quantify the effect of a crack on the stress distribution in a treated layer, since cracked layers are no longer continuous and the available computer programs, such as CHEVRON (4) and BISTRO (5), are therefore no longer suitable for the analysis. This greatly increases the complexity of designing pavements with treated layers. However, a recent development in finite-element analysis may be one of the keys to the solution of the problem.

The objectives of this paper are to (a) summarize a previous study on the application of finite-element analysis to a pavement that contains a cracked treated layer, (b) make a tentative recommendation about the procedure that should be adopted to determine the possible increases in stress that may result from the crack, and (c) determine the extent of the stress increase in some typical layouts used in South Africa.

PRISMATIC-SOLID FINITE ELEMENTS AND CRACKED TREATED LAYERS

The Program

The finite-element program used in this study was developed by Wilson and Pretorius (6) and uses constant-strain prismatic solids. These are defined as three-dimensional solids that have constant two-dimensional geometric shapes and infinite third dimensions. The loading into the third dimension is achieved by a Fourier series, and this makes the program essentially three-dimensional.

The program was previously used by Pretorius to study the fatigue behavior of a cement-treated layer. Luther and others (8) used this program to study reflection cracking through bituminous overlays. I have studied the application of the program to the analysis of a pavement that contains a cracked treated layer (9). This paper is a summary of that study.

Mesh

Based on the results of the previous study, it is recommended that the finite-element mesh shown in Figure 2 be used. More details on why the mesh is recommended and the crack widths and crack spacings considered are available elsewhere (9, 10).

Maximum Stress

The previous study (9, 10) and the work of Pretorius have indicated that the maximum horizontal tensile stress in a cracked treated layer will occur at the bottom of the treated layer and that it will act parallel to the crack. In structural pavement design, this maximum value should be used as the design stress and not the value for the uncracked, axisymmetric loading condition calculated by using, for example, CHEVRON (which is usually a lower value).

Increase in Tensile Stress

The increase in maximum horizontal tensile stress in the treated layer, which results from the crack in the treated material, can be defined and calculated as the difference between the maximum stress obtained from the finite-element model and the maximum calculated by a CHEVRON analysis. The maximum stress can be determined from the finite-element model by preparing stress contour maps (9). But an easier and faster method has been developed (9, 10).

The faster method involves a finite-element analysis and location of the maximum horizontal tensile stress, which usually occurs in the center of an element at the bottom of the treated layer. The next step is to record the stress in the center of the finite element directly above the element that contains the maximum stress. This stress value is generally lower. The stress gradient between these two points should be projected downward to calculate the maximum stress σ_{∞} at the bottom of the treated layer. It is suggested that the σ_{∞} value be taken as the maximum horizontal tensile stress in the

treated layer. Next, a CHEVRON analysis is performed to calculate the maximum tensile stress for the uncracked case (σ_{su}). The increase in maximum horizontal tensile stress as a result of the crack is expressed as the difference between the two stress values ($\sigma_{sc} - \sigma_{su}$). Mitchell and Monismith (11) have termed this stress increase the "edge loading condition".

Vertical Stress in the Subgrade

If a wide crack has formed in a treated layer, the loss of horizontal load transfer across the crack may result in a significant increase in vertical compressive stress in the lower-lying materials next to the crack (12). The increased stress may cause deformation in the untreated materials (subgrade) next to the crack, which could eventually lead to, for example, an unacceptable riding quality on the road. In the design of a pavement that contains a cracked treated layer, therefore, it is necessary to take notice of the increase in vertical compressive stress and the possibility that deformation may develop. The prismatic-solids finite-element program was also used to investigate this phenomenon (9, 10); in that investigation it was observed that the possibility of subgrade deformation after cracking should not be disregarded. This subject is dealt with later in this paper.

STRESS DISTRIBUTION IN CRACKED TREATED LAYERS

Layouts

In this study, it was intended that several typical structural layouts would be examined to obtain the percentage increase in stress in the treated layer after initial cracking has occurred. There are, however, a multitude of possible combinations of layer thickness and elastic properties. Thus, only two basic structural sections were chosen—one with and one without a crushed-stone base. The bituminous surfacing was omitted in all analyses. From the multitude of possible layouts, eight were selected and analyzed. In some, the elastic moduli of the treated layers were varied while the properties of the other layers were kept constant. A constant Poisson's ratio of 0.35 was assumed for all materials. The load applied was 40 kN, and the corresponding tire contact pressure was 500 kPa.

Figure 3 shows the selected thicknesses, elastic moduli, and material types in the various layouts. The depth of the crack considered in each analysis is indicated by the jagged vertical line. The thicknesses were based on South African experience, and the moduli were obtained from published literature.

Layouts A-C are typical of the upside-down designs in which an untreated crushed stone is usually used on top of a cement-treated natural gravel subbase (13). In layout D, a cement-treated crushed-stone base was included between the treated and untreated natural gravel layers. Layout E contains two treated natural gravel layers. In layout F, the upper treated layer is usually a cement-treated crushed-stone layer and the lower layer a treated natural gravel. Layout G was used on two roads in South Africa during the 1960s (Special Road S12 and a part of Route N4); its performance was not entirely satisfactory (3). Layout H is essentially the same as layout G but with thicker layers. Both have an untreated layer between two treated layers.

Results

The finite-element model shown in Figure 2 was modified to accommodate the changes in the depth of the crack. The model was analyzed 21 times to cover the combinations shown in Figure 3. The method described earlier was used to calculate the maximum horizontal tensile and vertical compressive stresses in the cracked pavement.

Tensile Stress in Treated Layers

In all cases, the maximum tensile stress occurred at the bottom of the treated layer and acted parallel to the crack. This confirms the observation of Pretorius (7). The maximum stress usually occurred between the center of the loaded area and the crack, whereas in CHEVRON it always occurred directly beneath the center of the loaded area.

Tables 1 and 2 give the maximum stresses recorded for the eight layouts and also the increase in maximum horizontal tensile stress (at the bottom of the treated layer).

It appears that the maximum increase in tensile stress as a result of the crack was about 1.4 times [illegible] occurred in the treated base of layout D (Table 2 [illegible] stress decrease was noticed in layouts A and H [illegible] interesting observation is the relatively high in[illegible] in stress in layouts B, C, and F, which had thi[illegible] layers (250-300 mm) in comparison with the sm[illegible] creases in layouts A and E, which had thin upper [illegible] (≤200 mm). This observation did not quite fit [illegible] but since the design of layout G and that of lay[illegible] unbalanced (3, 14) and should therefore prefera[illegible]

Figure 3. Schematic drawing of analyzed layouts.

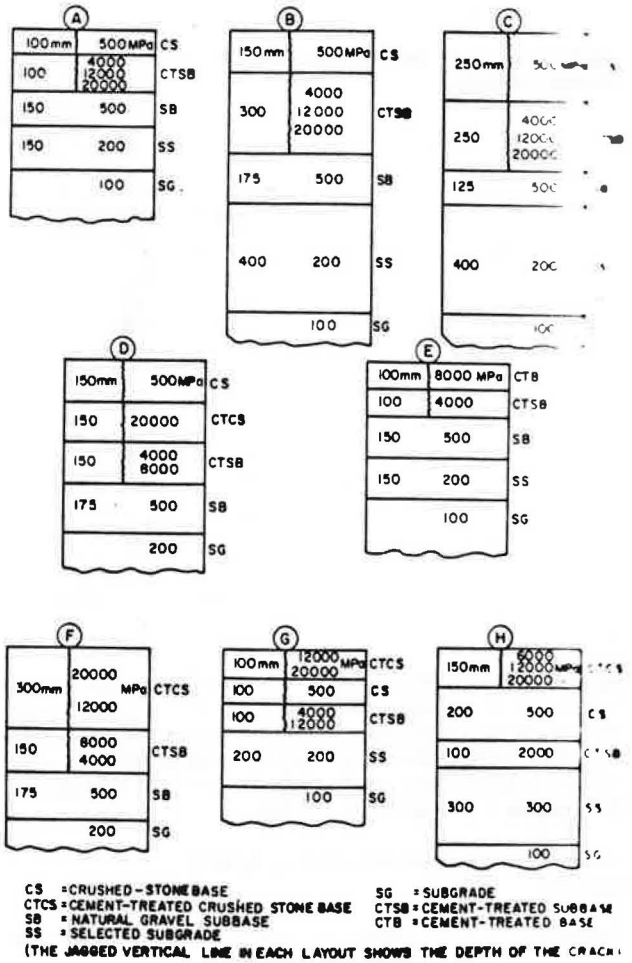

CS = CRUSHED-STONE BASE
CTCS = CEMENT-TREATED CRUSHED STONE BASE
SB = NATURAL GRAVEL SUBBASE
SS = SELECTED SUBGRADE
SG = SUBGRADE
CTSB = CEMENT-TREATED SUBBASE
CTB = CEMENT-TREATED BASE
(THE JAGGED VERTICAL LINE IN EACH LAYOUT SHOWS THE DEPTH OF THE CRACK)

Table 1. Increase in horizontal tensile stress in a cracked pavement layer: layouts A-C.

Layout	Elastic Modulus of Treated Layer (MPa)	Maximum Horizontal Tensile Stress in Treated Layer (kPa)		Increase in Stress Caused by Crack
		CHEVRON (uncracked)	Finite-Element Analysis (cracked pavement)	
A	4 000	658	595	0.90
	12 000	1438	1418	0.99
	20 000	1903	1964	1.03
B	4 000	217	254	1.17
	12 000	364	476	1.31
	20 000	430	587	1.37
C	4 000	213	254	1.19
	12 000	382	509	1.33
	20 000	466	644	1.38

Table 2. Increase in horizontal tensile stress in a cracked pavement layer: layouts D-H.

Layout	Elastic Modulus (MPa)		Base			Subbase		
			Maximum Horizontal Tensile Stress (kPa)			Maximum Horizontal Tensile Stress (kPa)		
	Base	Subbase	CHEVRON (uncracked)	Finite-Element Analysis (cracked)	Increase in Stress Caused by Crack	CHEVRON (uncracked)	Finite-Element Analysis (cracked)	Increase in Stress Caused by Crack
D	20 000	4 000	447	596	1.33	161	199	1.24
	20 000	8 000	239	333	1.39	256	337	1.32
E	8 000	4 000	-*	-*	-	513	514	1.0
F	20 000	8 000	225	289	1.28	153	202	1.32
	12 000	4 000	232	290	1.25	113	142	1.26
G	12 000	4 000	1352	1570	1.16	411	489	1.19
	12 000	12 000	1214	1430	1.18	805	933	1.16
	20 000	4 000	1829	2147	1.17	351	412	1.17
	20 000	12 000	1657	1967	1.19	697	820	1.18
H	6 000	2 000	719	675	0.94	-	-	-
	12 000	2 000	1042	1008	0.97	-	-	-
	20 000	2 000	1294	1271	0.98	-	-	-

*In compression.

Table 3. Increase in vertical strain in a cracked pavement.

Layout	First Underlying Layer			Second Underlying Layer		
	Vertical Compressive Strain (10^{-6} mm/mm)			Vertical Compressive Strain (10^{-6} mm/mm)		
	CHEVRON (uncracked)	Finite-Element Analysis (cracked)	Increase in Strain	CHEVRON (uncracked)	Finite-Element Analysis (cracked)	Increase in Strain
A	331	1028	3.1	346	634	1.8
	226	951	4.2	268	565	2.1
	178	888	5.0	227	516	2.3
B	84	588	7.0	92	403	4.4
	45	450	10.0	55	303	5.5
	32	399	12.5	42	242	5.8
C	79	675	8.5	103	520	5.0
	46	559	12.2	66	440	6.7
	34	503	14.8	51	357	7.0
D	61	461	7.6	72	298	4.1
	48	452	9.4	59	261	4.2
E	199	845	4.2	203	417	2.1
F	27	277	10.3	33	165	5.0
	41	343	8.4	47	219	4.7
G	201	1045	5.2	207	493	2.4
	148	897	6.1	173	433	2.5
	171	961	5.6	185	473	2.6
	129	815	6.3	156	410	2.6

be used in pavement design, very little attention is paid to them in the remainder of this paper. These two layouts were analyzed mainly as part of an ongoing study to evaluate their previously unacceptable performance (3). In both layouts, the increase in stress attributable to the cracks was less than 1.2 times.

Vertical Compressive Strain in Lower Layers

Table 3 gives the vertical strains in the two untreated layers under the cracked treated layer. In some of the layouts—for example, A, B, C, and E—these layers are the subbase and selected subgrade, whereas in others—for example, D and F—they are the subbase and subgrade. These values were calculated by using CHEVRON (for the uncracked pavement) and finite-element analysis (for the cracked pavement). The strain for the finite-element analysis was obtained by multiplying the strain obtained from the CHEVRON analysis by the ratio of the calculated corresponding vertical stresses (9, 10).

The data given in Table 3 show that the increase in

vertical strain caused by cracking depends on the layout and that it is considerable: The increase varies between 2 times (layout A) and 15 times (layout C). The magnitude of these values should not be regarded as very accurate since the finite-element mesh was often fairly coarse in the areas where the increases were calculated (9). For subgrade-quality materials, Dormon and Metcalf (15) have suggested a vertical strain of less than 650 $\mu\epsilon$ ($\mu\epsilon = 10^{-6}$ mm/mm) to withstand about a million load repetitions. Assuming that this order of strain also holds for both subbase-quality and selected subgrade-quality materials, it seems that the strains in the first layer below the treated layers of layouts A, E, and G (when cracked) are rather excessive and deformation will probably occur before a million load repetitions. The other layouts may withstand a million load repetitions without severe rutting and deformation next to the crack, but the strains are approaching the allowable limit and, should water penetrate the lower layers, severe deformation would probably take place. The strains in layout H are well below 300 $\mu\epsilon$, probably because of the intact treated subbase. Since the low strains in layout H result in a negligible chance of rutting, they are not given in Table 3.

DISCUSSION OF RESULTS

Horizontal Tensile Stress

In the development of a design procedure for a pavement that contains a treated layer, the presence of initial cracks—also called shrinkage cracks—has always caused some concern because it has been difficult to evaluate their effect. Tables 1 and 2 quantify the increase in horizontal tensile traffic-associated stress attributable to the crack. The increased stress acts parallel to the crack and occurs at the bottom of the treated layer. The increase seems to depend on the material properties and structural layout, but it will probably not exceed about 1.4 times. During the design process, therefore, it is possible to provide for the increased stress and to design for it. This can be done by calculating the maximum horizontal tensile stress σ_t for the uncracked structural layout by using, say, CHEVRON. σ_t is then increased—1.4 times, for example—and the new value (σ_n) is taken as the design horizontal tensile stress for the treated material in the particular layout.

Vertical Compressive Strain

Wide cracks and the corresponding loss of load transfer result in significant increases in the vertical compressive strains in the lower layers, and the increased strains approach the currently accepted design criterion for relatively dry materials—that is, materials at their natural moisture contents. If water penetrates the cracks and becomes trapped in the lower layers, it is highly probable that deformation will take place. The penetration of water should be prevented by providing effective drainage of surface water and/or sealing the cracks effectively after they have formed. It may also be possible to allow for the increase in strain during the design stage, in which case the suggestions given in Table 4 may be used.

Crack Length, Depth, and Width

In this analysis, the length of the crack was considered to be the width of the pavement—that is, a transverse crack across the pavement. The depth of the crack was varied, depending on the layout, but it was always taken through the cement-treated layers. A wide crack (6 mm) was considered across which no load transfer was assumed to take place.

In practice things are different. The length of cracks varies, and there are shorter cracks that do not extend across the pavement. Shorter cracks were not considered in this analysis, however, because the prismatic-solids finite-element program used to perform the analysis can only handle infinitely long cracks (6). The increase in stress calculated next to a short crack would probably be less than the increase calculated next to a crack that extends all the way across the pavement. This implies that recommendations for stress or strain increases based on the analysis described in this paper are conservative.

Cement-treated materials are brittle, and once a crack has formed it grows very rapidly. This implies that a crack that does not extend through the depth of the layer is not in a stable condition and that it will grow relatively quickly to become a full-depth crack and be in a stable condition. That is why only full-depth cracks were considered in this analysis. For the sake of the analysis and the computer program, it was assumed that the cracks reflected even through the crushed-stone-base layers.

Only wide cracks (6 mm) were considered in the analysis, and no load transfer was assumed to take place across them. In practice there are materials in which the cracks are relatively narrow, from hairline to 2 mm, and some degree of load transfer will probably occur across them. In materials that are known to exhibit

Table 4. Suggested increases in calculated maximum stresses and strains to accommodate initial cracking in treated layer.

Type of Cracking	Total Thickness of Treated Material (mm)	Increase in Maximum Horizontal Tensile Stress[a]	Increase in Maximum Vertical Stress	
			First Underlying Layer	Second Underlying Layer
No cracking expected (e.g., less than 2 percent lime or cement)		1.0	1.0	1.0
Moderate cracking; crack widths less than 2 mm (e.g., natural materials with lime or 2-3 percent cement)	≤200	1.10	2.5	1.5
	>200	1.20	7.0	3.5
Extensive cracking; crack widths more than 2 mm (e.g., crushed stone with 4-6 percent cement)	≤200	1.25	5.0	2.5
	>200	1.40	14.0	7.0

[a]Parallel and adjacent to initial crack.

narrow cracks (here called moderate cracking)—such as some cement-treated natural gravels and lime-treated soils—it is suggested that about 50 percent load transfer be assumed and that the stress and strain increases be taken as 50 percent of those calculated for wide cracks.

Increases Recommended for Design

If a pavement is to be designed to carry normal highway traffic, the available information can be used; if, however, a pavement is to be designed for a special purpose (for example, an airfield or a container terminal), the complete finite-element analysis may be justified. Since the increases seem to be dependent on the structural layout and the material properties, which also provide an indication of the crack width, the information in Tables 1-3 was interpreted and Table 4 was proposed. This table indicates the increases to be applied to the stresses and strains calculated in an uncracked layer (that is, by CHEVRON analysis). Further studies with this finite-element program indicated that these increases are equally applicable to calculated strains (10).

For practical pavement design it is suggested that, if the base is of a material that will blanket reflection of cracks to the surface (for example, crushed stone), the treated layer should be considered as falling in the category of moderate cracking and the values increased accordingly. The increase in the vertical compressive strain in the layers below the cracked treated layer is considerable—as much as 14 times. Although, as indicated earlier, the magnitude of the increase in vertical strain should not be regarded as very accurate, it may be used as an interim guide to warn the designer against possible deformation in the subgrade. In some layouts it is often very difficult to decide which is the second underlying layer, and in this case it is suggested that the designer consider only the first underlying layer.

Mitchell and Monismith (11) have suggested an increase of 1.5 times for the horizontal tensile strain, which is constant and not affected by the layer thickness or the crack width. I suggest that a constant increase is too insensitive and that the values in Table 4 should be used to accommodate the initial cracking in the treated material during the structural pavement design stage.

CONCLUSIONS AND RECOMMENDATIONS

1. It is recommended that the prismatic-solids finite-element program and the finite-element model used in this paper be used for the design of pavements that contain cracked treated layers.
2. After cracking, the maximum tensile stress acts parallel to the crack and occurs near the center of the loaded area at the bottom of the treated layer.
3. To calculate the increase in stress that results from the crack, the finite-element analysis should be performed and the element with the maximum stress located. From the stress gradient the maximum value (σ_{sc}) for the structure can be determined. The CHEVRON analysis should be performed to obtain the maximum value for an uncracked pavement (σ_{su}). The stress increase as a result of the crack is defined as the difference between the two maximum values ($\sigma_{sc} - \sigma_{su}$).
4. A wide crack—that is, one with no load transfer across it—causes a definite increase in the maximum horizontal tensile stress at the bottom of the treated layer. The increase seems to be dependent on the materials and structural layout. Use of Table 4 is recommended.
5. The increase in the vertical stress and strain in the subgrade as a result of the initial crack is significant, and the possibility of subgrade deformation cannot be excluded. It should be noted, however, that these calculated increases are localized in the vicinity of a crack and their eventual effect on subgrade deformation is indeterminate at this stage. But it could contribute to a loss of riding quality because of localized deformation near the crack. A more detailed analysis is also necessary to improve the values given in Table 4, but it is suggested that these values be used in the meantime as indicators for pavement design.
6. This computer analysis contributed to a better understanding of the stress distribution and possible behavior of a pavement that contains a cracked treated layer. Further work along these lines may eventually result in a complete understanding of the effects of a cracked layer on the remainder of the pavement.

ACKNOWLEDGMENT

This paper is published with the permission of the Director of the National Institute for Transport and Road Research, Council for Scientific and Industrial Research, Pretoria, South Africa. I also wish to acknowledge the advice and assistance of P. C. Pretorius on the use of the finite-element computer program and of W. D. O. Paterson in preparing Table 4.

REFERENCES

1. B. Brewer and R. I. T. Williams. An Assessment of the Performance of Dry Lean Concrete Bases for Roads. Road and Road Construction, Nov. - Dec. 1968.
2. K. P. George. Cracking in Soil-Cement. Proc., 7th Australian Road Research Board Conference, Adelaide, 1974.
3. E. Otte. The Performance of Two Pavements Containing Cement-Treated Crusher-Run Bases. NITRR-PCI Symposium on Cement-Treated Crusher-Run Bases, Johannesburg, South Africa, Feb. 1973.
4. H. Warren and W. L. Dieckman. Numerical Computation of Stresses and Strains in a Multilayered Asphalt Pavement System. California Research Corp., Richmond, 1963.
5. M. G. F. Peutz, H. P. M. Van Kempen, and A. Jones. Layered Systems Under Normal Surface Loads. HRB, Highway Research Record 228, 1968, pp. 34-45.
6. E. L. Wilson and P. C. Pretorius. A Computer Program for the Analysis of Prismatic Solids. Univ. of California, Berkeley, UC-SESM Rept. 70-21, 1970.
7. P. C. Pretorius. Design Considerations for Pavements Containing Soil-Cement Bases. Univ. of California, Berkeley, Ph.D. thesis, 1970.
8. M. S. Luther, K. Majidzadeh, and C. W. Chang. A Mechanistic Investigation of Reflection Cracking. Proc., 2nd Conference on Asphaltic Pavements for Southern Africa (CAPSA '74), Durban, South Africa, 1974.
9. E. Otte. Prismatic Solid Finite Elements and a Cracked Road Pavement. Council for Scientific and Industrial Research, NITRR Tech. Rept. RP/6/75, Pretoria, South Africa, Dec. 1975.
10. E. Otte. A Structural Design Procedure for Cement-Treated Layers in Pavements. Univ. of Pretoria, Pretoria, South Africa, D.Sc. (Eng) thesis, 1977.
11. J. K. Mitchell and C. L. Monismith. A Thickness Design Procedure for Pavements with Cement-

Stabilized Bases and Thin Asphalt Surfacings. Proc., 4th International Conference on the Structural Design of Asphalt Pavements, Univ. of Michigan, Ann Arbor, Vol. 1, 1977, p. 409.
12. P. E. Fossberg, J. K. Mitchell, and C. L. Monismith. Load-Deformation Characteristics of a Pavement with Cement-Stabilized Base and Asphalt Concrete Surfacing. Proc., 3rd International Conference on the Structural Design of Asphalt Pavements, Univ. of Michigan, Ann Arbor, Vol. 1, 1972, p. 795.
13. E. Otte and C. L. Monismith. Some Aspects of Upside-Down Pavement Design. Proc., 8th Australian Road Research Board Conference, Perth, 1976.
14. E. Otte. Factors Affecting the Behaviour of Cement-Treated Layers in Pavements. Proc., 9th Australian Road Research Board Conference, Brisbane, 1978.
15. G. M. Dormon and C. T. Metcalf. Design Curves for Flexible Pavements Based on Layered System Theory. HRB, Highway Research Record 71, 1965, pp. 69-84.

Publication of this paper sponsored by Committee on Flexible Pavement Design.

Design of Pavements with Lean-Concrete Bases

S. F. Brown, University of Nottingham, Nottingham, England

In the analytic approach to pavement design, structures with lean-concrete bases require certain distinctive considerations that arise from the incidence of cracks in the lean concrete attributable to thermal and shrinkage effects that influence stresses and strains in the rest of the structure. Details of a two-stage design process, for both conventional lean-concrete-base structures and for those that involve a "sandwich" layer of unbound granular material above the lean concrete, are presented. Both types of structures incorporate 100 mm of rolled-asphalt surfacing; the conventional structures use an additional thickness of dense bitumen macadam as part of a composite base. In stage 1 of the procedure, the full uncracked value of modulus is used for the lean concrete, and pavement life, in terms of numbers of standard axle loads, is calculated to the point at which secondary (traffic-induced) cracking occurs. In stage 2, the modulus of the lean concrete is substantially reduced as a consequence of this cracking, and additional life is calculated on the basis of asphalt fatigue cracking or permanent deformation, whichever is critical. The total life is the sum of stages 1 and 2. The results are compared with current design recommendations and with the results of full-scale trials. Since the granular material can only develop a modest value of modulus in sandwich construction, that technique does not appear to be very effective unless it can be shown to reduce the incidence of reflection cracking in the asphalt surface.

In applying the principles of analytic pavement design to structures that incorporate lean concrete layers, the occurrence of cracks, which develop in this material before traffic loading, introduces a problem that is not encountered with asphalt or unbound bases. If this "primary" cracking is augmented by the cracking caused by traffic, the resulting lean-concrete layer has an effective elastic modulus that is little better than that of granular material, and a figure of 500 MPa has been proposed (1). Alternatively, if this "secondary" (traffic-associated) cracking is avoided, then the full intact strength and stiffness of the lean concrete are available between cracks. Pell and Brown (2) have suggested, therefore, that this type of pavement should be designed in two stages, the first involving only primary cracking and the second involving secondary cracking. This approach has been developed by Walker and others (3), who produced analytical data related to the effects of primary cracking on the critical stresses and strains in the structure. This paper uses this and other relevant information in an analytically based design method for structures with lean-concrete bases, such as those used in Britain. It also considers the potential of "sandwich" construction, which involves a granular layer between the asphalt surfacing and the lean-concrete base.

DESIGN CONSIDERATIONS

Lean concrete, as used in British pavements (4), requires good-quality aggregate to a fairly strict grading and mix proportions that will produce a cube strength of 10-20 MPa at 28 days. Although this is the material considered in this paper, the design principles could well apply to lower-quality, cement-treated materials. The primary cracking of lean concrete is considered by Williams (5) to be caused by warping stresses and by subgrade restraint stresses that arise during contraction of the material under falling temperatures rather than by shrinkage in view of the good quality of aggregate used in lean concrete. Whatever the cause, these primary cracks are well spaced, and between them the virgin stiffness of lean concrete and its reasonable tensile strength are fully available to the designer. However, allowances must be made for the situation near the cracks; a procedure for estimating the critical stresses and strains in this location has been suggested by Walker and others (3). Stage 1 of the process assumes that primary cracking has taken place, whereas stage 2 allows consideration of an extensively cracked base. The occurrence (or otherwise) of this secondary cracking, which is largely caused by traffic-induced stresses, is indicated by the results of the stage 1 analysis. The total life of the pavement is simply the sum of the lives calculated for the two stages. Stage 2 will not occur in those pavements that are strong enough to prevent traffic-induced cracking in the lean concrete.

During stage 1 of the design, the modulus of the lean concrete is much greater than that of the overlying bituminous material. The horizontal strains at the bottom of this bituminous material are, therefore, compressive, and hence the question of fatigue cracking does not arise. This statement should be qualified by noting that tensile strain does develop in the vertical direction.

near the surface between dual wheels. Its magnitude was not large enough to be of importance in the designs considered in this paper, but it could be of some consequence in other situations and deserves further investigation. In stage 2, when the modulus of the lean concrete is substantially lower, the possibility of fatigue cracking in the bituminous material must be considered.

The subgrade strain criterion used to deal with permanent deformation in pavements that have bituminous bases (6) is suitable for stage 2 calculations on lean-concrete bases but not for stage 1. Lower allowable strains should be associated with this more rigid construction, and an adjustment has been effected by using the deflection criteria developed by Lister (7). He found that the allowable deflection for a given pavement life with cemented bases is about 75 percent of that for fully flexible construction. The justification for use of this finding is that subgrade strains do correlate well with surface deflections (8).

A major problem in the use of lean concrete in practice is reflection cracking. Even in pavements in which the lean concrete shows only primary cracking, these cracks can propagate through the overlying bituminous material if it is too thin. Because analytic methods have not yet been devised to consider reflection cracking in any detail, the matter is not considered in this paper. However, the thinnest total thickness of bituminous cover used in the design calculations was 100 mm. This should provide some resistance to reflection cracks, particularly since the material involved was hot-rolled asphalt, which has good inherent crack resistance.

MATERIAL CHARACTERISTICS

The modulus of elasticity of lean concrete is related to its tensile strength. The following relation can be derived from the results presented by Williams (9):

$$E = 7.125f + 20\,500 \text{ MPa} \quad (1)$$

where f = flexural strength (MPa). It should be noted that distinctly different relations apply for other cement-bound materials.

Flexural strength f can be estimated from compressive cube strengths u_c by using

$$f = 0.1\,u_c \quad (2)$$

Williams (9) has indicated this to be the lower-bound value, and it is therefore appropriate for design. Since current practice uses cube strength to specify the material quality, Equations 1 and 2 allow the elastic modulus to be estimated. The range of cube strengths allowed (4) is 10-20 MPa; these correspond approximately to moduli of 28 000-34 000 MPa, respectively. The other parameter required for analysis is Poisson's ratio. A study of relevant literature (10) indicates that 0.2 is an appropriate value to use. When a lean-concrete layer becomes extensively cracked as a result of traffic stresses, its effective modulus of elasticity is substantially reduced. It approaches a value similar to that for unbound granular material [a figure of 500 MPa has been suggested (1,3)]. The Poisson's ratio associated with this has been taken to be 0.3. The table below summarizes the elastic properties used for the lean concrete:

Condition of Material	E (MPa) u_c = 10 MPa	E (MPa) u_c = 20 MPa	ν
Primary cracking	28 000	34 000	0.2
Secondary cracking	5 000	5 000	0.3

Lean concrete is susceptible to fatigue cracking. Figure 1 shows the results of some work carried out at the Transport and Road Research Laboratory (TRRL) that indicates that the criterion is the tensile stress expressed as a proportion of the tensile strength (f_c, f). Superimposed on Figure 1 are the results of tests by Kolias (10), who used a different test technique but whose results show general agreement. For the purposes of design, the endurance limit was taken as

$$f_c/f = 0.6 \quad (3)$$

A straight-line relation was used to determine the fatigue lives N_f at higher stress levels, as follows:

$$N_f = 10 \exp(14.9 - 13.2\,f_c/f) \quad (4)$$

Figure 1 shows that this approximation is inappropriate at stress levels above 0.95, but the corresponding lives are so short that this is of no consequence.

Walker and others (3) and Mitchell and Monismith (12)

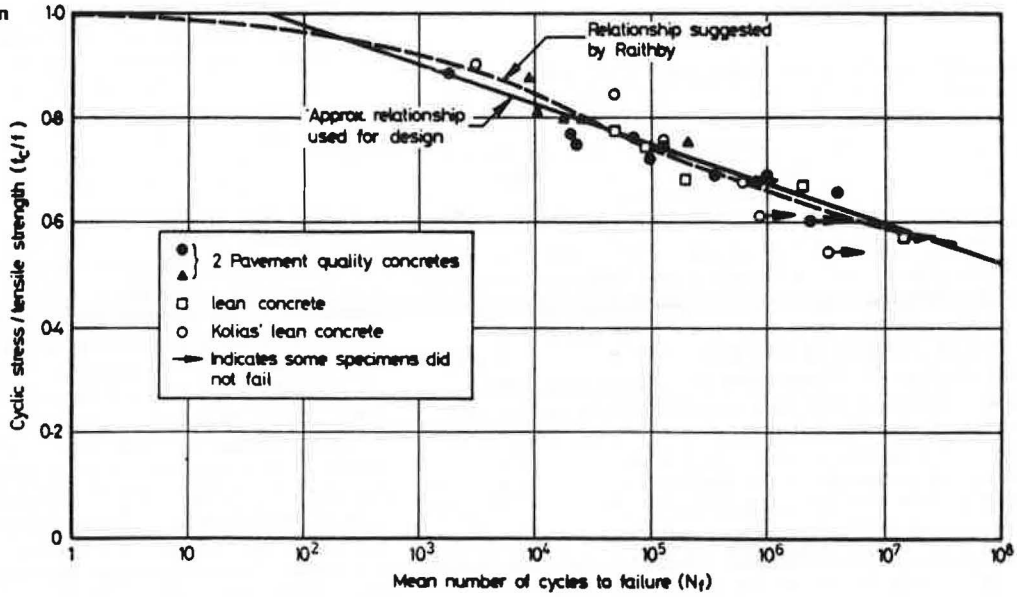

Figure 1. Fatigue results for lean concrete.

both used tensile strain rather than stress as their design criterion. The choice of stress for this work was dictated by the nature of the rather limited data available on the material used in Great Britain.

DESIGN CRITERIA

The design calculations generally took place in two stages that corresponded to the situations of primary and secondary cracking in the lean concrete. In stage 1, the two design criteria were as follows:

1. Tensile stress at the bottom of the lean concrete (σ_θ), expressed as a proportion of the tensile strength (f)—i.e., σ_θ/f—to deal with fatigue cracking.
2. Maximum compressive strain in the subgrade (ϵ_z) to deal with permanent deformation.

The modified relation to give allowable strains that are 75 percent of those appropriate to bituminous and unbound bases is

$$N_f = (1.07 \times 10^{15})/\epsilon_z^{3.57} \quad (5)$$

To take account of the intermittent primary cracks, stresses and strains calculated from pavement analysis were increased as follows (3): Tensile stress in the lean concrete × 1.25 and compressive strain in the subgrade × 2.5. These adjusted values were then used in assessing pavement lives.

In stage 2, the design criteria were those used in bituminous base constructions (6):

1. Tensile strain at the bottom of the bituminous layer to prevent fatigue cracking (the layer in question would be the one immediately above the lean concrete), and
2. Subgrade strain to limit permanent deformation.

DESIGN CALCULATIONS

Details of the structures that were considered are given in Table 1. A standard 40-kN dual wheel load was used in which each wheel had a contact pressure of 500 kPa. The space between contact areas was 110 mm.

Variability in the lean concrete was dealt with by considering the range of compressive strengths (10-20 MPa) allowed in current specifications (4). For each structure, the thickness of lean concrete was varied in 50-mm increments between 100 and 300 mm. A design life was then calculated for each.

Typical details for one of the design calculations are given in Table 2 and in the two text tables below (the lean-concrete specification is u_c = 10 MPa, f = 1050 kPa, and E = 28 000 MPa). The case considered in these tables is a design that has 75 mm of dense bitumen macadam (DBM) as the top of the composite base. The quality of the lean concrete is taken to be at the low bound of the specification (10 MPa).

For stage 1 (primary cracking only), the tensile stress in the lean concrete is multiplied by the factor 1.25 to allow for the cracks. This figure is then used to evaluate a life N_1, in millions of standard axle loads (msa), by using the fatigue relation of Equation 4 and the endurance limit. The latter implies that infinite lives result when the stress term $1.25\ \sigma_\theta/f$ is 0.6 or less. The stage 1 deformation analysis is considered on the right-hand side of Table 2. Here the design parameter is multiplied by a factor of 2.5, and a corresponding life N_1' is determined by using the modified relation of Equation 5.

The table below gives the stage 2 calculations (completely cracked):

Thickness of Lean Concrete (mm)	Tensile Strain in DBM × 10^{-6}	N_2 (msa)	Subgrade Strain × 10^{-6} (mm/mm)	N_2' (msa)
100	87	2.3	355	2.4
150	79	3.1	324	3.3
200	73	3.9	293	4.7

These calculations were only necessary for thicknesses of 100, 150, and 200 mm because the two larger thicknesses of lean concrete did not exhibit traffic-associated cracking. The analyses for stage 2 use the reduced modulus (500 MPa) for the lean concrete, and lives based on fatigue cracking in the DBM (N_2) and permanent deformation (N_2') are obtained. In this case, the fatigue lives (N_2) are slightly shorter and, therefore, critical.

Table 1. Details of analyzed structures.

Layer	Material	Stiffness (MPa)	Thickness (mm)
Wearing course	Rolled asphalt	6400	40
Base course	Rolled asphalt	7000	60
Composite road base	Dense bitumen macadam	9400	0, 75, 125
	Lean concrete, uncracked	28 000 or 34 000	100-300
	Lean concrete, cracked	500	
Subbase	Granular	75	200
Subgrade	3 percent California bearing ratio	30	-

Table 2. Details of typical design calculations: stage 1.

Thickness of Lean Concrete (mm)	Tensile Stress in Lean Concrete (σ_θ) (kPa)	1.25 σ_θ/f	N_1 (msa)	2.5 × Subgrade Strain × 10^{-6} (mm/mm)	N_1' (msa)
100	1110	1.32	0*	348	0.9
150	836	0.99	0*	248	3.0
200	645	0.77	0.05*	185	8.6
250	500	0.60	∞	140	23.0*
300	374	0.45	∞	113	50.0*

*Critical life.

The total pavement lives are calculated below:

Thickness of Lean Concrete (mm)	Life (msa)		
	Stage 1	Stage 2	Total (stage 1 + stage 2)
100	0	2.3	2.3
150	0	3.1	3.9
200	0.05	3.9	4.0
250	23.0	–	23.0
300	50.0	–	50.0

For the three smallest thicknesses of lean concrete, this involves summation of the lives from both stages, but for the 250- and 300-mm thicknesses, only stage 1 is involved.

The results of all calculations are summarized in Table 3.

A graphical representation of all the results is given in Figure 2, which shows the thicknesses of lean-concrete base for given pavement lives. A pair of curves is given for each of the three thicknesses of DBM used in the composite base. The asphalt thicknesses shown in the figure refer to the total thickness of bituminous material (including the surfacing). The shaded zones between each pair of lines show the effects of lean-concrete quality within the current specification. As may be expected, this effect decreases as the thickness of the DBM increases.

The recommended thicknesses from current British practice (13) are superimposed on these results for comparison. In Road Note 29, the thickness of bituminous cover varies continuously with traffic volume, and hence the thickness has been identified on the line in Figure 2 at various points to facilitate comparison with the analytic designs. This comparison is only possible at three discrete points and where the bituminous cover is of similar thickness. The analytic designs indicate between 60 and 100 mm more lean concrete for a given life.

The shape of the analytic curves in Figure 2 is of interest. The full lines indicate designs based on stage 1 only, which implies that traffic-associated cracking does not occur. The dotted lines are for designs that involve both stages. As DBM thickness increases, the lean-concrete stresses are reduced and less secondary cracking is apparent. The relation between the thickness of lean concrete and pavement life, when only primary cracking is involved, is a fairly steep one, best illustrated by the completely full line for the 225-mm bituminous thickness. The transition from primary to secondary cracking involves a shift to a lower life at the critical thickness, which explains the shape of the curves for the two smaller asphalt thicknesses. This shift is perhaps rather exaggerated, since the change in modulus from 28 000 or 34 000 MPa down to 500 MPa is applied suddenly and on the assumption that traffic-associated secondary cracking will occur rapidly once it begins. No reliable data on this transition are available, so the design calculations have erred on the safe side.

Table 3. Pavement lives at three DBM thicknesses.

Thickness of Lean Concrete (mm)	Pavement Life (msa)					
	Zero DBM Thickness		75-mm DBM Thickness		125-mm DBM Thickness	
	u_s = 10 MPa	u_s = 20 MPa	u_s = 10 MPa	u_s = 20 MPa	u_s = 10 MPa	u_s = 20 MPa
100	0.2	0.2	2.3	2.3	6.3	2.9
150	0.4	0.4	3.1	3.8	8.4	8.6
200	0.7	1.0	4.0	11.2	18.2	23.3
250	1.3	10.5	23.0	30.4	40.4	55.2
300	20.6	26.6	50.0	65.1	93.1	112.9

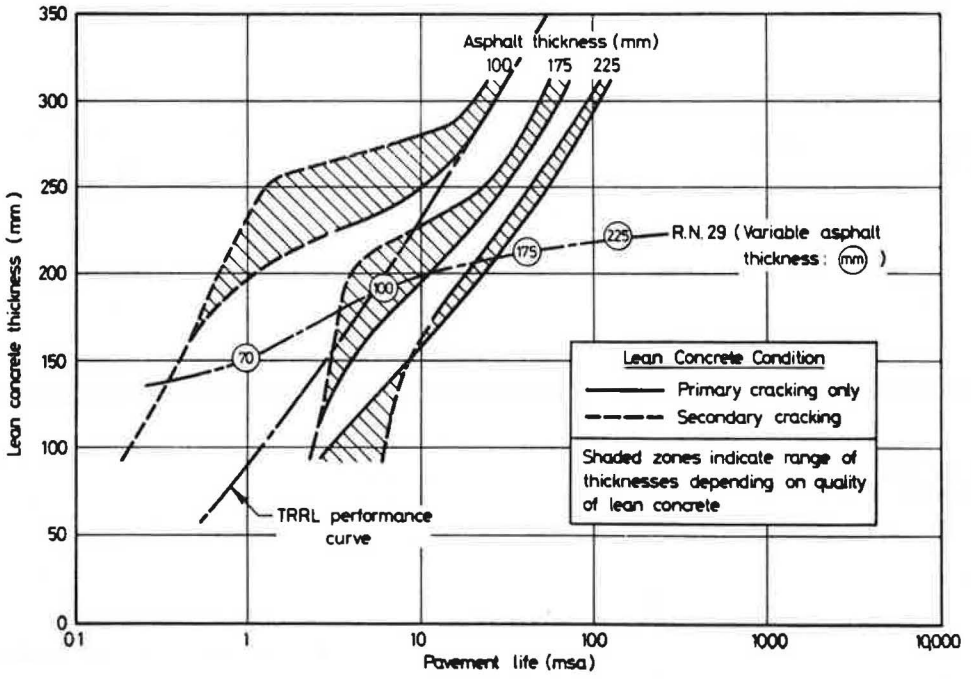

Figure 2. Life of pavements with lean-concrete bases.

The reason for the crossing of the curves in the case of the 225-mm asphalt thickness is interesting. When lean-concrete thickness is 100 mm, secondary cracking occurs in the weaker lean concrete but not in the stronger. During stage 2, for the weaker material, the additional life of the pavement based on fatigue resistance of the DBM exceeds that based on permanent deformation for the stronger material that has only primary cracks. Thus, when the lean-concrete layer is relatively thin, there is some advantage to be gained from keeping its strength down.

In order to relate the analytic designs reported here to the performance of actual pavements that incorporate lean-concrete bases, a curve is superimposed on Figure 2 to indicate the results of TRRL experimental sections at Alconbury Hill (14). The relevant sections had 100 mm of hot-rolled asphalt surfacing, and the curve is seen to converge on the analytic designs at the heavy-traffic end. The divergence at lower traffic volumes indicates that secondary cracking apparently had less effect on-site than the analytic procedure indicates. The sharp transition from the primary to the secondary cracking situation referred to above tends to exaggerate the discrepancy between the site curve and the design calculations. As may be expected, the site curve intersects the recommendations of Road Note 29 (13) at the appropriate point in Figure 2.

SANDWICH CONSTRUCTION

Design Considerations

The idea of using an unbound granular layer above a cement-treated layer is, in principle, attractive for several reasons:

1. The granular material can be compacted against a stiff supporting layer so that it develops a higher modulus.
2. Because it is placed above a stiffer layer, the stresses induced in the granular material are largely compressive.
3. There exists the potential, at least, for protecting the asphalt to some degree from reflection cracking induced by the cement-treated layer.

The basic approach to design that was used followed that described for conventional lean-concrete bases. There was a major difference in the pavement analysis, however, in respect to the granular layer. The stress-strain relations for unbound granular material are markedly nonlinear, but this fact only becomes important when the granular layer assumes a significant role in the structure. Hence, nonlinearity in the subbase was ignored in detail in the analysis of the structures discussed above. For sandwich construction, however, it was thought necessary to model the granular material in the composite base more accurately.

The nonlinearity of granular material can be expressed by an equation of the following form:

$$E = Kp^n \quad (6)$$

where p = mean normal stress = 1/3 (sum of any three orthogonal stresses at a point) and K and n are constants that depend on the particular material and its grading, density, and moisture content.

For the calculations reported here, the actual relation used was

$$E = 25 p_m^{0.67} \text{ MPa} \quad (7)$$

where p_m = mean value of p caused by a combination of overburden stress and traffic-induced stress, in kilopascals. The constants were taken from work carried out at Nottingham on a crushed-limestone base material (15). These design considerations are similar to those described by Otte and Monismith (16), although they differ in detail. Otte and Monismith were concerned primarily with the analysis of structures that have thin asphalt surfacings, and they only considered a single traffic volume. Their cement-treated material was of lower quality than the lean concrete considered here, and the supporting subbase and subgrade were stiffer

Details of the Analysis

Characteristics of the structures analyzed are given in Table 4. The quality of the lean concrete is taken to be at the low bound of the specification (10 MPa).

The choice of a stiffness (elastic modulus) of 200 MPa for the granular sandwich layer followed a number of preliminary analyses in which various values for this parameter were used. In each case, the stresses were calculated at the top, middle, and bottom of the layer at three horizontal locations: midway between the dual wheels, below the center of one wheel, and below the edge of one wheel. By using these stresses, as well as appropriate values for overburden pressure, the nonlinear modulus equation (Equation 7) was used to check the value of modulus. The results indicated that the values derived from the calculated stresses varied very little with the parameters investigated, which were (a) the initial modulus of the layer between 100 and 1000 MPa, (b) the modulus of the lean-concrete layer below (values of 28 000 and 500 MPa were used to represent the primary and secondary cracking situations), and (c) the thickness of the granular layer between 100 and 500 mm.

When the value of 200 MPa was used for the granular layer, the derived values at the various locations investigated varied between 130 and 300 MPa. Average values for the two extreme thicknesses and the two conditions

Table 4. Details of sandwich structures.

Layer	Material	Design Stiffness (MPa)	Thickness (mm)
Wearing course	Rolled asphalt	6400	40
Base course	Rolled asphalt	7000	60
Composite road base	Unbound granular	200	100-500
	Lean concrete, uncracked	28 000	150
	Lean concrete, cracked	500	
Subbase	Granular	75	200
Subgrade	3 percent California bearing ratio	30	-

of the lean-concrete base are given below:

Layer Thickness (mm)	Derived Modulus of Elasticity (MPa)	
	Primary Cracking	Secondary Cracking
100	280	184
500	192	161

These values were considered sufficiently close to 200 MPa for this measurement to be taken as a representative value. The finding is interesting, since it demonstrates that some of the potential advantages of the stiffer support are not realized. For instance, the well-graded crushed-limestone material used in laboratory tests developed a modulus of 1000 MPa under appropriate stress conditions (15). When this value was used in analysis, the largest derived modulus was only 340 MPa. It is apparent, therefore, that the stress conditions in a sandwich layer are such that granular materials do not develop very high modulus values.

During this analysis, consideration was given to the possibility of failure conditions developing in the granular layer, since this would cause a reduction in modulus. By using the modulus of 200 MPa, failure conditions were approached at some locations in the layer, which indicates that the actual effective modulus may be slightly lower than this. Failure is expressed in terms of the ratio q/p, where q = deviator stress and p = mean normal stress, both values being the maximum reached under the application of a wheel load. Otte and Monismith (16) simply ensured in their analyses that p did not become tensile. This is not considered a sufficiently rigorous check and will lead to higher effective moduli for the granular layer.

Design Calculations

Some details of the design calculations are given in Table 5 and in the two text tables below. During stage 1 (Table 5), the lean concrete cracked very early for all but the thickest granular layers. In stage 2, permanent deformation was the critical parameter below 300 mm, but asphalt fatigue became critical at 400 mm [critical life (N_2) = 4.7]:

Thickness of Granular Layer (mm)	Tensile Strain in Asphalt $\times 10^{-6}$	N_2 (msa)	Subgrade Strain $\times 10^{-6}$	N_2' (msa)
100	148	4.5	484	0.8
300	148	4.5	310	3.9
400	147	4.7	255	7.7

The final design lives indicate a rather small range between 0.8 and 5.5 msa for thicknesses of granular "sandwich" between 100 and 500 mm:

Thickness of Granular Layer (mm)	Life (msa)		
	Stage 1	Stage 2	Total (stage 1 + stage 2)
100	0	0.8	0.8
300	0.01	3.9	3.9
400	0.8	4.7	5.5
500	4.3	–	4.3

Table 5. Details of typical design calculations for sandwich construction: stage 1.

Thickness of Granular Layer (mm)	Tensile Stress in Lean Concrete (σ_θ) (kPa)	1.25 σ_θ/f	N_1 (msa)	Tensile Strain in Asphalt $\times 10^{-6}$	N_1' (msa)	2.5 × Subgrade Strain $\times 10^{-6}$	N_1'' (msa)
100	1060	1.26	0*	102	27	405	0.5
300	700	0.83	0.01*	132	7.8	300	1.5
400	571	0.68	0.8*	137	6.5	260	2.6
500	480	0.57	∞	140	5.8	225	4.3*

*Critical life.

Figure 3. Life of pavement in sandwich construction.

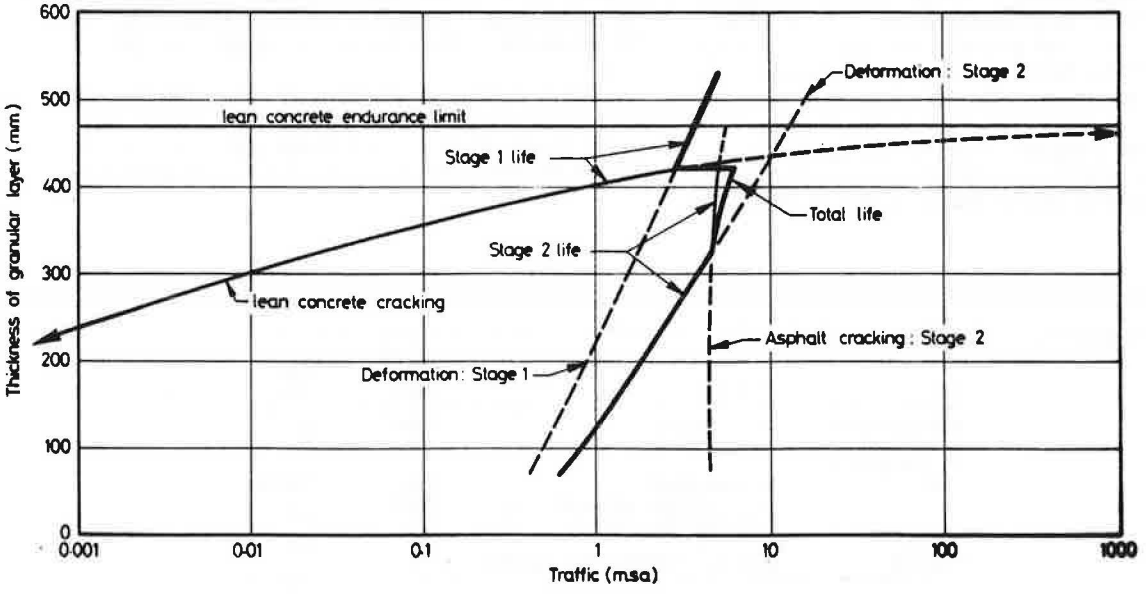

The low modulus of the granular material means that it does not play a very significant structural role in the pavement.

It is interesting to note that the calculated life in the final design table above for the 500-mm thickness is less than that with 400 mm of granular material. This arises from the fact that between these two thicknesses there is a change from stage 1 + stage 2 behavior to stage 1 only for the 500-mm situation. This, together with other interactions of the design parameters, is shown in Figure 3. Here the effect of the thickness of the granular layer on the critical design parameters for both stage 1 and stage 2 is shown and the total life is indicated by the thickest line. The endurance limit for the lean concrete in stage 1 comes in when the granular layer is 470 mm thick. The effect of this is to reduce the pavement life, since the permanent deformation criterion under stage 1 leads to a shorter life than the combined stage 1 and stage 2 lives at slightly lower thicknesses.

The detail shown in Figure 3 should not be allowed to lead to a false sense of accuracy in these designs, although it is helpful in explaining the interactions in this particular example. The final life may be influenced by several factors. In particular, use of a DBM base course instead of rolled asphalt would move the line that represents stage asphalt cracking to a position around 1 msa.

The effect of the thickness of the granular layer on some of the design parameters is interesting. During stage 1, when the lean-concrete modulus is high, increasing the thickness of granular material actually causes an increase in tensile strain in the asphalt surfacing. This parameter was not critical and is therefore excluded from Figure 3, but the values are given in Table 5. This effect results from the low modulus of the granular layer so that when it is thick it allows greater flexing of the surface material. During stage 2, when the lean-concrete modulus is low, the thickness of the granular layer has a negligible effect on the tensile asphalt strain, as shown by the nearly vertical line for this parameter in Figure 3.

The sandwich construction can be compared with the conventional lean-concrete base. For a surface thickness of 100 mm and a lean-concrete base of 150 mm—the conditions used for the sandwich structures—a life of 0.4 msa was obtained. This corresponds to the point in Figure 3 where the line for total life would intersect the horizontal axis, i.e., zero granular-layer thickness. The maximum benefit to be obtained by adding the granular layer is to increase the life to 6 msa when the layer thickness is 420 mm. Figure 2 indicates that 240 mm of lean-concrete base would be required to produce this same life. It is possible to extend this and compare equivalent thicknesses of lean concrete, greater than 150 mm, with those of granular sandwich to produce the same life, as follows:

Pavement Life (msa)	Equivalent Thickness (mm)	
	Granular	Lean Concrete
0.4	0	0
0.8	100	40
1.8	200	65
3.7	300	75
5.6	400	85

For granular layers as thick as about 200 mm, the lean concrete has an equivalence, in terms of thickness, of approximately 3 to 1. Above this, the equivalence increases considerably.

CONCLUSIONS

1. The analytic approach can be used to design pavements with lean-concrete bases.
2. The analytic designs indicate the need for greater thicknesses in lean-concrete bases than those currently specified in British practice.
3. The quality of lean concrete has an increasingly important influence on design thickness as the thickness of bituminous cover is decreased.
4. The analyses indicate that in sandwich construction the modulus of the granular layer can reach only a modest value, a fact that lessens the potential advantages of this type of construction. In view of this, the thickness of granular material in sandwich construction does not have a major effect on pavement life.

ACKNOWLEDGMENT

The work described in this paper formed part of a project sponsored by the British Department of Transport. I am grateful for the advice of P. S. Pell on the paper and the assistance of A. F. Stock in the analyses.

REFERENCES

1. P. S. Pell and S. F. Brown. The Characteristics of Materials for the Design of Flexible Pavement Structures. Proc., 3rd International Conference on the Structural Design of Asphalt Pavements, London, Vol. 1, 1972, pp. 326-342.
2. P. S. Pell and S. F. Brown. Authors' reply to discussion, Proc., 3rd International Conference on the Structural Design of Asphalt Pavements, London, Vol. 2, 1972, pp. 132-134.
3. R. N. Walker, W. D. O. Paterson, C. R. Freeme, and C. P. Marais. The South African Mechanistic Pavement Design Procedure. Presented at 4th International Conference on the Structural Design of Asphalt Pavements, Univ. of Michigan, Ann Arbor, 1977.
4. British Department of Transport. Specification for Road and Bridge Works. Her Majesty's Stationery Office, London, 1976.
5. R. I. T. Williams. Cement-Stabilised Materials. In Developments in Highway Pavement Engineering (P. S. Pell, ed.), Applied Science Publishers, Ltd., London, 1978.
6. S. F. Brown, P. S. Pell, and A. F. Stock. The Application of Simplified, Fundamental Design Procedures for Flexible Pavements. Proc., 4th International Conference on the Structural Design of Asphalt Pavements, Univ. of Michigan, Ann Arbor, Vol. 1, 1977, pp. 327-341.
7. N. W. Lister. Deflection Criteria for Flexible Pavements. Transport and Road Research Laboratory, Crowthorne, Berkshire, England, Rept. LR 375, 1972.
8. C. L. Saraf, W. S. Smith, and F. N. Finn. Rut Depth Prediction. TRB, Transportation Research Record 616, 1976, pp. 9-14.
9. R. I. T. Williams. Properties of Cement-Stabilized Materials. Journal of the Institute of Highway Engineers, Vol. 14, No. 2, 1972, pp. 5-19.
10. S. Kolias and R. I. T. Williams. Cement-Bound Road Materials: Strength and Elastic Properties Measured in the Laboratory. Transport and Road Research Laboratory, Crowthorne, Berkshire, England, Rept. SR 344, 1978.
11. K. D. Raithby. Some Flexural Fatigue Properties of Concrete: Effects of Age and Method of Curing.

Proc., 1st Australian Conference on Engineering Materials, Sydney, 1974.
12. J. K. Mitchell and C. L. Monismith. A Thickness Design Procedure for Pavements with Cement-Stabilised Bases and Thin Asphalt Surfacings. Proc., 4th International Conference on the Structural Design of Asphalt Pavements, Univ. of Michigan, Ann Arbor, Vol. 1, 1977, pp. 409-416.
13. British Road Research Laboratory. A Guide to the Structural Design of Pavements for New Roads, 3rd Ed. Her Majesty's Stationery Office, London, Road Note 29, 1970.
14. P. D. Thompson, D. Croney, and E. W. H. Currer. The Alconbury Hill Experiment and Its Relation to Flexible Pavement Design. Proc., 3rd International Conference on the Structural Design of Asphalt Pavements, London, 1972, pp. 920-937.
15. J. R. Boyce, S. F. Brown, and P. S. Pell. The Resilient Behaviour of a Granular Material Under Repeated Loading. Proc., Australian Road Research Board, Vol. 8, 1976, pp. 8-19.
16. E. Otte and C. L. Monismith. Some Aspects of Upside-Down Pavement Design. Proc., Australian Road Research Board, Vol. 8, 1976.

Publication of this paper sponsored by Committee on Flexible Pavement Design.

Evaluation of Structural Coefficients of Stabilized Base-Course Materials

M. C. Wang and T. D. Larson, Pennsylvania Transportation Institute, Pennsylvania State University, University Park

The structural coefficients of two stabilized base-course materials—bituminous concrete and aggregate cement—are evaluated by using two different methods of analysis: the American Association of State Highway and Transportation Officials (AASHTO) performance analysis and the limiting-criteria approach. The AASHTO performance analysis is based on the field performance of 11 bituminous concrete pavements and three aggregate cement pavements; the limiting-criteria approach is based on maximum tensile strain at the bottom of the base course, maximum compressive strain at the top of the subgrade, and maximum pavement surface deflection. The test pavements were constructed at the Pennsylvania Transportation Research Facility. The field performance data collected were rutting, cracking, and present serviceability index. Limiting criteria were developed by using the BISAR computer program and the rutting and cracking data for the test pavements. Results of the evaluation show good agreement between the two methods of analysis. The structural coefficients of the base-course materials were found to vary with many factors, such as the thickness and stiffness of each pavement constituent layer, structural coefficients of other pavement layers, and pavement life. It is concluded that it is very difficult to assign a constant value to the structural coefficient of a base-course material.

The design procedure of the American Association of State Highway and Transportation Officials (AASHTO) serves as the basis for the design of flexible pavements for many highway agencies. One of the requirements of the design procedure is that structural coefficients be assigned to all materials used above the subgrade. Structural coefficients of some pavement materials were determined at the AASHO Road Test; it was recommended, however, that the coefficients be refined to reflect local material properties and climatic conditions. The refinement of the structural coefficients for materials used in Pennsylvania was one of the principal objectives of research at the Pennsylvania Transportation Research Facility at Pennsylvania State University. The specific objective of the study was to determine structural coefficients for the various stabilized base-course materials used in Pennsylvania.

Two different approaches were taken in the evaluation of the structural coefficients of two stabilized base-course materials—namely, bituminous concrete and limestone aggregate cement. The first analysis was based on the use of performance data with analysis techniques similar to those used during the AASHO Road Test. The second approach was based on limiting criteria so that pavement deflection, tensile strain at the bottom of the stabilized base, and compressive strain at the top of the subgrade could be limited within permissible values. This paper presents the results of the analysis.

RESEARCH FACILITY AND FIELD TESTING

The Pennsylvania Transportation Research Facility was constructed in the summer of 1972. The original facility was a 1.6-km (1-mile), one-lane test road composed of sections with different base-course materials and different layer thicknesses. In the fall of 1975, four sections were replaced by eight shorter sections. The plan view and longitudinal profile of the facility are shown in Figure 1. More detailed information on the design, construction, and traffic operations of the facility are available elsewhere (1, 2).

The base-course materials studied were bituminous concrete, aggregate cement, aggregate-lime-pozzolan, and aggregate-bituminous. Three types of aggregate were used in the aggregate-cement base: limestone, slag, and gravel. Among these base-course materials, there was only one base thickness for the aggregate-bituminous material and for the slag and gravel aggregate-cement material. Although three different base thicknesses were available for the aggregate-lime-pozzolan, the pavements that had 10.1- and 15.2-cm (4- and 6-in) thick base—i.e., sections F and G—did not cure properly because of cold weather during construction. Thus, only bituminous concrete and limestone aggregate cement had three levels of base-course thickness. Since the calculation of structural coefficients using the AASHTO performance approach requires examining the change in the indicators of pavement performance across levels of layer thicknesses, only

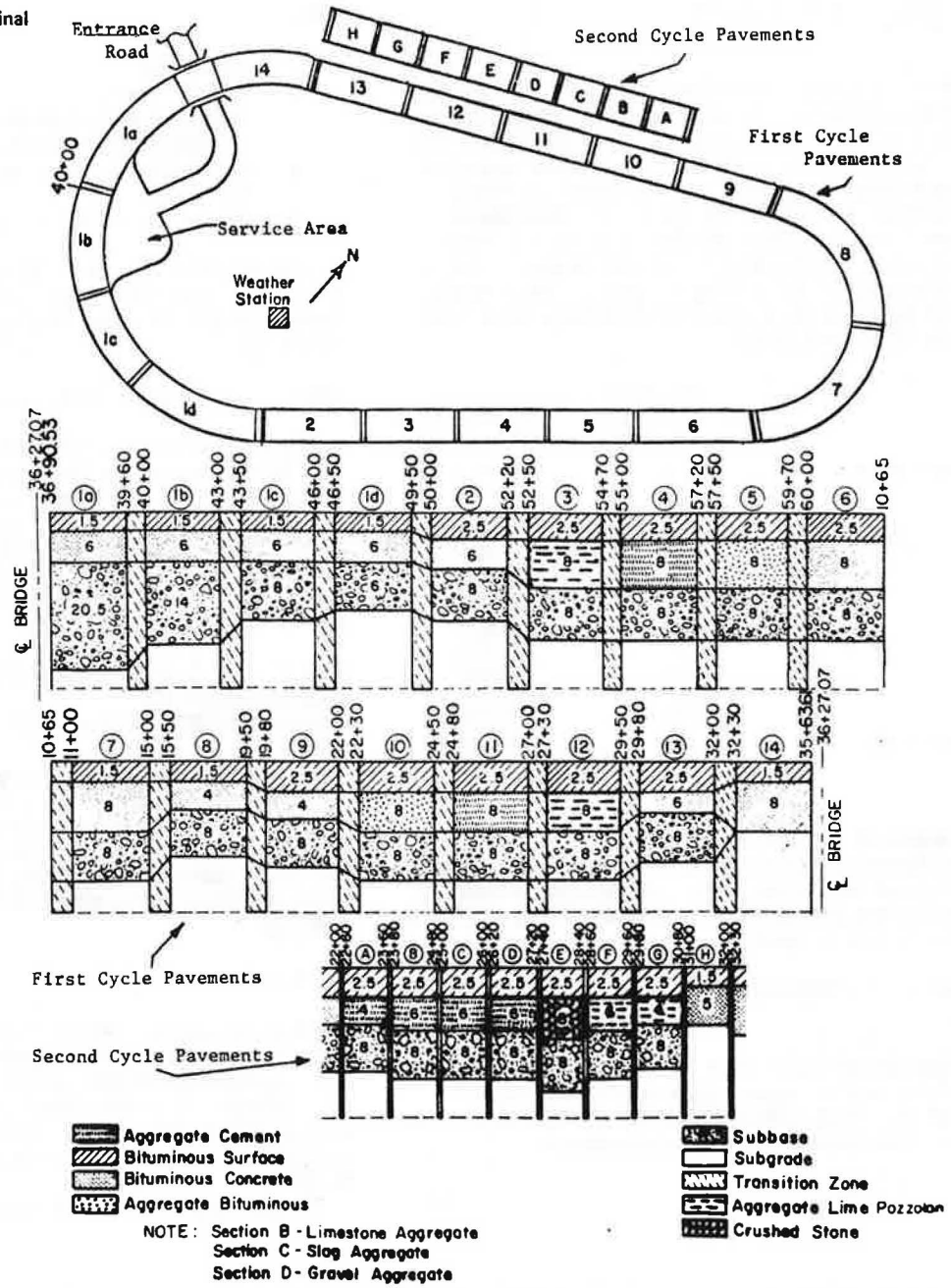

Figure 1. Plan view and longitudinal profile of test track.

bituminous concrete and limestone aggregate-cement pavements are analyzed in this paper.

Field testing of pavement performance was conducted periodically. Rut depth was measured biweekly every 12.2 m (40 ft) in both wheel paths by using an A-frame that was attached to a 2.1-m (7-ft) long base channel. Surface cracking was surveyed and mapped biweekly. Surface roughness was measured in both wheel paths by using a MacBeth profilograph. The roughness factors obtained from the profilograph data were converted into present serviceability index (PSI) by using the following equations (since these equations are formulated in U.S. customary units, no SI equivalents are given):

$$PSI = 11.33 - 4.06 (\log RF) - 0.01 \sqrt{C + P} - 1.34 \overline{RD}^2 \quad (1)$$

$$RF = 63.267 + 1.0831 (R) \quad (2)$$

where

RF = Mays meter roughness factor,
C = area of cracking (ft^2/1000 ft^2),
P = area of patching (ft^2/1000 ft^2),
$\overline{RD}$ = average rut depth (in), and
R = profilograph readings (in/mile).

Equation 2 was developed by the Bureau of Materials, Testing, and Research of the Pennsylvania Department of Transportation (PennDOT).

In addition, surface deflections, pavement temperature, depth of frost penetration, weather data, and subgrade moisture were collected. Detailed information on field testing is available elsewhere (1).

PAVEMENT PERFORMANCE DATA

Results of the crack survey for bituminous concrete and limestone-aggregate-cement pavements are summarized in Table 1 in terms of the number of 80-kN [18 000-lbf (18-kip)] equivalent axle-load (EAL) applications when significant fatigue cracking was observed, the total length of class 1 cracks, and the total area of class 2 and class 3 cracks. The table below gives rut-depth data at 1 million EALs and the number of 80-kN EALs when 6.4-mm (0.25-in) rutting occurred. Numbers of EALs for sections 13, 4, and B were extrapolated from field data (1 mm = 0.04 in):

Base	Section	Rut Depth at 1 Million EALs (mm)	Number of EALs at 6.4-mm Rutting
Bituminous concrete	1A	1.8	1 700 000
	1B	2.5	1 600 000
	1C	3.6	1 400 000
	1D	5.1	1 140 000
	2	3.1	1 650 000
	6	3.8	1 520 000
	7	4.1	1 420 000
	8	14.0	640 000
	9	12.5	570 000
	13	4.8	1 210 000
	14	4.3	1 180 000
	H	>50	270 000
Limestone aggregate cement	4	1.3	2 300 000
	A	9.4	760 000
	B	2.8	1 800 000

The variation of PSI with 80-kN EAL applications is shown in Figure 2. Note that each PSI value represents the average of both wheel paths. Performance data for other pavements appear in papers by Wang and Kilareski elsewhere in this Record.

PAVEMENT PERFORMANCE MODEL

The mathematical model used to describe the serviceability trends is the same as that used at the AASHO Road Test (3). It is assumed that the serviceability loss is a power function of axle-load applications:

$$c_0 - p = (c_0 - c_1)\,(W/\rho)^{\beta} \qquad (3)$$

where

c_0 = initial PSI,
p = PSI at time t,
c_1 = terminal serviceability index (TSI) = 2.5 for the models reported here,
ρ = pavement life expressed in terms of 80-kN EALs, and
β = rate of change of serviceability loss.

Fitting the model to the observed (PSI and EAL) data points was a straightforward application of simple linear regression with a transformed version of Equation 3 (3):

$$\log[(c_0 - p)/(c_0 - c_1)] = \beta\,(\log W - \log \rho) \qquad (4)$$

where the terms are as described for Equation 3.

Two parameters (β and $\log \rho$) were estimated for each test section as a result of fitting Equation 4. These two parameters were interpreted as the indicators of pavement performance for each section. The two indicators of pavement performance were instrumental in the calculation of structural coefficients, in which the performance approach described below was used.

STRUCTURAL COEFFICIENTS DETERMINED BY PERFORMANCE APPROACH

For relating pavement performance to design and load variables, the AASHTO analysis procedure assumed mathematical models to relate β and $\log \rho$ to layer thickness, type of axle, and magnitude of axle loads. In these mathematical models, the layer thicknesses were contained in the structural number (SN), as follows (4):

$$SN = a_1 D_1 + a_2 D_2 + a_3 D_3$$

where a_1, a_2, and a_3 = structural coefficients for the surface, base, and subbase, respectively, and D_1, D_2, D_3 layer thicknesses of the surface, base, and subbase, respectively. The structural coefficients were averaged partial regression coefficients that resulted from examining the change in β and $\log \rho$ across levels of D_1, D_2, and D_3.

To determine structural coefficients in the current

Table 1. Results of crack survey.

Base	Section	Number of EALs at First Appearance of Significant Cracking (000 000s)	Amount of Cracking: Class 1 (m/km^2)	Amount of Cracking: Classes 2 and 3 (m^2/km^2)
Bituminous concrete	1A	-	14 800	0[a]
	1B	-	13 200	0[a]
	1C	1.65	61 300	0[a]
	1D	1.45	85 900	26 000[a]
	2	2.35	56 400	0[a]
	6	-	4 900	0[a]
	7	2.38	8 900	0[a]
	8	0.386	0[b]	85 500[b]
	9	1.16	385 400	180 400[c]
	13	-	0[b]	0[b]
	14	0.906	47 600[d]	88 800[e]
	H	0.359	0[d]	133 300[d]
Limestone aggregate cement	4	2.3	195 800[a]	3 000[a]
	A	0.75	372 800[f]	94 200[f]
	B	-	32 900[f]	0[f]

Notes: 1 m/km^2 = 0.0003 $ft/1000\ ft^2$; 1 m^2/km^2 = 0.001 $ft^2/1000\ ft^2$.
[a] As of May 31, 1978, EALs = 2 377 000.
[b] At the end of the first cycle of study, EALs = 1 082 000.
[c] Before overlay, EALs = 2 021 000.
[d] Before overlay, EALs = 405 000.
[e] Before overlay, EALs = 1 487 000.
[f] As of May 31, 1978, EALs = 1 303 000.

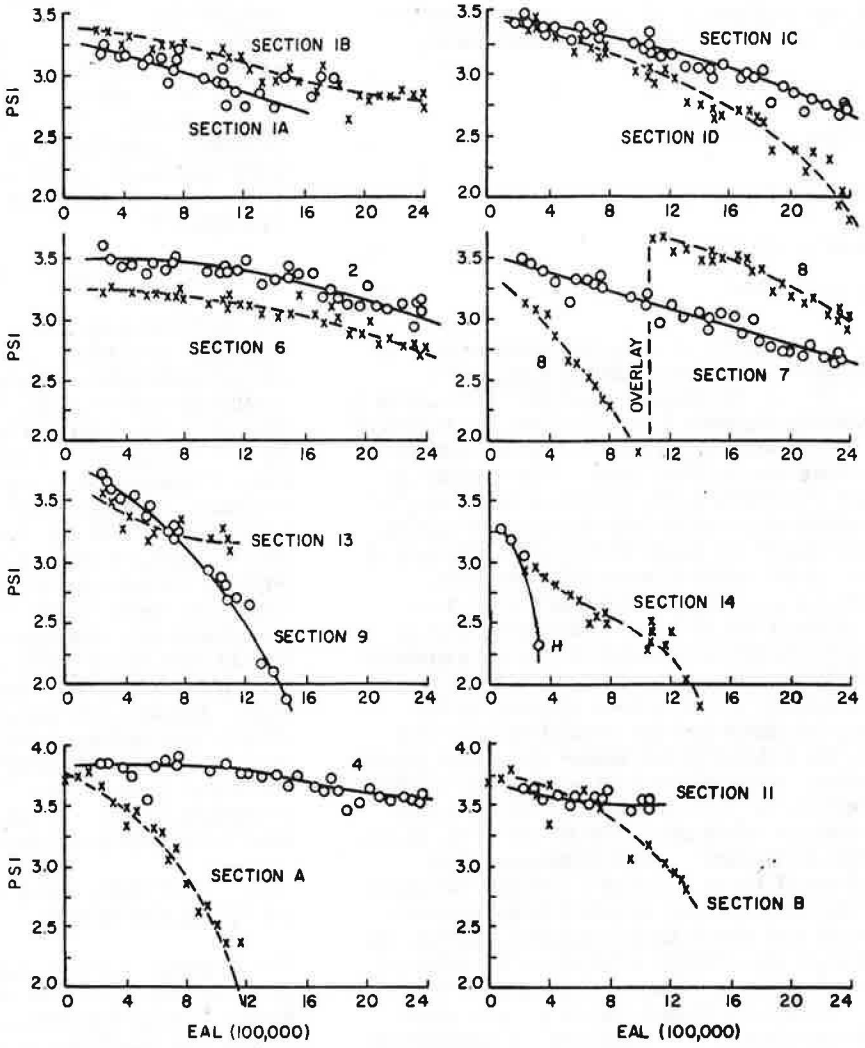

Figure 2. Performance data for pavements with bituminous concrete and limestone-aggregate-cement bases.

study, it was necessary to formulate a model that accommodated the differences between this study and the AASHO Road Test. The primary differences were (a) the use of two base-course materials; (b) the absence of load variables, since all axle loading was converted to 80-kN EAL; and (c) the need to determine if the base-course structural coefficients changed with base-course thickness.

The reduced model finally adopted to relate the pavement performance indicators to design variables (material type and thicknesses D_1 and D_2) was as follows (5):

$$Y_i = \lambda_0 + \lambda_1 M_i + \lambda_2 D_{1i} + \lambda_3 D_{2i}^2 + \lambda_4 (M_i \times D_{2i}) + \lambda_5 (M_i \times D_{2i}^2) + \epsilon_i \quad (6)$$

where

Y_i = β or log ρ;
λ_i = partial regression coefficients;
M_i = base-course material type: 1 = bituminous concrete and 0 = aggregate cement;
D_{1i} and D_{2i} = thicknesses of wearing and base courses, respectively; and
ϵ_i = error terms ~ ind $N(0, \sigma^2)$.

Note that D_3 is constant and therefore was not used in the model and that the subbase structural coefficient was calculated in a separate analysis.

The detailed analysis procedure is outlined elsewhere (5). The analysis assumed that the effect of the design variables was the same (although opposite in algebraic sign) on both β and log ρ. Accordingly, the reduced model (Equation 6) was fit alternately by using first β and then log ρ as the dependent variable in an iterative manner until the λ-coefficients closed to the same values when either β or log ρ was used as the dependent variable. All terms in Equation 6 were statistically significant at a 90 percent level of confidence except λ_2 (wearing-course structural coefficient). The term was left in the model because it is certainly reasonable to expect that D_1 has an effect on pavement performance. It was not possible to detect this effect as statistically significant because of the limited range of D_1 values [3.8-6.4 cm (1.5-2.5 in)] and the small number of observations in the data set (11). The presence of a significant nonlinear effect for D_2 (λ_3 and λ_5 in Equation 6) supports the conclusion that, for the materials and layer thicknesses included in this study, the base-course structural coefficient changes across levels of base-course layer thicknesses.

The results of fitting the model (Equation 6) yielded the following expression, which is referred to as KD only for identification purposes:

$$KD = -1.989M + 0.106D_1 + 0.020D_2^2 + 0.811 (M \times D_2) - 0.075 (M \times D_2^2)$$

where $M = 1$ for bituminous concrete base and 0 for aggregate cement base and D_1 and D_2 = thicknesses of

surface and base courses, respectively. In addition, the two indicators of pavement performance were obtained as follows. For bituminous concrete base,

$$\beta = 1.0 + 8.954/(KD + 1)^{5.175} \quad (8a)$$

$$\rho = 1.262 \times 10^5 (KD + 1)^{4.279} \quad (8b)$$

For limestone-aggregate-cement base,

$$\beta = 1.0 + 9.204/(KD + 1)^{5.735} \quad (9a)$$

$$\rho = 1.018 \times 10^5 (KD + 1)^{4.668} \quad (9b)$$

Because, as mentioned before, the structural coefficient of the subbase was evaluated in a separate analysis, no subbase thickness is included in Equation 7. Thus, by equating Equation 7 with the first two terms of Equation 5, the structural coefficients of the surface and base courses can be determined. The results of the calculated structural coefficients are shown in Figure 3. The structural coefficient of aggregate cement increases throughout the range of the data while that of bituminous concrete peaks at about 15.2 cm (6 in).

The structural coefficients shown in Figure 3 are those obtained for a TSI of 2.5 and after normalizing the raw analysis results to a wearing-course structural coefficient of 0.44. This was necessary because any analysis will determine coefficients specific to that analysis; e.g., consider that the coefficient indicates the change in log ρ (logarithmic scale) with a unit change in layer thickness and that the ρ-values for the AASHO Road Test were in the EAL range of 10^5-10^6 whereas those in the current study are in the 10^6-10^7 EAL range. Therefore, the coefficients would differ even if an additional 2.5 cm (1 in) of material increased the pavement life by the same number of EALs in both studies. The coefficients that result from a specific analysis do, however, indicate the relative abilities of the different layers to contribute to the structural adequacy of the pavement. The relative magnitudes of the raw coefficients were maintained by multiplying the coefficients by the ratio of 0.44 to the raw a_1 value. This normalized the coefficients to a value in common use (a_1 = 0.44) and facilitated interpretation of the base-course structural coefficients.

Figure 3. Structural coefficients of base-course materials determined by performance approach.

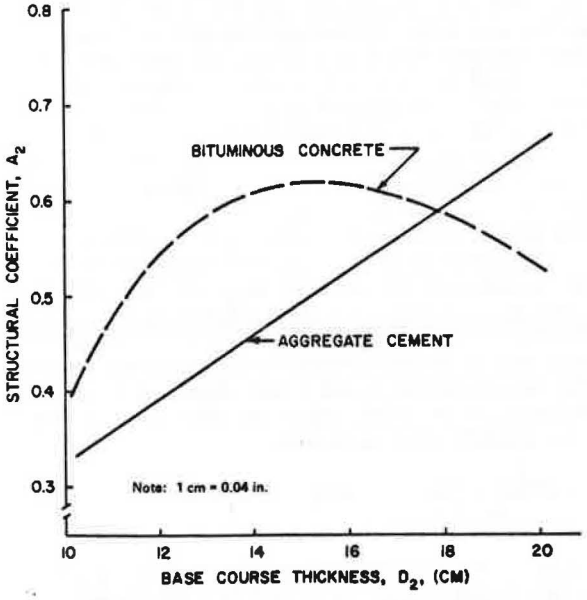

The subbase structural coefficient was calculated by using a similar but separate analysis of the performance data of three test sections whose only variable was subbase thickness [15.2, 20.3, and 35.6 cm (6.0, 8.0, and 14.0 in)]. Note that these three test sections contained base courses of bituminous concrete. The normalized value for a_3 supports the 0.11 value currently being used by PennDOT.

MATERIAL PROPERTIES

The material properties needed to analyze pavement response were modulus of elasticity and Poisson's ratio of each pavement constituent material. The elastic moduli of surface, bituminous concrete base, subbase, and subgrade materials have been reported elsewhere (6). The elastic modulus of limestone-aggregate-cement material was determined by using the same method as that used to determine bituminous concrete base material. It was found that the modulus of limestone aggregate cement did not vary significantly with the curing ages of the specimen, which ranged from two months to one year. In addition, the modulus was practically independent of confining pressures up to 0.21 MPa (30 lbf/in^2), deviatoric stress up to 0.41 MPa (60 lbf/in^2), and number of load applications up to 2000. The average modulus of limestone aggregate cement was approximately equal to 25 000 MPa (3.6 million lbf/in^2). Poisson's ratio of aggregate cement was found to range from 0.15 to 0.22 according to other researchers (7, 8). Thus, a Poisson's ratio of 0.20 was used in the following response analysis.

PAVEMENT RESPONSE AND LIMITING CRITERIA

The response of the test pavements to traffic loading was analyzed for the climate condition that is most critical to pavement performance. The analysis was made by using an elastic-layer computer program and appropriate material properties. The computer program adopted was the BISAR program developed at Koninklijke Shell Laboratorium in Amsterdam.

The traffic loading used was an 80-kN EAL on dual wheels that had a tire pressure of 552 kPa (80 lbf/in^2). The critical responses analyzed were maximum radial tensile strain in the surface and the base layers, maximum vertical compressive strain in the subgrade, and maximum surface deflection. These critical responses were considered because maximum tensile strain and maximum surface deflection are related to fatigue cracking whereas maximum compressive strain is associated with rutting. The pavement response analyzed was related to pavement performance to establish limiting strain criteria.

Since a rut of 6.4 mm (0.25 in) has been widely used for developing limiting strain criteria (9-11), the 80-kN EAL required to produce 6.4-mm rutting for each section concerned is related to the maximum compressive strain at the top of the subgrade (see Figure 4). Note that the relation for the bituminous concrete base material has been given elsewhere (6). Also shown are the results determined at the San Diego test road (9) and the criteria developed by Monismith and McLean (10) and Dormon and Metcalf (11).

Figure 4 demonstrates that, for the same subgrade compressive strain, the pavement that contains bituminous concrete base requires a greater number of EALs than that with aggregate-cement base in order to reach the same rutting of 6.4 mm. This is rather

Figure 4. Maximum compressive strain versus EAL at 6.4-mm rut depth.

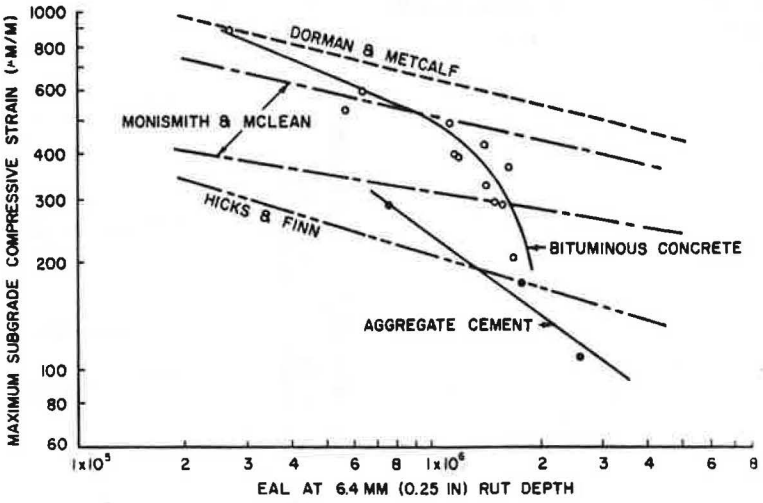

Figure 5. Maximum tensile strain at bottom of base course versus EAL applications.

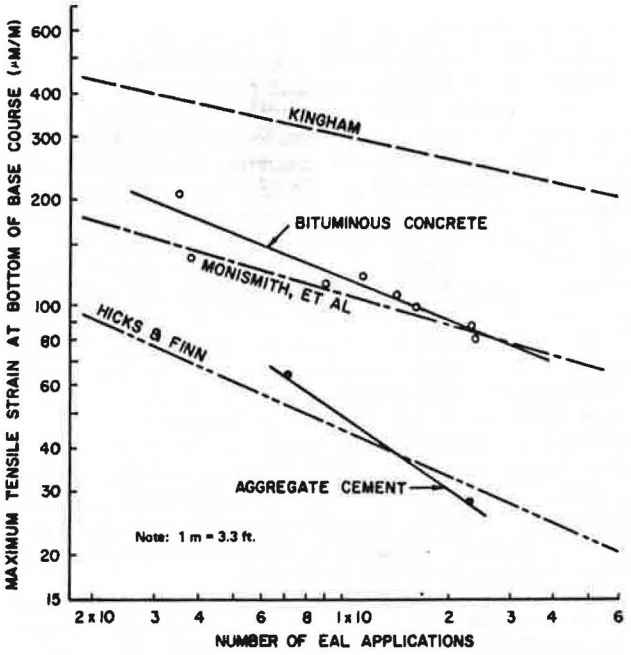

unexpected, for it is generally believed that under the same loading condition bituminous concrete base material will undergo more plastic deformation than aggregate-cement material, so that the pavement that contains bituminous concrete base course will display greater rutting. The possible reasons for this effect are yet to be investigated. Figure 4 indicates that the limiting compressive strain at 1 million EALs equals 450 μm/m (450 $\times$ 10^{-6} in/in) and 230 μm/m (230 $\times$ 10^{-6} in/in) for the bituminous concrete and limestone aggregate cement, respectively. One million EALs was adopted in the development of limiting criteria because that figure is widely associated with 20-year pavement life.

In Figure 5, the maximum tensile strain at the bottom of the base course is related to EAL based on the number of axle loadings at the first appearance of significant surface cracking. Note again that the relation for bituminous concrete base material has been established for field data collected up to July 1976. Results obtained by other researchers (9, 12, 13) are also included in the figure. The figure shows that the limiting tensile strain at 1 million EALs equals 120 μm/m (120 $\times$ 10^{-6} in/in) for the pavements that contain bituminous concrete base and 45 μm/m (45 $\times$ 10^{-6} in/in) for the limestone-aggregate-cement base.

Figure 6 summarizes the relation between the number of EALs at the first appearance of significant surface cracking and the maximum pavement surface deflection. Results obtained by others (9, 13, 14) are also included in the figure for comparison. Figure 6 indicates that the limiting maximum surface deflection at 1 million EALs equals 0.51 mm (0.020 in) for the pavements that contain bituminous concrete base and 0.30 mm (0.012 in) for the limestone-aggregate-cement base.

STRUCTURAL COEFFICIENTS DETERMINED BY LIMITING CRITERIA

The structural coefficients of the bituminous concrete and limestone-aggregate-cement base materials were computed by using the following basic equation developed from the AASHO Road Test (3):

$$\rho = 0.64\,(SN + 1)^{9.36}$$

where ρ = EALs at failure and SN = structural number as defined in Equation 5.

In the computation, the structural coefficient of 0.44, which was originally developed from the AASHO Road Test, was used for the bituminous concrete surface material. Details of the computation procedure are available elsewhere (6). The structural coefficients determined are shown in Figure 7 (6) for the bituminous concrete base and in Figure 8 for the aggregate-cement base material. The figures also show some results obtained from the performance approach; these are included for later discussion.

Figures 7 and 8 demonstrate that the structural coefficients of the base and subbase materials vary with the thicknesses of surface, base, and subbase layers for the conditions studied. The structural coefficient of aggregate cement, however, does not vary with the base-course thickness as much as that of the bituminous concrete base material. The structural coefficient of the subbase material determined from the pavements that contain bituminous concrete base course fluctuates around 0.10. This value is very close to that originally developed at the AASHO Road Test (3) for a sandy gravel

Figure 6. Maximum surface deflection versus EAL applications.

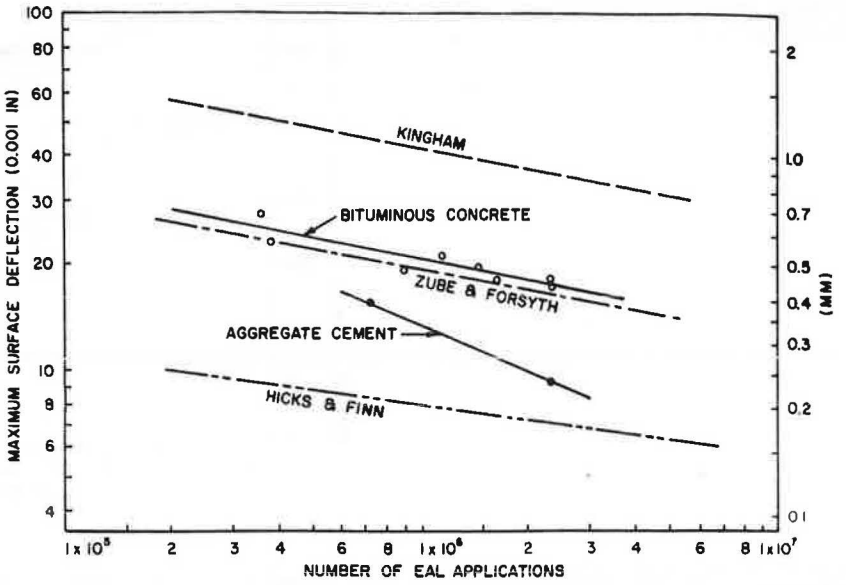

subbase. The structural coefficient of the subbase material determined from the pavements that contain aggregate-cement base course, however, fluctuates around 0.04. This deviation could be attributed to the difference in the relative stiffness between the base and subbase layers. The resilient moduli given earlier for the base and subbase materials indicate that the relative stiffness between the aggregate cement base and the subbase is considerably greater than that between the bituminous concrete base and the subbase materials. Since the layer-thickness combinations that satisfy the limiting criteria depend on the relative stiffness of the constituent layers, the effect on the base thickness of a unit change in the subbase thickness is less significant for the system that contains a base course much stiffer than the subbase course. As a consequence, the structural coefficient of the subbase material evaluated with the aggregate-cement base was lower than that evaluated with the bituminous concrete base. A similar effect of the stiffness of one layer on the structural coefficient of another layer has also been observed by VanTil and others (15).

DISCUSSION OF RESULTS

According to the findings of the AASHO Road Test and Equation 10, pavement life in terms of 80-kN EAL can be expressed as a function of a structural number. Based on this equation, the SNs required for pavement lives of 1 million, 2 million, and 3 million EALs are 3.59, 3.94, and 4.16, respectively. The performance analysis for pavements at the Pennsylvania Transportation Research Facility resulted in two different equations for the two stabilized base-course materials: Equation 8b for bituminous concrete and Equation 9b for aggregate cement. Note that in this analysis the SN is equal to the sum of KD and a_3D_3 (the subbase structural coefficient times the subbase layer thickness). According to these equations, the SNs required for pavement lives of 1 million, 2 million, and 3 million EALs are 3.45, 4.66, and 5.45, respectively, for bituminous concrete and 3.50, 4.57, and 5.28, respectively, for aggregate cement. The results for 1 million EALs are in good agreement with the AASHTO result, whereas those for 2 million and 3 million EALs are slightly higher. Note that the SNs required for different EALs for the two stabilized base-course materials studied are nearly the same; this suggests that for a given pavement life the SNs required are practically independent of the type of base-course material used in the pavement.

A comparison of the structural coefficients of the base-course materials determined by using the two different analysis approaches—namely, the AASHTO performance approach and the limiting-criteria approach—can be made for a common pavement life. The limiting-criteria approach was used for a pavement life of 1 million EALs. From the performance approach, the SN required for the bituminous concrete pavement with a pavement life of 1 million EALs is 3.45, as mentioned earlier. Assuming this SN, a relation between the layer thicknesses of surface and base is given by Equation 7. The base layer thicknesses required for each surface layer thickness of 3.8, 6.4, and 8.9 cm (1.5, 2.5, and 3.5 in) were determined by using this equation. The base-course structural coefficients were then calculated by using 0.44 and 0.11 as the structural coefficients of surface and subbase, respectively. The calculated results are plotted in Figure 7, and a good agreement between the two approaches is shown.

For the aggregate-cement pavement with a pavement life of 1 million EALs, the SN required is 3.50. Base-course structural coefficients were calculated for the same three surface layer thicknesses mentioned above by using Equation 7. In the calculation, a surface-layer structural coefficient of 0.44 was used. However, two different values were used for the subbase structural coefficient: 0.11 and 0.04. The 0.11 value was determined in the performance approach from three pavement sections that contained bituminous concrete base. This value was also produced in the evaluation of bituminous concrete pavement by use of the limiting-criteria approach. As mentioned before, because of the considerable difference in the base-course stiffness of the aggregate cement and the bituminous concrete, the subbase structural coefficient found in the evaluation of aggregate-cement pavements by use of the limiting-criteria approach was about 0.04 rather than 0.11. Because a similar effect has been reported by VanTil and others (15), it is reasonable to use 0.04 as the subbase structural coefficient for this comparison. The calculated results for $a_3 = 0.04$ are shown in Figure 8. Although the data points fall outside the range of the limiting approach for base layer thickness, a fairly good agreement between the two approaches is obtained.

Figure 7. Structural coefficients of bituminous concrete base and limestone subbase.

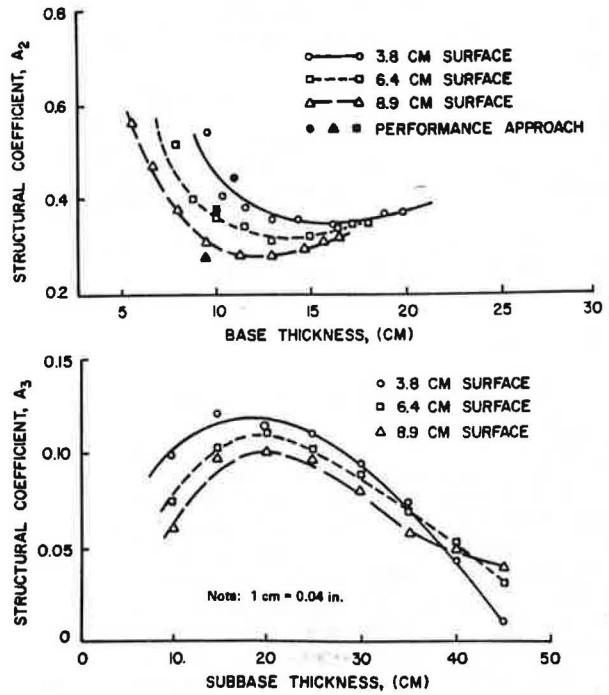

Figure 8. Structural coefficients of aggregate cement base and limestone subbase.

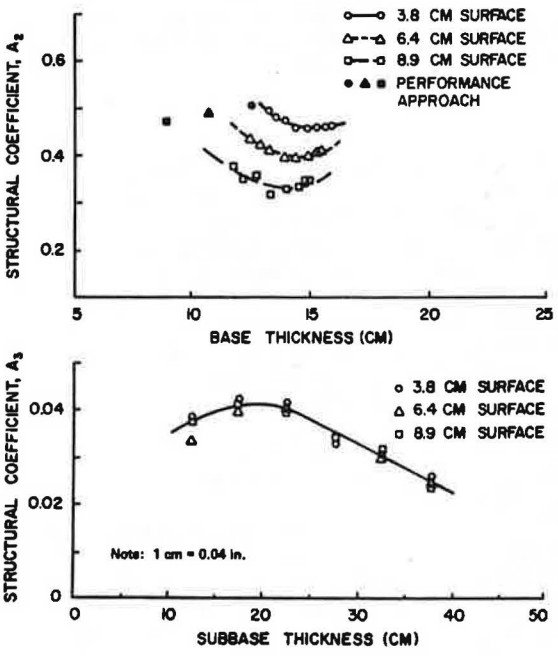

The performance approach can also roughly control the estimated pavement lives by specifying the TSI. For the pavement sections at the research facility, the TSI level that resulted in pavement lives closest to 1 million EALs was about 3.0. The structural coefficients calculated by using this TSI level are compared with the results of the limiting-criteria analysis in Figures 9 and 10. One important point that should be reiterated here is that the performance analysis was performed

Figure 9. Comparison of structural coefficients for bituminous concrete.

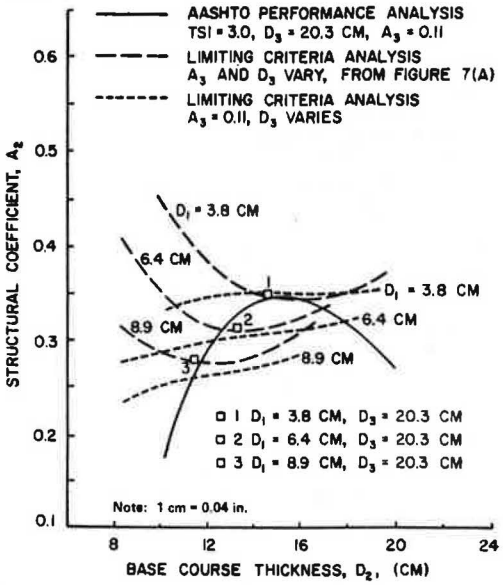

for a constant subbase layer thickness [D_3 = 20.3 cm (8 in)] and a constant subbase structural coefficient (a_3 = 0.11), whereas the limiting-criteria approach allowed both a_3 and D_3 to vary. Because of this basic difference, a direct comparison requires common a_3 and D_3 values.

For the bituminous concrete sections, three data points that have conditions common to both methods of analysis are shown in Figure 9. A very good agreement between the two different approaches is seen. It was valid to plot the results of the limiting-criteria approach for all three wearing thicknesses because no surface - base-course thickness interaction could be detected in the performance analysis. This implied that the base-course structural coefficient is independent of the surface layer thickness (within the range of the field data). This contradicts the findings of the limiting-criteria approach, which shows base-course structural coefficients to vary with surface layer thickness. The interpretation is that this effect was not sufficiently pronounced in the field data to be detected as statistically significant since the surface layer thickness only occurred at two levels in the field and the field data composed a very limited data set.

For aggregate cement, two values of the subbase structural coefficient a_3 were used for the reason stated earlier. Figure 10 shows that, when a constant value of a_3 is used, the structural coefficient of the aggregate cement (a_2) increases linearly with increasing thickness of the base course (D_2) regardless of the method of analysis used. The results of the limiting-criteria analysis indicate that, although the rate of increase of a_2 with D_2 for a_2 = 0.04 is almost equal to that obtained from the performance approach, the rate of increase for a_3 = 0.11 is much greater. Furthermore, a_2 varies considerably with surface layer thickness D_1 when a_3 = 0.04. When a_3 = 0.11, however, the effect of D_1 on a_2 is not as significant.

It should be noted that the only variable associated with the aggregate-cement base course in the field experimental design was the thickness of the aggregate-cement base course. The varying subbase thickness and varying surface layer thicknesses all occurred in sections that contained bituminous concrete. Accordingly, all conclusions of the performance analysis concerning

Figure 10. Comparison of structural coefficients for aggregate cement.

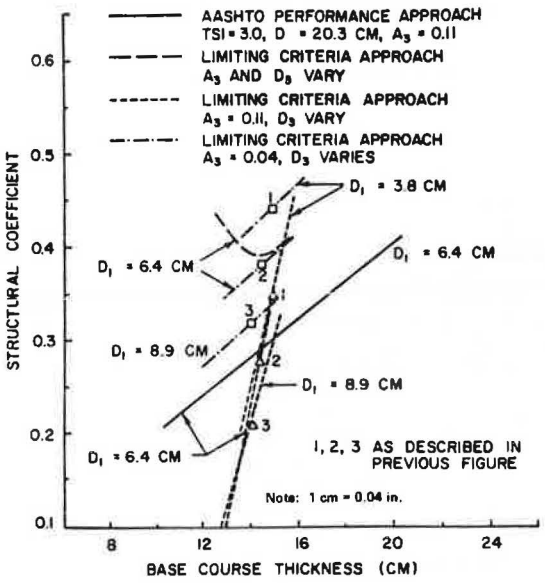

the surface course, surface × base interactions, and subbase were generated from the data of the bituminous concrete base. Of necessity, these results were "borrowed" by the analysis of the aggregate cement to identify surface and subbase structural coefficients to be used with the aggregate-cement structural coefficients. As noted before, in the performance analysis the thicknesses of the surface and subbase layers used with the aggregate-cement base course were 6.4 and 20.3 cm (2.5 and 8 in), respectively. The limiting-criteria data points that correspond to these layer thicknesses are identified by the number 2 in Figure 10. It is seen that a better agreement between the two approaches was obtained for $a_3 = 0.11$ simply because it was used in the performance analysis.

Both Figures 9 and 10 demonstrate that, for the two types of base-course materials studied, the base-course structural coefficient a_2 first decreases and then increases with increasing base-course thickness D_2, when both subbase structural coefficient a_3 and subbase layer thickness D_3 are allowed to vary. When a_3 is kept constant, however, a_2 increases with an increase in D_2. Furthermore, when both a_3 and D_3 are kept constant, a_2 also increases with D_2 for the aggregate-cement base material whereas, for the bituminous concrete base material, a_2 first increases and then decreases with increasing D_2 within the range of conditions studied.

The preceding results indicate that a_2 varies with many factors, such as the thickness and stiffness of each pavement constituent layer, structural coefficients of other pavement layers, and pavement life. This complex dependency of a_2 not only makes it difficult to assign a constant and unique value of a_2 for a base-course material but also complicates practical applications of a_2 in pavement design.

SUMMARY AND CONCLUSIONS

The structural coefficients of two stabilized base-course materials—bituminous concrete and aggregate cement—were evaluated. Two different methods of analysis were used: the AASHTO performance analysis and the limiting-criteria approach. The AASHTO performance analysis was based on the field performance of 11 bituminous concrete pavements and three aggregate-cement pavements, whereas the limiting-criteria approach was based on the maximum tensile strain at the bottom of the base course, the maximum compressive strain at the top of the subgrade, and the maximum pavement surface deflection.

The results of the evaluation showed good agreement between the two methods of analysis. It was found that the structural coefficients of the base-course materials varied with many factors, such as the thickness and stiffness of each pavement constituent layer, structural coefficients of other pavement layers, and pavement life. This complex dependency makes it very difficult to assign a constant and unique value to the structural coefficient of a base-course material.

ACKNOWLEDGMENT

The study presented here is a part of two research projects sponsored by the Pennsylvania Department of Transportation in cooperation with the Federal Highway Administration, U.S. Department of Transportation. This support is gratefully acknowledged. We wish to express our gratitude to the National Crushed Stone Association for lending us its repeated-load test apparatus for laboratory testing and to the Asphalt Institute for its cooperation in conducting the fatigue testing during the initial phase of the research. Our sincere appreciation is extended to S. A. Kutz, who performed the analysis in which the AASHTO performance approach was used, participated in the preparation of the manuscript, and assisted in the collection and reduction of the field data. Others who participated in the field testing and data reduction were B. A. Anani, R. P. Anderson, P. J. Kersavage, and W. P. Kilareski.

This paper represents our views and does not necessarily reflect those of the Pennsylvania Department of Transportation or the Federal Highway Administration.

REFERENCES

1. E. S. Lindow, W. P. Kilareski, G. Q. Bass, and T. D. Larson. An Evaluation of Pennsylvania's Flexible Pavement Design Methodology: Volume 2—Construction, Instrumentation, and Operation. Pennsylvania Transportation Institute, Pennsylvania State Univ., University Park, Interim Rept. PTI 7504, Feb. 1973.
2. W. P. Kilareski, S. A. Kutz, and G. Cumberledge. A Study of Flexible Pavement Base Course and Overlay Designs: Modification, Construction, and Instrumentation of an Experimental Highway. Pennsylvania Transportation Institute, Pennsylvania State Univ., University Park, Interim Rept. PTI 7607, April 1976.
3. The AASHO Road Test: Report 5—Pavement Research. HRB, Special Rept. 61E, 1962.
4. AASHO Interim Guide for the Design of Pavement Structures. AASHO, Washington, DC, 1972.
5. S. A. Kutz and T. D. Larson. Determination of the Structural Coefficients of Two Stabilized Base Course Materials Using the AASHTO Performance Method. Pennsylvania Transportation Institute, Pennsylvania State Univ., University Park, Res. Project 75-2, Interim Rept., July 1977.
6. M. C. Wang and T. D. Larson. Performance Evaluation for Bituminous Concrete Pavements at the Pennsylvania State Test Track. TRB, Transportation Research Record 632, 1977, pp. 21-27.
7. K. Nair, W. S. Smith, and C. Y. Chang. Characterization of Asphalt Concrete and Cement-Treated Granular Base Course. Materials Re-

search and Development, Inc., Oakland, CA, Feb. 1972.
8. S. Kolias and R. I. T. Williams. Cement-Bound Road Materials: Strength and Elastic Properties Measured in the Laboratory. Transport and Road Research Laboratory, Crowthorne, Berkshire, England, TRRL Supplementary Rept. 344, 1978.
9. R. G. Hicks and F. N. Finn. Prediction of Pavement Performance from Calculated Stresses and Strains at the San Diego Test Road. Proc., AAPT, Vol. 43, 1974, pp. 1-40.
10. C. L. Monismith and D. B. McLean. Structural Design Considerations. Proc., AAPT, Vol. 41, 1972, pp. 258-305.
11. G. M. Dormon and T. Metcalf. Design Curves for Flexible Pavements Based on Layered System Theory. HRB, Highway Research Record 71, 1965, pp. 69-84.
12. C. L. Monismith, J. A. Epps, D. A. Kasianchuk, and D. B. McLean. Asphalt Mixture Behavior in Repeated Flexure. Institute of Transportation and Traffic Engineering, Univ. of California, Berkeley, Rept. TE70-5, 1970.
13. R. I. Kingham. Fatigue Criteria Developed from AASHO Road Test Data. Proc., 3rd International Conference on the Structural Design of Asphalt Pavements, Univ. of Michigan, Ann Arbor, 1972, pp. 656-669.
14. E. Zube and R. Forsyth. Flexible Pavement Maintenance Requirements as Determined by Deflection Measurements. HRB, Highway Research Record 129, 1966, pp. 60-75.
15. C. J. VanTil, B. F. McCullough, B. A. Vallerga, and R. G. Hicks. Evaluation of AASHO Interim Guides for Design of Pavement Structures. NCHRP, Rept. 128, 1972.

Publication of this paper sponsored by Committee on Flexible Pavement Design.

Behavior and Performance of Aggregate-Cement Pavements

M. C. Wang and W. P. Kilareski, Pennsylvania Transportation Institute, Pennsylvania State University, University Park

Field performance of six aggregate-cement pavements at the Pennsylvania Transportation Research Facility was evaluated based on their rutting and cracking behavior and values of present serviceability index. Three types of aggregate were used in the aggregate-cement bases: limestone, slag, and gravel. The results of an analysis of relative performance among the three types of aggregate-cement materials are presented. The pavement response to an 80-kN [18 000-lbf (18-kip)] equivalent single-axle load was analyzed by using an elastic-layer computer program. The pavement response was related with the field performance data to establish limiting criteria. Among the three types of aggregate studied, limestone possesses the greatest strength and performs best in terms of rutting, cracking, and change in serviceability index. Gravel possesses greater compressive strength but smaller resilient modulus and fatigue strength than slag. The pavement with a base of slag aggregate cement performs better than that with a base of gravel aggregate cement. The limiting criteria developed were a maximum compressive strain of 230 μm/m (0.000 230 in/in) for limestone aggregate and 180 μm/m (0.000 180 in/in) for both slag and gravel aggregates, a maximum tensile strain of 45 μm/m (0.000 45 in/in), and a maximum pavement surface deflection of 0.30 mm (0.012 in) for all three types of aggregate studied. With these limiting criteria, it would be possible to design aggregate-cement pavements to withstand 1 million 80-kN equivalent axle-load applications without significant surface cracking or excessive rutting.

The use of cement-stabilized material in pavement structures has increased steadily over the past decades. Most available procedures for thickness design of cement-stabilized layers are largely based on empirical rules. Recognizing the need for developing an improved method of thickness design, the Committee on Structural Design of Roadways of the American Society of Civil Engineers identified steps required for achieving this goal (1). Among the steps identified are the establishment of failure criteria and performance studies in the field. A number of studies have provided information relative to these steps, including those by Bofinger (2), Shen and Mitchell (3), Larsen and Nussbaum (4), Larsen (5), Mitchell and Freitag (6), and Nussbaum and Larsen (7). However, most of these studies dealt with cement-stabilized soils; very few studies on cement-stabilized aggregates are currently available.

An investigation of the field performance of various stabilized base-course materials was conducted at the Pennsylvania Transportation Research Facility at Pennsylvania State University. The stabilized materials studied were aggregate cement, bituminous concrete, aggregate-lime-pozzolan, and aggregate-bituminous. Three types of aggregate were used in the aggregate-cement material. The performance of bituminous concrete and aggregate-lime-pozzolan pavements has been discussed elsewhere (8, 9). This paper presents the results of a performance evaluation for pavements that contain aggregate-cement base courses. Limiting strain and limiting deflection criteria are developed from field performance data and pavement response. The results provide information that is useful in the steps identified above.

AGGREGATE-CEMENT MATERIAL

The aggregate-cement base material was composed of six percent by weight of type 1 portland cement and 94 percent by weight of aggregate. The mix design was determined by the Bureau of Materials, Testing, and Research of the Pennsylvania Department of Transportation (PennDOT).

Three types of aggregate were used: crushed limestone, gravel, and slag. The limestone and gravel are natural to central Pennsylvania. The slag was a blast-furnace slag obtained from Johnstown, Pennsylvania. Some basic characteristics of the slag are summarized

below (1 kg/m^3 = 0.062 lb/ft^3):

Characteristic	Measurement
Specific gravity	2.34
Weight	1237 kg/m^3
Absorption	4.9 percent
Sodium sulfate loss	0.78
Los Angeles abrasion loss	35.2 percent
Loss by washing	0

The gradations of the three types of aggregate are about the same. The average gradation is given below (1 mm = 0.039 in):

Sieve Size (mm)	Percentage Passing
51	100
19	96
9.5	79.6
4.75	66.2
1.18	25.6
0.15	6.7

The strength and fatigue properties of the aggregate-cement materials were determined on specimens both compacted in the laboratory and taken from the test pavements. The laboratory-compacted specimens were 15.2 cm (6 in) in diameter and 25.4 cm (10 in) in height and were molded to the same moisture content and dry density as those in the test pavements by using the modified American Association of State Highway and Transportation Officials (AASHTO) compaction effort. Table 1 summarizes the moisture content and dry density of the test specimens. The compacted specimens were embedded in the soil near the test pavements to cure under the same environmental conditions as the pavements. Core samples were 10.2 cm (4 in) in diameter and 20.4 cm (8 in) in height. They were taken from the test pavement after about 1.1 million 80-kN [18 000-lbf (18-kip)] equivalent axle-load (EAL) applications (EAL, as used in this paper, indicates an 80-kN load). The 1.1 million EALs were achieved after approximately 20 months of traffic operation. Test results indicate that the laboratory specimens had practically the same strength property as the core samples.

Triaxial compression test results with confining pressures up to 0.21 MPa (30 lbf/in^2) showed no significant effect of confining pressure on the compressive strength of the aggregate-cement material. Tensile strength was determined by using the double-punch test (8). Table 1 gives some results of the compression and double-punch tests as well as the average resilient modulus of the aggregate-cement materials. The repeated loading used for the determination of resilient modulus had a load duration of 0.1 s and a frequency of 20 cycles/min. Test results indicate that the resilient modulus was practically independent of confining pressures up to 0.21 MPa, deviatoric stress up to 0.41 MPa (60 lbf/in^2), and number of load applications up to 2000. In addition, the resilient modulus did not vary significantly for specimens cured at different durations (from two months to one year).

The fatigue property was evaluated by using the repeated-load flexure test on beam specimens. The beam specimens, which were compacted in the laboratory, were 8.25 cm (3.25 in) square by 46 cm (18 in) long. The beams were simply supported and were loaded with two symmetrically placed interior concentrated loads. The repeated loading had the same duration and frequency as that used in the repeated triaxial compression test. It was found that the fatigue property remained almost constant for different specimen ages, from two months to one year. Test results are given in Table 1 in terms of K_1 and K_2 of the following fatigue equation:

$$N = K_1(1/\epsilon)^{K_2}$$

where N = number of load applications to fail[illegible] and ϵ = tensile strain.

The material properties given in Table 1 [illegible] that, among the three types of aggregate stu[illegible] stone aggregate is superior to slag and grave[illegible] of strength, resilient modulus, and fatigue pr[illegible]. A comparison between the properties of slag a[illegible] reveals that the gravel has considerably gre[illegible] than the slag. The resilient modulus of slag, however, is significantly greater than that of gravel. The difference in fatigue property between the slag and gravel is small, although the slag appears to be better in this area than the gravel. Thus, it is rather difficult to rank the slag aggregate cement and the gravel aggregate cement based merely on their laboratory properties.

Table 1. Properties of aggregate-cement materials.

Property	Limestone	Gravel	Slag
Moisture content (%)	7.7	8.7	11.2
Dry density (kg/m^3)	2296	2152	2001
Compressive strength (MPa)			
7 days	10.34	9.65	6.20
4 weeks	13.79	-	-
1 year	21.18	16.79	13.50
Tensile strength[a] (MPa)	2.07	-	-
Resilient modulus[a] (MPa)	25 000	17 000	22 000
Fatigue[a]			
K_1	6.56×10^{-21}	1.83×10^{-8}	4.48×10^{-9}
K_2	6.05	2.93	3.08

Note: 1 kg/m^3 = 0.062 lb/ft^3; 1 MPa = 145 lbf/in^2.

[a]Average values for specimens cured between 2 months and 1 year.

TEST PAVEMENTS

Six pavements containing aggregate-cement base [illegible] constructed at the Pennsylvania Transportation Research Facility. Among the six pavements, two were constructed in the summer of 1972 and the other four were built in the fall of 1975. Each of the first two pavements contained a 20.3-cm (8-in) limestone-aggregate-cement base. One of the last four pavements had a 10[illegible] (4-in) limestone-aggregate-cement base, while the other three pavements contained a 15.2-cm (6-in) base made up of all three types of aggregate. One of the first two pavements was in a cut and the other in a fill section. In fact, the pavement in the fill section was removed after about 1.1 million EALs. At that time the last four pavements were constructed at the site of the removed pavement. Each of the first two pavements was 67.1 m (220 ft) long, and each of the last four was 30.5 m (100 ft) long. All six pavements were 3.7 m (12 ft) wide and contained a 6.4-m (2.5-in) bituminous concrete surface course and a 20.3-cm subbase layer.

The materials for the aggregate-cement bases were mixed in a central plant. For the 10.2-cm (4-in) and 16.2-cm (6-in) base, the aggregate cement was placed in one lift; for the 20.3-cm (8-in) base, the aggregate cement was placed in two 10.2-cm compacted layers. The top of the first lift was scarified before placement of the second lift. Compaction was accomplished by using a roller with three steel wheels for the breakdown and compaction operation and a two-wheel roller for the breakdown and compaction operation and a two-wheel tandem roller for the finish operation. When the finishing operation was completed, a bituminous seal coat was

applied to the surface of the aggregate-cement base course.

In addition to the aggregate-cement pavements, the research facility also contained several other pavements that had different base materials and layer thicknesses. The subgrade soil at the research facility was predominantly classification A-7. The first two pavements were subjected to traffic approximately two months after completion of the base-course construction. For the last four pavements, traffic was started about one month after the base course was completed. The traffic consisted of a conventional truck tractor that pulled a semitrailer and a full trailer. After about 1.5 million EALs, another full trailer was added to increase the rate of loading. The axle loading was within the range of 80-107 kN (18 000-24 000 lbf). Complete information on design, construction, material properties, and traffic operation is available elsewhere (9, 10).

FIELD EVALUATION

Field testing of pavement performance was conducted periodically. Rut depth was measured biweekly every 12.2 m (40 ft) in both wheel paths by using an A-frame that was attached to a 2.1-m (7-ft) long base channel. Surface cracking was surveyed and mapped biweekly. Surface roughness was measured in both wheel paths by using a MacBeth profilograph. The roughness factors obtained from the profilograph data were converted into pavement present serviceability index (PSI) by using Equations 1 and 2 given in the paper by Wang and Larson elsewhere in this Record. In addition, data on surface deflections, pavement temperature, depth of frost penetration, air temperature, wind velocity, precipitation, and subgrade moisture were collected.

Figure 1. Rut depth versus EAL applications for limestone-aggregate-cement pavements.

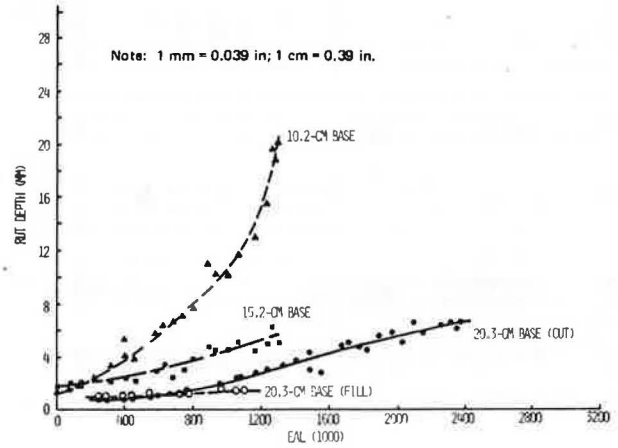

Figure 2. Rut depth versus EAL applications for three types of aggregate-cement pavement.

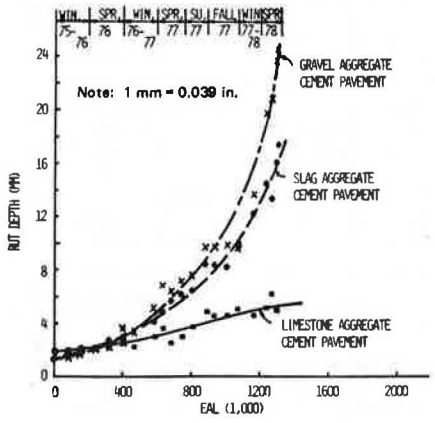

PAVEMENT DISTRESS

Rutting

Figures 1 and 2 show the variation of rut depth with number of EAL applications. The effect of base layer thickness on rutting for the pavements that contain limestone aggregate cement is shown in Figure 1. As expected, the pavement with a thick base course undergoes less rutting. The data on rut depth are quite consistent for the two 20.3-cm (8-in) base pavements, one in a cut and the other in a fill section. A comparison of the rut-depth data among the three types of aggregates under study is shown in Figure 2. Also shown in this figure are seasons within which the rut-depth data were taken. No clear indication is seen of significant seasonal variation in rutting. The figure indicates that, for the three types of aggregates studied, the limestone appears to have the greatest resistance and the gravel the least resistance to rutting.

It is generally recognized that rutting is primarily caused by the permanent deformation of each constituent pavement material. Because of the rigid and brittle nature of aggregate cement, permanent deformation in the aggregate-cement base is usually very small and can be neglected in the evaluation of rutting. Thus, for the three pavement systems that contain different types of aggregate but the same layer thicknesses, the difference in rutting would probably result from different permanent deformations in the subgrade. Permanent deformation in the subgrade depends greatly on the vertical compressive stress that is acting on the top of the subgrade. The vertical compressive stress decreases with increasing base-course modulus, other factors being equal. Since the resilient modulus of the aggregate cement decreases in order from limestone to slag to gravel, rutting would be expected to be smallest in the limestone, intermediate in the slag, and greatest in the gravel-aggregate-cement pavements.

According to Figures 1 and 2, for pavements that contain limestone-aggregate-cement bases, the number of EAL applications required for 6 mm (0.25 in) of rutting is approximately 760 000 for 10.2-cm (4-in) base, 1 800 000 for 15.2-cm (6-in) base, and 2 700 000 for 20.3-cm (8-in) base. For the pavements that contain 15.2-cm base, the number of EALs is about 900 000 for the slag aggregate and 800 000 for the gravel aggregate. These data will form the basis for the later development of limiting strain criteria.

Cracking

No cracking was observed in the fill section with the 20.3-cm (8-in) limestone-aggregate-cement base when the pavement was removed. In the cut section with the 20.3-cm limestone-aggregate-cement base, however, a transverse shrinkage crack developed across the entire pavement width about 3.2 m (10 ft) from one end of the pavement. This transverse crack was observed at approximately 1 million EALs, which was equivalent to about 16 months after construction. Figure 3 shows crack patterns mapped at about 2.4 million EALs. Longitudinal cracking appeared along the edge at approximately 1.4 million EALs. After about 1.8 million,

some longitudinal cracks developed in the wheel path. The rate of growth of class 1 cracking is shown in Figure 4. All class 2 and class 3 cracking developed along the transverse crack. The total area of class 2 and class 3 cracking was about 3000 m^2/km^2 (3 $ft^2/1000\ ft^2$).

In the pavement that contained 15.2-cm (6-in) limestone-aggregate-cement base, there was only one transverse shrinkage crack across the entire pavement width. This shrinkage crack was observed at approximately 1.27 million EAL applications. In the pavement that contained 10.2-cm (4-in) limestone-aggregate-cement base, the first transverse shrinkage crack developed about 3.2 m (10 ft) from one end of the pavement and was observed at approximately 84 000 EALs. The second transverse shrinkage crack developed at about the middle of the pavement at about 565 000 EAL applications. Longitudinal cracking appeared in both wheel paths after about 700 000 EALs. Class 2 cracking was not observed until about 1.07 million EALs. The length of class 1 cracking and the area of class 2 and class 3 cracking are shown in Figure 4. Figure 5 shows the crack pattern as it was mapped at three different times.

In the pavement that contained 15.2-cm (6-in) slag-aggregate-cement base, the first transverse shrinkage crack developed at about the middle of the pavement after approximately 565 000 EAL applications. At approximately 622 000 applications, a second transverse shrinkage crack appeared about 3.6 m (12 ft) from one end of the pavement. At almost that same time, longitudinal cracking developed in the wheel paths. Class 2 cracking appeared at about 1.2 million EAL applications. Figure 4 summarizes the length of class 1 cracking and the area of class 2 cracking. Figure 6 shows the growth of cracking.

For the pavement that contained 15.2-cm (6-in) gravel-aggregate-cement base, three transverse shrinkage cracks developed almost simultaneously during the early stage of pavement life. The locations of the three cracks are shown in Figure 7. The length of class 1 cracking and the area of class 2 cracking are shown in Figure 4.

Figure 4 shows that, for pavements of the same thickness that contained the three types of aggregate-cement base, cracking was greatest in the gravel-

Figure 3. Crack patterns in pavement with 20.3-cm limestone-aggregate-cement base.

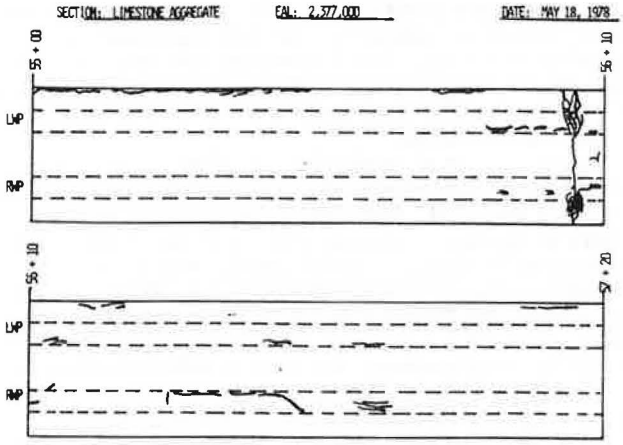

Figure 4. Length and area of cracking at various EAL applications.

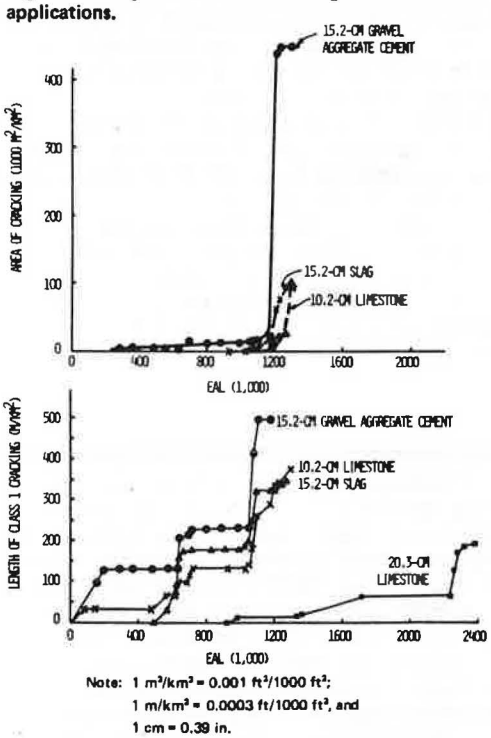

Note: 1 m^3/km^2 = 0.001 $ft^3/1000\ ft^2$;
1 m/km^2 = 0.0003 $ft/1000\ ft^2$, and
1 cm = 0.39 in.

Figure 5. Crack patterns at different EALs in 10.2-cm limestone-aggregate-cement pavement.

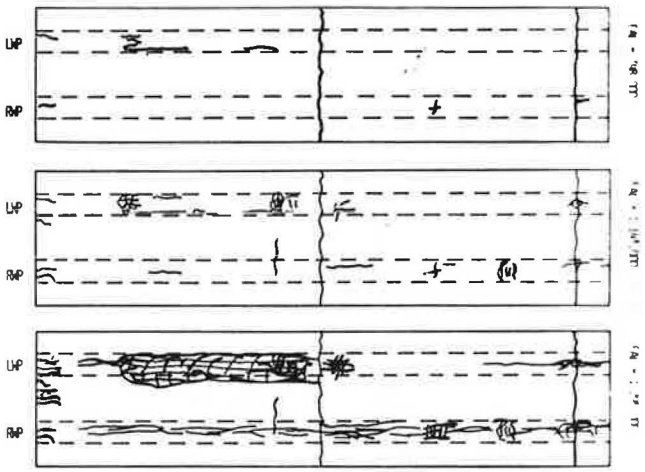

Figure 6. Crack patterns at different numbers of EAL applications in slag-aggregate-cement pavement.

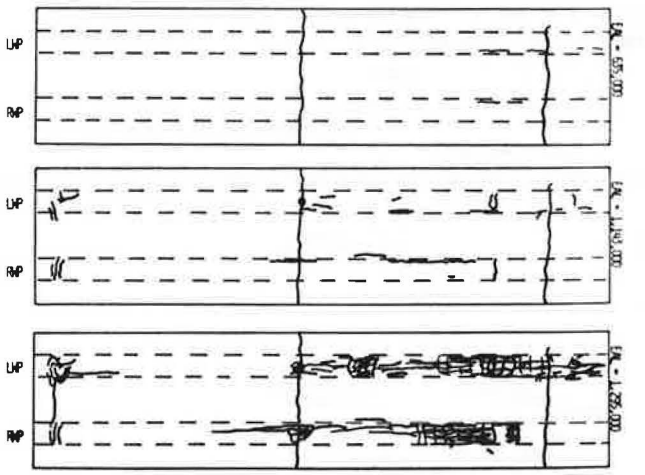

Figure 7. Crack patterns at different numbers of EAL applications in gravel-aggregate-cement pavement.

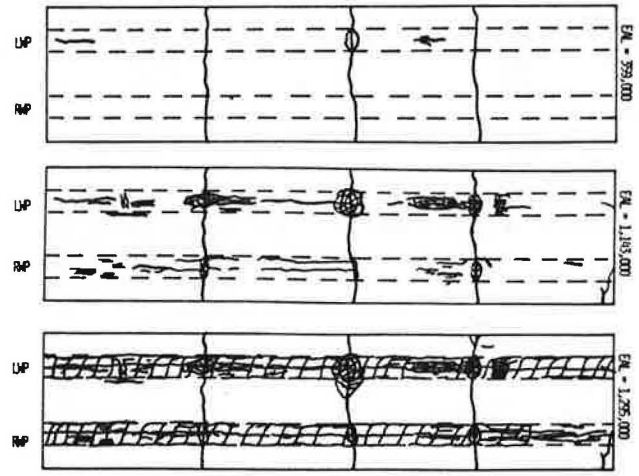

Figure 8. PSI versus EAL applications for limestone-aggregate-cement pavements.

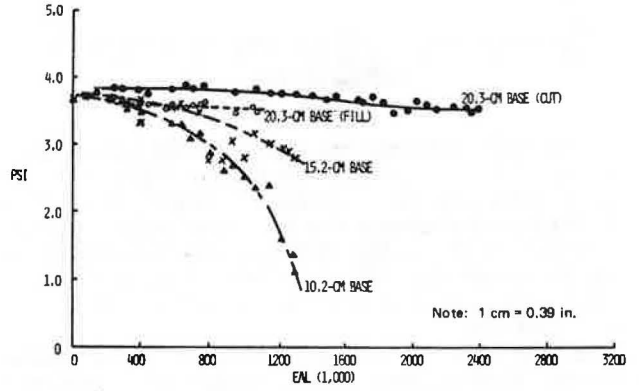

Figure 9. PSI versus EAL applications for 15.2-cm aggregate-cement pavement.

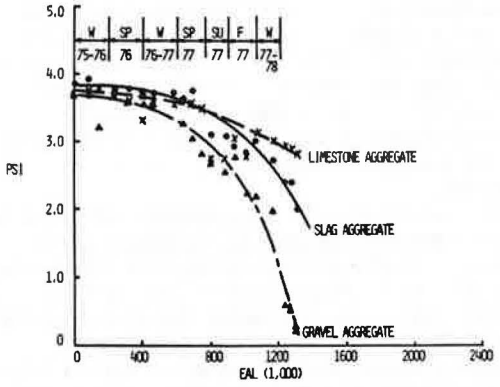

aggregate pavement, intermediate in the slag-aggregate pavement, and least in the limestone-aggregate pavement. Furthermore, the surface cracking appeared earliest in the gravel-aggregate pavement and last in the limestone-aggregate pavement. In addition, the rate of crack growth was fastest in the gravel pavement, intermediate in the slag pavement, and slowest in the limestone pavement.

These differences in cracking behavior among the three types of aggregate under investigation could be attributable to the difference in the fatigue and modulus properties given in Table 1. The fatigue life of a pavement system decreases exponentially with an increase in tensile strain at the bottom of the stabilized base course. The tensile strain decreases as the modulus of the base course increases. Since the resilient moduli of the three types of aggregate descend in order from limestone to slag to gravel, the tensile strain at the bottom of the base course will increase with type of aggregate in the same order and the fatigue strength will decrease with type of aggregate in the same order. Therefore, the combined effect of the difference in resilient modulus and fatigue strength would result in the observed cracking behavior.

Figure 4 also shows, as expected, that among the three limestone-aggregate pavements, more cracking developed in the pavement with a thin base course than the pavement with a thick base course. It is interesting to note that transverse shrinkage cracking developed in all aggregate-cement pavements except the pavement that contained a 20.3-cm (8-in) limestone-aggregate base, which was removed after about 20 months of traffic operation.

Transverse shrinkage cracking developed earlier than load-associated cracking. In most cases, the presence of shrinkage cracking aided to various degrees in the growth of load-associated cracking.

PAVEMENT PERFORMANCE

The variation of PSI with the number of EAL applications is shown in Figures 8 and 9. For all six pavements under study, the initial PSI values were almost the same, about 3.8. Figure 8 shows, as expected, that as the base-course thickness increased the rate of drop in PSI value decreased. For the 20.3-cm (8-in) base, the PSI values remained almost constant at 3.5 after about 2.4 million EAL applications. For the 10.1-cm (4-in) base, however, the PSI values dropped to 2.5 after only 1 million EALs.

Among the three types of aggregate studied, the drop in PSI value was fastest for the gravel aggregate, intermediate for the slag aggregate, and slowest for the limestone aggregate. This order of difference could be expected since development of both rutting and cracking was fastest in the gravel, intermediate in the slag, and slowest in the limestone pavements. The service life of the pavements to reach a PSI of, say, 2.5 was about 960 000, 1 200 000, and 1 400 000 EAL applications for the gravel, slag, and limestone aggregates, respectively. Thus, based on the performance data, the three types of aggregate can be ranked in the order limestone, slag, and gravel.

Both Figures 8 and 9 also show the seasons during which the PSI values were determined. It can be seen that, although the PSI values fluctuate within seasons, there is no apparent seasonal trend in the variation of PSI.

PAVEMENT RESPONSE AND LIMITING CRITERIA

The response of the test pavements to traffic loading was analyzed for the climatic condition that is most critical to pavement performance. The analysis was made by using an elastic-layer computer program and appropriate material properties. The computer program adopted was the BISAR program developed at Koninklijke Shell Laboratorium in Amsterdam. Material properties required were the modulus of elasticity and Poisson's ratio of each pavement constituent material. The elastic moduli of the aggregate cement are given in Table 1.

Table 2. Results of analysis of pavement response.

Type of Aggregate	Pavement Layer Thickness (cm)			Maximum Tensile Strain (μm/m)	Maximum Compressive Strain (μm/m)	Maximum Surface Deflection (mm)
	Surface	Base	Subbase			
Limestone	63.5	10.1	20.3	65.0	288.0	0.400
	63.5	15.2	20.3	42.2	171.5	0.301
	63.5	20.3	20.3	28.5	107.5	0.240
Slag	63.5	15.2	20.3	46.1	185.5	0.311
Gravel	63.5	15.2	20.3	54.4	216.0	0.330

Note: 1 cm = 0.39 in; 1 μm/m = 0.000 001 in/in; 1 mm = 0.039 in.

Figure 10. Maximum compressive strain at top of subgrade for EALs at 6.4-mm rutting.

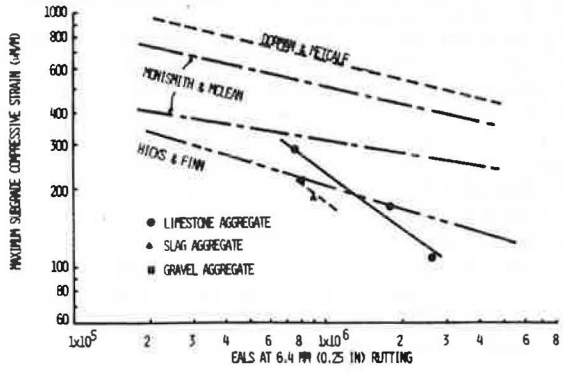

Figure 11. Maximum tensile strain at bottom of base course versus EAL applications.

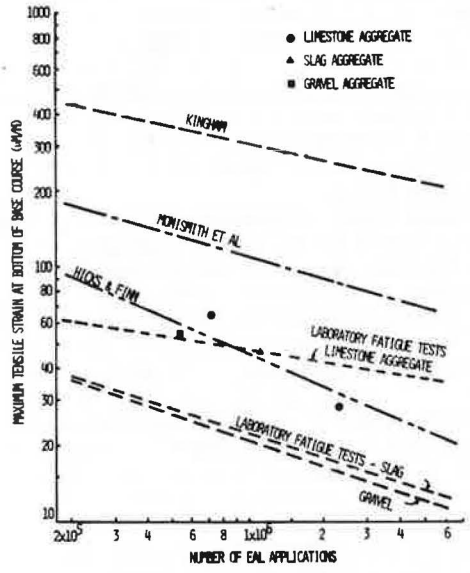

The Poisson's ratio of the aggregate cement was taken at 0.20, according to the results of other researchers (11, 12).

The subgrade moisture data indicated that the highest subgrade moisture content occurred around late spring and early summer. At this time of the year, the average subgrade moisture content was approximately 21 percent and the average pavement temperature was about 21°C (70° F). For these temperature and moisture conditions, the elastic moduli of the bituminous concrete surface, crushed-limestone subbase, and subgrade soil were 965 MPa (140 000 lbf/in^2), 331 MPa (48 000 lbf/in^2), and 69 MPa (10 000 lbf/in^2), respectively (13). Poisson's ratios were 0.40, 0.40, and 0.45 for the surface, subbase, and subgrade materials, respectively.

Figure 12. Maximum surface deflection versus EAL applications.

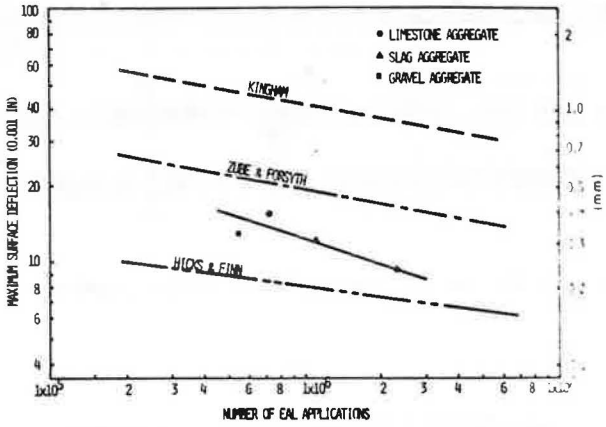

The traffic loading used was an 80-kN EAL on dual wheels with a tire pressure of 552 kPa (80 lbf/in^2). Results of the response analysis are summarized in Table 2. Pavement response was related to performance by using a base of 1 million EALs in order to develop limiting strain criteria. This level of EAL application was adopted because it is widely associated with 20-year pavement life.

In Figure 10, the number of EALs required to produce 6.4-mm (0.25-in) rutting for each pavement concerned is related to maximum compressive strain in the subgrade. A rut depth of 6.4 mm is used because it has been widely adopted for developing limiting strain criteria (14-16). According to Figure 10, the limiting compressive strain at 1 million EALs approximately equals 230 μm/m (0.000 230 in/in) for the limestone-aggregate-cement pavement. An extrapolation is needed for slag and gravel because only one test pavement for each of the two types of aggregate is available for analysis. It is estimated that the limiting compressive strain for slag and gravel equals about 180 μm/m (0.000 180 in/in).

The number of EALs at first appearance of significant cracking decreases with increasing maximum tensile strain at the bottom of the base course; this follows the trend of the laboratory fatigue curve shown in Figure 11. Among the four data points available, the data point for the pavement with the 20.3-cm (8-in) limestone-aggregate-cement base falls below the laboratory fatigue curve, which indicates that the laboratory fatigue test results overpredict the number of EALs required for fatigue failure in the field. Similar overprediction was also encountered at the San Diego test road (12) and in the performance analysis for the bituminous concrete pavements at the Pennsylvania research facility (13). Among the several possible reasons previously discussed in the literature (13), the effect of weathering could be a plausible one, since this pavement section had been exposed to severe weather conditions longer than the other three pavements. Figure 11 also includes the results obtained by other researchers (14, 16, 18) for

different base materials. The data points scatter around the finding of Hicks and Finn (14), and the limiting tensile strain at 1 million EAL applications equals about 45 μm/m (0.000 45 in/in) for all three types of aggregate cement studied.

In Figure 12, maximum surface deflection is related to EALs based on the number of axle loadings at the first appearance of significant surface cracking. The test results are bracketed between the findings of Hicks and Finn (14) and Zube and Forsyth (19). The figure indicates a limiting maximum surface deflection of approximately 0.30 mm (0.012 in) for all three types of aggregate-cement pavement for a life of 1 million EAL applications.

SUMMARY AND CONCLUSIONS

The behavior and performance of six pavements that contained aggregate-cement bases were evaluated. Three types of aggregate were used in the aggregate-cement bases: limestone, slag, and gravel. Performance data were collected on PSI, rutting, and cracking. Pavement response to 80-kN EALs was analyzed by using the BISAR computer program and appropriate material properties. The response was then related to the performance data to establish limiting criteria.

Among the three types of aggregate studied, limestone possesses the greatest strength and resilient modulus. Pavement that contained limestone-aggregate-cement base performed much better in terms of rutting, cracking, and change in PSI than did pavements with the other two types of base materials. Gravel aggregate has greater compressive strength but lower resilient modulus and fatigue strength than slag aggregate. Pavement that contained slag-aggregate-cement base performed better than that with the gravel aggregate. The limiting criteria developed can provide a basis for designing aggregate-cement pavements to withstand 1 million 80-kN EAL applications without significant surface cracking or excessive rutting.

ACKNOWLEDGMENT

The study presented here is part of a research project sponsored by the Pennsylvania Department of Transportation in cooperation with the Federal Highway Administration, U.S. Department of Transportation. Their support is gratefully acknowledged. We wish to express our gratitude to the National Crushed Stone Association for use of its repeated-load test apparatus in laboratory testing. Sincere appreciation is due to T. D. Larson of the Pennsylvania Transportation Institute for his encouragement and review of the manuscript. We are also thankful to R. P. Anderson, B. A. Anani, P. J. Kersavage, and S. A. Kutz, who assisted in collecting and reducing the field data.

This paper represents our views and does not necessarily reflect those of the Pennsylvania Department of Transportation or the Federal Highway Administration.

REFERENCES

1. Problems of Designing Roadway Structures. Transportation Engineering Journal, Proc., ASCE, Vol. 95, No. TE2, May 1969, pp. 289-315.
2. H. E. Bofinger. The Fatigue Behavior of Soil-Cement. Journal of Australian Road Research Board, Vol. 2, No. 4, June 1965, pp. 12-20.
3. C. K. Shen and J. K. Mitchell. Behavior of Soil-Cement in Repeated Compression and Flexure. HRB, Highway Research Record 128, 1966, pp. 68-100.
4. T. J. Larsen and P. J. Nussbaum. Fatigue of Soil-Cement. Portland Cement Assn., Bull. D119, 1967.
5. T. J. Larsen. Test on Soil-Cement and Cement-Modified Bases in Minnesota. Journal of Portland Cement Assn. Research and Development Laboratories, Vol. 9, No. 1, Jan. 1967, pp. 25-47.
6. J. K. Mitchell and D. R. Freitag. A Review and Evaluation of Soil-Cement Pavements. Journal of Soil Mechanics and Foundations Division, Proc., ASCE, Paper 2294, Dec. 1959.
7. P. J. Nussbaum and T. J. Larsen. Load-Deflection Characteristics of Soil-Cement Pavements. HRB, Highway Research Record 86, 1965, pp. 1-14.
8. W. F. Chen. Double-Punch Test for Tensile Strength of Concrete. ACI Journal, Vol. 67, Dec. 1970, pp. 993-995.
9. E. S. Lindow, W. P. Kilareski, G. Q. Bass, and T. D. Larson. An Evaluation of Pennsylvania's Flexible Pavement Design Methodology: Volume 2—Construction, Instrumentation, and Operation. Pennsylvania Transportation Institute, Pennsylvania State Univ., University Park, Interim Rept. PTI 7504, Feb. 1973.
10. W. P. Kilareski, S. A. Kutz, and G. Cumberledge. A Study of Flexible Pavement Base Course and Overlay Designs: Modification Construction and Instrumentation of an Experimental Highway. Pennsylvania Transportation Institute, Pennsylvania State Univ., University Park, Interim Rept. PTI 7607, April 1976.
11. K. Nair, W. S. Smith, and C. Y. Chang; Materials Research and Development, Inc. Characterization of Asphalt Concrete and Cement-Treated Granular Base Course. Federal Highway Administration, U.S. Department of Transportation, Final Rept. Feb. 1972.
12. S. Kolias and R. I. T. Williams. Cement-Bound Road Materials: Strength and Elastic Properties Measured in the Laboratory. Transport and Road Research Laboratory, Crowthorne, Berkshire, England, Supplementary Rept. 344, 1978.
13. M. C. Wang and T. D. Larson. Performance Evaluation for Bituminous-Concrete Pavements at the Pennsylvania State Test Track. TRB, Transportation Research Record 632, 1977, pp. 21-27.
14. R. G. Hicks and F. N. Finn. Prediction of Pavement Performance from Calculated Stresses and Strains at the San Diego Test Road. Proc., AAPT Vol. 43, 1974, pp. 1-40.
15. C. L. Monismith and D. B. McLean. Structural Design Considerations. Proc., AAPT, Vol. 41, 1972, pp. 258-305.
16. G. M. Dormon and T. Metcalf. Design Curves for Flexible Pavements Based on Layered System Theory. HRB, Highway Research Record 71, 1965, pp. 69-84.
17. R. I. Kingham. Fatigue Criteria Developed from AASHO Road Test Data. Proc., 3rd International Conference on the Structural Design of Asphalt Pavements, Univ. of Michigan, Ann Arbor, 1972, pp. 656-669.
18. C. L. Monismith, J. A. Epps, D. A. Kasianchuk, and D. B. McLean. Asphalt Mixture Behavior in Repeated Flexure. Institute of Transportation and Traffic Engineering, Univ. of California, Berkeley, Rept. TE70-5, 1970.
19. E. Zube and R. Forsyth. Flexible Pavement Maintenance Requirements as Determined by Deflection Measurements. HRB, Highway Research Record 129, 1966, pp. 60-75.

Publication of this paper sponsored by Committee on Flexible Pavement Design.

Field Performance of Aggregate-Lime-Pozzolan Base Material

M. C. Wang and W. P. Kilareski, Pennsylvania Transportation Institute, Pennsylvania State University, University Park

The behavior and performance of pavements that contain aggregate-lime-pozzolan (ALP) base are evaluated and compared with those of a pavement that contains a crushed-stone base. Performance data collected include present serviceability index, rut depth, and cracking. The response of the ALP pavement to 80-kN [18 000-lbf (18-kip)] equivalent axle loadings (EALs) is analyzed by using an elastic-layer computer program. Pavement response is related to performance data to establish limiting criteria. The limiting criteria developed constitute the basis for the determination of the structural coefficient of ALP material. The results of the study indicate that the ALP material, in comparison with the crushed-stone aggregate, provided a stiff base that considerably reduced rutting. Furthermore, the PSI value decreased much slower in the ALP pavement, and cracking developed much earlier and propagated much faster in the crushed-stone pavement. No non-traffic-associated cracking appeared in either type of pavement. The limiting criteria, which were developed for the ALP pavement to withstand 1 million EALs without significant surface cracking and excessive rutting, were a maximum pavement surface deflection of 0.28 mm (0.011 in), a maximum radial tensile strain at the bottom of the base course of 41.0 μm/m (0.000 041 in/in), and a maximum compressive strain at the top of the subgrade of 160.0 μm/m (0.000 160 in/in). Within the range of layer thicknesses studied, the structural coefficients of the ALP material were, approximately, 0.33, 0.29, and 0.25 for surface layer thicknesses of 3.8, 6.4, and 8.9 cm (1.5, 2.5, and 3.5 in), respectively.

There is ample evidence to indicate that lime with fly ash is an effective agent in stabilizing aggregate for pavement construction (1). The total energy required in the production of aggregate—lime—fly-ash (ALFA) mixes is very low because the mixes generally require a small amount of lime. On the other hand, the required fly-ash content is considerably high, usually from three to five times that of the required lime content. Thus, the use of fly ash for stabilization can at least alleviate the problem of disposing of the ever-increasing quantity of fly ash. These two factors have aided in the increasing use of ALFA material in recent years.

In spite of the increase in the use of ALFA material in pavement construction, most agencies base the thickness and quality design of ALFA layers on empirical rules. Although it is likely that some degree of empiricism will always be required to account for factors that are not readily analyzable, improved methods of thickness design are needed. General steps required for the development of an improved design technique have been proposed by the Committee on Structural Design of Roadways of the American Society of Civil Engineers (ASCE) (2). Included in these steps are the establishment of failure criteria and performance studies in the field.

A research program on the field performance of various base-course materials was undertaken at the Pennslyvania Transportation Research Facility of the Pennsylvania State University. The base-course materials studied were aggregate-lime-pozzolan (fly ash), dense-graded crushed stone, aggregate cement, bituminous concrete, and aggregate bituminous. The performance of aggregate cement and bituminous concrete pavements is discussed in papers by Wang and Larson and by Wang and Kilareski elsewhere in this Record. This paper discusses the performance of pavements that contain aggregate-lime-pozzolan base courses. Limiting strain criteria and limiting deflection criteria were developed from field performance data and data on pavement response. The results of this study provide information that would be useful in the design steps identified by ASCE.

AGGREGATE-LIME-POZZOLAN MATERIAL

The aggregate-lime-pozzolan (ALP) base material studied was composed of 3 percent by weight of lime, 15 percent by weight of fly ash, and 82 percent by weight of aggregate. The mix design was determined by the Bureau of Materials, Testing, and Research of the Pennsylvania Department of Transportation (PennDOT). The aggregate was a crushed limestone. The tables below summarize the gradation and the basic properties of the aggregate, lime, and fly ash (1 mm = 0.039 in):

	Percentage Passing		
Sieve Size (mm)	Aggregate	Lime	Fly Ash
50	100		
19	93		
9.5	53		
4.75	28		
2.36	17		
1.18	10		
0.6	7		
0.3	4		
0.15	2	97.7	94.7
0.075	-	85.4	82.7
0.045	-	82.9	68.8

	Percentage		
Property	Aggregate	Lime	Fly Ash
Specific gravity	2.78	-	2.40
Loss on ignition	-	16.0	-
Chemical composition			
SiO_2		Trace	45.3
Fe_2O_3		2.0	15.6
Al_2O_3			24.6
CaO		47.4	4.2
MgO		32.6	1.3
C		1.3	2.4

The chemical properties of lime and fly ash given in the second table are taken from the work of Cumberledge and others (3).

TEST PAVEMENTS

Four test pavements that contained ALP base were constructed at the Pennsylvania Transportation Research Facility. Two were installed in the summer of 1972, and the other two were constructed in the fall of 1975 (the construction of the base course took place from October 22 through November 3). Each of the four pavements contained a 6.4-cm (2.5-in) bituminous concrete surface and a 20.3-cm (8-in) subbase layer. The first two pavements had a 20.3-cm base; the other two pavements contained a 15.2-cm (6-in) and a 10.2-cm (4-in) base, respectively. One of the first two pavements was in a cut, and the other was in a fill section. The fill section was replaced by the last two pavements after about 1.1 mil-

lion applications of 80-kN [18 000-lbf (18-kip)] equivalent axle loads (EALs) (EAL, as used in this paper, refers to an 80-kN load). Each of the first two pavements was 67.1 m (220 ft) long, and the length of each of the last two pavements was 30.5 m (100 ft). All pavements were 3.7 m (12 ft) wide.

The ALP material was mixed in a central plant at Talmage, Pennsylvania. The 10.2-cm (4-in) and 15.2-cm (6-in) ALP bases were placed in one lift, whereas the 20.3-cm (8-in) bases were placed in two 10.1-cm (4-in) compacted layers. The top of the first lift was scarified before placement of the second lift. Compaction was achieved by using a tandem-axle steel-wheel roller. After compaction, a bituminous seal coat was applied to the surface of the ALP base course. The moisture content and dry density were 6.7 percent and 2251 kg/m^3 (139.6 lb/ft^3), respectively, which corresponds to the optimum moisture content and maximum dry density of the modified American Association of State Highway and Transportation Officials (AASHTO) compaction effort.

In addition to the ALP pavements, the research facility also contained one pavement with a 20.3-cm (8-in) dense-graded, crushed-stone base and several other pavements with different base materials. The crushed-stone base had a 6.4-cm (2.5-in) bituminous concrete surface and a 20.3-cm subbase. This pavement was used to provide a comparative basis for the data obtained at the research facility with AASHO Road Test findings as well as with numerous other published findings on crushed-stone base courses. The design data for the crushed-stone base material are given below. The materials used were bituminous concrete fine aggregate and Pennsylvania 2B aggregate at a maximum dry density of 2327.7 kg/m^3 and an optimum moisture content of 7.5 percent. The field data represent an average of nine tests (1 mm = 0.039 in):

Sieve Size (mm)	Percentage Passing: Specification Limits	Percentage Passing: Field Data
50	100	100
19	52-100	85.0
9.5	36-70	55.1
4.75	24.50	41.2
2.36	–	32.2
1.18	10-30	21.3
0.6	–	14.8
0.3	–	10.9
0.15	–	8.8
0.075	0-10	–

The crushed-stone pavement was overlaid with 6.4 cm (2.5 in) of bituminous concrete after approximately 940 000 EAL applications.

The subgrade soil at the research facility was predominantly soil classification A-7. The first two ALP pavements (constructed in 1972) were subjected to traffic approximately two months after completion of the base-course construction. For the last two ALP and crushed-stone pavements (constructed in 1975), traffic was started about one month after the base course was completed. The traffic was initially provided by a conventional truck tractor that pulled a semitrailer and a full trailer. After about 1.5 million EALs, another full trailer was added to increase the rate of loading. The single-axle loading was within the range of 80-107 kN (18 000-24 000 lbf). Complete information on design, construction, material properties, and traffic operation is available elsewhere (4, 5).

FIELD EVALUATION

Field testing of pavement performance was conducted periodically. Rut depth was measured biweekly every 12.2 m (40 ft) in both wheel paths by using an A-frame that was attached to a 2.1-m (7-ft) long base channel. Surface cracking was surveyed and mapped biweekly. Surface roughness was measured in both wheel paths by using a MacBeth profilograph. The roughness factors obtained from the profilograph data were converted into pavement present serviceability index (PSI) by using Equations 1 and 2 given in the paper by Wang and Larson elsewhere in this Record.

Surface deflections were determined in the wheel paths by using the Benkelman beam and road-rater measurements. Pavement temperature profile and distribution of subgrade moisture were measured by using thermocouples and moisture cells. Two frost-depth indicators were installed at the research facility to measure the depth of frost penetration. Weather data such as wind velocity, precipitation, and temperature were collected by using various meteorological gages.

DISTRESS BEHAVIOR

The distress behavior of the test pavements was evaluated in terms of rutting and cracking. Figure 1 shows the rut-depth data for the ALP and crushed-stone pavements (the two short ALP pavements are not included since they did not cure properly because of cold weather during construction). The figure also shows the seasons in which the rut depths were measured. The two ALP pavements show almost the same amount of rutting until the point at which the fill section was replaced, which indicates that the material properties of the two pavements were quite consistent. Figure 1 clearly indicates that the ALP pavement has much greater resistance to rutting than the crushed-stone pavement. The rate of rutting seems to vary insignificantly with the seasons while the pavements are in structurally sound condition but to increase rapidly in the spring season when the pavements approach a state of failure.

Figure 1 shows that the crushed-stone pavement displayed rutting of about 25.4 mm (1.0 in) at the end of 1 million EAL applications, whereas the ALP pavement had only about 3.8-mm (0.15-in) rutting. The ALP pavement reached a rut depth of 6 mm (0.25 in) at about 1.4 million EALs, whereas the crushed-stone pavement reached this rut depth at only about 0.2 million EALs. The 6-mm rut depth is widely used as a criterion in the design of

Figure 1. Rut depth versus EAL for pavements with ALP and crushed-stone bases.

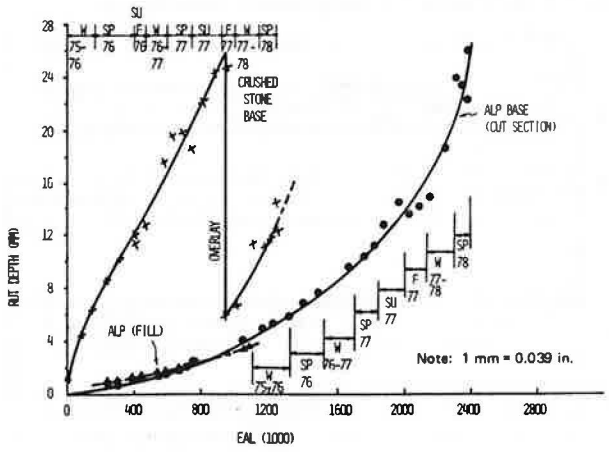

flexible highway pavements (6, 7). These data will be used later as a basis for the determination of the structural coefficient of the ALP material.

The results of a crack survey showed that there was no cracking in either 20.3-cm (8-in) ALP-base pavement at the time when the fill section was removed. A few hairline cracks appeared in the wheel paths in the cut section at approximately 1.12 million EAL applications. After about 2.3 million EALs, two potholes had formed in the ALP pavement. The first pothole developed at about 1.17 million EALs and the second at about 1.36 million EALs. Figures 2-5 show crack patterns mapped at four different times to illustrate the growth of surface cracking in the ALP pavement. It is interesting to note that nearly all cracks initiated in the longitudinal direction. The more numerous longitudinal cracks along the left side of the pavement were probably a result of the installation of a skid-testing facility adjacent to the left edge of the pavement. The construction of the skid-testing facility could have disturbed the original support along the edge of the test pavement. As a result, the edge of the test pavement is under less confinement and is thus more susceptible to the formation of longitudinal cracking.

Figure 2. Crack patterns in ALP pavement: April 1976.

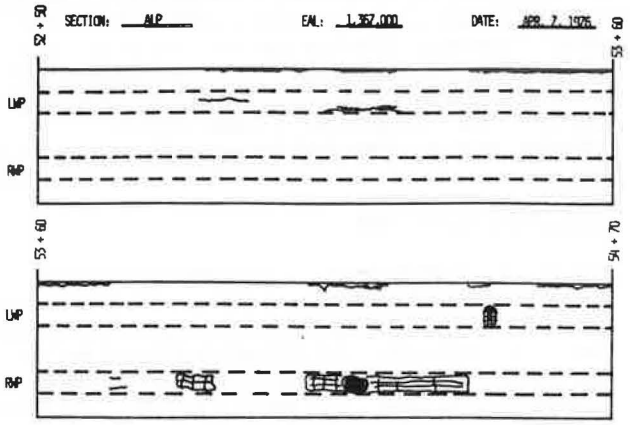

Figure 3. Crack patterns in ALP pavement: March 1977.

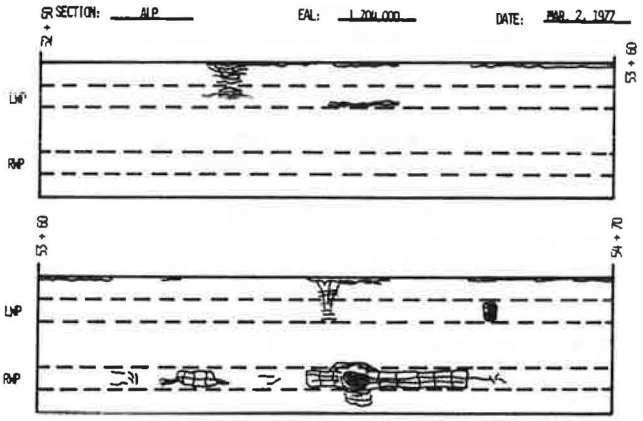

Figure 4. Crack patterns in ALP pavement: November 1977.

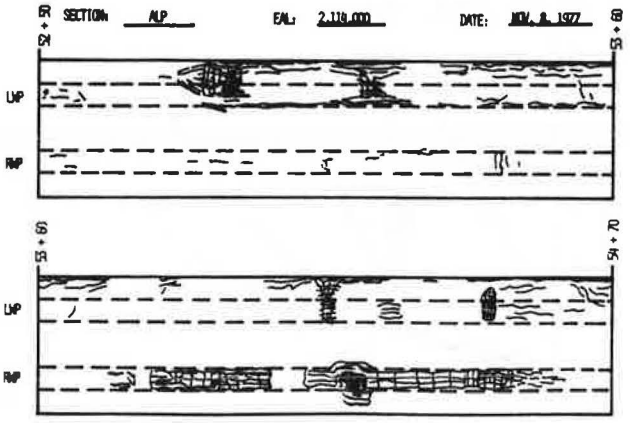

Figure 6 shows crack patterns developed in the crushed-stone pavement. Hairline cracks initiated in both wheel paths at approximately 56 500 EAL applications. The contrast in the development of surface crack patterns in the ALP and crushed-stone pavements is shown in Figures 2-6. In the ALP pavement, surface cracking initiated in some localized areas; in the crushed-stone pavement, surface cracking developed in the wheel paths at almost the same time throughout the entire pavement. One possible reason for the difference could be the nonuniformity of the ALP material, which is probably attributable to imperfect mixing. But no attempt was made to verify this. Figures 2-6 also show that the rate of growth from class 1 to class 2 and class 3 cracking was much faster in the crushed-stone pavement than in the ALP pavement. Furthermore, no apparent temperature or shrinkage cracking was observed in either pavement.

The total areas of class 2 and class 3 cracking that developed in both ALP and crushed-stone pavements are shown in Figure 7. The area of cracking increased very rapidly when the pavements approached a state of failure. A rapid increase in cracking occurred in the ALP pavement during the spring of 1976, primarily because of the development of the second pothole. During the spring season, the thawing of frozen material and relatively heavy rainfall contributed to the formation of potholes. It should be noted that, among the many test pavements at the research facility, potholes were observed only in the ALP pavement. Possible reasons for this are yet to be investigated.

PAVEMENT PERFORMANCE

The variation of PSI with EAL applications for the ALP and crushed-stone pavements is shown in Figure 8. The initial PSI values for the three pavements were almost the same, approximately 3.8. The performance trends of the two ALP pavements were also nearly equal until

Figure 5. Crack patterns in ALP pavement: March 1978.

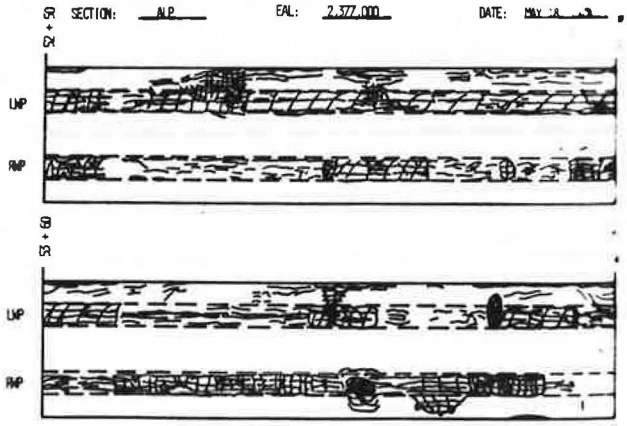

Figure 6. Crack patterns in crushed-stone pavement.

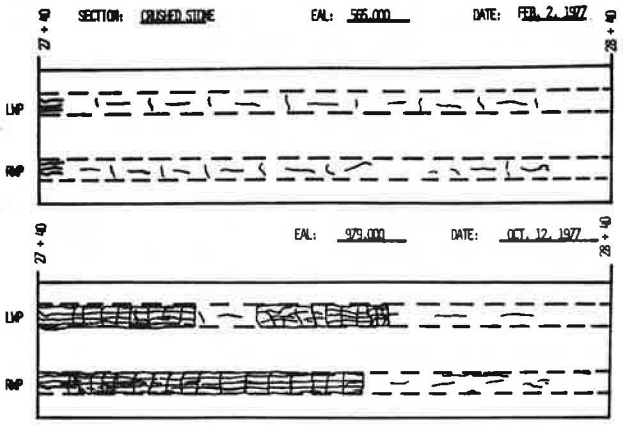

Figure 7. Crack area versus number of EALs.

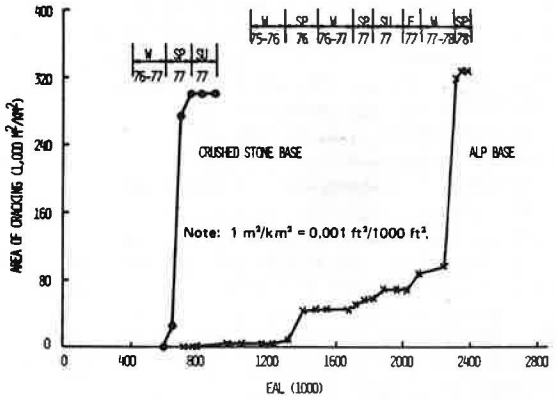

the fill section was removed. For the first million EAL applications, the PSI value decreased by only about 0.3. After that, however, the PSI value dropped at an ever-increasing rate. The data seem to show that the PSI dropped slightly faster in the spring-summer seasons than in the fall-winter seasons. According to the data, it required about 2.15 million EAL applications to reach a PSI of 2.0.

From the beginning, the PSI value dropped much faster for the crushed-stone pavement than for the ALP pavement, which would indicate a shorter service life for the crushed-stone pavement. The performance data also indicate that the crushed-stone pavement can only sustain 0.7 million EAL applications before it reaches a PSI of 2.0. This service life is much shorter than that of the ALP pavement. The PSI value immediately after overlay was only about 2.6, which is much lower than the PSI after initial construction. A possible reason for this could be that the crushed-stone pavement is so short—only 33 m (100 ft) long—that it is rather difficult to control the thickness of overlay uniformly by using routine construction equipment.

MATERIAL PROPERTIES

The strength and fatigue properties of the ALP material were determined based on specimens both compacted in the laboratory and taken from the pavement. The laboratory-compacted specimens were 15.2 cm (6 in) in diameter and 25.4 cm (10 in) in height and were molded by using the modified AASHTO compaction effort to the same moisture content and dry density as those in the

Figure 8. Variation of PSI with number of EALs.

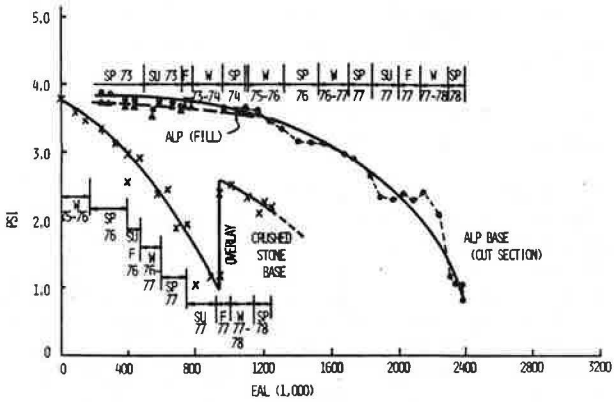

pavement. The compacted specimens were embedded in the soil at the research facility to cure under the same environmental conditions as the test pavement. Several core samples 10.2 cm (4 in) in diameter and 20.4 cm (8 in) in height were taken from the test pavement after about 1.1 million EALs. Note that the 1.1 million EALs were achieved after approximately 20 months of traffic. Test results indicated that the laboratory-compacted specimens had almost the same strength properties as the core samples.

Triaxial compression tests were conducted on four-week-old and one-year-old specimens under various confining pressures up to 0.14 MPa (20 lbf/in^2). Test results indicated no significant effect of confinement on the compressive strength within the range of conditions studied. Based on the results of six tests, average compressive strength and strain at failure were 17.1 MPa (2480 lbf/in^2) and 0.0142, respectively, for one-year-old specimens and 5.2 MPa (750 lbf/in^2) and 0.010, respectively, for four-week-old specimens.

The tensile strength of the test specimens was determined by using the double-punch test (8). For specimens aged 4 weeks, 10 weeks, 1 year, and 2 years, the tensile strengths were 0.24, 0.39, 0.84, and 0.97 MPa (34, 57, 121, 140 lbf/in^2), respectively. By comparison with the previous values of compressive strength, the ratios of tensile to compressive strength are approximately 4.5 and 4.9 percent for 4-week-old and 1-year-old specimens, respectively. These two ratios are close to the lower limit of the range of values documented elsewhere (9).

The fatigue property was evaluated by using repeated-load flexural tests on beam specimens. The beam specimens, which were compacted in the laboratory, had dimensions of 8.25x8.25x45.75 cm (3.25x3.25x18 in). The beam specimens were simply supported at both ends and were subjected to repeated loading at two points within the span. Each loading point was located at equal distance from its nearest support to ensure pure bending at the middle of the span. The repeated loading had a duration of 0.1 s and a frequency of 20 cycles/min. Test results gave $K_1 = 2.80 \times 10^{-4}$ and $K_2 = 2.17$ for the following fatigue equation:

$$N = K_1(1/\epsilon)^{K_2} \quad (1)$$

where N = number of load repetitions to failure and ϵ = tensile strain.

In addition, repeated-load triaxial compression tests were conducted by using the same repeated loading to determine the modulus of resilient deformation. For confining pressures up to 0.21 MPa (30 lbf/in^2) and de-

viatoric stresses up to 0.45 MPa (65 lbf/in^2), the resilient modulus was found to be practically independent of confining pressure, deviatoric stress, and the number of load repetitions. The resilient modulus was averaged at 16 400 MPa (2.38 million lbf/in^2).

PAVEMENT RESPONSE AND LIMITING CRITERIA

Pavement response was analyzed for the weather conditions that are most critical to pavement performance by using an elastic-layer computer program and the appropriate material properties. The computer program adopted was the BISAR program developed at Koninklijke Shell in Denmark. Material properties needed are the modulus of elasticity and Poisson's ratio of each pavement constituent material. The elastic modulus of the ALP material has already been given. Poisson's ratio is taken to be 0.15, according to previous research results (11).

The data on subgrade moisture indicated that the maximum subgrade moisture content occurred around the late spring and early summer. At this time of the year, the subgrade moisture content was approximately 21 percent and the average pavement temperature was about 21°C (70°F). The elastic moduli of the bituminous concrete surface, crushed-limestone subbase, and subgrade materials that correspond to these temperature and moisture conditions are 965.5 MPa (140 000 lbf/in^2), 330.9 MPa (48 000 lbf/in^2), and 68.9 MPa (10 000 lbf/in^2), respectively (10). In addition, Poisson's ratio values are 0.40, 0.40, and 0.45, respectively, for the surface, subbase, and subgrade materials. The critical response analyzed included maximum tensile strain in the surface and base courses, maximum vertical compressive strain in the subgrade, and maximum deflection on the pavement surface. These responses were considered because maximum tensile strain and maximum surface deflection are associated with fatigue cracking (11-14), whereas maximum vertical compressive strain is associated with rutting (6, 7, 13).

According to the results of the response analysis, maximum pavement surface deflection, maximum tensile strain at the bottom of the base course, and maximum subgrade compressive strain equal 0.27 mm (0.0107 in), 41.10 μm/m (0.000 041 in/in), and 142.78 μm/m (0.000 143 in/in), respectively. The field data presented earlier indicate that surface cracking appeared at approximately 1.1 million EAL applications. Thus, it would be appropriate to state that, for an ALP pavement to withstand 1 million EALs without surface cracking, the maximum pavement surface deflection and maximum tensile strain in the base course should be no greater than 0.28 mm (0.011 in) and 41.0 μm/m (0.000 041 in/in).

As mentioned before, the number of EAL repetitions required for 6 mm (0.25 in) of rutting is about 1.4 million (Figure 1). The maximum subgrade compressive strain obtained above is related to 1.4 million EAL repetitions in Figure 9. Figure 9 also shows the relations established for pavements with bituminous concrete bases at the research facility (10) and relations established by other researchers (6, 7, 13). It is estimated by extrapolation that the subgrade compressive strain at 1 million EALs equals approximately 160 μm/m (0.000 160 in/in). These three values—maximum surface deflection = 0.28 mm (0.011 in), maximum tensile strain = 41.0 μm/m (0.000 041 in/in), and maximum subgrade compressive strain = 160 μm/m (0.000 160 in/in)—constitute the limiting criteria for the ALP pavement to withstand 1 million EAL applications. One million EAL applications was adopted because it is widely associated with 20-year pavement service life.

Figure 9. Maximum compressive strain in subgrade versus EAL at 6-mm (0.25-in) rutting.

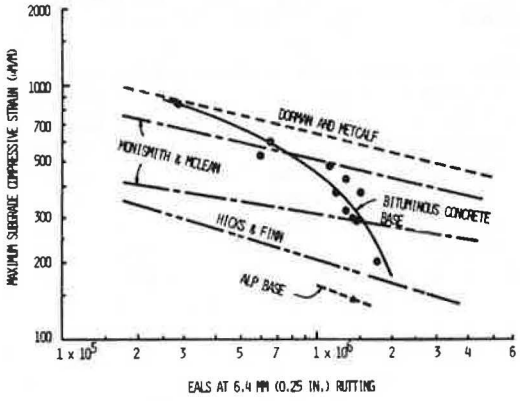

STRUCTURAL COEFFICIENT

The structural coefficient of the ALP base material was evaluated by following the same approach as that presented before (10). For this approach, the BISAR computer program was used to determine pavement sections that had various combinations of layer thickness that satisfied the preceding limiting criteria. Table 1 summarizes the results of the computation. The layer thicknesses in the first, second, and last columns of this table provide pavement sections for the calculation of the structural coefficient.

The structural coefficient was computed by using the

Table 1. Layer-thickness combinations that satisfy limiting criteria for ALP pavements.

Subbase Thickness (cm)	Surface Thickness (cm)	Base Thickness (cm) Based on 0.028-cm Deflection	41.10-μm/m Tensile Strain	160.10-μm/m Compressive Strain	Combined
0	3.8	22.1	22.6	16.5	22.6
	6.4	21.3	19.6	15.7	21.3
	8.9	20.6	17.8	15.0	20.6
10.2	3.8	21.3	22.4	18.8	22.4
	6.4	20.8	21.3	18.3	21.3
	8.9	20.1	20.3	17.5	20.3
20.3	3.8	20.3	21.3	18.0	21.3
	6.4	19.6	20.3	17.5	20.3
	8.9	18.8	19.3	16.8	19.3
40.6	3.8	17.3	19.8	14.7	19.8
	6.4	16.5	18.8	14.2	18.8
	8.9	15.5	17.5	13.5	17.5

Note: 1 cm = 0.39 in; 1 μm/m = 0.000 001 in/in.

Figure 10. Structural coefficients of ALP and subbase materials.

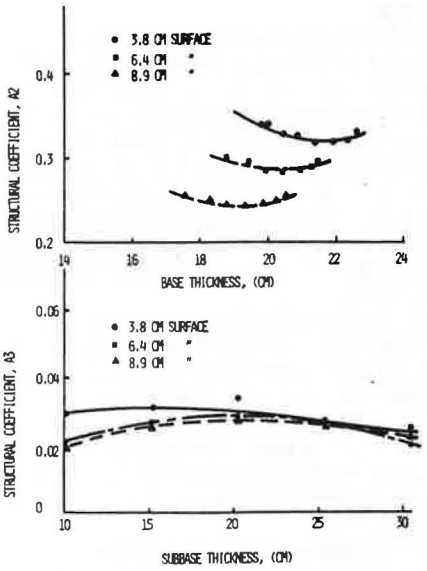

following basic equation, developed from the AASHO Road Test:

$$\rho = 0.64(SN + 1)^{9.36} \quad (2)$$

where ρ = EALs at failure and SN = structural number, which is defined as follows:

$$SN = a_1 H_1 + a_2 H_2 + a_3 H_3 \quad (3)$$

where a_1, a_2, and a_3 = structural coefficients of surface, base, and subbase materials, respectively, and H_1, H_2, and H_3 = layer thicknesses of surface, base, and subbase courses, respectively.

In the computation, a structural coefficient of 0.44, which was originally developed from the AASHO Road Test, was used for the bituminous concrete surface material. It was assumed that the structural coefficient of the subbase material does not change appreciably within a thickness of 5.1 cm (2 in). A more detailed computation procedure is available elsewhere (10). The structural coefficients determined are shown in Figure 10.

Figure 10 shows that, for a given surface-layer thickness, the structural coefficient of the ALP material is nearly constant within the range of base thicknesses studied. The structural coefficient of the ALP material, however, is smaller for thicker surface layers. The same effect was also observed for bituminous concrete base material (10). Figure 10 shows that the structural coefficients equal approximately 0.33, 0.29, and 0.25 for surface thicknesses of 3.8, 6.4, and 8.9 cm (1.5, 2.5, and 3.5 in), respectively. These values are close to those determined by Ahlberg and Barenberg (15) for other ALP materials; the values ranged between 0.34 and 0.20 for different qualities of ALP materials.

The structural coefficient of the limestone subbase material is also roughly independent of the subbase layer thickness, as shown in Figure 10. For the range of layer thicknesses studied, the average structural coefficient of the subbase material equals approximately 0.03. This value is relatively low compared with 0.10, the value that was reported before for bituminous concrete base material (10). This deviation could be attributed to the difference in relative stiffness between the base and subbase layers. As given earlier, the resilient modulus of the ALP material equals 16 400 MPa (2.38 million lbf/in^2) and that of the bituminous concrete base was approximately 2410 MPa (0.35 million lbf/in^2), which corresponds to the spring temperature condition (10). Thus, the relative stiffness between the ALP base and the subbase is considerably greater than that between the bituminous concrete base and the subbase materials. Since the combinations of layer thickness that satisfy the limiting criteria depend on the relative stiffness of the constituent layers, the effect on the base thickness of a unit change in the subbase thickness is less significant for the system that contains a base course much stiffer than the subbase course. As a consequence, the structural coefficient of the subbase material evaluated with the ALP base was lower than that of the subbase material evaluated with the bituminous concrete base. A similar effect of one layer's stiffness on another layer's structural coefficient has also been observed by VanTil and others (16).

SUMMARY AND CONCLUSIONS

The behavior and performance of pavements that contained ALP base were evaluated and compared with those of pavement that contained crushed-stone base. The critical response of the ALP pavement was analyzed by using the BISAR computer program and appropriate material properties. The response analyzed was related to performance data to establish limiting criteria. The structural coefficient of the ALP material was evaluated based on the limiting criteria developed.

The results of this study indicate that ALP material provides a stiffer base with longer service life than crushed-stone aggregate. The ALP pavement displayed much less severe rutting than the crushed-stone pavement. In addition, the PSI value decreased at a much lower rate for ALP pavement than for crushed-stone pavement. Cracking developed much earlier and faster in the crushed-stone pavement. No apparent non-traffic-associated cracking was observed in either type of pavement.

For the ALP pavement to withstand 1 million applications of 80-kN EAL, the maximum surface deflection, maximum tensile strain in the base, and maximum vertical compressive strain in the subgrade must be limited to 0.28 mm (0.011 in), 41 μm/m (0.000 041 in/in), and 160 μm/m (0.000 160 in/in), respectively. The structural coefficient of the ALP material remains relatively constant with respect to the base thickness but varies with the surface thickness. For surface thicknesses of 3.8, 6.4, and 8.9 cm (1.5, 2.5, and 3.5 in), the structural coefficients equal 0.33, 0.29, and 0.25, respectively.

ACKNOWLEDGMENT

The study presented here is part of a research project sponsored by the Pennsylvania Department of Transportation in cooperation with the Federal Highway Administration, U.S. Department of Transportation. Their support is gratefully acknowledged. We wish to express our gratitude to the National Crushed Stone Association for lending us its repeated-load test apparatus for laboratory testing. Our sincere appreciation is extended to T. D. Larson of the Pennsylvania Transportation Institute for his encouragement and review of the manuscript. We are also thankful to S. A. Kutz for his participation in the preparation of the paper. The field data reported here were collected and reduced with the assistance of R. P. Anderson, B. A. Anani, P. J. Kersavage, and S. A. Kutz.

This paper represents our views and does not necessarily reflect those of the Pennsylvania Department of Transportation or the Federal Highway Administration.

REFERENCES

1. State of the Art: Lime Stabilization Reactions, Properties, Design, Construction. TRB, Circular 180, Sept. 1976.
2. Problems of Designing Roadway Structures. Transportation Engineering Journal, Proc., ASCE, Vol. 95, No. TE2, May 1969, pp. 289-315.
3. G. Cumberledge, G. L. Hoffman, and A. C. Bhajandas. Curing and Tensile Strength Characteristics of Aggregate-Lime-Pozzolan. TRB, Transportation Research Record 560, 1976, pp. 21-30.
4. E. S. Lindow, W. P. Kilareski, G. O. Bass, and T. D. Larson. An Evaluation of Pennsylvania's Flexible Pavement Design Methodology: Volume 2—Construction, Instrumentation, and Operation. Pennsylvania Transportation Institute, Pennsylvania State Univ., University Park, Interim Rept. PTI 7504, Feb. 1973.
5. W. P. Kilareski, S. A. Kutz, and G. Cumberledge. A Study of Flexible Pavement Base Course and Overlay Designs: Modification, Construction, and Instrumentation of an Experimental Highway. Pennsylvania Transportation Institute, Pennsylvania State Univ., University Park, Interim Rept. PTI 7607, April 1976.
6. G. M. Dormon and T. Metcalf. Design Curves for Flexible Pavements Based on Layered System Theory. HRB, Highway Research Record 129, 1966, pp. 60-75.
7. C. L. Monismith and D. B. McLean. Structural Design Considerations. Proc., AAPT, Vol. 41, 1972, pp. 258-305.
8. W. F. Chen. Double-Punch Test for Tensile Strength of Concrete. ACI Journal, Vol. 67, Dec. 1970, pp. 993-995.
9. Lime-Fly Ash-Stabilized Bases and Subbases. NCHRP, Synthesis of Highway Practice 37, 1976.
10. M. C. Wang and T. D. Larson. Performance Evaluation for Bituminous-Concrete Pavements at the Pennsylvania State Test Track. TRB, Transportation Research Record 632, 1977, pp. 21-27.
11. C. L. Monismith, J. A. Epps, D. A. Kasianchuk, and D. B. McLean. Asphalt Mixture Behavior in Repeated Flexure. Institute of Transportation and Traffic Engineering, Univ. of California, Berkeley, Rept. TE70-5, 1970.
12. R. I. Kingham. Fatigue Criteria Developed from AASHO Road Test Data. Proc., 3rd International Conference on the Structural Design of Asphalt Pavements, Univ. of Michigan, Ann Arbor, 1972, pp. 656-660.
13. R. G. Hicks and F. N. Finn. Prediction of Pavement Performance from Calculated Stresses and Strains at the San Diego Test Road. Proc., AAPT, Vol. 43, 1974, pp. 1-40.
14. E. Zube and R. Forsyth. Flexible Pavement Maintenance Requirements as Determined by Deflection Measurements. HRB, Highway Research Record 129, 1966, pp. 60-75.
15. H. L. Ahlberg and E. J. Barenberg. Pozzolan Pavements. Engineering Experiment Station, University of Illinois, Urbana-Champaign, Bull. 473, 1967.
16. C. J. VanTil, B. F. McCullough, B. A. Vallerga, and R. G. Hicks. Evaluation of AASHO Interim Guides for Design of Pavement Structures. NCHRP Rept. 128, 1972.

Publication of this paper sponsored by Committee on Flexible Pavement Design.

Structural Design of PCC Shoulders

Jihad S. Sawan and Michael I. Darter, Department of Civil Engineering, University of Illinois, Urbana-Champaign

A structural design procedure for plain jointed portland cement concrete (PCC) highway shoulders has been developed. The procedure can be used to provide PCC shoulders either for rehabilitation of existing pavement or for new pavement construction. All major factors that are known to affect the behavior of PCC shoulders are considered in the mechanistic design approach, including encroaching moving trucks, parked trucks, foundation support, load transfer across the longitudinal joint, shoulder slab thickness and tapering, width of shoulder, and traffic lane slab. The finite-element structural analysis technique was used along with a model for concrete fatigue damage to sum damage for both moving encroaching trucks and parked trucks. A relation was established between accumulated fatigue damage and slab cracking. The shoulder can thus be designed for an allowable amount of cracking, which can vary depending on the performance level desired. Procedures for tying the PCC shoulder to the mainline PCC slab are recommended to provide adequate load transfer and avoid joint spalling. Long-term, low-maintenance performance of the PCC shoulder, as well as significant improvement in the performance of the traffic lane, can be obtained if the shoulder is properly designed.

Portland cement concrete (PCC) shoulders have been constructed for several years on urban expressways and rural highways. They were first constructed on an experimental basis but more recently as regular construction. Since no structural design procedure is available, design has been based on engineering judgment and the performance of a few experimental sections. The purpose of this study is to develop a structural design procedure that considers the major design variables that affect the behavior of PCC shoulders. The design includes the placement of PCC shoulders for the purpose of rehabilitating existing pavements and also for new pavement construction.

Shoulders are an integral part of today's major highways and are required to provide structural support to (a) encroaching traffic loads from the adjacent traffic lane, (b) emergency parking, and (c) regular traffic if the shoulder is used as a detour around a closed lane or as an additional lane during peak traffic hours. Field results of this study (1) have shown that the PCC shoulder contributes to the structural support of traffic in the adjacent lane so that distress in the lane is significantly

reduced. The lack of adequate shoulder design in the past (usually attributable to minimizing construction costs) has often led to considerable distress and maintenance requirements.

The major design variables for PCC shoulders have been shown to include (a) slab thickness and tapering of thickness, (b) joint spacing, (c) foundation support and loss of support, (d) tie between shoulder and traffic lane (including load transfer of the longitudinal joint), (e) width of the shoulder slab, and (f) design and condition of the adjacent traffic lane (1). The shoulder must withstand both repeated moving loads and static loads from parked vehicles. Both of these conditions involve edge-loading conditions from heavy trucks. The edge-loading condition has been determined to be the most critical for fatigue damage (2) and the point at which cracking initiates.

The influence of these major design variables for PCC shoulders has been analyzed in a previous study (1), and the following conclusions have been drawn:

1. Two load positions must be considered to determine the required shoulder thickness—the inside edge near the lane-shoulder longitudinal joint (encroached traffic) and the outside "free" edge (parked traffic).
2. A minimum thickness of 15 cm (6 in) is recommended, since thinner slabs will have very high stresses when they are loaded by typical heavy trucks and tend to crack after only a few load applications.
3. Tapering of the shoulder thickness between the two edges is not recommended.
4. Tied-shoulder width should be at least 90-152 cm (3-5 ft) to provide maximum structural benefits to the traffic lane and shoulder. However, a wider shoulder of 3.0-3.6 m (10-12 ft) is mostly used for geometric and safety considerations.
5. Use of a tie system that provides at least 50 percent load transfer is a very effective way to reduce critical stresses near the longitudinal joint in both the traffic lane and the shoulder.
6. Provision of a "moderate" foundation support, i.e., $k = 54.2$ N/cm^3 (200 lbf/in^3), appears justified.
7. A maximum slab length of 3.6 m (15 ft) is recommended.

Finite-element models and procedures for slab stress-strain computation were used in the initial study. A comprehensive procedure for fatigue analysis is developed in this study that gives accumulated fatigue damage at both edges of the PCC shoulder. Therefore, fatigue damage produced by the encroachment of traffic from the mainline pavement at the inner edge of the shoulder can be compared with the fatigue damage from the parked traffic at the outer edge of the shoulder. This procedure is computerized. The computer program—called JCS-1—provides cumulative fatigue-damage data for selecting the structural design of the PCC shoulder and is written in FORTRAN.

DEVELOPMENT OF DESIGN PROCEDURE

Location of the critical point at which cracking initiates in the PCC slab is vital to the development of a fatigue analysis when the objective is controlling slab cracking. The location of the critical point is determined by using both field and slab fatigue analysis results (1, 3, 4). These results indicate that, for normal highway loadings and slab widths, the critical fatigue damage is in the center third of the slab at the edge.

Development of Analysis of Fatigue Damage

A comprehensive analysis of fatigue damage in PCC shoulders was developed based on the following factors:

1. The location of critical fatigue damage in the shoulder is at the longitudinal edge of the slab midway between the transverse joints.
2. Critical edge stresses caused by traffic loads are considered to prevent transverse cracking.
3. Load stresses are computed by using a finite-element program that has been shown to provide good results.
4. The proportion of mainline traffic encroaching on the inner edge of the shoulder and/or parking on the shoulder is used in the fatigue analysis.
5. Fatigue damage is computed and accumulated according to Miner's hypothesis (5).
6. A correlation between computed fatigue damage and measured cracking is determined, and a limiting damage criterion for PCC shoulder design is selected.

PCC Fatigue

Several laboratory studies have shown that plain PCC beams experience fatigue failure when they are subjected to high repetitive flexural stresses (6-8). In addition, in several road tests and in many slabs in service, PCC slabs have been observed to experience fatigue cracking when they were subjected to many applications of heavy truck traffic (3, 9).

Results from laboratory studies have shown that the number of repeated loads that PCC can sustain in flexure before fracture depends on the ratio of applied flexural stress to ultimate static flexural strength or modulus of rupture. In this study, Miner's hypothesis (5) is used to represent the cumulative-damage characteristics of concrete.

Fatigue data were obtained for plain PCC beams from three studies (10-12). An S-N plot of 140 tests from these studies, presented by Darter (1), shows a considerable scatter of data. A design curve was fit through the data that provides for a safety factor (the curve was moved back one decade of load applications from the average regression line):

$$\text{Log}_{10}N = 16.61 - 17.61\,(R)$$

where N = number of stress applications to failure of beam and R = ratio of repeated flexural stress to modulus of rupture. This equation represents a failure probability of 0.24 or 24 percent.

Truck Traffic on Shoulders

Truck traffic on shoulders includes moving encroachments near the longitudinal joint, parked trucks with wheel loads near the outside edge, and the use of shoulders as an additional traffic lane. One of the most important factors that affects the lateral distribution of truck traffic in the outside traffic lane is the existence of shoulders and whether or not they are paved. The encroachment of truck traffic onto the shoulders depends mainly on lateral placement in the adjacent traffic lane. Available evidence (1) indicates that, when there is a paved shoulder and there are no lateral obstructions, trucks traveling on the outer lane show a definite tendency to shift several centimeters toward the slab edge. Data collected by Taragin (13) for 3.6-m (12-ft) concrete traffic lanes show the mean lateral distance of mainline trucks from the slab edge

to be 28 cm (11 in) when paved shoulders are used and 63.5 cm (25 in) when gravel or grass shoulders are used. This lateral shift toward the slab edge increases the number of truck encroachments onto the shoulder accordingly.

Another aspect to be considered is the number of parked trucks along a given highway section. Some of the main factors that affect this factor are the geometric layout of the section, its location relative to a weighing station, and, most important, its proximity to an interchange. In addition, PCC shoulders are sometimes used for regular traffic as a detour around a closed lane or as an additional lane during peak traffic hours. These conditions will thus have an effect on the structural and geometric adequacy of PCC shoulders and must be considered in design.

If a PCC shoulder is to perform its functions, it is crucial that the truck traffic used in design be based on the actual future uses of the shoulder under local conditions along the project.

Computation of PCC Fatigue

A procedure of fatigue analysis was developed based on previous results to provide a method of estimating the traffic damage that would result in cracking of the PCC slab. The basic purpose in fatigue design for plain jointed concrete shoulders is to control linear cracking. This is possible through direct consideration of traffic loading, joint spacing, lane-shoulder tie, shoulder width, and foundation support and loss of support. Fatigue damage is investigated at two critical locations in the concrete shoulder: the inner and outer edges. As discussed earlier, these two locations are very important in design and must therefore be analyzed separately in the design procedure.

The major steps in the fatigue analysis are as follows:

1. Determine axle applications, at each of the two critical edge locations, in each single- and tandem-axle load group.
2. Select the trial slab-subbase structure, lane-shoulder load transfer, PCC strength and variability, PCC shoulder width, and other required factors.
3. Compute the fatigue damage at each of the shoulder edges for a given year by using Miner's cumulative damage hypothesis (5) and sum yearly over the entire design period:

$$\text{Damage} = \sum_{j=1}^{j=p} \sum_{i=1}^{i=m} (n_{ij}/N_{ij}) \qquad (2)$$

where

- Damage = total accumulated fatigue damage over the design period at either of the slab edges;
- j = a counter for years beyond the design period;
- p = total number of years in the design period;
- i = a counter for axle-load magnitude, both single and tandem axle;
- m = total number of single- and tandem-axle load groups;
- n_{ij} = number of applied axle-load applications of the ith magnitude for the jth year; and
- N_{ij} = number of allowable axle-load applications of the ith magnitude for the jth year, determined from the PCC fatigue curve.

The fatigue damage is computed at each of the shoulder-slab longitudinal edges because results from field observations of many jointed concrete pavements (both traffic lanes and shoulders) and analytical fatigue analysis (1) have shown the midpoint between the transverse joints at the slab edge to be the critical point at which cracking initiates.

Applied traffic n_{ij} is computed from traffic data for the year under consideration by using the following expression:

$$n_{ij} = (ADT_y)(T/100)(DD/100)(LD/100)(A)(365)(P/100) \times (C/100)(CON) \qquad (3)$$

where

- ADT_y = average daily traffic at the end of the specific year under consideration;
- T = percentage trucks in ADT;
- DD = percentage trucks in the direction of the traffic lane adjacent to the shoulder;
- LD = lane distribution factor (percentage trucks in the design lane in one direction);
- A = mean number of axles per truck;
- P = percentage axles in the ith load group;
- C = percentage total axles in the truck traffic lane that park on or otherwise use the adjacent PCC shoulder (used for computing fatigue damage at the outer edge) or percentage total axles in the traffic lane that encroach on or otherwise use the adjacent PCC shoulder (used for computing fatigue damage at the inner edge); and
- CON = 1 for single axles, 2 for tandem axles.

Allowable traffic N_{ij} is computed from PCC fatigue considerations. The loading stress is computed at either of the two edges of the shoulder for a given axle load (single or tandem) by using a finite-element model.

The JCS-1 computer program was developed to compute accumulated fatigue damage over the design life of the PCC shoulder. These data can be used to incorporate consideration of fatigue damage in the evaluation and design of a plain jointed concrete shoulder.

Limiting Fatigue Consumption

The fatigue analysis that has been developed considers directly the effects of traffic loadings, shoulder width, lane-shoulder tie, and loss of foundation support (i.e., pumping). There are several factors, however, that are not considered because of insufficient information. One of the most important factors may be the use of PCC fatigue curves for small beams in estimating the fatigue life of large, fully supported pavement slabs. Traffic loading conditions also differ considerably between the laboratory and the field. Other inadequacies could be cited, but the point to be made is that the final accumulated fatigue damage computed for a pavement slab based on Equation 2 must be correlated with measured slab cracking before a limiting fatigue consumption can be selected for design.

According to Miner's hypothesis (5), a material should fracture when the accumulated damage equals 1.0. Even if Miner's hypothesis were exact, the variability in material strengths along a concrete pavement would cause a variation in accumulated computed damage in the various slabs that would range from much less than to much greater than 1.0, since an average strength that represents all of the slabs is used.

To determine a limiting value of fatigue damage for use in the design procedure, Equation 2 was used in fatigue analysis of many in-service pavements. The

Figure 1. Cracking index versus computed fatigue damage developed for in-service pavements.

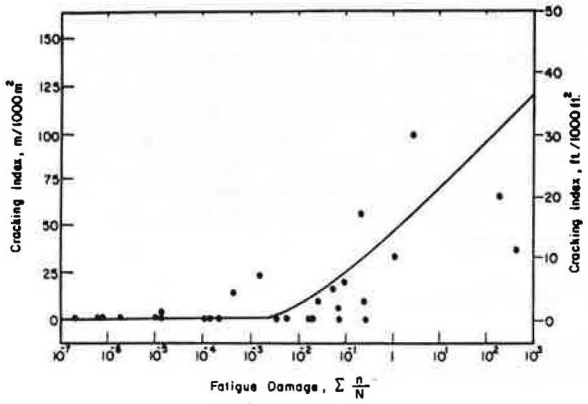

field data from 27 projects needed for the analysis were obtained from the zero-maintenance design project (2). The cracking index of each pavement project was measured. The curve shown in Figure 1 was developed from the analysis of sections that had joint spacing of 4.6-6.1 m (15-20 ft). The data for the curve were taken from plain jointed concrete pavements located in various states. By using this curve, the designer can select a limiting design value of fatigue damage to limit the cracking of the pavement slabs or, once the value of fatigue damage is computed for a given design, estimate the cracking index over the design period.

During the field survey conducted on I-74 (1), it was found that about 60 percent of the 7.6-m (25-ft) shoulder slabs showed transverse cracking. The severity of these cracks, however, is low to medium and therefore has not affected the performance of the PCC shoulder so far and is tolerated by highway users. The cracking index for this amount of cracking is 83 m/1000 m^2 (25 ft/1000 ft^2). According to Figure 1, the corresponding fatigue damage is between 10^1 and 10^2. Even with this amount of cracking, the PCC shoulder is still relatively smooth to drive on and provides adequate structural support to the traffic lane. It is believed, therefore, that the highway user will tolerate a higher level of cracking index when driving on the shoulder and that additional cracking can be tolerated without significantly reducing the amount of support provided to the traffic lane. Therefore, a fatigue damage of 10^3 [cracking index = 116 m/1000 m^2 (35 ft/1000 ft^2)] is recommended for use as a design limiting criterion for PCC shoulders on heavily trafficked highways. Recommended fatigue-damage values for pavement shoulders for high, medium, and low traffic volumes are as follows: Low traffic volume = 10^5 (ADT of the mainline = <2000), medium traffic volume = 10^4 (2000 < ADT < 20 000), and high traffic volume = 10^3 (ADT = >20 000).

JCS-1 COMPUTER PROGRAM

The JCS-1 (Jointed Concrete Shoulders-1) computer program was written to provide fatigue data for use in design. It is written in FORTRAN computer language for the IBM-360 digital computer but can be adapted for use on other computers with only minor modifications. The computer processing time for a design problem such as analyzing a range of shoulder thicknesses is about 9 s. The program requires 40 000 bytes of storage area. The designer must specify trial structural designs, determine the required inputs, run the JCS-1 program, and analyze the output fatigue data. The program is written to analyze any one or a combination of the following: shoulder thickness, mainline slab thickness, shoulder width, and mainline-shoulder tie. It can provide output for each combination while holding all other inputs constant. The designer can therefore examine a range of shoulder designs for a given traffic volume and foundation support in only one run of the program.

A complete, detailed example of the use of the program in the structural design of a PCC shoulder is given later in this paper.

JOINT DESIGN

PCC shoulders properly tied to either new or existing concrete pavement serve to stiffen the traffic lane and thereby decrease the deflection and consequent pumping near the longitudinal joint (1). The method of tying the PCC shoulder to the mainline concrete pavement is a primary factor in determining the magnitude and extent of load-transfer efficiency across the longitudinal joint throughout the design life. Therefore, some recommended methods for constructing concrete shoulders that are tied to both new and existing traffic lanes are discussed.

When a PCC shoulder is constructed for an existing slab, adequate load transfer can be provided for by means of closely spaced tiebars. Holes are drilled in the edge of the existing slab. This can be done by using a tractor-mounted drill that can drill several holes in the side of the mainline slab at one time. Tiebars are installed in the holes by using epoxy or a cement grout. The bars should be placed into the slab over such a length as to develop full bond strength [at least 22.9 cm (9 in) to avoid spalling over the base].

Malleable tiebars of smaller diameter (no. 4 or no. 5) and spacing 0.3-0.6 m (12-24 in) midway across the slab depth are preferable to stiffer, short bars at large spacing intervals. This will substantially reduce the possibility of stress concentrations above the tiebar, which will cause spalling of the joint in the vicinity of the bar and the eventual breakage of the slab and the loss of load transfer. The possibility of upward heave or drop-off of the shoulder in the area between the bars will also be substantially reduced when a short tiebar spacing is used [< 60 cm (<24 in) is recommended], since there will be more steel to hold the lane and shoulder together. Problems with upward heave in the shoulder and spalling of the lane concrete were experienced in Pennsylvania and New York, where two-piece tie bolts [152 cm (60 in) center to center] were used to tie a 15-cm (6-in) concrete shoulder to the existing mainline pavement.

On I-80 in Illinois, shoulders were tied to the mainline slab (smooth edge) with no. 4 hooked bolts, 37.5 cm (15 in) in length, turned into 5-cm (2-in) snapoff expanding end anchors set into the edge of the mainline slab at 75-cm (30-in) intervals by use of a pneumatic hammer. Recent measurements of this project showed that the deflection efficiency of the lane-shoulder joint was very poor, ranging from 31 to 47 percent. The joint had opened an average of about 10 mm (0.4 in), and many of the bars had spalled the concrete over the bar in the traffic lane, where the 5-cm snapoff expanding end anchors were set. Some of the bars were set within 5 cm of the surface, which also contributed to the spalling and loss of load transfer. It is believed that placing bars at middepth of the slab would minimize any potential spalling.

The practice of not placing tiebars within 75 cm (30 in) of the transverse shoulder joint results in loss of load transfer along 150 cm (60 in) of traffic lane. On one continuously reinforced concrete pavement (CRCP)

project in Indiana (I-65), several edge punchouts have occurred within this area because of no load transfer. Based on results from the I-74 and I-80 projects in Illinois, tie-bars can be placed much closer—e.g., half the normal tiebar spacing—to the transverse shoulder joint.

In the case of new construction, tiebars can be inserted into the plastic concrete near the rear of the slip-form paver. Bent bars can be installed by mechanical means or manually. The bent portion can be straightened later to tie the shoulder to the mainline pavement. A three-piece tie bolt can be used, half of which is inserted in the traffic lane by machine, along with the coupler, and the other half of which is screwed into the coupler before the shoulder is added (15-17). In addition to the tiebars, a keyway can be formed to provide additional load-transfer capability.

A keyed joint with tiebars was used in the construction of the experimental shoulder sections built on I-74 in Illinois. The efficiency of load-deflection transfer on I-74 is still quite high (70-100 percent) after 10 years in service (2). This shows that with proper joint design and construction a high efficiency (i.e., >70 percent) can be attained over a long period of time. More comprehensive analysis of concrete pavement joint designs for different load-transfer systems was conducted at the University of Illinois (18). This study provides guidelines for the degree of efficiency to be expected from one load-transfer system or a combination of two or more (e.g., tiebars, dowel bars, aggregate interlock, and keyway) that can be used across the joint between the traffic lane and the shoulder.

On I-74, it was also found that a joint opening of as much as 25 mm (1 in) is experienced on a keyed joint when no tiebars are used. This opening results in complete loss of load deflection and an upward heave or a drop-off in the PCC shoulder.

The longitudinal joint between the traffic lane and the shoulder should be provided with a sealant reservoir and sealed with an effective sealant to reduce the possibility of foreign materials collecting inside the joint and thus reduce the potential for the joint to spall and minimize the amount of deicing salt that penetrates to the tiebars. There was significant corrosion of tiebars on I-80 after 11 years, which shows the necessity of providing either a good seal or corrosion-resistant tiebars to ensure long-term structural adequacy of the bar in transferring load across the joint (if the pavement is subjected to deicing salts).

The cross-slope of the bottom surface of the concrete shoulder should be great enough to permit drainage away from the longitudinal shoulder-pavement joint and avoid pocketing water at this critical location. This will contribute directly to a more effective and lasting load-transfer system across the joint.

Finally, for plain jointed concrete pavements, the shoulder joint pattern should match that of the traffic lane, although intermediate joints can be placed if the joint spacing of the traffic lane is greater than 6.1 m (20 ft). Intermediate contraction joints must be placed where the traffic lane is jointed reinforced concrete with long joint spacing. None of the transverse shoulder joints require dowels unless the shoulder is to be used as a regular traffic lane.

SHOULDER DESIGN

The design example presented here is for a PCC shoulder located on a stretch of I-80 near Joliet, Illinois. The existing asphalt paved shoulder has reached a point of severe deterioration that requires complete reconstruction. Moreover, the mainline pavement is a 20-cm (8-in) CRCP that is experiencing excessive edge deflections because of the combined effects of heavy truck traffic and loss of support at the vicinity of the outer edge of the pavement as a result of the excessive pumping of fine materials from under the CRCP slab. Edge punchouts have occurred to the extent that major rehabilitation of the pavement is needed before deterioration becomes excessive. Construction of a PCC shoulder was selected as part of the rehabilitation to replace the existing deteriorated shoulder and to improve the performance of the adjacent traffic lane through edge support.

Structural Design Inputs

The design life of the PCC shoulder is 20 years.

The slab properties are as follows:

1. Slab thickness—Trial thicknesses of 12.5, 15, 17.5, 20, and 22.5 cm (5, 6, 7, 8, 9 in) are chosen for the shoulder slab to provide a range of results that should encompass the appropriate slab thickness. The adjacent CRCP traffic lane is 20 cm (8 in) thick.
2. Slab width—A shoulder width of 3 m (10 ft) is standard practice for use on Interstate highways to accommodate emergency stops and other uses by traveling vehicles.
3. Shoulder-joint spacing—The design procedure was developed for a shoulder-joint spacing of <6 m (<20 ft). The length selected for this project is 4.76 m (15 ft).
4. Mean PCC modulus of rupture—The mean modulus of rupture that is used in this design example (third-point loading at 28 days curing) is 5,17 MPa (750 lbf in'
5. Coefficient of variation of PCC modulus of rupture—An average coefficient of variation of 10 percent is typical for the PCC used in shoulder construction.

The traffic factors considered are as follows:

1. ADT at the beginning of the design period—The current ADT in both directions is 17 100.
2. ADT at the end of the design period—The final ADT after 20 years is estimated from transportation planning studies to be 39 100.
3. Percentage trucks in the ADT—The average percentage of trucks for the highway, including panels and pickups, is estimated to be 21 percent. This percentage is for the entire 20-year period.
4. Percentage trucks in the most heavily traveled lane—The percentage of trucks in the most heavily traveled lane (the outer lane) is determined from manual counts to be 85 percent.
5. Percentage directional distribution of traffic—Since traffic is approximately equal in each direction, a value of 50 percent traffic in the design direction is selected.
6. Mean axles per truck—Traffic data from W-4 tables for the highway show an average of 2.6 axles/truck (including pickups and panels).
7. Percentage trucks that use the shoulder—For encroached traffic, a 16.1-km (10-mile) shoulder stretch was surveyed and the average length of total encroachments per truck over the 16.1 km was 0.39 km (0.24 mile), which produces 2.4 percent trucks encroaching on the shoulder (this estimate was obtained by following behind randomly selected trucks and recording the length of their encroachment over the 16.1-km section). For parked traffic, the percentage of trucks that park on a specific slab of the shoulder is generally estimated as follows. The surveyed stretch of shoulder is 3.2 km (2 miles) or 3221 m (10 560 ft) long. There are seven hundred and four 4.6-m (15-ft)

slabs in the surveyed stretch. A truck drives on the outer shoulder edge an average distance of about 61 m (200 ft) before it can come to a stop and then start up and move over to the traffic lane. This translates into thirteen 4.6-m slabs and divides the surveyed stretch into 53 groups of thirteen 4.6-m slabs each. If we assume, for example, that only one truck per day will park on the surveyed stretch and the probability of this truck using any one of the 53 slab groups is equal, the probability of any group of slabs being used by this truck on any day is 1/53; or, in other words, one truck will use a given group of slabs every 53 days on the average. The ADT in one direction on I-80 per day is ADT × T × DD = 28 100 × 0.21 × 0.5 = 2951 trucks/day/direction, and 2951 × 53 = 156 371 trucks in 53 days. Therefore, the percentage of truck traffic that will park on a given group of slabs is 1/156 371 × 100 = 0.000 64 percent of mainline trucks. Based on the limited field survey conducted on the stretch of I-80, it is believed that the average number of trucks that park within a 3.4-km (2-mile) stretch of shoulder could range from 1 to 25; therefore, this range is used in the design. Additional surveys would be necessary to determine the average number of parked trucks more accurately and whether the number varied along the project (particularly at interchanges). The percentage of truck traffic that will travel on a given group of slabs when 25 trucks park within the limits of the surveyed stretch is 0.000 64 × 25 = 0.016 percent.

8. Axle-load distribution—The axle-load distribution was established by weighing axle loads at a loadometer station near the project. This distribution should be modified if conditions indicate that legal loads will change during the 20-year period.

Foundation Support

The shoulder will be placed on embankment materials that are mostly fine textured. The soil is American Association of State Highway and Transportation Officials classification A-6 and A-7-6. The materials are principally relatively thin glacial drift of Wisconsinan age overlying dolomitic limestone bedrock (14). A 20-cm (8-in) layer of open-graded granular materials was evaluated as a subbase for the shoulder concrete slab. The k-value on top of the subbase is estimated to be about 54.2 N/cm^3 (200 lbf/in^3). The initial erodibility of the shoulder foundation is zero, and the final erodibility is estimated to be 20 cm (8 in) for the granular subbase.

Lane-Shoulder Tie

Tiebars could be installed in the existing mainline pavement and the new PCC shoulder to provide adequate load transfer across the joint. In this example, a load-transfer system that consists of a tied-butt joint with 76-cm (30-in) long no. 4 tiebars placed 46 cm (18 in) center to center is used to provide load transfer across the longitudinal joint. An average value of 80 percent (based on deflection) is used for the load-transfer efficiency of this joint to account for any lack of quality control of construction and materials that might occur during the construction phase and for the effect of millions of repeated loads applied near the joint.

The degree of load-transfer efficiency, which is defined as the ratio of the deflection of the unloaded slab to that of the loaded slab at the joint, is not necessarily the same as the degree of load-transfer efficiency when it is defined as the ratio of the flexural stress experienced by both slabs at the joints. The finite-element model used in the analysis does not take this factor into consideration. Thus, an adjustment for the difference between the two efficiencies is needed. A more comprehensive finite-element model (18) that accounts for the difference between the two efficiencies is used to establish an adjustment curve that can be used in design.

Figure 2 shows the relation between the load-transfer efficiency based on deflections and that based on stresses. Thus, for this design example, assuming 80 percent load-transfer efficiency (based on deflection) and using Figure 2 for adjustment, 42 percent load-transfer efficiency (based on stress) is obtained and is used for design.

Selection of Shoulder Design

A summary of the results obtained from the computer program output is given below (1 cm = 0.39 in):

Slab Thickness (cm)	Fatigue Damage Attributable to	
	Parked Traffic	Encroaching Traffic
12.5	4.81×10^{24}	3.53×10^{3}
15.0	5.74×10^{11}	6.95×10^{-1}
17.5	3.34×10^{4}	6.52×10^{-3}
20.0	1.06×10^{0}	3.16×10^{-4}
22.5	1.04×10^{-3}	3.51×10^{-5}

The volume of parked traffic used is 25 trucks/day in the 3.3-km (2-mile) shoulder stretch surveyed. These results are shown in Figure 3. The minimum design

Figure 2. Effect of thickness of PCC shoulder slab on accumulated fatigue damage at both shoulder edges.

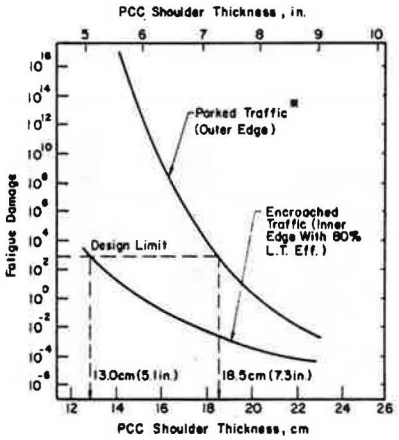

Figure 3. Load-transfer efficiency based on deflection versus that based on stress.

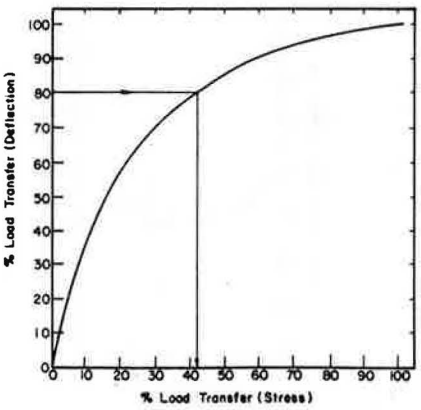

slab thickness at the inner and outer edges of the shoulder is determined as indicated [although the inner-edge thickness is shown in Figure 3 at 13 cm (5.1 in), a minimum of 15 cm (6 in) (2) will be used].

The outer-edge minimum thickness = 18.5 cm (7.3 in) due to parked traffic, and the inner-edge minimum thickness = 15 cm due to encroached traffic, with 80 percent load-transfer efficiency across the joint. Therefore, for these conditions of design life, slab properties, traffic, foundation support, and load transfer across the lane-shoulder joint, the structural design thickness would be 18.5 cm (7.3 in) minimum of PCC over a 20-cm (8-in) layer of open-graded granular subbase. By decreasing the volume of shoulder parked traffic in the 3.3-km (2-mile) surveyed stretch from 25 trucks/day to only 1 truck/day, as previously discussed, the structural design thickness of the PCC shoulder would be reduced to 17.8 cm (7 in), as shown in Figure 4.

Figure 4. Effect of the number of parked trucks on accumulated fatigue damage at the outer edge of the shoulder.

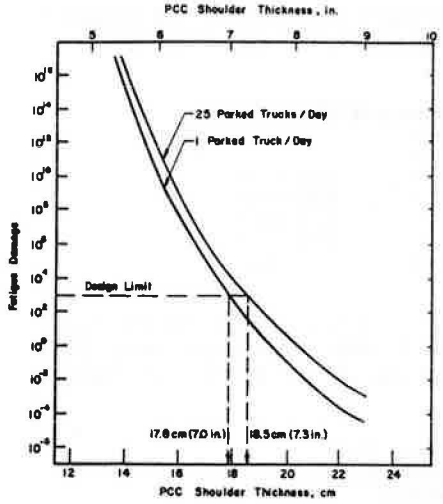

The previous structural design selections (Figure 3) were obtained for a specific subbase, shoulder width, and concrete strength. There are other alternatives, however, that could be analyzed to obtain the most economical structural design. A summary of a few alternatives is given in Table 1. The other design inputs were held constant for each of these alternatives as a single parameter was varied. Required thickness varies from 15.0 to 18.8 cm (6.0-7.4 in), depending on the values of the design parameters controlled by the designer. Each alternative should be further designed and economic analysis conducted to determine the most economical alternative.

Table 1. Summary of alternate structural designs for PCC shoulder design example.

Alternate	Design Parameter: Slab Width (m)	Subbase Type	Strength (kPa)	Design Thickness (cm)
1	3	20 cm, granular	5171	18.5
2	3	15 cm, stabilized	5171	16.3
3	3	20 cm, granular	6205	16.8
4	3	15 cm, stabilized	6205	14.7*
5	2.1	20 cm, granular	5171	18.8
6	2.1	15 cm, stabilized	5171	16.5
7	2.1	20 cm, granular	6205	17.0
8	2.1	15 cm, stabilized	6205	14.8*

Note: 1 m = 3.3 ft; 1 kPa = 0.145 lbf/in²; 1 cm = 0.39 in.
*Minimum 15 cm.

Final Design Selection Relative to Cost

A complete cost analysis of alternative designs that meet the limiting criteria can be conducted. Since no shoulder structural maintenance is expected over the 20-year design period, the cost analysis can be based on the first cost of the pavement. The design alternative that provides the lowest initial construction cost should be chosen as the optimum structural design alternative.

Sensitivity Analysis

A sensitivity analysis is conducted to illustrate the effect of changes in several of the design parameters on required shoulder slab thickness and to show the reasonableness of the design procedures. The average conditions are set as described in the design of the example project, and then one parameter at a time is varied over a range that might exist in actual situations. Shoulder width is the first parameter varied, from 0.46 to 3.05 m (1.5-10 ft), as shown in Figure 5. The shoulder slab thickness required decreases from 20.0 to 17.8 cm (8-7 in) as shoulder width increases from 0.46 to 3.05 m (1.5-10 ft). A change in the 28-day modulus of rupture from 4.48 to 6.2 MPa (650-900 lbf/in², produces a change of about 3.6 cm (1.4 in) in PCC shoulder slab thickness, as shown in Figure 6. A change in

Figure 5. Sensitivity analysis of design parameters: shoulder slab thickness versus shoulder width.

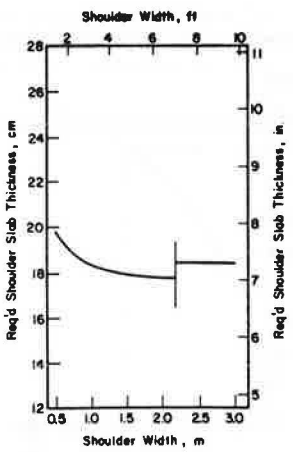

Figure 6. Sensitivity analysis of design parameters: shoulder slab thickness versus modulus of rupture.

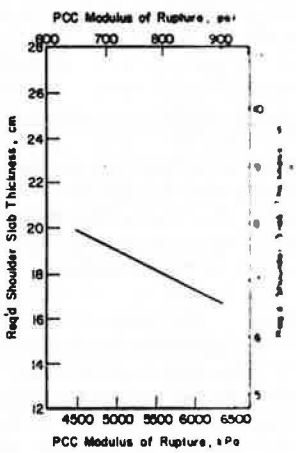

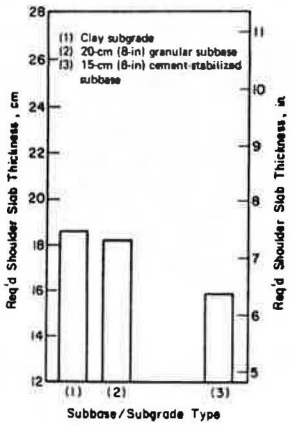

Figure 7. Sensitivity analysis of design parameters: shoulder slab thickness versus type of subbase or subgrade.

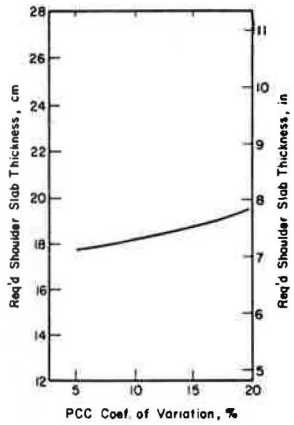

Figure 8. Sensitivity analysis of design parameters: shoulder slab thickness versus PCC coefficient of variation.

foundation conditions from no subbase over clay subgrade to 20-cm granular subbase to 15 cm (6 in) of cement-stabilized subbase reduces the required shoulder slab thickness by about 0.50 cm (0.2 in) and 2.8 cm (1.1 in) respectively, as shown in Figure 7. The variation in PCC strength shown in Figure 8 is indicated by the coefficient of variation. The variation from excellent quality control (5 percent) to poor (20 percent) causes an increase in the required PCC shoulder slab thickness of approximately 1.8 cm (0.7 in).

The effect of increasing the number of trucks that park on the shoulder stretch from 1 to 25 trucks/day, as shown in Figure 4, produces a change in required PCC shoulder slab thickness of 0.8 cm (0.3 in).

CONCLUSIONS

This paper describes the development of a comprehensive structural design procedure for plain jointed concrete shoulders as well as a design example that contains all the procedures necessary in actual design. A computer program designated JCS-1 is used to obtain fatigue-damage data for use in structural design. The program is written in FORTRAN and is easily adapted to most computers. The design procedure developed in this research can be used for both new construction and rehabilitation. Detailed documentation and a complete description of use of the JCS-1 program are presented elsewhere (19).

A procedure for comprehensive fatigue-damage analysis was developed that permits direct control of slab cracking. Stress attributable to traffic loadings is directly considered in the analysis through the use of the finite-element method. A fatigue-damage limiting design criterion was determined from field data.

The joint between the shoulder and the traffic lane has a major influence on the structural adequacy of PCC shoulders and on improving the performance of the adjacent traffic lane. Recommendations concerning the joint design are presented.

An example design application is provided that describes the use of the procedure in detail. The economic justification of the selection of the final PCC shoulder design is an important factor and should be a criterion in giving one design priority over another.

The design procedure discussed here can be used for new construction of PCC shoulders and also for rehabilitation of existing concrete pavements. The effect of many variables can be analyzed, including shoulder slab thickness, mainline slab thickness, concrete strength and variation, shoulder width, traffic that uses the shoulder, traffic overloads, foundation support (subbase and subgrade, including degree of saturation), and systems of load transfer across the lane-shoulder longitudinal joint.

ACKNOWLEDGMENT

This research was conducted at the University of Illinois at Urbana-Champaign. We wish to thank the sponsor—the Federal Highway Administration, U.S. Department of Transportation.

REFERENCES

1. J. S. Sawan and M. I. Darter. Structural Evaluation of PCC Shoulders. TRB, Transportation Research Record 666, 1978, pp. 51-60.
2. M. I. Darter. Design of Zero-Maintenance Plain Jointed Concrete Pavements: Volume 1—Development of Design Procedures. Federal Highway Administration, U.S. Department of Transportation, Tech. Rept. FHWA-RD-77-111, 1977.
3. The AASHO Road Test: Report 5—Pavement Research. HRB, Special Rept. 61E, 1962.
4. E. A. Finney and L. T. Ochler. Final Report on Design Project, Michigan Test Road. HRB, Proc., Vol. 38, 1959.
5. M. A. Miner. Cumulative Damage in Fatigue. Trans., ASCE, Vol. 67, 1945, pp. A159-A164.
6. J. W. Murdock. A Critical Review of Research on Fatigue of Plain Concrete. Engineering Experiment Station, Univ. of Illinois at Urbana-Champaign, Bull. 476, 1965, 32 pp.
7. H. K. Hilsdorf and C. E. Kesler. Fatigue Strength of Concrete Under Varying Flexural Stresses. Proc., ACI, Vol. 63, 1966, pp. 1059-1076.
8. J. W. Murdock and C. E. Kesler. Effect of Range of Stress on Fatigue Strength of Plain Concrete Beams. Proc., ACI, Vol. 55, 1959, pp. 221-231.
9. M. I. Darter and E. J. Barenberg. Zero-Maintenance Pavement: Results of Field Studies on the Performance Requirements and Capabilities of Conventional Pavement Systems. Federal Highway Administration, U.S. Department of Transportation, Tech. Rept. FHWA-RD-76-105, 1976.
10. G. M. Nordby. Fatigue of Concrete: A Review of Research. Proc., ACI, Vol. 55, 1959, pp. 191-220.
11. C. A. Ballinger. Cumulative Fatigue Damage Characteristics of Plain Concrete. HRB, Highway Research Record 370, 1972, pp. 48-60.
12. K. D. Raithby and J. W. Galloway. Effects of Moisture Conditions, Age, and Rate of Loading on Fatigue of Plain Concrete. ACI, Detroit, SP-41, 1974.

13. A. Taragin. Lateral Placement of Trucks on Two-Lane Highways and Four-Lane Divided Highways. Public Roads, Vol. 30, No. 3, Aug. 1958.
14. L. J. McKenzie. Experimental Paved Shoulders on Frost-Susceptible Soils. Illinois Department of Transportation, Springfield, Project IHR-404, Final Rept., March 1972.
15. G. K. Ray. Concrete Shoulders for CRC Pavements. Presented at Continuously Reinforced Concrete Pavement Workshop, New Orleans, Feb. 14-15, 1978.
16. R. H. Florence, Jr. Design and Construction of Several Maintenance Techniques for Continuously Reinforced Concrete Pavements. Purdue Univ., West Lafayette, IN, Joint Highway Res. Project 76-12, Interim Rept., March 1976.
17. A. M. Tabatabaie-Raissi. Structural Analysis of Concrete Pavement Joints. Univ. of Illinois at Urbana-Champaign, Ph.D. thesis, Jan. 1978.
18. M. M. Alexander and R. A. Gaves. Determination of the Level Distribution of Truck Traffic on Freeway Facilities. Georgia State Highway Department, Atlanta, Final Rept., 1971.
19. J. S. Sawan, M. I. Darter, and B. J. Dempsey. Structural Design of PCC Jointed Shoulder. Univ. of Illinois at Urbana-Champaign, Tech. Rept., 1978.

Publication of this paper sponsored by Committee on Shoulder Design.